ITUPublications

International Telecommunication Union
Radiocommunication Sector

Report ITU-R M.2547-0

(12/2024)

M Series: Mobile, radiodetermination, amateur and related satellite services

Various aspects of non-safety aeronautical mobile service systems in the frequency bands 15.4-15.7 GHz and 22-22.21 GHz

Foreword

The role of the Radiocommunication Sector is to ensure the rational, equitable, efficient and economical use of the radio-frequency spectrum by all radiocommunication services, including satellite services, and carry out studies without limit of frequency range on the basis of which Recommendations are adopted.

The regulatory and policy functions of the Radiocommunication Sector are performed by World and Regional Radiocommunication Conferences and Radiocommunication Assemblies supported by Study Groups.

Policy on Intellectual Property Right (IPR)

ITU-R policy on IPR is described in the Common Patent Policy for ITU-T/ITU-R/ISO/IEC referenced in Resolution ITU-R 1. Forms to be used for the submission of patent statements and licensing declarations by patent holders are available from https://www.itu.int/ITU-R/go/patents/en where the Guidelines for Implementation of the Common Patent Policy for ITU-T/ITU-R/ISO/IEC and the ITU-R patent information database can also be found.

Series of ITU-R Reports

(Also available online at https://www.itu.int/publ/R-REP/en)

Series	Title
BO	Satellite delivery
BR	Recording for production, archival and play-out; film for television
BS	Broadcasting service (sound)
BT	Broadcasting service (television)
F	Fixed service
M	**Mobile, radiodetermination, amateur and related satellite services**
P	Radiowave propagation
RA	Radio astronomy
RS	Remote sensing systems
S	Fixed-satellite service
SA	Space applications and meteorology
SF	Frequency sharing and coordination between fixed-satellite and fixed service systems
SM	Spectrum management
TF	Time signals and frequency standards emissions

***Note**: This ITU-R Report was approved in English by the Study Group under the procedure detailed in Resolution ITU-R 1.*

Electronic Publication
Geneva, 2025

REPORT ITU-R M.2547-0

Various aspects of non-safety aeronautical mobile service systems in the frequency bands 15.4-15.7 GHz and 22-22.21 GHz

(2024)

The present ITU-R Report contains the various studies conducted during the study cycle 2019-2023 which were the basis for discussion leading to the decision taken at WRC-23. This Report in no way, whatsoever, would compromise, undermine, or impact the decision taken by WRC-23 on agenda item 1.10.

TABLE OF CONTENTS

1 Scope

This Report addresses studies on spectrum needs, compatibility and sharing studies with radio communication services and regulatory measures for possible new allocations for the aeronautical mobile (off-route) service (AM(OR)S) for the use of non-safety aeronautical mobile applications in the 15.4-15.7 GHz and 22-22.21 GHz frequency bands.

These tasks are further divided as follows:

– Sections 4 and 5 provide information on the use of airborne sensors in various fields of the industry, and introduces non-safety data links that are an essential component thereof;

– Section 6 presents a list of operational scenarios involving airborne datalinks, and evaluates the deployment densities as well as the spectrum resource associated to the aforementioned scenarios. These scenarios are used throughout the Report for sharing and compatibility studies with incumbent services;

– Section assesses the spectrum needs associated to future non-safety AM(OR)S applications;

– Section 8 summarizes the result of sharing and compatibility studies.

AM(OR)S[1] allocations, rather than AMS are considered. This is due to the fact that the possible future applications in these bands will be restricted to professional and governmental usages. In that regard, they would take place at specific locations and for limited periods of time. Therefore, mass-market applications, and in particular these taking place on national and international civil air routes in the context of commercial aviation, would be excluded.

2 Related Recommendations and Reports

ITU-R Recommendations

Recommendation ITU-R SM.337 – Frequency and distance separations

Recommendation ITU-R P.452 – Prediction procedure for the evaluation of interference between stations on the surface of the Earth at frequencies above about 0.1 GHz

Recommendation ITU-R P.453 – The radio refractive index: its formula and refractivity data

Recommendation ITU-R S.465 – Reference radiation pattern for earth station antennas in the fixed-satellite service for use in coordination and interference assessment in the frequency range from 2 to 31 GHz

Recommendation ITU-R P.528 – A propagation prediction method for aeronautical mobile and radionavigation services using the VHF, UHF and SHF bands

Recommendation ITU-R S.580 – Radiation diagrams for use as design objectives for antennas of earth stations operating with geostationary satellites

Recommendation ITU-R SA.509 – Space research earth station and radio astronomy reference antenna radiation pattern for use in interference calculations, including coordination procedures, for frequencies less than 30 GHz

Recommendation ITU-R P.619 – Propagation data required for the evaluation of interference between stations in space and those on the surface of the Earth

Recommendation ITU-R S.672 – Satellite antenna radiation pattern for use as a design objective in the fixed-satellite service employing geostationary satellites

Recommendation ITU-R P.676 – Attenuation by atmospheric gases and related effects

---

[1] AM(OR)S is, according to RR No. **1.34**, an aeronautical mobile service intended for communications, including those relating to flight coordination, primarily outside national or international civil air routes.

Recommendation ITU-R F.699 – Reference radiation patterns for fixed wireless system antennas for use in coordination studies and interference assessment in the frequency range from 100 MHz to 86 GHz

Recommendation ITU-R F.758 –System parameters and considerations in the development of criteria for sharing or compatibility between digital fixed wireless systems in the fixed service and systems in other services and other sources of interference

Recommendation ITU-R RA.769 – Protection criteria used for radio astronomical measurements

Recommendation ITU-R P.835 – Reference standard atmospheres

Recommendation ITU-R F.1245 – Mathematical model of average and related radiation patterns for point-to-point fixed wireless system antennas for use in interference assessment in the frequency range from 1 GHz to 86 GHz

Recommendation ITU-R F.1336 – Reference radiation patterns of omnidirectional, sectoral and other antennas for the fixed and mobile service for use in sharing studies in the frequency range from 400 MHz to about 70 GHz

Recommendation ITU-R S.1340 – Sharing between feeder links for the mobile-satellite service and the aeronautical radionavigation service in the Earth-to-space direction in the band 15.4-15.7 GHz

Recommendation ITU-R P.1409 – Propagation data and prediction methods for systems using high altitude platform stations in the stratosphere at frequencies greater than about 0.7 GHz

Recommendation ITU-R M.1461 – Procedures for determining the potential for interference between radars operating in the radiodetermination service and systems in other services

Recommendation ITU-R F.1495 – Interference criteria to protect the fixed service from time varying aggregate interference from other radiocommunication services sharing the 17.7-19.3 GHz band on a co-primary basis

Recommendation ITU-R RA.1513 – Levels of data loss to radio astronomy observations and percentage-of-time criteria resulting from degradation by interference for frequency bands allocated to the radio astronomy service on a primary basis

Recommendation ITU-R SM.1541 – Unwanted emissions in the out-of-band domain

Recommendation ITU-R F.1565 – Performance degradation due to interference from other services sharing the same frequency bands on a co-primary basis, or from other sources of interference, with real digital fixed wireless systems used in the international and national portions of a 27 500 km hypothetical reference path at or above the primary rate

Recommendation ITU-R S.1586 – Calculation of unwanted emission levels produced by a non-geostationary fixed-satellite service system ta radio astronomy sites

Recommendation ITU-R RA.1631 – Reference radio astronomy antenna pattern to be used for compatibility analyses between non-GSO systems and radio astronomy service stations based on the epfd concept

Recommendation ITU-R M.1730 – Characteristics of and protection criteria for the radiolocation service in the frequency band 15.4-17.3 GHz

Recommendation ITU-R RS.1813 – Reference antenna pattern for passive sensors operating in the Earth exploration-satellite service (passive) to be used in compatibility analyses in the frequency range 1.4-100 GHz

Recommendation ITU-R M.1825 – Guidance on technical parameters and methodologies for sharing studies related to systems in the land mobile service

Recommendation ITU-R M.1851 – Mathematical models for radiodetermination radar systems antenna patterns for use in interference analyses

Recommendation ITU-R RS.1861 – Typical technical and operational characteristics of Earth exploration-satellite service (passive) systems using allocations between 1.4 and 275 GHz

Recommendation ITU-R RS.2017 – Performance and interference criteria for satellite passive remote sensing

Recommendation ITU-R M.2089 – Technical characteristics and protection criteria for aeronautical mobile service systems in the frequency range 14.5-15.35 GHz

Recommendation ITU-R M.2114 – Technical and operational characteristics of and protection criteria for aeronautical mobile service systems in the frequency bands 22.5-23.6 GHz and 25.25-27.5 GHz

Recommendation ITU-R M.2115 – Technical and operational characteristics of and protection criteria for aeronautical mobile systems operating in the 45.5-47 GHz frequency range

Recommendation ITU-R M.2116 – Technical characteristics and protection criteria for the aeronautical mobile service systems operating within the 4 400-4 990 MHz frequency range

Recommendation ITU-R M.2120 – Technical characteristics and protection criteria for aeronautical mobile systems operating in the mobile service in the frequency range 21.2-22 GHz

ITU-T Recommendations

Recommendation ITU-T G.826 – End-to-end error performance parameters and objectives for international, constant bit-rate digital paths and connections

ITU-R Reports

Report ITU-R RA.2188 – Power flux-density and e.i.r.p. levels potentially damaging to radio astronomy receivers

3 List of acronyms and abbreviations

Acronyms

ADT	Airborne data terminal
AGL	Above ground level
AI	Agenda item
ALS	Automatic landing system
ATPC	Automatic transmit power control
AMS	Aeronautical mobile service
AM(OR)S	Aeronautical mobile (off-route) service
AMSL	Above mean seal level
APO	Availability performance objective
ARNS	Aeronautical radio navigation service
ARP	Antenna radiation pattern
A2A	Air-to-air
A2G	Air-to-ground
BAQ	Block adaptative quantization
BER	Bit error rate
BLOS	Beyond line of sight
BPSK	Binary phase shift keying
BSS	Broadcasting-satellite service
BW	Bandwidth
CDMA	Code division multiple access
CDF	Cumulative distribution function
C/*N*	Carrier-to-noise

CO	Continuous observation
CR	Compression ratio
Codec	Coder, decoder
DAA	Detect and avoid
DC	Duty cycle
DEM	Digital elevation model
DFS	Dynamic frequency selection
DR	Data rate
DSSS	Direct sequence spread spectrum
ECDF	Empirical cumulative distribution function
EESS	Earth exploration-satellite service
EFOV	Effective field of view
e.i.r.p.	Equivalent isotropic radiated power
EPO	Error performance objective
ES	Earth station
ESR	Errored second ratio
FDMA	Frequency division multiple access
FDR	Frequency dependent rejection
FM	Fade margin
FM	Frequency modulation
FOV	Field of view
FPS	Frame per second
FR	Frame rate
FR	Frequency reuse
FS	Fixed service
FSK	Frequency shift keying
FSPL	Free space path loss
FSS	Fixed-satellite service
FTBR	Front-to-back ratio
GBT	Green bank telescope
GDT	Ground data terminal
GSO	Geostationary orbit
G2A	Ground-to-air
HD	High-definition
HPBW	Half-power beam width
ICDF	Inverse cumulative distribution function
IF	Intermediate frequency
IMT	International Mobile Telecommunications
INR	Interference-to-noise ratio
IR	Infrared

IR	Image resolution
ITU-R	International Telecommunication Union, Radiocommunication Sector
IWS	Interfered-with system
LAMEA	Latin America, Middle East and Africa
LEO	Low Earth orbit
LFM	Linear frequency modulation
LIDAR	Light detection and ranging
LMS	Land mobile service
LOS	Line-of-sight
MAI	Mission area of interest
MCL	Minimum coupling loss
MIFR	Master of International Frequency Register
MS	Mobile service
NATS	North Atlantic Track System
NF	Noise figure
Non-GSO	Non-geostationary-satellite orbit
NM	Nautical mile
NPAS	National Police Air Service
OOB	Out-of-band
OTR	On-tune rejection
PD	Pixel depth
pfd	Power flux-density
PGDT	Portable ground data terminal
PL	Path loss
PRF	Pulse repetition frequency
PRR	Pulse repetition rate
PSD	Power spectral density
PSK	Phase shift keying
PTMP	Point-to-multipoint
PTP	Point-to-point
QAM	Quadrature amplitude modulation
QPSK	Quadrature phase shift keying
RAS	Radio astronomy service
RF	Radio frequency
RFI	Radio frequency interference
RGB	Red green blue
RHD	Radio horizon distance
RLS	Radiolocation service
RP	Remote pilot

RPSD	Relative power spectral density
RR	Radio Regulations
RR	Repetition rate
SAA	Sense and avoid
SAR	Synthetic aperture radar
SAR	Search and rescue
SEM	Spectrum emission mask
SESR	Severely errored second ratio
SHF	Super high frequency
SLA	Side lobe attenuation
SLAR	Side-looking-airborne-radar
SLO	Spectral line observation
SNR	Signal-to-noise ratio
SRS	Space research service
SRTM	Shuttle Radar Topography Mission
TPO	Transmit power output
UHF	Ultra-high frequency
U.K.	United Kingdom
U.S.A.	United States of America
VHF	Very high frequency
VLA	Very large array
WBLOSDL	Wideband line of sight datalink

4 Airborne sensors

Airborne sensors are typically used to provide accurate and if relevant real-time measurements of physical characteristics related to the surface of the Earth or its atmosphere. Some applications include (the list is not exhaustive):

– *Agriculture*. Crops health can be monitored from the sky using special types of airborne sensors such as red green blue (RGB) or infrared (IR) cameras. In particular, areas in need of water, fertilizer or pesticide can be located with high accuracy, which improves the overall efficiency of the farming (see Fig. 1).

– *Forestry*. Airborne sensors can be used for forest inventory and tree height measurement (see Fig. 2).

FIGURE 1

RGB images taken over crop fields using airborne sensors; specific sensors can detect different kinds of anomalies[2]

FIGURE 2

Digital elevation model (DEM), representing a forest area[3]

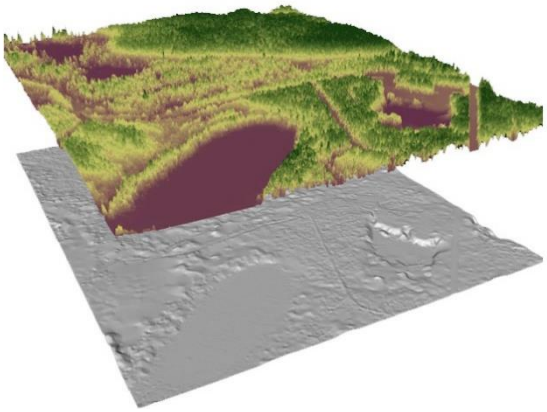

– *Survey*. Airborne sensors are an efficient and cost-effective solution to monitor large and potentially inaccessible areas. In this regard, petroleum pipelines, power-lines, railway tracks, or large cities can be monitored during a single flight and provide valuable information to prevent vandalism and theft of equipment;

– *Topography*. Country-wide terrain models can be generated using synthetic aperture radars (SAR) or light detection and ranging (LIDAR) sensors (see Figs 3 and 4). Other examples include seabed mapping, natural resource survey and monitoring of the ice thickness in Arctic regions using special new-generation sonars;

– *Disaster management*. Oil spill can be detected and monitored from the sky using Side-Looking-Airborne-Radars (SLAR) (see Figs 5 and 6);

– *Aerospace*. Intelligence gathering, surveillance, reconnaissance operations;

– *Local and national law enforcement.*

2 *Source*: https://botlink.com/blog/rgb-versus-nir-which-sensor-is-better-for-measuring-crop-health

3 *Source*: A best practices guide for generating forest inventory attributes from airborne laser scanning data using an area-based approach, J. White, M. Wulder, A. Varhola, M. Vastaranta, N. Coops, B. Cook, D. Pitt, M. Woods, Environmental Science, Forestry Chronicle, December 2013.

FIGURE 3

Topographic measurement using a LIDAR[4]

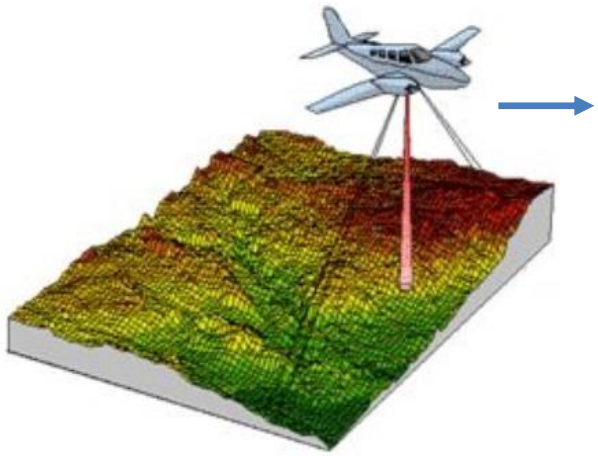

FIGURE 4

Topographic map generated using LIDAR technology[5]

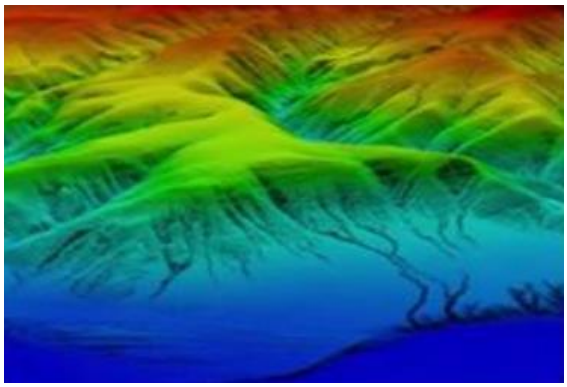

FIGURE 5

Principle of detection of oil slick using an SLAR

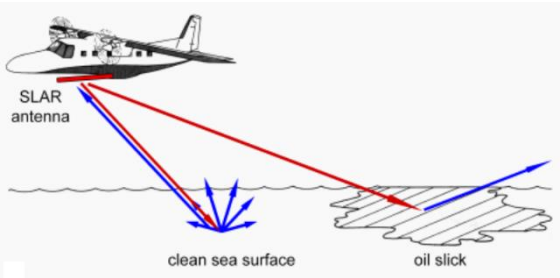

The rough sea surface causes diffuse reflection of the radar wave, and a small fraction of the reflected wave is detected by the SLAR antenna. An oil slick dampens the waves on the sea surface, and therefore backscattering decreases[7]

FIGURE 6

SLAR image of a ship (white spot) spilling oil (seen as a dark structure due to backscatter reduction)[6]

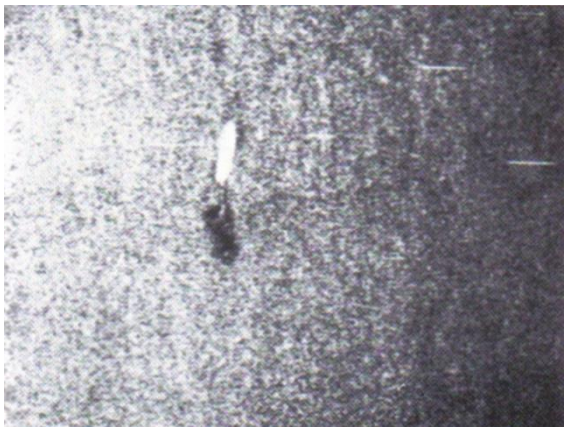

Some examples of airborne sensors include (the list is not exhaustive):

– IR cameras that are used principally for observations by night, or to locate hot spots on the ground that could be wildfires or human bodies in the snow after an avalanche;

– high-definition (HD) optical cameras that are used for observations by day, whenever and wherever weather and atmospheric conditions allow it;

– humidity and pressure sensors that are used in meteorological or Earth exploration missions;

---

4 *Source*: https://www.cdema.org/virtuallibrary/index.php/charim-hbook/data-management-book/3-base-data-collection/3-2-digital-elevation-models

5 *Source*: https://www.cdema.org/virtuallibrary/index.php/charim-hbook/data-management-book/3-base-data-collection/3-2-digital-elevation-models

6 *Source*: https://seos-project.eu/marinepollution/marinepollution-c02-s02-p03.html

7 *Source*: https://seos-project.eu/marinepollution/marinepollution-c02-s02-p03.html

– SAR that are used to produce HD images of the surface of the Earth, independently of the weather and the observation conditions;
– LIDAR that can produce high resolution images in the same way as SAR, but using laser light instead of radio frequencies (RF).

Typical data rates (DR) produced by such sensors are provided in Table 1.

TABLE 1

Typical DR of airborne sensors

Type of sensor	Payload throughput (Mbit/s)
HD optical camera(1)	≈5
IR camera(2)	
SAR(3)	≈30
Light Detection And Ranging (LIDAR)(4)	
Humidity/pressure sensors	A few kbit/s

(1) The DR of an optical camera depends on the required Image Resolution (IR), the Frame Rate (FR), the Pixel Depth (PD) and the Coder-Decoder (Codec). A typical setup for an HD optical camera used on board aircraft is the following:

– IR = 4 096 × 3 072 pixels;
– FR = 50 Frames per second (FPS);
– PD = 16 bits;
– Codec = H.264, achieving a Compression Ratio (CR) of about 1:2000.

Equation (1) is used to compute the DR from these elements:

$$DR = \frac{PD \cdot IR \cdot FR}{CR} \quad (1)$$

(2) The DR of an IR camera is assumed to be roughly the same as an optical camera.

(3) The DR is computed for a SAR installed on board an aircraft flying at the altitude h = 3 000 m Above Ground Level (AGL). The following parametrization is used:

– images are generated using 1 channel in the X-band;
– the pulse BW is B = 760 MHz;
– the pulse repetition frequency (PRF) is PRF = 5 kHz;
– block adaptive quantization (BAQ) is used;
– the angle from the nadir to the far end of the swath is $\theta_f = 20°$;
– the angle from the nadir to the near end of the swath is $\theta_n = 10°$.

Therefore, the angle from the nadir to the centre of the swath is 15° and the incidence angle of the signal on the ground is $\theta_i = 10°$. The resolution of the SAR can be computed from equation (2) and equals approximately 20.4 cm.

$$\delta = \frac{c}{2.B.\sin(\theta_i)} \quad (2)$$

where:

c: speed of light in vacuum ($2.998 \cdot 10^8$ m/s);

The DR of the SAR can be computed using equation (3):

$$DR = PRF.N_r \quad (3)$$

where:

N_r: number of data bits per window of the echo signal received from the direction of range in the area of interest.

N_r can be computed from equation (4):

$$N_r = 2.W.B.Q.N_r \quad (4)$$

Notes to Table 1:

where:

W: swath width window time (s) which is the time per scan between the near and far end of the swath

Q: quantization level, which is 4 bits as BAQ is used;

W can be computed from equation (5) below:

$$W = \tau_p + \frac{2(R_f - R_n)}{c} B \quad (5)$$

where:

τ_p: $1/B$, which is the pulse width

R_f: slant distance (m) from the SAR antenna to the far end of the swath

R_n: slant distance (m) from the SAR antenna to the near end of the swath;

R_f and R_n can be computed from equation (6) below:

$$R_f = \frac{h}{\cos(\theta_f)}, R_n = \frac{h}{\cos(\theta_n)} \quad (6)$$

where:

h: flying altitude of the aircraft;

By putting equations (3) and (6) together, equation (7) is obtained:

$$DR = 2.PRF\left(1 + \frac{2.B.h}{c}\left(\frac{1}{\cos(\theta_f)} - \frac{1}{\cos(\theta_n)}\right)\right) \quad (7)$$

By using numerical values in equation (4-7), DR ≈ 29.7 Mbit/s.

(4) The DR of a LIDAR is assumed to be roughly the same as a SAR.

5 Airborne datalinks

Section 4 has introduced significant applications of airborne sensors. In some of these applications, the data captured by these sensors can be stored on-board the flying platform and processed at a later stage. However, some time-critical missions like surveillance, require that the data is transmitted to other flying platforms or to ground facilities in real time. Two-way digital data links allowing this transmission will be referred to as wideband line of sight datalinks (WBLOSDL) in this Report. The present section provides a technical description of these datalinks.

5.1 Definition

As seen in § 1 of this Report, WBLOSDLs are mostly used in governmental and professional applications. They are established on a time-limited basis between platforms having low density deployment. In that regard, they can operate under AM(OR)S allocations. WBLOSDL are further characterized by the fact that:

– The transported data are not related to the safety of flight, which means that WBLOSDL cannot be used to support command and control components;

– The platforms that communicate using WBLOSDL must be visible to each other, as frequency bands are used that only allow line-of-sight (LOS) transmission modes;

– WBLOSDL are established using wideband channels (sometimes spread over several tens of MHz) so that significant amount of data can be transported. This enables data-intensive applications like for instance HD video transmission.

Aircraft stations operating WBLOSDLs are referred to as airborne data terminals (ADTs) and aeronautical stations are referred to as ground data terminals (GDTs). GDTs may be installed at a permanent location or they can be transportable, depending upon operational requirements. In the latter case, the term portable GDT (PGDT) is used.

5.2 Link distance

Depending upon operational requirements, the link distance covered by WBLOSDLs can be relatively short, but it is in theory only limited by the radio LOS horizon. For example, an ADT flying at an altitude of 20 km above ground level (AGL) could reach a GDT over a distance of approximately 450 km[8]. Note however that this distance can be significantly reduced in case of unfavourable conditions whose effect on radio wave propagation is addressed in various ITU-R Recommendations of the P-series.

5.3 Control and data channels

In typical use cases of WBLOSDL, most of the data traffic is transported unidirectionally from one station to the other, for example from an ADT equipped with sensors to a GDT. In that case, WBLOSDL are operated in a broadband mode on a so-called *data channel*. The reverse direction is operated in a narrowband mode on a *control channel* and is used to implement certain features like closed-loop power control algorithms, packet acknowledgement, remote control of the sensors, or maintaining of the antennas' alignment for link budget optimization between stations. Illustrations thereof are provided in § 6 of this Report, which describes typical operational scenarios.

5.4 Bi-directionality

WBLOSDLs can be divided into two groups, depending on the direction of the data channel (in the sense given in § 5.3):

– Air to Air (A2A) WBLOSDLs have their data channel from an ADT to another ADT;

– Air to Ground (A2G) WBLOSDLs have their data channel from an ADT to a GDT.

Note applications of non-safety AM(OR)S intend to transport data from a flying platform to a ground facility. In that regard, ground-to-air (G2A) WBLOSDLs are irrelevant from the application standpoint and are not considered in this Report.

WBLOSDLs are bidirectional by design, but in typical situations, the ADTs are equipped with airborne sensors and therefore generate most of the data. Illustrations thereof are provided in § 6 of this Report.

WB LOS DL can also be divided into three categories, depending on the relative location of the receiver with respect to the receiver.

– "Downwards WBLOSDL" are A2G, or A2A WBLOSDL when the transmitting ADT is at higher altitude than the receiving ADT so that most of the energy is radiated towards the surface of the Earth;

– "Horizontal WBLOSDL" are A2A WBLOSDL established between ADTs with an elevation angle with respect to the local horizon close to zero, or slightly negative when the ADTs are separated by large distances;

– "Upwards WBLOSDL" are A2A WBLOSDL when the transmitting ADT is a lower altitude than the receiving ADT so that most of the energy is radiated towards space.

The distinction above makes sense in particular from the regulatory point of view. Indeed, it is easily understood that 'downwards WBLOSDL' have the strongest effect on other terrestrial services operating in the same or in an adjacent frequency band, and 'upwards WBLOSDL', on space services. The effect of 'horizontal WBLOSDL' is more difficult to predict in practice and heavily depends on the altitude of the ADTs.

---

8 Value computed using equation (A11-1) in Annex 11 to this Report.

5.5 Transmission modes

WBLOSDLs can be operated in a narrowband or in a broadband mode. The broadband mode is used to transport the data collected by the sensors, whilst the narrowband mode can be used to remotely control the sensors, acknowledge reception of data packets, or to implement the return loop of the ATPC. The control channel may as well be used by the tracking to maintain alignment of the antennas and ensure maximum directivity.

5.6 Power control

ATPC, sometimes simply referred to as *power control*, is an efficient way of reducing the power consumption of transceivers installed onboard ADTs while limiting interferences with other services operating in the same or in adjacent frequency bands. The principle is to adapt the output power of the transmitter in order to reach a desired power level at the receiver. A simplified implementation of the power control algorithm is described in § A11.6.1.

5.7 Operation modes

WBLOSDL can operate in three different modes:

– Point-to-point (PTP) mode. One station communicates with a single other station.

– Point-to-multipoint (PTMP) mode. One station disseminates data among a number of other stations.

– Relay mode. One station relays data from a first to a second station. This mode is used for instance when the two stations are out of each other's reach. Another application is the establishment of ad-hoc networks using some stations as communication nodes.

5.8 Multiple access

Several WBLOSDLs can be established in the same frequency band using multiple access mechanisms as for instance:

– Frequency division multiple access (FDMA). The available frequency band is divided into a number of communication channels. Before transmitting, stations sense the available spectrum and select a channel that is not used by another station in the network. This mechanism is known as sense and avoid (SAA). While optimizing the use of the available spectrum, it also allows a dynamic and flexible configuration of the network without requiring a central node for coordination.

– Code division multiple access (CDMA). The available spectrum contains a single communication channel. Before being put on the channel, baseband signals are multiplied with a spreading code by the transmitting station. The same code is used for de-modulation at the receiving station.

Note also that the use of highly directive antennas can support geographic separation of the links, which in turn makes it possible to reuse the same frequency channel over a limited area.

5.9 Frequency planning

In the case where WBLOSDLs use the same frequency band as other aeronautical systems installed on board the same aircraft (such as meteorological or proximity radars), frequency planning is a solution to mitigate interference and to guarantee the operation of all systems with an acceptable level of performance.

5.10 Antennas

ADTs and GDTs are equipped with different kinds of antennas, depending upon the operational requirements of the mission:

– *Omnidirectional antennas* are used on board small ADTs or hand-held PGDTs. Communication with other stations is only possible over limited distances.

– *Highly directive antennas* are used on board large ADTs or GDTs. These antennas must be coupled with a tracking system to maintain close alignment with the communication partner. The link budget performance is significantly improved, and link distances of several hundreds of kilometres can be overcome. As side benefit, directional antennas can also improve coexistence or sharing with other systems as emissions outside of the main beam are kept to an acceptable level.

5.11 Frequency allocations

Several frequency bands are allocated on a primary basis to the AMS (and thus to the AM(OR)S) and can therefore be used to establish WBLOSDL. Table 2 references Recommendations from the M-series that provide technical and operational characteristics of typical AM(OR)S systems operating in these frequency bands.

TABLE 2

Applicable ITU-R Recommendations for various frequency bands in the aeronautical mobile (off-Route) service

Frequency band	Recommendation
4 400-4 990 MHz	ITU-R M.2116-0
14.5-15.35 GHz	ITU-R M.2089-0
21.2-22 GHz	ITU-R M.2120-0
22.5-23.6 GHz	ITU-R M.2114-0
25.25-27.5 GHz	
45.5-47 GHz	ITU-R M.2115-0

Note however that the use of a certain band in a given mission is not always possible due to some constraints including:

– Unfavourable propagation characteristics, noting that certain bands are optimal for certain types of applications.

– Additional constraints imposed by administrations on a national basis, for instance in regards of co-primary allocations.

6 System deployment scenarios

6.1 Introduction

This section introduces four representative scenarios of non-safety AM(OR)S and WBLOSDL. Each scenario is described in terms of mission purpose in § 6.2. The configuration of the ADTs and GDTs, the setting of the sensors, flying altitude, etc. are further described from a technical perspective in § 6.3. Section 6.4 derives deployment densities associated to the missions and § 6.5 analyses the spectrum occupancy of each scenario.

The scenarios presented in this section cover a variety of current and future usages of non-safety AM(OR)S and will be used as a basis for sharing and compatibility studies throughout this Report. Note however that the responsibility, authorization and verification of these missions remain a national matter and could differ from country to country. Hence these aspects will not be considered here.

6.2 Mission description

6.2.1 Wildfire detection

Global climatic change has made natural disasters and in particular wildfires more frequent and difficult to predict. Forest fires often occur in remote areas like natural reserves and have led over the recent years to dramatic destructions of the environment. Such consequences could in many cases be avoided if wildfires would be detected and extinguished early enough.

One possible solution consists in using a fleet of rotorcraft to observe large forestry areas from the sky. In the event of a fire outbreak, firefighters on the ground would be informed about the location of the fire, which would greatly improve the efficiency of the response. On the other hand, if the fire has already spread over large areas, recording images from the sky would improve situational awareness for rescue or evacuation purposes.

The operational scenario shown in Fig. 7 describes such a mission. Two helicopters equipped with several optical and IR cameras are used. Optical cameras can detect fire outbreaks through the smoke that they produce and IR cameras, through thermal anomalies under the vegetation. Using several cameras increases the monitoring capacity of the helicopters and improves the efficiency of the detection. The data recorded by the two helicopters is sent back in real time to a fire truck through a dedicated WBLOSDL.

FIGURE 7

Typical scenario of a wildfire observation mission

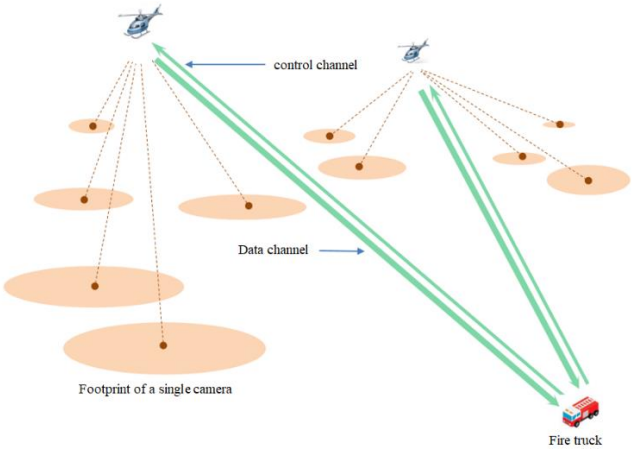

6.2.2 Search and rescue

The use of aircraft in search and rescue missions have gained popularity in the second half of the 20th century as they allow quick and efficient searches over wide areas as well as deployment flexibility. Helicopters or fixed-wing aircraft are best suited for these missions because they can be operated both at low speed and low altitude.

However, the main challenge in these mission remains the research of crash zones over areas partially or fully covered with dense vegetation, for which observations from the aircraft cockpit can be enhanced using special types of radars, for instance SAR. The immediate advantage over direct

observations is the fact that SAR can operate independently of light and weather conditions. Furthermore, if the right frequency band is chosen, SAR radio waves can penetrate the foliage and produce high-resolution images of the ground. Post-processing interferometry algorithms can then locate crash zones using surface deformations as evidences.

However, images captured by SAR may in some cases not be used directly because they are degraded due to turbulences experienced at low flying altitudes, and therefore post-processing correction algorithms need to be applied. Moreover, evidences of a potential crash zone can only be discovered after the application of some interferometry algorithms.

Such algorithms require significant computational effort and dedicated hardware resources. For this reason, they cannot be performed on board each aircraft involved in search and rescue operations. One solution would be to record and store images for later post-processing. However, this would dramatically affect the reactivity, the flexibility and the duration time of the mission and potentially reduce chances of rescuing victims in time. On the other side, direct transmission of the data to a ground station is not practically feasible as soon as the distance is too important.

A technical solution is to use a fleet of aircraft equipped with SAR that transmit their data to a central aircraft equipped with the necessary hardware to post-process and analyse this kind of data in real time. Figure 8 shows a fleet of fixed-wing observation aircraft performing a search and rescue mission. All the data recorded is transmitted to the central aircraft 4 using dedicated WBLOSDL

FIGURE 8

Typical scenario of a search and rescue mission

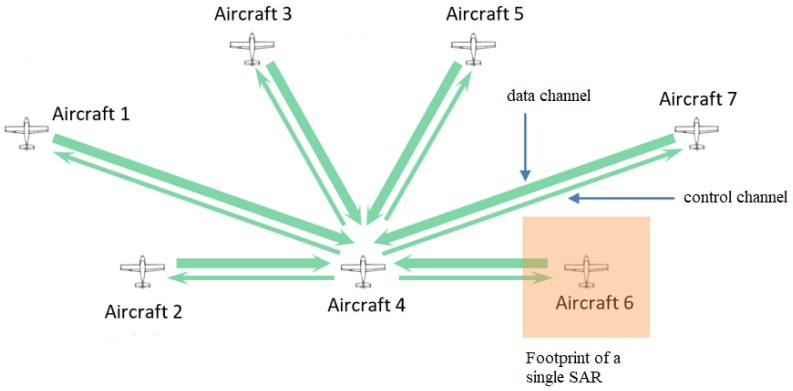

6.2.3 Border surveillance

Airborne surveillance can represent a substantial saving of time and money as compared to on-site surveillance. In particular, observing remote and hardly accessible areas from the sky is relevant in various contexts such as facility monitoring, local and national law enforcement, and border surveillance. However, real-time data exchange between aircraft and ground facilities can reveal challenging when direct visibility is not provided. Therefore, such missions often require that secondary aircraft are used as relay for data forwarding.

The configuration shown in Fig. 9 illustrates a typical airborne surveillance mission, where two observation aircraft equipped with optical cameras are deployed over the area of interest. Using a backup IR camera can also make observations independent of weather and visibility conditions. As the distance between the ground centre and the area of interest may reach over the horizon, the communication link is built via a relay aircraft flying at high altitude.

FIGURE 9

Typical scenario of a border surveillance mission

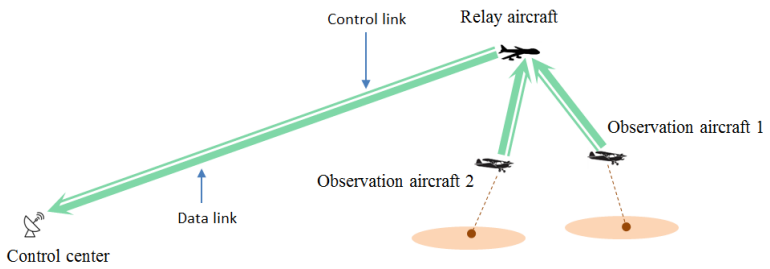

6.2.4 Data networks

Exchanging sensor data in a network composed of several aircraft can find applications in several other contexts than search and rescue and border surveillance. For instance, the information captured by one aircraft can be sent to another aircraft for further processing or gathering purposes in the context of an Earth observation mission. The configuration shown in Fig. 10 describes a formation of five aircraft connected to their closest neighbour through WBLOSDL. Some of these aircraft can be used to relay information between communication partners that are out of reach of each other.

FIGURE 10

Typical scenario of data networks applications

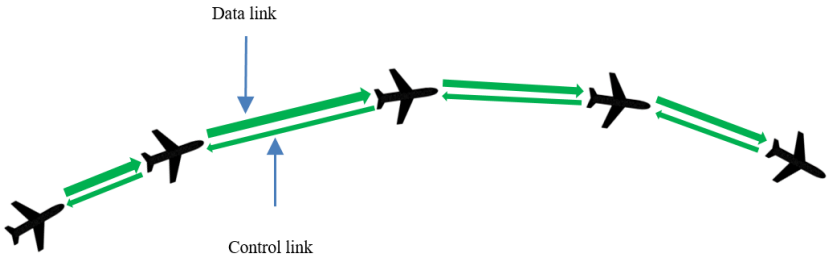

6.2.5 New applications

Section 6.2 of this Report presents a number of current applications of non-safety AM(OR)S operated under an AM(OR)S used in various contexts of the industry. It is also important to note that the last years have seen a range of new trends towards further usages of airborne sensors addressing to new challenges. One example is the COVID-19 (coronavirus disease 2019) crisis which has fostered the development of airborne sensors that can detect high pathogens concentrations from the sky and therefore improve public health sector resilience in the event of a pandemic.

6.3 Technical setup of the scenarios

Table 3 provides a technical description of the AM(OR)S scenarios presented in § 6.2. The AM(OR)S systems used in the various scenarios are addressed in further detail in Annex 1.

TABLE 3

Technical description of the operational scenarios for systems operating in the aeronautical mobile (off-Route) service

			Operational scenario			
		Units	**Wildfire detection (6.2.1)**	**Search and rescue (6.2.2)**	**Border surveillance (6.2.3)**	**Data networks (6.2.4)**
Frequency band		GHz	15.4-15.7 or 22-22.21[(1)]			
Assumed nadir speed of the clusters		km/h	200[(2)]	400	400	900
AM(OR)S system	1		–	Aircraft 1, 2, 3, 5, 6 and 7	Observation aircraft, Relay aircraft[(11)]	–
	2		Helicopters[(3)]	Aircraft 4[(9)]	Relay aircraft[(11)]	–
	3		–	–	–	All aircraft
	4		Fire truck[(4)]	–	–	–
	5		–	–	Ground centre	–
Altitude AGL	GDT	m	2[(5)]	–	2[(5)]	–
	ADT		300[(6)]	Coordinates[(10)] of aircraft 1: (−12; 3; −2.6), 2: (−8; 0; −2.6), 3: (−4; 5; −2.6), 4: (0; 0; 0), 5: (4; 5; −2.6), 6: (8; 0; −2.6), 7 (12; 3; −2.6)	3 000, 10 000[(12)]	10 000
Horizontal link distance	A2A	km	–		5	150 to 800[(14)]
	A2G		1, 1.2[(7) (8)]	-	50 to 150 or 50 to 100[(7) (13)]	–

(1) The four missions described in § 6.2 can use either one of the frequency bands, but not the two simultaneously.

(2) This value corresponds to the typical cruise speed of a helicopter. Note that the two helicopters do not necessarily remain connected to the same fire truck over the whole duration of the mission, but at a given point in time, they are both connected to a unique truck. This feature allows for flexibility of the mission (the ADTs can travel from one area of interest to another and connect to the closest truck available).

(3) AM(OR)S system 2 has an omnidirectional antenna which is best suited for helicopters whose roll and pitch may vary quickly over time.

(4) The antenna associated to AM(OR)S system 4 is typically an antenna mounted on the rooftop of a ground vehicle.

(5) 2 m is the lower bound of the applicability range of Rec. ITU-R P.528-5, which is used to compute propagation losses between the fire truck and the helicopters in scenario 6.2.1 and between the relay and the control centre in scenario 6.2.3;

(6) The quality of the images captured by the cameras mounted on the helicopters is best for low distances to the target. 300 m is the lowest flying altitude of a helicopter;

(7) 1 km if the 22-22-21 GHz band is used, 1.2 km if the 15.4-15.7 GHz band is used.

Notes to Table 3:

(8) The separation distance is chosen smaller in the band 22-22.21 GHz so that the maximum TPO of AM(OR)S system 2 is attained in both frequency bands. Figure A11-7 shows the distribution of the transmit output power of AM(OR)S system 2 in different scenarios.

(9) The use of AM(OR)S system 2 for aircraft 4 coupled with an omnidirectional antenna allows simultaneous reception of signals from the observation aircraft.

(10) The location of aircraft is defined in the coordinate system centred at aircraft 4 which is at the altitude 3.6 km AGL.

(11) In scenario 6.2.3, the relay aircraft is equipped with two AM(OR)S systems: system 2 is used to gather data from the observation aircraft, and system 1 to forward this data to the control centre.

(12) The altitude of the observation aircraft and the relay in scenario 6.2.3 is 3 000 and 10 000 m AGL, respectively.

(13) The separation distance is between 50 and 150 km if the 15.4-15.7 GHz band is used, and between 50 and 100 km if the 22-22.21 GHz band is used.

(14) The horizontal link distance between aircraft in scenario 6.4.4 is lower-bounded by safety separation distances, and upper-bounded by the radio LOS distance at this altitude, calculated using equation (A11-1).

6.4 Deployment density

Table 4 references typical deployment densities associated with the operational scenarios introduced in § 6.2. The details of the calculations are provided in §§ 6.4.1 to 6.4.4. Densities are given in terms of clusters or links per area unit. A cluster is a representative group of ADTs and GDTs involved in a particular scenario:

– In scenario 6.2.1, Wildfire Detection, a cluster is composed of one GDT (fire truck) communicating with two ADTs (the observation helicopters). Two A2G WBLOSDL are established per cluster.

– In scenario 6.2.2, Search and Rescue, a cluster is composed of one GDT (the control centre) communicating with one ADT (the relay aircraft). This same ADT is also communicating with two other ADTs (the observation aircraft). Three WBLOSDL (one A2G and two A2A) are established per cluster.

– In scenario 6.2.3, Border Surveillance, a cluster is composed of six ADTs communicating with a same seventh ADT. Six A2A WBLOSDL are established per cluster.

– In scenario 6.2.4, Data Networks, a cluster is composed of a five ADTs communicating with each other on a sequential basis. Four A2A WBLOSDL are established per cluster.

TABLE 4

Deployment density associated with the four operational scenarios considered in § 6.2

	Units	Scenario			
		6.2.1	6.2.2	6.2.3	6.2.4
Density of clusters	Clusters/10^6 km²	4.93	1.36	1.46	2.89
Density of A2A WBLOSDL	links/10^6 km²	0	8.15	2.92	11.6
Density of A2G WBLOSDL		9.87	0	1.46	0
Radius of the circle in which one A2A WBLOSDL is found at any point in time (1)	km	0	198	330	166
Radius of the circle in which one A2G WBLOSDL is found at any point in time (1)		180	0	467	0
Radius of the circle in which one cluster is found at any point in time (1)	km	254	484	467	332

(1) The radius of the circle in which one cluster, A2A or A2G WBLOSDL can be found at any point in time is calculated using equation (8):

$$R = \frac{1}{\sqrt{\pi . d}} \quad (8)$$

where:

R: radius (km) of the circle in which one cluster, A2A or A2G WBLOSDL can be found, at any point in time

d: density (clusters or links per km²).

6.4.1 Wildfire detection

Table 5 shows the yearly statistics of wildfires for some countries frequently subject to such disaster events. Using the total area of these countries and the average duration of a wildfire detection mission as described in § 6.2.1, one can determine the radius of the circle in which one cluster is expected. Note that the final value computed in Table 5 represents an average value for any day of the year and any piece of land in a given country, noting that most wildfires tend to only occur in densely forested areas during exceptional heat waves and long periods of drought.

TABLE 5

Typical cluster densities in a wildfire detection mission

Country	California	Texas	Australia	Turkey	Spain	Average
Total area in km² (1)	423 970	695 621	7 692 024	783 356	505 990	
Average yearly number of wildfires	7 874(2)	10 200(3)	52 000(4)	3 500(5)	18 034(6)	
Average surface in which one wildfire is expected per day in km² (7)	19 653	2 892	53 992	81 693	10 241	
Average mission duration in hours	4	4	4	4	4	

TABLE 5 (*end*)

Country	California	Texas	Australia	Turkey	Spain	Average
Average surface in km² in which one cluster is expected at any point in time(8)	117 918	149 352	323 952	490 158	61 446	
Radius in km of the circle in which one cluster is expected at any point in time(9)	194	218	321	395	140	254

(1) *Source*: Wikipedia.

(2) *Source*: California Department of Forestry and Fire Protection. The average yearly number of wildfires was computed from the statistics provided from 2016 to 2020, according to which 6 959 wildfires occurred in 2016, 9 270 in 2017, 7 948 in 2018, 7 860 in 2019 and 7 335 in 2020 in the State of California.

(3) *Source*: Texas Forestry Service.

(4) According to the Australian Productivity Commission, 46 000 to 62 000 wildfires per year occurred in Australia between 2001 and 2002 and between 2006 and 2007. According to the Australian Institute of Criminology, 52 000 wildfires per year were reported between 1995 and 2006 (30% of them being deliberately lit).

(5) *Source*: Daily Sabah, "Fires, flood, mucilage: What's happening in Turkey", 16 August 2021.

(6) According to the *Estadística General de Incendios Forestales* (EGIF), there has been a total of 360 672 wildfires in Spain between 1988 and 2007.

(7) The average surface C in which one cluster is expected per day is computed using equation (9):

$$C = \frac{365.A}{B} \quad (9)$$

where:

A: total country area (km²)

B: average yearly number of wildfires in the country.

(8) The average surface E in which one cluster is expected at any point in time is computed using equation (10):

$$E = \frac{C.D}{24} \quad (10)$$

where:

C: average surface in which one cluster is expected per day (km²)

D: mission duration (hours).

(9) Equation (11) is used to convert E into the radius R of the circle having the same area as E:

$$R = \sqrt{\frac{E}{\pi}} \quad (11)$$

6.4.2 Search and rescue

In general, aircraft-supported search and rescue operations are performed by police forces or other local or national bodies. Table 6 examines for some countries, the aircraft fleet that could take part in a search and rescue missions as described in § 6.2.2. The average area in which one of these aircraft formations (called cluster for the purpose of this Report), is derived following the same methodology as in § 6.4.1.

TABLE 6

Typical cluster densities in a search and rescue mission

Country	U.K.	France	Italy	Victoria	Texas	Average
Total area in km² (1)	242 495	632 734	301 340	227 444	695 662	
Number of aircraft per country that can participate in scenario 6.2.2	23 (2)	56 (3)	35 (4)	5	23 (5)	
Number of aircraft per formation in scenario 6.2.2	7	7	7	7	7	
Equivalent number of clusters (6)	3	8	5	1	3	
Average surface in which one cluster is expected per day in km² (7)	80 832	79 092	60 628	227 444	231 887	
Average mission duration in hours	4	4	4	4	4	
Average surface in km² in which one cluster is expected at any point in time (8)	481 992	420 552	363 768	1 364 664	1 391 322	
Radius in km of the circle in which one cluster is expected at any point in time (9)	392	366	340	659	665	484

(1) *Source*: Wikipedia.

(2) In the United Kingdom (U.K.), search and rescue operations are performed by the National Police Air Service (NPAS), which runs a fleet of 19 helicopters and 4 fixed-wing aircraft from a network of 15 bases across England and Wales (*Source*: West Yorkshire Police).

(3) In France, air-supported search and rescue operations are led by the *Forces Aériennes de la Gendarmerie Nationale*, which operates a fleet of 56 helicopters (*Source*: Gendarmerie Nationale).

(4) In Italy, the *Protezione Civile* comprises 35 aircraft and rotorcraft suited for scenario 6.2.2 (*Source*: Italian Government, Civil Protection Department).

(5) In the State of Texas, the Department of Public Safety Operations Division operates a fleet of 15 helicopters and 8 fixed-wing aircraft (*Source*: Texas Department of Public Safety).

(6) The maximum number C of clusters that can take part in a search and rescue mission is simply the number of aircraft divided by the number of aircraft in a formation, as shown in equation (12):

$$C = \frac{B}{N} \tag{12}$$

where:

B: number of aircraft in the country that can participate in scenario 6.2.2

N: average number of aircraft per formation in scenario 6.2.2.

(7) The average surface D in which one cluster is expected in one day is given by equation (13):

$$D = \frac{\mathrm{A}}{\mathrm{C}} \tag{13}$$

where:

A: total area of the country (km²)

C: maximum number of clusters that can take part in a search and rescue scenario.

(8) The average surface F in which one cluster is expected at any point in time is calculated using equation (10).

(9) The radius R in which one cluster is expected at any point in time is calculated using equation (8).

6.4.3 Border surveillance

Table 7 compares, for various countries of the world, the border length against the total area of the country, and from there derives the density of aircraft that could take part in a border surveillance mission as described in § 6.2.3.

TABLE 7

Cluster density associated to scenario 6.2.3 'Border surveillance'

	Country					
	USA	**Canada**	**Brazil**	**Paraguay**	**Argentina**	**Egypt**
Border to area ratio in km/km² (1)	0.00126	0.000891	0.00173	0.00964	0.00348	0.00266
Assumed border section in km monitored by a cluster of aircraft	250	250	250	250	250	250
Average country area in km² covered by one cluster(2)	198 413	280 584	144 509	25 934	71 839	93 985
Average mission duration in hours	4					
Average surface in km² in which one cluster is expected at any point in time(3)	1 190 47	1 503 50	867 054	155 604	431 034	563 910
Radius in km of the circle in which one cluster is expected at any point in time(4)	616	692	525	223	370	424
Border to area ratio in km/km² (1)	0.00398	0.00206	0.0033	0.00231	0.00117	
Assumed border section in km monitored by a cluster of aircraft	250	250	250	250	250	
Average country area in km² covered by one cluster of aircraft(2)	62 814	121 359	75 758	108 225	213 675	
Average mission duration in hours	4	4	4	4	4	
Average surface in km² in which one cluster is expected at any point in time(3)	376 884	728 154	454 548	649 350	1 282 050	
Radius in km of the circle in which one cluster is expected at any point in time(4)	332	481	380	455	639	467

(1) *Source*: Wikipedia. This value represents the sum of all borders with other countries (excluding maritime borders), divided by the total area of the country.

(2) The average surface C in which one cluster (composed of two observation aircraft and one relay) is to be found is given by equation (14):

$$C = \frac{B}{A} \tag{14}$$

where:

A: border to area ratio of the country (km/km²)

B: border section monitored by one cluster (km).

(3) The average surface D in which one cluster is to be expected at any point in time is calculated using equation (10).

(4) The radius R in which one cluster is expected at any point in time is calculated using equation (8).

6.4.4 Data networks

As explained in § 6.2.4, synchronizing data between aircraft organised in an ad-hoc network can find applications in various contexts, including Earth observation missions performed over extended areas. This example is used to derive a reference density of platforms in this scenario.

A typical Earth observation mission could take place over the North Atlantic, a large oceanic region shown in Fig. 11. Assuming a maximum number of aircraft taking part in the mission, Table 8 computes the corresponding cluster density.

FIGURE 11

Oceanic area over the North Atlantic

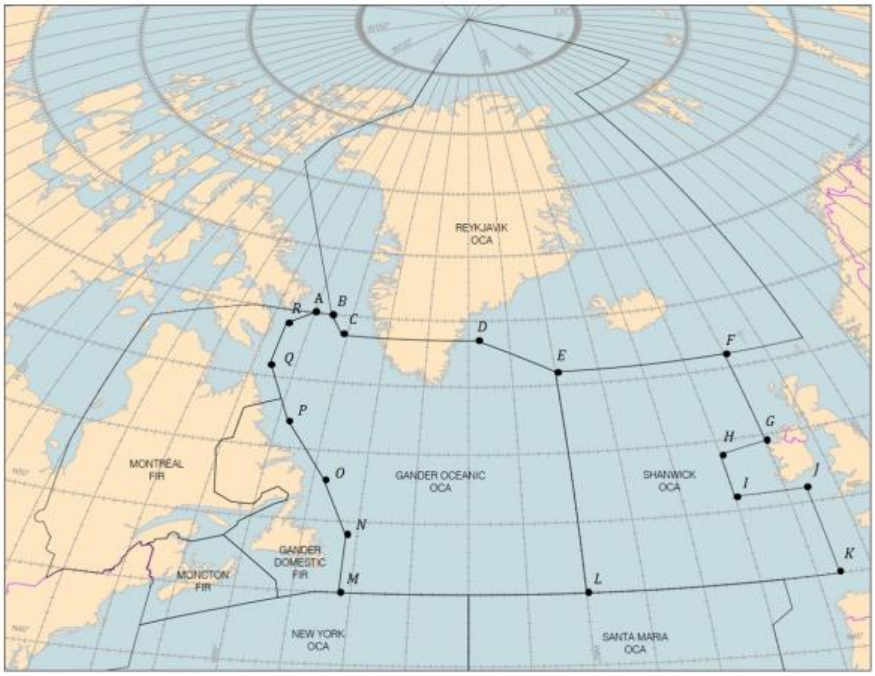

TABLE 8

Cluster density associated to scenario 6.2.4

Area	Shanwick	Gander
Polygon in Fig. 11	EFGHIJKL	ABCDELMNOPQR
Partial area in km² (1)	3 318 500	3 617 546
Total area in km²	6 936 046	
Number of aircraft participating in the Earth observation mission(2)	80	
Equivalent number of clusters(3)	20	
Average surface in km² in which one cluster is expected at any point in time(4)	346 800	
Radius in km of the circle in which one cluster is expected at any point in time(5)	332	

Notes to Table 8:

(1) The area of the two regions composing the North Atlantic is computed by decomposing the areas into triangles.

(2) Aircraft participating in the Earth observation mission are assumed to be evenly spread over the area of interest.

(3) See note (6) under Table A2-2.

(4) The average surface in which one cluster is expected at any point in time is calculated using equation (10).

(5) The radius R in which one cluster is expected at any point in time is calculated using equation (8).

6.5 Spectrum occupancy

This section determines the spectrum occupancy associated to the four operational scenarios introduced in § 6.2. It does not assess currently available allocations to the AM(OR)S. Note that the figures in Table 9 were derived on a per-cluster basis, where a cluster denotes a set of ADTs and GDTs involved in one particular scenario.

TABLE 9

Estimation of the spectrum occupancy per cluster for the four operational scenarios considered in § 6.2

		Units	Scenario			
			6.2.1	**6.2.2**	**6.2.3**	**6.2.4**
Number of WBLOSDL per cluster(1)		ø	2	6	3	4
Data	Payload throughput per link	Mbit/s	50(2)	30(3)	10, 20(4)	80, 160, 240, 320(5)
	Overhead factor(6)	%	10	10	10	10
	Raw throughput per link	Mbit/s	55	33	11, 22	88, 176, 264, 352
Control	Payload throughput per link		0.5	0.5	0.5	0.5
	Overhead factor(6)	%	10	10	10	10
	Raw throughput per link	Mbit/s	0.55	0.55	0.55	0.55
Multiplexing scheme(7)		ø	FDMA			
Aggregate raw throughput per cluster(8)		Mbit/s	111.1	201.3	46.65	352.55
Spectrum efficiency		bit/s/Hz	1			3
Spectrum resource per cluster(9)		MHz	111.1	201.3	46.65	117.52

(1) The number of ADTs, GDTs and WBLOSDL per cluster is determined based on the examples presented in § 6.2. See in particular Fig. 7 for scenario 6.2.1, Fig. 8 for scenario 6.2.2, Fig. 9 for scenario 6.2.3 and Fig. 10 for scenario 6.2.4.

(2) In scenario 6.2.1, each helicopter is assumed to be equipped with five HD cameras (each of them generates 5 Mbit/s of payload according to Table 2). Each of these cameras is coupled with an IR camera that having the same throughput. The aggregate payload throughput is therefore 5x5 Mbit/s + 5x5 Mbit/s = 50 Mbit/s.

(3) In scenario 6.2.2, the six-observation aircraft are assumed to be equipped with a SAR whose payload throughput is 30 Mbit/s as per Table 2.

(4) In scenario 6.2.3, the two-observation aircraft are assumed to be equipped with one HD camera coupled with an IR camera. The payload throughput of the two data links from the observation aircraft to the relay is therefore 10 Mbit/s. The data link from the relay aircraft to the remote-control centre aggregates these data flows and therefore must have a payload capacity of 20 Mbit/s.

(5) In scenario 6.2.4, the formation assumed to operate in a relay mode and data is forwarded between aircraft that are out of reach of each other. It is therefore relevant to assume different throughputs for different links.

Notes to Table 9:

(6) The overhead factor denotes the additional data that is transmitted on top of the payload. It can be composed of error correction codes, medium access information, metadata, acknowledgement, etc. The sum of the payload and the overhead constitutes the raw data flux.

(7) All links are established within a cluster using different non-overlapping channels. The same channels can be re-used between different clusters. Guard bands are not taken into consideration.

(8) The aggregate raw throughput per cluster is computed by summing the raw throughput of all data and control links in the cluster i.e. using equation (15):

$$T_{\text{raw}} = \text{N}.\, R_{\text{raw}}^{\text{control}} + \sum_{i=1}^{N} \left(T_{\text{raw}}^{\text{data}}\right)_i \quad (15)$$

where:

T_{raw}: raw throughput (Mbit/s) per cluster

N: number of WBLOSDL per cluster

$T_{\text{raw}}^{\text{data}}$: raw throughput (Mbit/s) of a control link in the cluster

$\left(T_{\text{raw}}^{\text{data}}\right)_i$: raw throughput (Mbit/s) of the *i*-th data link in the cluster.

(9) The spectrum resource per cluster is given by equation (16):

$$S = \frac{T_{\text{raw}}}{s} \quad (16)$$

where:

S: necessary spectrum resource (MHz) per cluster

T_{raw}: raw throughput (Mbit/s) per cluster as computed in equation (14)

s: spectral efficiency (bit/s/Hz) associated to the scenario.

7 Future needs for spectrum allocated to the aeronautical mobile (off-Route) service

The four operational scenarios presented in § 6.2 typically use AM(OR)S allocations in the Ku and K frequency bands i.e. from about 12 to 27 GHz. The available spectrum in this range is 5.1 GHz as per Table 2. This section proposes a methodology to determine the future spectrum needs of non-safety AM(OR)S.

7.1 Introduction

Section 6.2 has introduced four representative scenarios where AM(OR)S is used to transmit sensor data between ADTs and GDTs, or between ADTs, in different contexts such as wildfire detection (Scenario 6.2.1), search and rescue operations (Scenario 6.2.2), border surveillance (Scenario 6.2.3) and data exchange in aircraft networks (Scenario 6.2.4). These scenarios typically operate under an AM(OR)S allocation, which is a subset of the AMS, or more broadly of the Mobile Service (MS), in the Ku or K band (i.e. from about 12 to 27 GHz). This is chiefly because this frequency range provides optimal LOS propagation conditions over a broad range of distances and thus allows flexibility in the technical implementation.

As seen in Table 2, the total spectrum usable for AMS applications in the Ku and K band is currently 5.1 GHz (850 MHz as per Recommendation ITU-R M.2089, 800 MHz as per Recommendation ITU-R M.2120, and 3.35 GHz as per Recommendation ITU-R M.2114).

The number of aircraft equipped with sensors has grown significantly in the past twenty years, and hence the need for bidirectional low to high data rate communications between aeronautical stations and aircraft stations, or between aircraft stations, has consequently increased.

The following sections compute, in the four operational scenarios introduced in § 6.2, the necessary increase of the spectrum resource to cover the growth of the number of aircraft participating in these scenarios.

7.2 Methodology

This section evaluates the additional amount of spectrum to allocate to the AM(OR)S in the Ku and K bands to support the foreseen increased number of aircraft equipped with sensors. For completeness, the analysis considers a wide range of assumptions regarding the growth rate of aircraft.

The methodology followed in this annex computes the necessary additional AM(OR)S spectrum resource in the Ku and K frequency bands so that the future performance of systems operating under this allocation is not changed in spite of increased aircraft density.

7.3 Calculation

The performance of WBLOSDL is chiefly limited by self-interference, i.e. interference between links established in close proximity with antenna pointing leading to higher probability of mutual interference.

The probability that two particular ADTs interfere with each other is denoted by $p_{collision}$. It can be decomposed as in equation (17).

$$p_{collision} = P(A \cap B \cap C) \tag{17}$$

where:

A denotes the event "The frequency channels used by the two ADTs are overlapping"

B denotes the event "The two ADTs are in LOS"

C denotes the event "the PL between the two ADTs (including the antenna gains) is such that interference occurs".

The event A is clearly independent of the events B and C. In addition, equation (17) can be further decomposed using conditional probabilities, as in equation (18):

$$p_{collision} = P(A) \cdot P(B \cap C) = P(A) \cdot P(B) \cdot P(C \mid B) \tag{18}$$

The three components of $p_{collision}$ are computed in §§ 7.3.1, 7.3.2, 7.3.3 and 7.3.4, respectively.

7.3.1 Probability of the event A

The probability $P(A)$ is computed using equation (19):

$$P(A) = \frac{2.S_{\text{scenario}}}{S_{\text{total}}} \tag{19}$$

where:

S_{scenario}: total spectrum resource used in a particular scenario in the Ku and K frequency bands

S_{total}: overall available spectrum resource that can be used in the Ku and K frequency bands.

Note that equation (19) is only valid if $2.S_{\text{scenario}} \leq S_{\text{total}}$, which is the case in all scenarios presented in § 6.2 (the highest spectrum resource per scenario is 201.3 MHz according to Table 9 whereas $S_{\text{total}} = 5.1$ GHz). If $2.S_{\text{scenario}} > S_{\text{total}}$, then $p_{overlap} = 1$, regardless of the values of S_{scenario} and S_{total}.

It also follows that, if $P(A)_{current}$ denotes the overlap probability before an increase of the ADTs number, and if $P(A)_{future}$ denotes the overlap probability after an increase by a factor g (g being above 1) of the ADTs number, equation (20) holds:

$$\frac{P(A)_{future}}{P(A)_{current}} = \frac{S_{total\,|\,current}}{S_{total\,|\,future}} \tag{20}$$

where:

$S_{total\,|\,current}$: total spectrum that is currently usable for AM(OR)S applications

$S_{total\,|\,future}$: total spectrum that needs to be usable in the future for AM(OR)S applications.

7.3.2 Probability of the event B

Figure 12 shows the geometry associated with two ADTs deployed with uniform probability on the surface of the Earth and flying at an altitude h AGL. The rest of the explanations are provided beside the Figure.

Event B occurs when the point H_2 is chosen within the spherical cap of centre E and forming an angle of 4α at the centre of the Earth, in other words the spherical cap of centre E and of height x.

Equations (21) and (22) are obtained by considering the triangle CBD.

$$\widehat{CBD} = 90° - 2\alpha \tag{21}$$

$$\sin\left(\widehat{CBD}\right) = 1 - \frac{x}{R_e} \tag{22}$$

By combining equations (21) and (22), and using the equation $\cos(2x) = 1 - 2\sin^2(x)$, equation (23) is obtained:

$$1 - 2\sin^2(\alpha) = 1 - \frac{x}{R_e} \tag{23}$$

On the other hand, by considering the triangle CEA_2, equations (24) and (25) are obtained:

$$\sin(\alpha) = \frac{A_2E}{R_e+h} \tag{24}$$

$$A_2E = \sqrt{(R_e+h)^2 - R_e^2} \tag{25}$$

FIGURE 12

Required spectrum increase as a function of the aircraft number increase

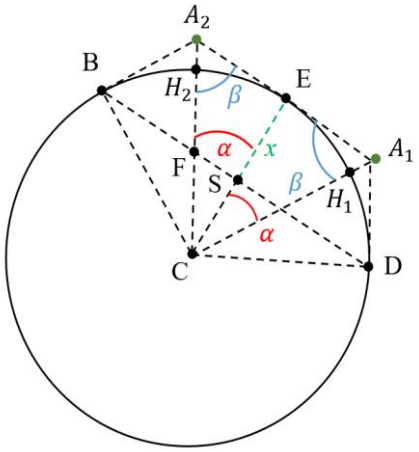

- A_1 and A_2 denote the two ADTs;
- H_1 and H_2 denote the points on the surface of the Earth just below A_1 and A_2 ;
- C denotes the centre of the Earth;
- The curved diameter of the visibility area of A_1 and A_2 are $[BE]$ and $[ED]$, respectively;
- $BC = H_2C = EC = H_1C = DC = R_e$, the radius of the Earth;
- S is the intersection between (BD) and (EC), so that x denotes the height of the spherical cap drawn on the surface of the Earth when the spherical cap corresponding to the visibility area of H_2"rolls" around the border of the visibility area of H_1;

By combining equations (24) and (25), equation (26) is obtained:

$$\sin(\alpha) = \frac{\sqrt{(R_e+h)^2 - R_e^2}}{R_e+h} \tag{24}$$

Finally, by replacing $\sin(\alpha)$ in equation (23) by the value found in equation (24), the value of x is found to be:

$$x = 2R_E\left(1 - \left(\frac{R_e}{R_e+h}\right)^2\right) \tag{25}$$

It follows that the area S where H_2 should not be placed if there should not be visibility between A_1 and A_2 is given in equation (26).

$$S = 2\pi R_e x = 4\pi R_e^2\left(1 - \left(\frac{R_e}{R_e+h}\right)^2\right) \tag{26}$$

The total area of the Earth S_{tot} is given in equation (27).

$$S_{tot} = 4\pi R_e^2 \tag{27}$$

Therefore, it follows that:

$$P(B) = \frac{S}{S_{tot}} = 1 - \left(\frac{R_e}{R_e+h}\right)^2 \tag{28}$$

It also follows that, if the number of ADTs deployed across the world increases by a factor g (g being greater than 1), then the probability $P(A)$ can be re-calculated by assuming that the same number of ADTs are deployed on a 'virtual' Earth radius of radius $\frac{R_e}{\sqrt{g}}$ (the density of ADTs being inversely proportional to the square of the radius of the sphere on which they are deployed). Therefore, before an increase of the number of ADTs, the probability $P(B)_{current}$is given in equation (29), and after an increase by a factor g, $P(B)_{future}$ is given in equation (30).

$$P(B)_{current} = 1 - \left(\frac{R_e}{R_e+h}\right)^2 \tag{29}$$

$$P(B)_{future} = 1 - \left(\frac{\frac{R_e}{\sqrt{g}}}{\frac{R_e}{\sqrt{g}}+h}\right)^2 \tag{30}$$

By combining equations (29) and (30), it follows that:

$$\frac{P(B)_{future}}{P(B)_{current}} = \frac{\sqrt{g}(2+h'\sqrt{g})}{2+h'}\left(\frac{1+h'}{1+h'\sqrt{g}}\right)^2 \tag{31}$$

where:

h': reduced height, $h' = h / R_e$.

7.3.3 Probability of the event $C|B$

Once the event B has occurred, meaning that the two particular ADTs are in LOS, the occurrence of the event C depends on the distance between them and the pointing of their antenna towards each other. The probability $P(C|B)$ however does not change when the number of aircraft deployed increases, in other terms:

$$\frac{P(C|B)_{future}}{P(C|B)_{current}} = 1 \tag{32}$$

7.4 Results

The condition under which the operation of AM(OR)S systems is not degraded when the number of ADTs increases by a factor g is that the probability of collisions remains constant between the current situation and the future. Equation (17) gives the probability for two given ADTs to interfer with each other. This probability can be assumed to scale linearly with the number of ADTs deployed. This means that is needed:

$$N_{ADT|current} \cdot p_{collision\,|\,current} = N_{ADT|future} \cdot p_{collision\,|\,future} \quad (33)$$

$$\frac{N_{ADT|current}}{N_{ADT|future}} . P(A)_{current} \cdot P(B)_{current} \cdot P(C|B)_{current} = P(A)_{future} \cdot P(B)_{future} \cdot P(C|B)_{future} \quad (34)$$

Noting that $\frac{N_{ADT|current}}{N_{ADT|future}} = \frac{1}{g}$ and using equations (20), (30) and (31), it follows that the necessary condition that $S_{total\,|\,future}$ must fulfil to guarantee that $p_{collision}$ remains constant is:

$$S_{total\,|\,future} = \frac{1}{g} . \frac{\sqrt{g}(2+h'\sqrt{g})}{2+h'} \left(\frac{1+h'}{1+h'\sqrt{g}}\right)^2 \cdot S_{total\,|\,current} \quad (35)$$

7.5 Summary

Based on equation (35), an increase of 20% in the number of ADTs would require an increase of 7.9% of the spectrum allocated to AM(OR)S in the Ku and K frequency bands. This corresponds to about 403.75 additional MHz. Changing the altitude h from 0.3 km to 15 km (which are the boundaries of altitude for all AM(OR)S systems planned to operate in the frequency bands 15.4-15.7 and 22-22.21 GHz) has only very minor influence on the results.

8 Sharing and compatibility studies

8.1 Existing allocations

8.1.1 Frequency range 15.4-15.7 GHz

An extract of Article **5** of the RR (Edition of 2020) is provided in Table 10, showing details of the bands under study.

TABLE 10

Allocation information in the frequency range 15.35-15.7 GHz (as of 2020)

Allocation to services		
Region 1	**Region 2**	**Region 3**
15.35-15.4	EARTH EXPLORATION-SATELLITE (passive) RADIO ASTRONOMY SPACE RESEARCH (passive) 5.340 5.511	
15.4-15.43	RADIOLOCATION 5.511E 5.511F AERONAUTICAL RADIONAVIGATION	
15.43-15.63	FIXED-SATELLITE (Earth-to-space) 5.511A RADIOLOCATION 5.511E 5.511F AERONAUTICAL RADIONAVIGATION 5.511C	
15.63-15.7	RADIOLOCATION 5.511E 5.511F AERONAUTICAL RADIONAVIGATION	

5.340 All emissions are prohibited in the following bands:

[…]

15.35-15.4 GHz, except those provided for by No. **5.511**,

[…] (WRC-03)

5.511 *Additional allocation*: in Saudi Arabia, Bahrain, Cameroon, Egypt, the United Arab Emirates, Guinea, Iran (Islamic Republic of), Iraq, Israel, Kuwait, Lebanon, Oman, Pakistan, Qatar, the Syrian Arab Republic and Somalia, the band 15.35-15.4 GHz is also allocated to the fixed and mobile services on a secondary basis. (WRC-12)

5.511A Use of the frequency band 15.43-15.63 GHz by the fixed-satellite service (Earth-to-space) is limited to feeder links of non-geostationary systems in the mobile-satellite service, subject to coordination under No. **9.11A**. (WRC-15)

5.511C Stations operating in the aeronautical radionavigation service shall limit their effective e.i.r.p. in accordance with Recommendation ITU-R S.1340-0. The minimum coordination distance required to protect the aeronautical radionavigation stations (No. **4.10** applies) from harmful interference from feeder-link earth stations and the maximum e.i.r.p. transmitted towards the local horizontal plane by a feeder-link earth station shall be in accordance with Recommendation ITU-R S.1340-0. (WRC-15)

5.511E In the frequency band 15.4-15.7 GHz, stations operating in the radiolocation service shall not cause harmful interference to, or claim protection from, stations operating in the aeronautical radionavigation service. (WRC-12)

5.511F In order to protect the radio astronomy service in the frequency band 15.35-15.4 GHz, radiolocation stations operating in the frequency band 15.4-15.7 GHz shall not exceed the power flux-density level of −156 dB(W/m²) in a 50 MHz bandwidth in the frequency band 15.35-15.4 GHz, at any radio astronomy observatory site for more than 2 per cent of the time. (WRC-12)

8.1.2 Frequency range 22-22.21 GHz

An extract of Article **5** of the RR (Edition of 2020) is provided in Table 11, showing details of the bands under study. The bands under study are highlighted with bold letters.

TABLE 11

Allocation information in the frequency band 21.4-22.5 GHz (as of 2020)

Allocation to services		
Region 1	**Region 2**	**Region 3**
21.4-22 FIXED MOBILE BROADCASTING-SATELLITE 5.208B 5.530A 5.530B	**21.4-22** FIXED 5.530E MOBILE 5.530A	**21.4-22** FIXED MOBILE BROADCASTING-SATELLITE 5.208B 5.530A 5.530B 5.531
22-22.21	FIXED MOBILE except aeronautical mobile 5.149	
22.21-22.5	EARTH EXPLORATION-SATELLITE (passive) FIXED MOBILE except aeronautical mobile RADIO ASTRONOMY SPACE RESEARCH (passive) 5.149 5.532	

5.149 In making assignments to stations of other services to which the bands:

[…]

22.01-22.21 GHz,

22.21-22.5 GHz,

[…]

are allocated, administrations are urged to take all practicable steps to protect the radio astronomy service from harmful interference. Emissions from spaceborne or airborne stations can be particularly serious sources of interference to the radio astronomy service (see Nos. **4.5** and **4.6** and Article **29**). (WRC-07)

5.208B In the frequency bands:

[…]

21.4-22 GHz,

Resolution **739** (**Rev.WRC-19**) applies. (WRC-19)

5.530A Unless otherwise agreed between the administrations concerned, any station in the fixed or mobile services of an administration shall not produce a power flux-density in excess of −120.4 dB(W/(m² · MHz)) at 3 m above the ground of any point of the territory of any other administration in Regions 1 and 3 for more than 20% of the time. In conducting the calculations, administrations should use the most recent version of Recommendation ITU-R P.452-17 (see also the most recent version of Recommendation ITU-R BO.1898). (WRC-15)

5.530B In the band 21.4-22 GHz, in order to facilitate the development of the broadcasting-satellite service, administrations in Regions 1 and 3 are encouraged not to deploy stations in the mobile service and are encouraged to limit the deployment of stations in the fixed service to point-to-point links. (WRC-12)

5.531 *Additional allocation*: in Japan, the band 21.4-22 GHz is also allocated to the broadcasting service on a primary basis.

5.532 The use of the band 22.21-22.5 GHz by the Earth exploration-satellite (passive) and space research (passive) services shall not impose constraints upon the fixed and mobile, except aeronautical services.

8.2 Propagation models

The propagation models used in sharing and compatibility studies between the AM(OR)S and incumbent services are referenced in Table 12.

TABLE 12

Propagation models to be used for sharing and compatibility studies with systems operating in the non-safety aeronautical mobile (off-Route) service

Frequency band	Incumbent service	Propagation model
15.4-15.7 GHz	ARNS	Rec. ITU-R P.528-5 (for ground-to-air path)
	Radiolocation	
	FSS (Earth-to-space)	Rec. ITU-R P.619-5 for ground-to-space paths and Rec. ITU-R P.1409-2 for air-to-space paths
	EESS (passive)	
	SRS (passive)	
22-22.21 GHz	FS	Rec. ITU-R P.528-5 (for ground-to-air path) and Rec. ITU-R P.1409-2 for air-to-space paths
	LMS	
	Radio astronomy	
	EESS (passive)	Rec. ITU-R P.619-5 for ground-to-space paths
	SRS (passive)	

8.3 Summary of studies

8.3.1 Sharing studies

8.3.1.1 Systems operating in the Radiolocation service in the frequency band 15.4-17.3 GHz

Study A is an MCL analysis providing the required separation distance between an AM(OR)S and an RLS system to ensure $I/N < -6$ dB at the RLS receiver. Following conclusions can be drawn from this study:

– Under certain conditions (alignment of the side lobe of AM(OR)S transmitter and main lobe of the RLS receive, maximum power of the interferer, propagation conditions from Recommendation ITU-R P.528-5), separation distances of 61 to 701 km would be necessary;

– Under alignment of the side lobe of AM(OR)S transmitter and side lobe of the RLS receiver condition, these distances would be 1.6 to 41 km.

Study E shows that, when considering the scanning behaviour of RLS radars and the directivity of antennas used for AM(OR)S and RLS, a typical encounter between an AM(OR)S station and an RLS radar would produce interference occurring four times in 30 minutes and each interference event will last for approximately 6 seconds.

Study B is a Monte Carlo multiple-entry analysis, that assesses the impact of the envisaged AM(OR)S scenarios and systems onto receivers operating in the RLS. The results have shown that, in all AM(OR)S scenarios, I/N level at RLS receivers is more than −6 dB for at most 0.001% of the time.

Study C includes two analyses:

– A single-entry Monte-Carlo analysis that considers one AM(OR)S cluster within the radio horizon of the RLS receiver. This analysis concludes that I/N level at the RLS receiver is greater than −6 dB for at most 0.000 1% of the time with the separation distance of 885 km.

– A multiple-entry Monte-Carlo study. AM(OR)S channels are randomly selected within the tuning range. This analysis concludes that I/N level at the RLS receiver is greater than −6 dB for at most 0.000 1% of the time with the separation distance of 1 440 km.

Study D has determined separation distances between several AM(OR)S clusters and an RLS receiver so that the probability that the I/N value exceeds −6 dB at the RLS receiver is less than 10^{-5}. As in Study C, the choice of this probability was arbitrary as the interference threshold of RLS radars as stipulated in Recommendation M.1730-1 is not associated with any time percentage. Taking ATPC into account, this analysis concludes that I/N level at the RLS receiver is greater than −6 dB for at most 0.000 1% of the time when the separation distance is 1 335 km in the worst of the four studied scenarios.

Study E has shown that interference events can happen in rare configurations (for instance when the AM(OR)S station and the RLS station are flying towards each other). In this case, the interference occurs four times in 30 minutes and each interference event last for approximately 6 seconds. It is worth mentioning that it is expected that the duration of an interference event is very dependent on the scanning behaviour of the radar. The study assumed 1 deg/s vertical and horizontal scan rate, while horizontal scan rate can range between 1 to 30 deg/s and vertical scan rate can range between 1 and 5 deg/s, according to Recommendation ITU-R M.1730-1.

8.3.1.2 Automatic landing systems operating in the aeronautical radionavigation service in the frequency band 15.4-15.7 GHz

Study A is a Monte Carlo multiple-entries analysis, that assesses the impact of the envisaged AM(OR)S scenarios and systems into ALS receivers operating in the ARNS. The results have shown that, in all AM(OR)S scenarios, the I/N level at ARNS ALS receivers is more than −10 dB for at most 0.01 % of the time.

8.3.1.3 Detect and avoid systems operating in the aeronautical radionavigation service in the frequency band 15.4-15.7 GHz

Study A is a Monte Carlo multiple-entries analysis, that assesses the impact of the envisaged AM(OR)S scenarios and systems into DAA receivers operating in the ARNS. The results have shown that, in all AM(OR)S scenarios, the *I*/*N* level at DAA receivers operating in the ARNS is more than −10 dB for at most 0.1 % of the time.

Study B is an MCL analysis. The study assumes aircraft stations operating in the AM(OR)S with transmit power of 25 or 40 dBm (no ATPC was taken into account), co-frequency operation, the antenna side-lobe gain of AM(OR)S and DAA are both 0 dBi and propagation from Recommendation ITU-R P.528-5. It shows such an airborne AM(OR)S system would need separation distances of 3 to 68 km when its side lobe is aligned with the side lobe of the DAA system and 12 to 720 km when its side lobe is aligned with the main lobe of the DAA system.

8.3.1.4 Systems operating in the fixed service operating in the frequency range 21.2-23.6 GHz

Three sharing studies contained in Annex 8 to this Report have assessed the feasibility of sharing the frequency band 22-22.21 GHz between future non-safety AM(OR)S systems and FS. Studies A and B contain Monte Carlo simulations and show that sharing is in general possible when AM(OR)S systems use directive antennas. However, the short-term protection criteria of the FS are exceeded in some configurations corresponding to study scenario described in § 6.2.1. Therefore, three pfd masks are derived in Study C. The following two alternatives have been found efficient to protect the FS when AM(OR)S deployment densities are roughly comparable to the typical densities provided in § 6.4. Note that, whilst equivalent to ensure the short-term protection of FS stations, the option 1 provides an additional margin of 20 dB with the long-term criterion. Note also that these pfd masks must be revised if deployment densities of AM(OR)S stations significantly differ from the typical values provided in § 6.4.

Pfd mask option 1:

$$PFD_{\max} = \begin{cases} 0.875 \cdot \theta - 130 & \text{for } 0° \leq \theta \leq 8° \\ 5 \cdot \theta - 163 & \text{for } 8° < \theta \leq 12° \\ 0.89 \cdot \theta - 113.68 & \text{for } 12° < \theta \leq 30° \\ 0.233 \cdot \theta - 93.99 & \text{for } 30° < \theta \leq 90° \end{cases} \quad (36)$$

where:

θ: elevation angle (degrees) at the FS station

$PFD_{\max}$: maximum allowable spectral pfd for ADTs, measured at the FS station in the frequency band 22-22.21 GHz (in dB(W/(m^2 · MHz))).

Pfd mask option 2:

$$PFD_{\max} = \begin{cases} A & \text{for } 0° \leq \theta < 10° \\ 50 \log_{10}\left(\frac{\theta}{10}\right) + A & \text{for } 10° \leq \theta < 30° \\ 50 \log_{10}(3) + A & \text{for } 30° \leq \theta \leq 90° \end{cases} \quad (37)$$

where:

θ: elevation angle (degrees) at the FS station

PFD_{max}: maximum allowable spectral pfd for ADTs, measured at the FS station in the frequency band 22-22.21 GHz (in dB(W/(m^2 · MHz))).

The variable A is given in equation (38).

$$A = -110 + MOD + FDR + L \tag{38}$$

where:

MOD: constant depending on the modulation scheme used by the FS station, 0 dB for 128-QAM and 5 dB for FSK modulation.

FDR: constant depending on the bandwidth BW_{FS} of the FS station and on the bandwidth $BW_{AM(OR)S}$ of the AM(OR)S stations i.e. 0 dB if $BW_{AM(OR)S} \leq BW_{FS}$, and $10 \log_{10}\left(\frac{BW_{AM(OR)S}}{BW_{FS}}\right)$ otherwise. BW_{FS} = 25 MHz if FSK modulation is used at the FS station, and BW_{FS} = 30 MHz if 128-QAM is used

L: feeder loss (FL) at the FS station that lies between 0 and 3 dB.

Pfd mask option 3:

$$PFD_{max} = \begin{cases} 0.88 \cdot \theta - 130 & \text{for} \quad 0° \leq \theta \leq 8° \\ 2.86 \cdot \theta - 146 & \text{for} \quad 8° < \theta \leq 15° \\ 0.87 \cdot \theta - 116 & \text{for} \quad 15° < \theta \leq 30° \\ 0.067 \cdot \theta - 92 & \text{for} \quad 30° < \theta \leq 90° \end{cases} \tag{39}$$

where:

θ: elevation angle (degrees) at the FS station

PFD_{max}: maximum allowable spectral pfd for ADTs, measured at the FS station in the frequency band 22-22.21 GHz (in dB(W/(m^2 · MHz))).

8.3.1.5 Systems operating in the fixed satellite service operating in the frequency range 15.43-15.63 GHz

Study A is a Monte Carlo multiple-entries analysis, that assesses the impact of the envisaged AM(OR)S scenarios and systems onto receivers operating in the FSS (Earth-to-space). The results have shown that, in all AM(OR)S scenarios, the protection criteria for systems operating in the FSS (Earth-to-space) in the frequency band 15.43-15.63 GHz are met. The long-term protection criterion is met with a margin of at least 20 dB.

8.3.2 Compatibility studies

8.3.2.1 Systems operating in the radio astronomy service operating in the frequency bands 15.35-15.4 GHz and 22.21-22.5 GHz

Four compatibility studies are contained in Annex 7 to this Report and consider different aspects of the compatibility between future non-safety AM(OR)S systems planned to operate in the frequency bands 15.4-15.7 GHz and 22-22.21 GHz and RAS operating in the adjacent bands 15.35-15.4 GHz and 22.21-22.5 GHz.

Study A analyses a scenario where a single ADT is flying with azimuth bearing towards a RAS station. The study showed that the aggregate incident power from steerable synthetic aperture antennas will be dominated by ADTs at large nadir distances and steering of directional ADTs antenna beams should be used to avoid the direction of the RAS station. The requirements of RR No. **5.340** may be satisfied if the mean incident pfd in the frequency bands 15.35-15.4 GHz and

22.21-22.5 GHz from aggregated emissions of the ADT does not exceed −233 dB(W/(m^2 · Hz)) at the RAS station.

Study B is a multiple-entries Monte Carlo study that considers the four operational AM(OR)S scenarios depicted in § 6.2, together with reference deployment densities provided in § 6.4. Moreover, the study takes the specificities of eight RAS sites operating in the world in the bands 15.35-15.4 GHz and 22.21-22.5 GHz. Actual trajectories of AM(OR)S stations around the RAS station are simulated over the 2 000 s integration time of RAS measurements and the analysis determines the expected percentage of erroneous measurements as a function of the elevation at the RAS station. In that respect, it follows the methodology laid out in Recommendation ITU-R S.1586-1. The study concludes that study scenario described in § 6.2.1 is the most detrimental for coexistence with RAS, and that mitigations measures are needed. Study C applies the same methodology and shows that a 10 MHz guard band between the AM(OR)S channels and the RAS band is sufficient to lower this percentage below 2% in all studied scenarios. Study D finally provides a methodology to fine-tune the necessary guard band in scenarios involving low-altitude ADTs and shows that the operation is possible if the terrain profile around the RAS station is carefully taken into consideration.

8.3.2.2 Systems operating in the broadcast-satellite service operating in the frequency band 21.4-22 GHz

A multiple-entries Monte Carlo analysis contained in Annex 10 to this Report has considered the four operational AM(OR)S scenarios presented in § 6.2, together with expected deployment densities. The study concludes that coexistence between BSS and future non-safety AM(OR)S systems can be achieved without any mitigation measures, if the deployment density of AM(OR)S stations is in the same order of magnitude as presented in § 6.4.

8.3.2.3 Systems operating in the Earth exploration satellite service (passive) operating in the frequency band 22.21-22.5 GHz

Study A reproduces the effective trajectory of a typical spacecraft operating an EESS (passive) sensor in this band, as well as the scanning behaviour of the sensor antenna. Moreover, it computes the trajectory according to a random but constant azimuth bearing, a constant altitude of 10 000 m AGL and a constant ground speed of 900 km/h. The number of deployed AM(OR)S stations within the 10 000 000 km^2 area analysed by the sensor was chosen as a typical value of 50. This study has determined that the maximum power level of unwanted emissions in 22.21-22.31 GHz for AM(OR)S stations operating in a 10 000 000 km^2 area analysed by the sensor and in the adjacent frequency band 22-22.21 GHz is $-21\,\frac{\text{dBW}}{100\text{MHz}}$ for omnidirectional systems, and according to equation (40) for directive AM(OR)S systems:

$$P_{max}(\theta) = \begin{cases} -28 & \text{if } |\theta| \le 1° \\ -28\left(1 - \dfrac{\log_{10}(|\theta|)}{\log_{10}(45)}\right) & \text{if } 1° \le |\theta| \le 45° \\ 0 & \text{if } |\theta| \ge 45° \end{cases} \quad (40)$$

where:

θ : elevation angle (deg) above the local horizontal (positive values above the horizon)

P_{max} : maximum permissible unwanted emissions $\left(\frac{\text{dBW}}{100\text{MHz}}\right)$ in the frequency band 22.21-22.31 GHz of directive AM(OR)S systems operating in the frequency band 22-22.21 GHz.

Complying with these limits may require the introduction of a guard band between the AM(OR)S channels and the lower edge of the passive band 22.21-22.5 GHz, depending of the necessary BW and the TPO of AM(OR)S stations.

The objective of Study B is to determine the maximum density of AM(OR)S systems operating near the band edge (within 100 MHz of the edge), which can be supported and simultaneously protecting incumbent EESS systems in the neighbouring band. The full deployment of AM(OR)S clusters for the various scenarios would likely make use of the 22-22.21 GHz range and some subset of systems could be assigned near the band edge. The results of Study B indicate that certain AM(OR)S scenarios, link modes, or system configurations, are less impactful to OOB interference seen in the neighbouring segment 22.21-22.31 GHz used by EESS (passive) service and can therefore allow greater population density of AM(OR)S near this segment and should be given preference over the other configurations. Conversely, the more impactful configurations/modes in adherence to the indicated power emission limits determined by this study will also help support protection of EESS passive service. This study concluded that the maximum allowable density of AM(OR)S stations and the associated limits of unwanted emissions are:

– at most 32 omnidirectional WBLOSDLs limited to $-23\,\frac{\mathrm{dBW}}{100\mathrm{MHz}}$ in the band 22.21-22.31 GHz or
– at most 20 directional and horizontal WBLOSDLs limited to $-22\,\frac{\mathrm{dBW}}{100\mathrm{MHz}}$ in the band 22.21-22.31 GHz or
– at most 64 directional tilted WBLOSDLs or
– at most 4 G2A WBLOSDLs in scenario 6.2.1

can operate simultaneously in the 10 000 000 km^2 mission area of interest (MAI) observed by the sensor without imposing harmful interference to this sensor.

Annexes: 11

Annex 1

Characteristics of future non-safety aeronautical mobile (off-route) service systems planned to operate in the frequency bands 15.4-15.7 GHz and 22-22.21 GHz

TABLE OF CONTENTS

This Annex introduces the technical characteristics of the new non-safety AM(OR)S systems planned to operate in the frequency bands 15.4-15.7 GHz and 22-22.21 GHz.

A1.1 Technical and operational characteristics

Technical and operational characteristics of future non-safety AM(OR)S systems planned to operate in the frequency bands 15.4-15.7 GHz and 22-22.21 GHz are provided in Table A1-1. An AM(OR)S system denotes the association of a transceiver and an antenna, and can be installed on-board a flying platform (systems 1, 2 and 3) or be ground-based (systems 4 and 5). As explained in § 5.1, airborne AM(OR)S systems are referred to as ADTs, and ground-based AM(OR)S systems, as GDTs.

A WBLOSDL is established between two AM(OR)S systems of the same or of different types. For example, an A2A link can be established using system 1 both at the transmitter and the receiver side. Another option is to use system 1 as transmitter and system 2 as receiver. This is for instance the case in scenario 6.2.2 (see Table 3).

TABLE A1-1

Technical and operational characteristics of future systems operating in the non-safety AM(OR)S in the frequency bands 15.4-15.7 GHz and 22-22.21 GHz

	Units	AM(OR)S system				
		1	**2**	**3**	**4**	**5**
Deployment						
Platform	–	Airborne			Ground-based	
Minimum operational altitude AGL	m	300			2	
Maximum operational altitude AGL		15 000			2	
Transmitter						
Tuning ranges	MHz	15 400 to 15 700 22 000 to 22 210				
Control link BW		0.5	0.5	0.5	0.5	0.5
Minimum data link BW		10	10	10	N/A[1]	
Maximum data link BW		200	150	150		
Maximum TPO[2]	dBm	40	25	40, 50[2]	40	40
Spectrum emission mask (SEM) expressed in relative power spectral density (RPSD)[3] [4] [5]	dB	*RPSD* = | 0 at $f_c + 0.5 \cdot B$ | −40 at $f_c + 1.35 \cdot B$ | −53 at $f_c + 2.5 \cdot B$ | −59 at $f_c + 3.1 \cdot B$ | −69 at $f_c + 5 \cdot B$				
Modulation		PSK[6]	QAM[7], PSK		BPSK[8]	
Multiplexing		FDMA				
Maximum duty cycle (DC)	%	100	100	100	100	100
Receiver						
Target SNR sensitivity threshold	dB	3	3	3	3	3
Noise figure (NF)		5	5	5	5	5

(1) N/A – Not applicable; systems 4 and 5 are typically used to receive data from another AM(OR)S system.

(2) The maximum TPO is 40 dBm in the 15.4-15.7 GHz frequency band and 50 dBm in the 22-22.21 GHz frequency band.

(3) The TPO is measured at the antenna port. It is adjusted by the transmitting system to match the target SNR value at the receiver using an ATPC algorithm. This algorithm is based on the feedback given by the receiver through the control channel. One possible ATPC implementation is described in § A11.6.1.

(4) The level of OOB emissions produced by the SEM provided in this Table complies with the limits laid out in § 2 of Annex 11 to Rec. ITU-R SM.1541-6. This is also the case for the spurious emissions level which matches the limit values mentioned in RR Appendix **3**).

(5) f_c denotes the centre frequency of the emission, and B, the necessary BW.

(6) Between the points provided in this Table, the SEM can be linearly interpolated, as shown in Fig. A1-1.

(7) PSK – Phase Shift Keying.

(8) QAM – Quadrature Amplitude Modulation.

(9) BPSK – Binary Phase Shift Keying.

FIGURE A1-1

Assumed spectrum emission mask of future systems operating in the non-safety aeronautical mobile (off-Route) service planned to operate in the frequency bands 15.4-15.7 GHz and 22-22.21 GHz

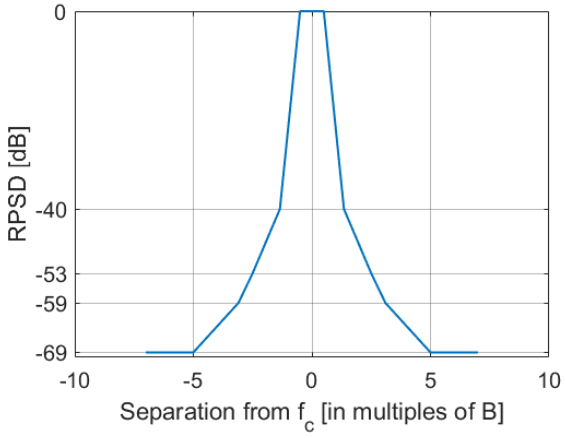

A1.2 Antenna characteristics

Future non-safety AM(OR)S systems planned to operate in the frequency bands 15.4-15.7 GHz and 22-22.21 GHz can use a variety of antennas, ranging from omnidirectional antennas to highly directive phased arrays, depending upon the configuration of the platforms and the operational requirements of the mission.

Typical antenna types are provided in Table A1-2 for the five systems introduced in Table A1-1. Their technical characteristics are further described in §§ A1.2.1 through A1.2.4.

TABLE A1-2

Antenna types used for systems planned to operate in the non-safety aeronautical mobile (off-route) service in the frequency bands 15.4-15.7 GHz and 22-22.21 GHz

		AM(OR)S system				
	Units	**1**	**2**	**3**	**4**	**5**
Antenna type	–	Phased array	Omni-directional	Phased array	Whip	Parabolic reflector
Peak gain	dBi	25	3	38	14	38
Related section	–	A1.2.1	A1.2.2	A1.2.1	A1.2.3	A1.2.4
Polarization		Circular	Horizontal, vertical or circular			

A1.2.1 Phased arrays

Phased arrays of antennas can achieve high directivity and allow for dynamic steering of the main beam in the desired direction. Such antenna arrays are composed of number of elementary radiators fed individually with electric signals that are offset in phase, which makes beam steering possible. The radiation pattern of such antennas can be computed using Recommendation ITU-R M.1851-1. It is to be noted that this Recommendation was under revision at the time of writing this Report.

Attachment A to this Annex provides the typical parameters of phased arrays used in AM(OR)S systems and calculates the radiation pattern of such antennas using the methodology laid out in Recommendation ITU-R M.1851-1.

A1.2.2 Omnidirectional antennas

Omnidirectional antennas are mainly used on-board data terminals that do not allow for the installation of a directive antenna coupled with a tracking system i.e. typically for small ADTs or hand-held PGDTs. Note however that such antennas can only be used for short distance communications.

The antenna can be installed either on the belly or on the roof of the platform. To account for the attenuation provided by the frame of the platform, it is assumed that, when installed on the belly, the gain is −3 dBi for positive elevation angles, and +3 dBi for negative elevation angles. Conversely, when mounted on the roof of the platform, the gain is +3 dBi for positive elevation angles, and −3 dBi for negative elevation angles.

A1.2.3 Whip antennas

Whip antennas can be mounted on the roof of a vehicle and provide omnidirectional gain in azimuth. A whip antenna can be modelled using a half-wave dipole over an infinite conducting surface. The mathematical equations to derive the corresponding radiation pattern are detailed in Attachment B to this Annex.

A1.2.4 Parabolic reflectors

Parabolic reflectors are often used for antennas mounted on GDTs and can achieve high gain values.

Attachment A
to Annex 1

Modelling of phased array antennas used in future systems operating in the non-safety aeronautical mobile (off-Route) service in the frequency bands 15.4-15.7 GHz and 22-22.21 GHz

This attachment provides the technical parameters of phased array antennas used in future non-safety AM(OR)S systems planned to operate in the frequency bands 15.4-15.7 GHz and 22-22.21 GHz. Furthermore, a modelling of the radiation pattern is provided based on these parameters.

Section A1A.1 is dedicated to the elementary radiators that compose the phased arrays. Section A1A.2 builds upon § A1A.1 and derives the compound radiation pattern.

A1A.1 Elementary radiator

The relative gain[9] of a typical elementary radiator used in AM(OR)S phased array antennas is given in equation (A1-1). Figure A1-2 further shows the coordinate system used to establish these equations. By convention, the boresight of the elementary radiators is aligned with the x-axis.

$$A_{\mathrm{EH}}(\phi) = -\min\left(12\left(\frac{\phi}{\phi_{3\mathrm{dB}}}\right)^2; A_m\right) \tag{A1-1}$$

[9] The reference for the relative gain is the peak gain of the elementary radiator.

$$A_{\mathrm{EV}}(\theta) = -\min\left(12\left(\frac{\theta}{\theta_{3\mathrm{dB}}}\right)^2 ; \mathrm{SLA}\right)$$

where:

$A_{EH}(\varphi)$: relative gain (dB) of the elementary radiator in the horizontal plane

$A_{EV}(\theta)$: relative gain (dB) of the elementary radiator in the vertical plane

φ: azimuth angle (deg.)

θ: elevation angle (deg.)

$\Phi_{3\mathrm{dB}}$: HPBW (deg.) of the elementary radiator in the horizontal plane

$\theta_{3\mathrm{dB}}$: HPBW (deg.) of the elementary radiator in the vertical plane

A_m: back lobe suppression factor (dB)

SLA: side lobe attenuation (dB).

It follows that the composite gain $A_E(\theta, \varphi)$ of the elementary radiator is computed using equation (A1-2):

$$A_E(\theta, \varphi) = G_{e,max} - min(- A_{EH}(\varphi) - A_{EV}(\theta) ; A_m) \quad \text{(A1-2)}$$

where:

$G_{e,max}$: peak gain (dBi) of the elementary radiator

$A_{EH}(\varphi)$: relative gain (dB) of the elementary radiator in the horizontal plane, as defined in equation (A1-1)

$A_{EV}(\theta)$: relative gain (dB) of the elementary radiator in the vertical plane, as defined in equation (A1-1).

Typical values of the parameters used in equations (A1-1) and (A1-2) are given in Table A1-3.

A1A.2 Compound radiation pattern

The compound radiation pattern $\mathrm{G}(\theta, \phi)$ of the phased array builds upon the pattern of a single radiator using the array factor (AF) defined in equation (A1-3):

$$\begin{aligned} G(\theta, \phi) &= A_E(\theta, \phi) + 10.\log_{10}\left(\mathrm{AF}(\theta, \phi)\right) \\ \mathrm{AF}(\theta, \phi) &= \mathrm{AF}_y(\theta, \phi).\mathrm{AF}_z(\theta, \phi) \end{aligned} \quad \text{(A1-3)}$$

The horizontal and vertical components $AF_y(\theta, \phi)$ and $AF_z(\theta, \phi)$ of the AF are defined in equation (A1-4):

$$AF_y(\theta, \phi) = \frac{\sin\left(\frac{N_y.\psi_y}{2}\right)}{\sin\left(\frac{\psi_y}{2}\right)}, \quad AF_z(\theta, \phi) = \frac{\sin\left(\frac{N_z.\psi_z}{2}\right)}{\sin\left(\frac{\psi_z}{2}\right)} \quad \text{(A1-4)}$$

where:

N_y: number of elementary radiators in the horizontal direction

N_z: number of elementary radiators in the vertical direction

$\Psi_y(\theta,\varphi)$: variable ($\emptyset$) defined in equation (A1-5)

$\Psi_z(\theta,\varphi)$: variable ($\emptyset$) defined in equation (A1-5).

$$\psi_y(\theta, \phi) = 2\pi\frac{d_y}{\lambda}\left(\sin(\theta).\cos(\phi) - \sin(\omega_\theta).\cos\left(\omega_\phi\right)\right) \quad \text{(A1-5)}$$

$$\psi_z(\theta,\phi) = 2\pi\frac{d_z}{\lambda}\left(\sin(\theta).\sin(\phi) - \sin(\omega_\theta).\sin\left(\omega_\phi\right)\right)$$

where:

d_y : spacing (m) between elements in the horizontal direction

d_z : spacing (m) between elements in the vertical direction

λ : wavelength (m)

ω_θ : electronic beam steering angle (deg.) in the vertical plane

ω_φ : electronic beam steering angle (deg.) in the horizontal plane.

Typical input parameters for equations (A1-4) and (A1-5) are provided in Table A1-4. Figure A1-3 finally shows on left-hand side, a 3D representation of the radiation pattern of the phased array. The top corresponds to the case where no electrical beam steering is applied (i.e. when $\omega_\theta = 0°$ and $\omega_\varphi = 0°$), and the bottom, the case where $\omega_\theta = 30°$.Finally on the right-hand side, a 2D visualization of the elementary radiator pattern (in blue) and composite array pattern (in red) are shown.

FIGURE A1-2

Coordinate system used in equation (A1A-1)

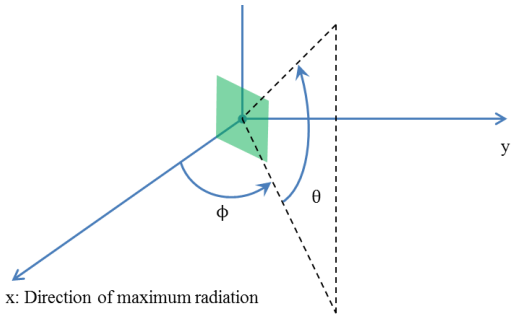

TABLE A1-3

Assumed parameters of elementary radiators

			AM(OR)S_system	
	Units	**Notation**	**1**	**3**
Antenna type	**–**		**Square patch**	
Vertical HPBW	deg	θ_{3dB}	65	
Horizontal HPBW		ϕ_{3dB}		
Peak gain	dBi	$G_{e,\max}$	5	8.5
Front-to-back ratio (FTBR)	dB	A_m	30	
Side lobe attenuation (SLA)		SLA		

TABLE A1-4

Assumed parameters of antenna arrays

			AM(OR)S system	
	Units	**Notation**	**1**	**3**
Elementary radiators in the horizontal direction	–	N_y	10	30
Elementary radiators in the vertical direction		N_z		
Horizontal spacing		d_y	$\lambda/2$	
Vertical spacing		d_z		

FIGURE A1-3

Graphical representation of the antenna radiation pattern of system 3 operating in the non-safety aeronautical mobile (off-Route) service

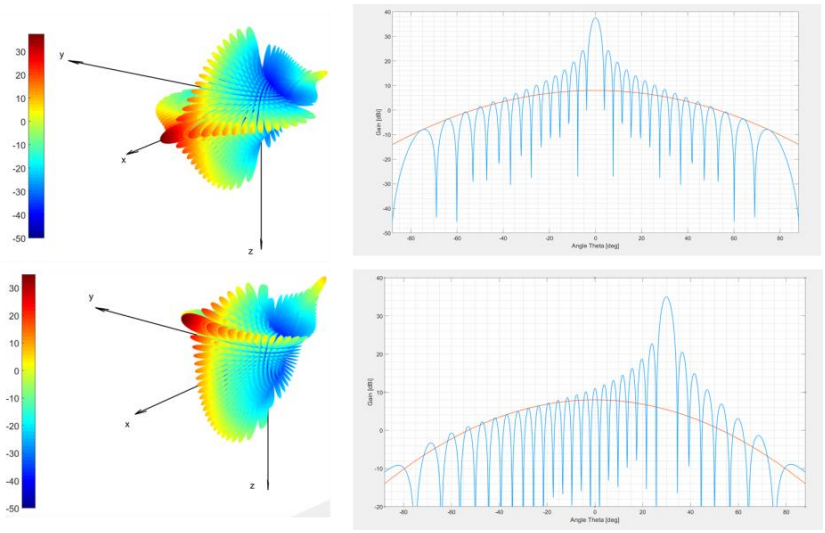

Attachment B
to Annex 1

Modelling of parabolic reflector antennas used in certain ground data terminals of future non-safety aeronautical mobile (off-Route) service systems operating in the frequency bands 15.4-15.7 GHz and 22-22.21 GHz

This Attachment proposes a mathematical modelling of parabolic reflector antennas used in certain GDTs of future AM(OR)S systems. Section A1B.1 computes the peak gain of such antennas, which is used in § A1B.2 to determine the complete radiation pattern.

A1B.1 Peak gain

The peak gain G_{max} of a parabolic reflector antenna is well approximated by equation (A1-6):

$$G_{max} = 20 \cdot \log_{10}(\pi \cdot D / \lambda) + 10 \cdot \log_{10}(e_A) \quad \text{(A1-6)}$$

where:

e_A: aperture efficiency of the antenna; a typical value of 0.7 is assumed

D: diameter of the parabolic reflector (m)

λ: wavelength (m).

A1B.2 Radiation pattern

The relative gain[10] G_{rel} of a parabolic reflector is given in equation (A1-7):

$$G_{rel} = 20 \cdot \log_{10}(2 \cdot J_1(x) / x) \quad \text{(A1-7)}$$

The reduced off-axis angle x in equation (A1B-2) is given in equation (A1-8):

$$x = \frac{\pi . D}{\lambda} . \sin(\theta) \quad \text{(A1-8)}$$

where:

θ: off-axis angle (deg.) from the main beam direction.

In equation (A1B-2), J_1 denotes the Bessel function that can be approximated using the infinite series shown in equation (A1-9):

$$J_1(x) = \sum_{S=0}^{+\infty} \frac{(-1)^s}{(1+s)!s!} . \left(\frac{x}{2}\right)^{1+2s} \quad \text{(A1-9)}$$

Note that equation (A1-9) is only valid for θ values between −90° and +90°. For off-axis angles between −180° and −90° or between 90° and 180° (i.e. towards the rear of the parabolic reflector), the gain is assumed to be −100 dBi.

Figure A1-4 shows the complete radiation pattern. Table A1-5 provides some data points that can be read from Fig. A1-4 for some particular off-axis angle values.

[10] The reference for the relative gain G_{rel} is the peak gain G_{max}.

FIGURE A1-4

Radiation pattern of a parabolic reflector antenna at 15.4 GHz, assuming an antenna efficiency of 0.7

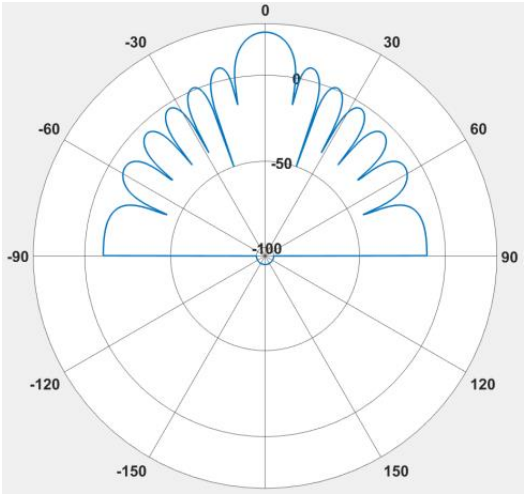

TABLE A1-5

Data points extracted from Fig. A1-1

Off-axis angle (degree)	Gain (dBi)
0	38
5	14.1
10	−30.6
15	0.1
20	−14.4
25	−6.1
30	−15.8
35	−21.5
40	−17
45	−21.4

Off-axis angle (degree)	Gain (dBi)
50	−24.1
55	−14.7
60	−27.8
65	−23.4
70	−23.4
75	−31.7
80	−17.1
85	−24.4
90	−100

Annex 2

Characteristics of existing services operating in the frequency bands 15.4-15.7 GHz, 22-22.21 GHz, or in an immediately adjacent band

TABLE OF CONTENTS

This Annex provides the technical and operational characteristics, as well as antenna characteristics and protection criteria, of the systems operating in the frequency bands 15.4-15.7 GHz or 22-22.21 GHz, or in an immediately adjacent band. These characteristics are used in this Report for sharing and compatibility studies with future non-safety AM(OR)S systems planned to operate in these bands.

A2.1 Systems operating in the radiolocation service in the frequency range 15.4-17.3 GHz

The frequency band 15.4-17.3 GHz is globally allocated to the RLS on a primary basis.

A2.1.1 Technical and operational characteristics

Recommendation ITU-R M.1730-1 introduces six representative RLS systems operating in the frequency range 15.4-17.3 GHz. Among them only one system (referred to as System 6) operates in-band with the AM(OR)S systems presented in § A1.1 of this Report. The technical and operational characteristics of the RLS System 6 are shown in Table A2-1.

TABLE A2-1

Technical and operational characteristics of system 6 operating in the radiolocation service operating in the frequency range 15.4-17.3 GHz

Characteristics	Value
Deployment	Airborne
Operational altitude AGL (m)	300 to 13 700
Transmitter	
Tuning range (MHz) (1)	15 400 to 17 300
Modulation	Linear FM(2) chirp
Transmit peak power (kW)	0.5, 2, 10
Pulse repetition rate (pps)	200 to 20 000
Maximum DC	Up to 0.2
Chirp BW	< 1 900
Transmitter RF BW (MHz): −3 dB −20 dB	 1 850 1 854
Receiver	
1st/2nd receiver intermediate frequency (IF) −3 dB BW (MHz)	25
Selectivity	See note (3)
NF (dB)	5

(1) Regarding the channelization of the frequency range 15.4-17.3 GHz, Rec. ITU-R M.1730-1 states in § 2 that "Radar operating frequencies can be assumed to be uniformly spread throughout each radar's tuning range".

(2) FM – Frequency Modulation.

(3) The selectivity of RLS radars is found in section 3.2 of Rec. ITU-R M.1461-2: "If the radar receiver IF selectivity response is not provided, a selectivity fall-off of 80 dB per decade should be used from the 3 dB bandwidth edge frequency down to a selectivity of 70 dB which is the floor." Note that this IF selectivity performance is not specific to RLS radars, but also applies to other radars operating in the ARNS (see § A2.2).

A2.1.2 Antenna characteristics

Antenna characteristics of RLS systems operating in the frequency range 15.4-17.3 GHz are provided in Attachment A to this Annex.

A2.1.3 Protection criteria

Recommendation ITU-R M.1461-2 provides general methods to assess the interference potential between radars operating in the radiodetermination service and systems in other services. The interference impact onto radars can be analysed using three different metrics:

– the receiver front-end overload

– the intermodulation

– the degradation of the sensitivity.

When the interfering signal under study has a high DC and appears noise-like to the radar, the degradation of the sensitivity is the most appropriate analysis criterion. As seen in § A1.1, this is applicable to the AM(OR)S systems, which can theoretically be active 100% of the time.

This assumption is substantiated by Recommendation ITU-R M.1730-1 which states in § 3:

> "For the portion of the 15.4-17.3 GHz band where there is a radiolocation allocation, a signal from another service resulting in an *I*/*N* ratio below −6 dB is acceptable by the radar users for signals from the other service with high-duty cycle […]. When multiple interferers are present, the recommended *I*/*N* protection criteria remains unchanged."

A2.2 Systems operating in the aeronautical radionavigation service in the frequency range 15.4-15.7 GHz

The frequency band 15.4-15.7 GHz is globally allocated to the ARNS on a primary basis. Technical and operational characteristics of ARNS radars operating in this frequency band are based on an ITU-R Recommendation that was being drafted at the time of writing this Report.

The draft Recommendation considers two types of systems operating under the ARNS allocation in the frequency band 15.4-15.7 GHz:

– Detect and avoid (DAA) radars, addressed in § A2.2.1.

– Aircraft landing systems (ALS), addressed in § A2.2.2.

A2.2.1 Detect and avoid radars operating in the frequency band in 15.4-15.7 GHz

DAA radars can be installed on board unmanned aircraft[11] or on the ground[12] to detect non-cooperative targets and constitute an essential component for the integration of UA in non-segregated airspace. The information collected by these radars is ultimately transmitted to the Remote Pilot (RP) using a dedicated communication system (either the control and command link in the case of an airborne DAA radar, or a land line in the case of a ground DAA radar).

A2.2.1.1 Technical and operational characteristics

Table A2-2 shows the technical and operational characteristics of three airborne DAA radars (Radars 1, 3 and 4) and one ground DAA radar (Radar 2).

TABLE A2-2

Technical and operational characteristics of DAA radars operating in the frequency range 15.4-15.7 GHz

		DAA Radars			
Parameters	**Units**	**1**	**2**	**3**	**4**
Deployment	-	Airborne, ground(1)	Ground(1)	Airborne, ground (1)	
Radar type		A2A, G2A	G2A	A2A, G2A	
Operating range if airborne	km	0.8 (small UAS); 2.0 (small general aviation aircraft)	No data available	1.8 (small UAS); 4.5 (small general aviation aircraft)	9
Operating height AGL		Up to 20		Up to 20	
Ground speed if airborne	km/h	200	N/A (2)	200	Up to 700

[11] Referred to as airborne DAA radars.

[12] Referred to as ground DAA radars.

		DAA Radars			
Parameters	**Units**	**1**	**2**	**3**	**4**
Transmitter					
Tuning range	MHz	15 400 to 15 700 [3]			
Channel selection	-	Uniformly selected in the tuning range			
Modulation type		FMCW [4]	No data available	FMCW	LFM [5]
Average transmitter power (conducted)	W	2		10	30
Pulse width	µs	220		197	0.25 to 20
Pulse rise and fall times		5/5		0.5/0.5	Up to 0.1
PRR [6]	ps	4 000		4 000	1 to 200
RF BW at: −3 dB −20 dB −40 dB	MHz	 176 184 201		 152 164 269	 25 80 155
Receiver					
IF BW at: −3 dB −20 dB −40 dB	MHz	 15 32 58			 Up to 200 Up to 300 Up to 400
Sensitivity	dBm	−147	No data available	−141	−121
NF	dB	1.5			4
Calculated Rx noise power	dBW	−130.7			−133

(1) On and off airports.

(2) N/A – Not applicable.

(3) The radar is pre-programmed at the factory to any centre frequency inside this band. Some settings may allow the radar to self-configure on-the-fly based on detected spectrum conflict with other radars. See also note (1) in Table A2-1.

(4) FMCW – frequency modulation continuous wave.

(5) LFM – linear frequency modulation.

(6) PRR – pulse repetition rate.

A2.2.1.2 Antenna characteristics

Table A2-3 presents the antenna characteristics of DAA radars as provided in the Recommendation on ARNS in the frequency range 15.4-15.7 GHz mentioned in § A2.2.

DAA radars antennas are composed of phased arrays, and therefore these characteristics must be complemented to obtain the complete radiation pattern. Hence, assumptions were made and gathered in Table A2-4 regarding the characteristics and the number of elementary radiators, the spacing between them, etc. that match with the best possible precision the characteristics presented in Table A2-3.

For instance, Fig. A2-1 shows the horizontal and vertical radiation pattern of DAA radar 1 that is obtained using the data provided in Table A2-4. This pattern can then be compared against the target characteristics in Table A2-3:

– The peak gain of the elementary radiator is 2 dBi (target value is 2 dBi), and the peak gain of the phased array is 11.5 dBi (target value is 12 dBi).

– The horizontal and vertical HPBW are 38.8° (target value is 40°).

– The first side lobe has a gain of −3 dBi for an off-axis angle of 74° (target value is −3 dBi for an off-axis angle of −50°).

Following the same methodology, Figs A2-2A and A2-2B respectively show the horizontal and vertical radiation patterns of DAA radar 4. These charts are also compared against the target values in Table A2-3:

– the peak gain of the elementary radiator is 2 dBi (target value is 2 dBi), and the peak gain of the phased array is 26.9 dBi (target value is 27 dBi);

– the horizontal HPBW is 4.2° (target value is 4°);

– the vertical HPBW is 2.4° (target value is 2°);

– in both the horizontal and the vertical directions, the first side lobe level is below 20 dBi, which was the maximum value specified in Table A2-3 for this radar.

TABLE A2-3

Antenna characteristics of DAA radars operating in the frequency range 15.4-15.7 GHz

		DAA radars			
Parameters	**Units**	**1**	**2**	**3**	**4**
Antenna type	-	Bi-Static phased array			
Antenna placement		Aircraft (manned or unmanned) if airborne; Tower (<20 m) if ground based			
Peak gain of elementary radiators	dBi	2			
Antenna peak gain		12	25	15	27
Horizontal HPBW	degree	40	2.5	32	4
Vertical HPBW			40	28	2
First side lobe	dBi	−3 at 50°	No data available	−1 at 52°	< 20
Radiation pattern model	-	Rec. ITU-R M.1851-1, section 7.2[13]			
Polarization		Linear			
Horizontal antenna scan	degree	±60			±65
Vertical antenna scan		±20		±60	−40 to +50

[13] This Recommendation was under revision at the time of writing this Report.

TABLE A2-4

Antenna characteristics of DAA radars operating in the frequency range 15.4-15.7 GHz – array elements

<table>
<tr><th rowspan="2">Parameters</th><th rowspan="2">Units</th><th colspan="4">DAA radars</th></tr>
<tr><th>1</th><th>2</th><th>3</th><th>4</th></tr>
<tr><td>Horizontal elements</td><td rowspan="2">–</td><td rowspan="2">3</td><td>3</td><td>5</td><td>18</td></tr>
<tr><td>Vertical elements</td><td>67</td><td>4</td><td>17</td></tr>
<tr><td>Element horizontal HPBW</td><td rowspan="2">degree</td><td colspan="4" rowspan="2">140</td></tr>
<tr><td>Element vertical HPBW</td></tr>
<tr><td>Horizontal element spacing</td><td rowspan="2">Lambda units[14]</td><td rowspan="2">0.45</td><td colspan="2">0.4</td><td rowspan="2">0.7</td></tr>
<tr><td>Vertical element spacing</td><td>0.3</td><td>0.4</td></tr>
<tr><td>FTBR</td><td rowspan="2">dB</td><td colspan="4" rowspan="2">30</td></tr>
<tr><td>SLA</td></tr>
</table>

FIGURE A2-1

Radiation pattern in the horizontal and vertical planes of detect and avoid Radar 1 computed using Table A2-3 and Table A2-4 (elementary radiator in red, compound pattern in blue)

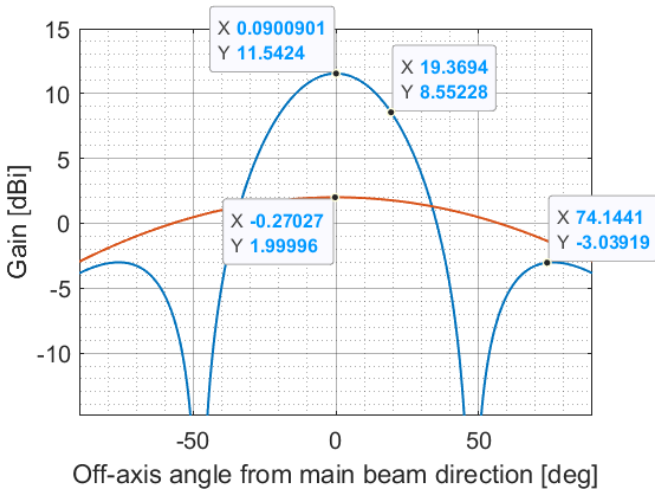

[14] Fraction of the wavelength.

FIGURE A2-2A

Horizontal radiation pattern of DAA radar 4 computed using Table A2-3 and Table A2-4 (elementary radiator in red, compound pattern in blue)

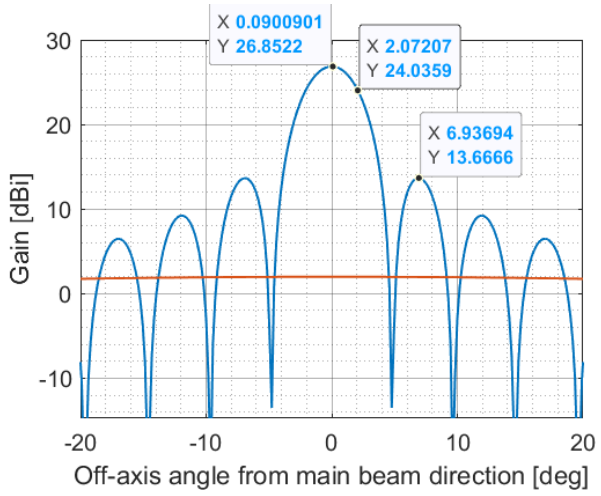

FIGURE A2-2B

Vertical radiation pattern of DAA radar 4 computed using Table A2-3 and Table A2-4 (elementary radiator in red, compound pattern in blue)

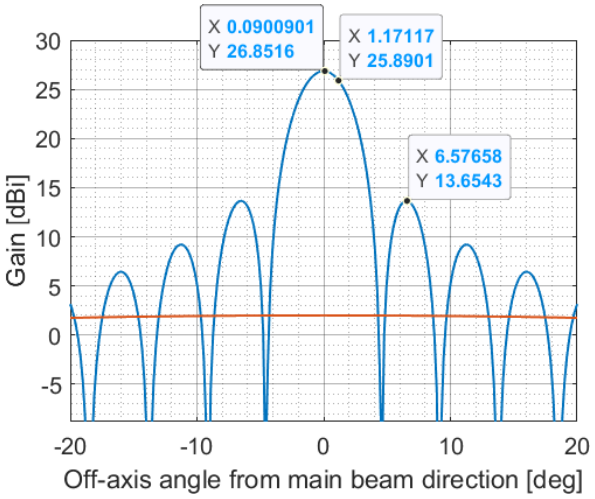

A2.2.1.3 Protection criteria

As explained in § A2.1.3, the impact of AM(OR)S systems onto radiodetermination radars is best evaluated using the desensitization criterion, because AM(OR)S transmitters exhibit noise-like characteristics and a high DC.

For radars operating under an RLS allocation, an increase of about 1 dB in the noise floor would constitute a significant degradation of the detection capability. This is equivalent to a *I*/*N* ratio of −6 dB, which is therefore used as a protection criterion for this type of radars (see § A2.1.3).

However, radars operating under an ARNS allocation implement safety-of-life functions and therefore it is appropriate to choose a more stringent protection criterion. It is assumed that an increase in the noise floor of 0.5 dB already constitutes a significant performance degradation, which is equivalent to a *I*/*N* ratio of −10 dB. This protection criterion accounts for the aggregate effect of multiple interferers, when present.

A2.2.2 Automatic landing systems operating in the frequency range 15.4-15.7 GHz

The ALS system presented in this section is an electronic aid that provides information to an approaching aircraft about its horizontal and vertical positioning with respect to the runway. There are two separate surface transmitters, one transmitting data about the azimuth, one transmitting data about the elevation, and one receiver on-board the aircraft. This section will focus on this receiver.

A2.2.2.1 Technical and operational characteristics

Table A2-5 presents the technical and operational characteristics of a typical ALS system operating in the frequency range 15.4-15.7 GHz.

TABLE A2-5

Technical and operational characteristics of a typical ALS in the frequency range 15.4-15.7 GHz

Parameter	Units	Value
Deployment	–	On-board aircraft (rx) and on the ground (tx)
Operating height AGL	km	Up to 2
ALS **transmitter on the ground**		
Tuning range	MHz	15 400 to 15 700
ALS **receiver on-board aircraft**		
IF BW −3 dB −20 dB −60 dB	MHz	 12 17 24
Sensitivity	dBm	−72
NF	dB	11.5
Calculated noise power	dBW	−121.7

A2.2.2.2 Antenna characteristics

The antenna characteristics of the typical ALS system introduced in § A2.2.2.1 are provided in Attachment B to this Annex.

A2.2.2.3 Protection criteria

The protection criteria of ALS systems operating in the frequency range 15.4-15.7 GHz are the same as the protection criteria of DAA radars operating under the same ARNS allocation (see § A2.2.1.3).

A2.3 Systems operating in the fixed satellite service (Earth-to-space) in the frequency band 15.43-15.63 GHz

The frequency band 15.43-15.63 GHz is globally allocated to the FSS (Earth-to-space) on a primary basis. The usage of the band is limited to the feeder links of non-GSO MSS systems as per RR No. **5.511A**.

A2.3.1 Technical and operational characteristics

The technical and operational characteristics of non-GSO FSS (Earth-to-space) satellites using the frequency band 15.43-15.63 GHz are provided in Table A2-6.

TABLE A2-6

Technical and operational characteristics of non-GSO systems operating in the FSS (Earth-to-space) in the frequency band 15.43-15.63 GHz

Characteristics	Notation	Units	Value
Altitude AGL	–	km	400 to 2 000 (1)
Centre frequency		MHz	15 530
Carrier BW			200
Beam characteristics	–		Single circular beam
Antenna pointing			Any point at the surface of the Earth within the footprint of the satellite (2)
IF BW	B	MHz	1
Receiver noise temperature	T	K	600

(1) This is the range of altitude values for a low Earth orbit (LEO) satellite.

(2) The footprint is assumed to be composed of all the points at the surface of the Earth that are visible (with sufficient elevation above the local horizon) from the satellite.

A2.3.2 Antenna characteristics

The characteristics of antennas installed on-board FSS (Earth-to-space) satellites operating in the frequency range 15.43-15.63 GHz are provided in Table A2-7.

TABLE A2-7

Antenna characteristics of a typical non-GSO systems operating in the FSS (Earth-to-space) in the frequency band 15.43-15.63 GHz (three carriers considered)

Characteristics	Notation	Units	Value		
Carrier	–		1	2	3
Diameter	D	m	1.2	1.8	2.4
HPBW	$2\psi_b$	degree	1.3	0.75	0.56
Aperture efficiency(1)	e_A	∅	0.6		
Peak gain(2)	$G_{\max}$	dBi	43.6	47.1	49.6
Major axis/Minor axis for the radiated beam(3)	z	∅	1		
Near-in-side-lobe level relative to the peak gain	L_N	dB	−25		
Far side-lobe level	L_F		0		

(1) Typical aperture efficiency values for a parabolic antenna range from 0.55 to 0.7.

(2) The peak gain $G_{\max}$ of a parabolic antenna is computed from the diameter D of the antenna, the aperture efficiency e_A, and the frequency f according to equation (A1-6) in Attachment B to Annex 1.

(3) This ratio equals 1 because the beam is supposed circular.

The pattern is rotationally symmetrical around the main beam direction and is described using equation (A2-1), which is an extract of *recommends* 1 in Recommendation ITU-R S.672-4:

$$G(\psi) = \begin{cases} G_{\max} & \text{for } 0° \le \psi \le \psi_b \text{ [15]} \\ G_{\max} - 3(\psi/\psi_b)^{\alpha} & \text{for } \psi_b \le \psi \le a \cdot \psi_b \\ G_{\max} + L_N + 20\log_{10}(z) & \text{for } a \cdot \psi_b < \psi \le 0.5b \cdot \psi_b \\ G_{\max} + L_N & \text{for } 0.5b \cdot \psi_b < \psi \le b \cdot \psi_b \\ X - 25\log_{10}(\psi) & \text{for } b \cdot \psi_b < \psi \le Y \\ L_F & \text{for } Y < \psi \le 90° \\ L_B & \text{for } 90° < \psi \le 180° \end{cases} \quad \text{(A2-1)}$$

where:

$$X = G_{\max} + L_N + 25\log(b\psi_b) \text{ and } Y = b\psi_b 10^{0.04(G_{\max}+L_N-L_F)}$$

ψ: off-axis angle (degree) with respect to the direction of peak gain

$G(\psi)$: gain (dBi) of the antenna at the off-axis angle ψ

L_B: constant (dBi) defined in equation (A2-2):

$$L_B = \max(0; 15 + L_N + 0.25G_{\max} + 5\log_{10}(z)) \quad \text{(A2-2)}$$

$\left.\begin{array}{l} \alpha = 2.58 \\ b = 6.32 \\ \alpha = 2 \end{array}\right\}$ as per Table 1 in Recommendation ITU-R S.672-4.

The constants G_{max}, ψ_b, L_N, z and L_F are defined in Table A2-7. Note also that Recommendation ITU-R S.672-4 provides a typical radiation pattern for parabolic dish antennas installed on-board GSO satellites. By extension, it is assumed usable for non-GSO satellites. Figure A2-3 shows a graphical representation of the radiation pattern associated to carrier 1 in Table A2-7.

FIGURE A2-3

Radiation pattern of the antenna installed on board a non-GSO systems operating in the FSS (Earth-to-space) in the frequency band 15.43-15.63 GHz in FSS (Earth-to-space) (parameters of carrier 1)

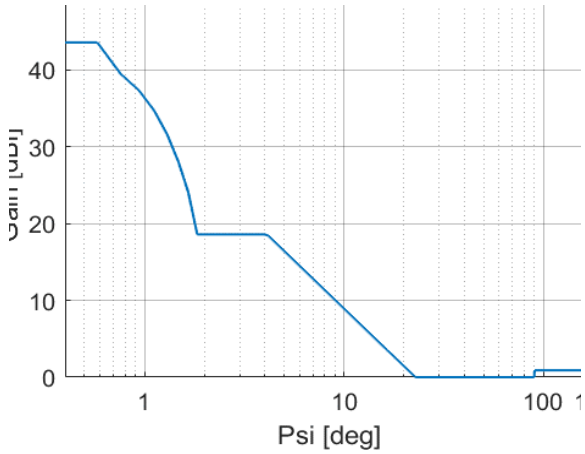

[15] Note that Recommendation ITU-R S.672-4 does not explicitly define the radiation pattern inside the main beam i.e. for absolute values of ψ below ψ_b. Therefore, equation (A8-1) made the assumption that the gain value inside the main beam simply assumed equals the peak gain. This is a worst-case assumption for coexistence studies where the FSS (Earth-to-space) is the Interfered-With System/Service (IWS).

A2.3.3 Protection criteria

The protection criterion of FSS (Earth-to-space) satellite receiver operating in the frequency range 15.43-15.63 GHz is expressed in terms of desensitization. In the presence of one or multiple interferers, the statistical distribution of the total aggregate unwanted power I at the FSS (Earth-to-space) receiver should meet the conditions expressed in equation (A2-3):

$$I/N \leq \begin{cases} -10.5 \text{ dB} & \text{for } 80\% \text{ of the time} \\ -6 \text{ dB} & \text{for } 99.4\% \text{ of the time} \\ 0 \text{ dB} & \text{for } 99.98\% \text{ of the time} \end{cases} \quad \text{(A2-3)}$$

where:

N: system receiver noise (dBm).

The system receiver noise N (dBm) is computed using equation (A2-4):

$$N = 10\log_{10}(\text{kTB}) + 30 \quad \text{(A2-4)}$$

where:

k: Boltzmann's constant $\left(\text{k} = 1.38 \cdot 10^{-23} \text{ W} \cdot \text{s}/\text{K}\right)$.

The constants T and B are defined in Table A2-7.

A2.4 Systems operating in the RAS in the frequency bands 15.35-15.4 GHz and 22.21-22.5 GHz

The frequency bands 15.35-15.4 GHz and 22.21-22.5 GHz are globally allocated to the RAS on a primary basis.

A2.4.1 Technical and operational characteristics

A list of the major RAS stations in the world operating in the frequency bands 15.35-15.4 GHz and 22.21-22.5 GHz is provided in Table A2-8. Note that, in the cases where radio observatories comprise several antennas, the characteristics are provided for a single antenna. Also note that the impact of future non-safety AM(OR)S systems planned to operate in the adjacent band 15.4-15.7 GHz and 22-22.21 GHz is only assessed in terms of unwanted emissions falling into the RAS operating bands 15.35-15.4 GHz and 22.21-22.5 GHz. In that regard, it is assumed that RAS receivers are equipped with perfect selectivity masks, which is a common assumption.

TABLE A2-8

Technical and operational characteristics of the major radio astronomy stations operating in the frequency bands 15.35-15.4 GHz and 22.21-22.5 GHz

			Antenna characteristics					
	Geodetic coordinates	**Height AMSL**	**Number**	**Diameter**	**Peak gain (1) (2)**	**HPBW (1) (2)**	**Efficiency(3)**	**Elevation range (4)**
Notation	**-**			D	G_0	$2\varphi_0$	η	–
Units	**degree**	**m**	Ø	**m**	**dBi**	**degree**	Ø	**degree**
Effelsberg	50.52472° N 6.884167° E	369	1	100	82.6 | 85.8	.0068 | .0046	0.7	5 to 90
MeerKAT	30.72111° S 21.41111° E	1 054	64	13.5	84 | 87	.0068 | .0046	0.7	5 to 90

TABLE A2-8 (*end*)

			Antenna characteristics					
Green Bank Telescope (GBT)	38.43306° N 79.83972° W	250	1	100	82.6 | 85.8	.0068 | .0046	0.7	5 to 90
Jansky VLA	33.97278° N 107.4111° W to 34.24889° N 107.8061° W	2 000	27	25	84 | 87	.0106 | .0073	0.7	5 to 90
Parkes	33.0000° S 148.2622° E	372	1	64	78.7 | 82	.0104 | .0073	0.7	5 to 90
Tianma	31.08694° N 121.1633° E	5	1	65	78.8 | 82.1	.0104 | .0071	0.7	5 to 90
Nobeyama	35.94444° N 138.4725° E	1 350	1	45	75.6 | 78.9	.0150 | .0103	0.7	5 to 90
Plateau de Bure	44.63389° N 5.924583° E	2 250	12	15	84 | 87	.0150 | .0103	0.7	5 to 90

(1) The peak gain and the HPBW of the antenna are calculated from the diameter and the aperture efficiency using equation (A2-6). The peak gain of antennas using a phased array is taken from Rec.n ITU-R RA.1631-0 *recommends* 3.

(2) The two values indicated in this column correspond to the frequency bands 15.35-15.4 and 22.21-22.5 GHz, respectively.

(3) In the absence of other information, a default antenna efficiency of 0.7 is chosen for all RAS antennas, in accordance with Report ITU-R RA.2188-0.

(4) According to section 7.5.1 of the Handbook On Radio Astronomy, “Radio telescopes can cover the sky down to about a 5° elevation angle.” In absence of other data, this value of 5° will be assumed as a minimum elevation angle for all the referenced RAS stations.

A2.4.2 Antenna characteristics

Compatibility studies with RAS often assume a constant gain of 0 dBi for the antenna used at the observatory. This is because interference signals are in most cases received through the side lobes of the antenna and not through the main beam. While being a valid assumption for interferers located on the ground, this no longer holds when considering airborne stations which, due to their high altitude, can also send parasitic emission through the main lobe of the RAS antenna.

Therefore, it is necessary to consider the complete radiation pattern rather than the envelope. As stated in section 1.3 of Recommendation ITU-R RA.769-2, the reference radiation pattern for RAS antennas is given in Recommendation ITU-R SA.509-3. This model considers both an average and a peak level. The peak level should be chosen when assessing the interference potential of a single interferer towards the RAS station. In cases where the aggregate interference from multiple sources is assessed, the average pattern should be preferred, which is the case in all the compatibility studies performed in this Report. The average radiation pattern provided in Recommendation ITU-R SA.509-3 (see equation (A2-5)) is rotationally symmetrical around the direction of maximum gain.

$$G(\varphi) = \begin{cases} G_0 - 3(\varphi/\varphi_0)^2 & \text{for } 0° \le \varphi < \varphi_1 \\ G_0 - 20 & \text{for } \varphi_1 \le \varphi < \varphi_2 \\ G_0 - 25\log_{10}(\varphi) & \text{for } \varphi_2 \le \varphi < 48° \\ -13 & \text{for } 48° \le \varphi < 80° \\ -8 & \text{for } 80° \le \varphi < 120° \\ -13 & \text{for } 120° \le \varphi \le 180° \end{cases} \quad \text{(A2-5)}$$

where:

G_0: peak gain of the antenna (dBi)

φ_0: half of the HPBW of the antenna (degree)

φ_1: $\varphi_0\sqrt{17/3}$ (degree)

φ_2: $10^{(49-G_0)/25}$ (degree).

In cases where a single interferer is considered, the constants 20, 13 and 8 in equation (A2-5) should be replaced by 17, 10 and 5, respectively.

If the peak gain G_0 and the HPBW φ_0 of the RAS antenna are not available, they can be evaluated using equation (A2-6), extracted from *recommends* 1.3 of Recommendation ITU-R SA.509-3. Note that equation (A2-6) was used to compute the peak gain and the HPBW of the major RAS sites listed in Table A2-8, which were not part of the original set of specifications.

$$\begin{cases} G_0 = 10 \cdot \log_{10}\left[\eta\left(\frac{\pi \cdot D}{\lambda}\right)^2\right] \\ \varphi_0 = \frac{20\sqrt{3}}{D/\lambda} \end{cases} \quad \text{(A2-6)}$$

where:

η: Aperture efficiency (∅) of the antenna

D: Diameter of the antenna (m)

λ: Wavelength (m).

FIGURE A2-4

Radiation pattern of the RAS in Effelsberg (Germany), measurement band 15.35-15.4 GHz

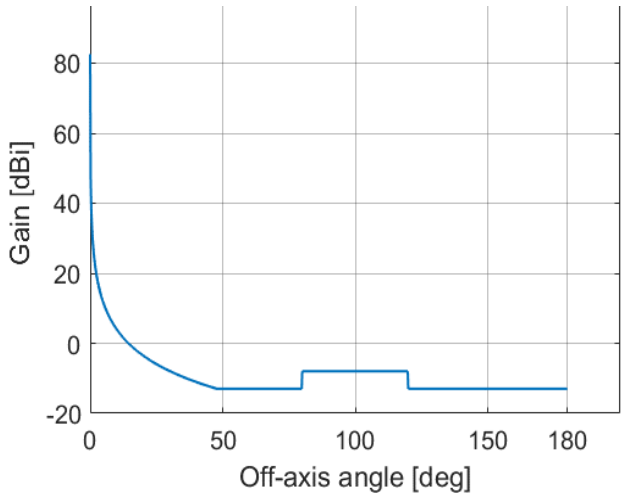

As an example, Fig. A2-4 above shows the antenna pattern of the RAS station in Effelsberg (Germany).

A2.4.3 Protection criteria

Due to unwanted emissions falling in the frequency bands allocated to the RAS, active services can potentially interfere with RAS stations by degrading the sensitivity of measurements.

Recommendation ITU-R RA.769-2 has computed the detrimental levels of interference power at the receiver's input that degrade the sensitivity of RAS measurements to an unacceptable level. An extract of Table 1 in Recommendation ITU-R RA.769-2 is provided in Table A2-9 for the frequency bands 15.35-15.4 GHz and 22.21-22.5 GHz. Two types of measurements are considered: Continuum Observations (CO) and Spectral Line Observations (SLO).

The same methodology is used to determine the protection criteria of RAS stations operating in the frequency band 22.21-22.5 GHz. However, in this frequency band, contrary to the band 15.35-15.4 GHz, Recommendation ITU-R RA.769-2 mentions both CO and SLO.

Recommendation ITU-R RA.1513-2 further provides the maximum percentage of data that can be corrupted due to the interference of other services in *recommends* 1 and 2:

> "1 […] for the evaluation of interference, a criterion of 5% be used for the aggregate data loss to the *RAS* due to interference from all other networks, in any frequency band allocated to the *RAS* on a primary basis […]"
>
> "2 that, for evaluation of interference, a criterion of 2% be used for data loss to the *RAS* due to interference from any one network, in any frequency band, which is allocated to the *RAS* on a primary basis".

The term "data loss" must be understood as the result of erroneous measurements due to interference with active services. Hence, at most 2% of the measurements can be lost because of interference with one active service (at most 5% if all active services susceptible to interfere with RAS measurements are considered). Note that a measurement consists in a 2 000-s[16] integration time with a fixed pointing of the RAS antenna.

[16] The measurement duration depends on various factors, but CO made with single antennas are well represented by a 2 000-s integration time. See section 1.2 in Recommendation ITU-R RA.769-2.

TABLE A2-9

Detrimental interference thresholds for continuous observation and spectral line observation radio astronomy measurements in the frequency bands 15.35-15.4 GHz and 22.21-22.5 GHz

	Centre frequency	Assumed BW	Minimum antenna noise temperature	Receiver noise temperature	System sensitivity (noise fluctuations)		Threshold interference levels		
					Temperature	PSD	Input power	Pfd	Spectral pfd
Notation	f_c	Δf	T_A	T_R	ΔT	ΔP	ΔP_H	$S_H \Delta f$	S_H
Units	MHz		K		mK	dB(W/Hz)	dBm	dB(W/m^2)	dB(W/(m^2 · Hz))
Value	15 375 CO	50	15	15	0.095	–269	–172	–156	–233
	22355 CO	290	35	30	0.085	–269	–165	–146	–231
	22200 SLO	0.25	35	30	2.91	–254	–190	–162	–216

A2.5 Systems operating in the Earth exploration satellite service (passive) in the frequency bands 15.35-15.4 GHz and 22.21-22.5 GHz

The frequency band 15.35-15.4 GHz and 22.21-22.5 GHz are globally allocated to the EESS (passive) on a primary basis. However, Working Party 7C cannot confirm any use of the band 15.35-15.4 GHz by passive sensors of the EESS (passive) nor provide any technical and operational characteristics. On the contrary, the band 22.21-22.5 GHz is globally allocated to the EESS (passive) on a primary basis. Space borne passive sensors are used in this frequency band to collect radiometric data on water vapour content.

A2.5.1 Technical and operational characteristics

Technical and operational characteristics of EESS (passive) sensors operating in the frequency band 22.21-22.5 GHz are provided in Recommendation ITU-R RS.1861-1. This Recommendation was in revision at the time of writing this Report. Table A2-10 contains the characteristics of a typical EESS (passive) sensor as included in the latest available version of the working document towards a preliminary draft revision of Recommendation ITU-R RS.1861-1.

TABLE A2-10

Technical and operational characteristics of space borne sensors operating in the EESS (passive) in the frequency band 22.21-22.5 GHz

Parameters	Notation	Units	Values
Sensor type	–		Conical
Orbit parameters			
Altitude AGL	–	km	833
Inclination		degree	98.6
Eccentricity		∅	0
Repeat period		day	25
Antenna parameters of the sensor			
Number of beams	–		1
Antenna size	D	m	0.61
Peak gain	$G_{\max}$	dBi	40.0
Polarization	–	-	vertical

TABLE A2-10 (*end*)

Parameters	Notation	Units	Values
Maximum HPBW		degree	2.09
Instantaneous field of view		km	46.5 × 73.6 (footprint size due to 1 × 2 averaging)
Off-nadir pointing angle		degree	45
Incidence angle at Earth			53.1
Swath width		km	1707
Antenna efficiency	η	∅	0.50
Beam dynamics	–	s	1.9
Sensor antenna pattern		-	Rec. ITU-R RS.1813-1
Total Field of View (FOV) cross/along-track		km	Effective field of view (EFOV): 44.8 (along scan) × 73.6 (90° to scan); 1 × 2 spatial averaging
Sensor receiver parameters			
Sensor integration time	–	ms	4.22 (for a single unaveraged sample)
Channel BW		MHz	290
Horizontal resolution		km	73.6
Vertical resolution			46.5

A2.5.2 Antenna characteristics

The antenna characteristics of the sensor R1 presented in Table A4-5 is given in Recommendation ITU-R RS.1813-1, and highlighted in equation (A2-7). Note that this equation corresponds to the average antenna pattern i.e. *recommends* 1 of Recommendation ITU-R RS.1813-1, which is applicable when no source of interference dominates over the others.

$$G(\varphi) = \begin{cases} G_{max} - 1.8 \cdot 10^{-3}\left(\frac{D}{\lambda}\varphi\right)^2 & \text{for } 0° \le \varphi \le \varphi_m \\ \max\left(\begin{matrix} G_{max} - 1.8 \cdot 10^{-3}\left(\frac{D}{\lambda}\varphi\right)^2; \\ 33 - 5\log_{10}\left(\frac{D}{\lambda}\right) - 25\log_{10}(\varphi) \end{matrix}\right) & \text{for } \varphi_m < \varphi \le 69° \\ -13 - 5 \cdot \log_{10}\left(\frac{D}{\lambda}\right) & \text{for } 69° < \varphi \le 180° \end{cases} \quad \text{(A2-7)}$$

where:

G_{max}: peak gain (dBi) of the antenna

D: antenna diameter (m)

φ: off-axis angle (deg.) from the direction of peak gain

λ: wavelength (m)

φ_m: breakpoint defined in equation (A2-8):

$$\varphi_m = \frac{22\lambda}{D}\sqrt{5.5 + 5\log_{10}\left(\frac{D}{\lambda}\eta^2\right)} \quad \text{(A2-8)}$$

where:

η: antenna efficiency (Ø).

Note that a floor value of −23 dBi is to be used when equation (A2-7) yields a smaller value than −23 dBi. A graphical representation of the complete radiation pattern associated to the sensor S1 is provided in Fig. A2-5.

FIGURE A2-5

Radiation pattern of a typical sensor (sensor S1) operating in EESS in the frequency band 22.21-22.5 GHz

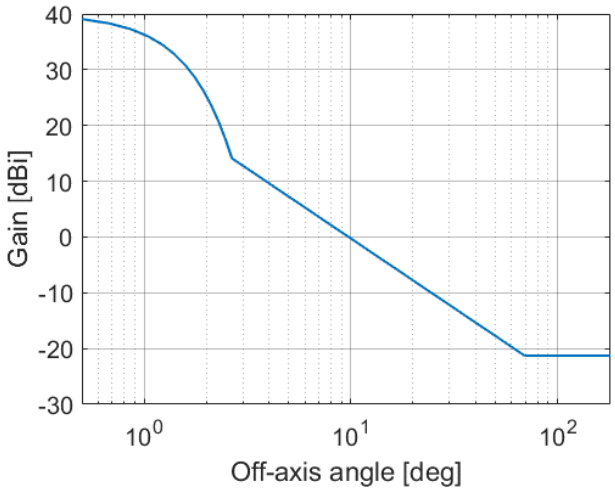

A2.5.3 Protection criteria

The detrimental interference level for passive EESS sensors operating in the frequency band 22.21-22.5 GHz is taken from Table 2 in Recommendation ITU-R RS.2017-0 and equals to −139 dBm/100 MHz, which is equivalent to −134.4 dBm over a channel bandwidth of 290 MHz. This detrimental interference level should not be exceeded for more than 0.1% of the time.

A2.6 Systems operating in the SRS (passive) in the frequency bands 15.35-15.4 GHz and 22.21-22.5 GHz

The frequency bands 15.35-15.4 GHz and 22.21-22.5 GHz are globally allocated to the SRS (passive) on a primary basis. However, WP 7C cannot confirm any use of the band by passive sensors of the SRS (passive) nor provide any technical and operational characteristics.

A2.7 Systems operating in the fixed service in the frequency range 21.2-23.6 GHz

The frequency range 21.2-23.6 GHz is globally allocated to the FS on a primary basis.

A2.7.1 Technical and operational characteristics

Technical and operational parameters of typical PTP FS systems operating in the frequency band 21.2-23.6 GHz are extracted from Table 9 of Recommendation ITU-R F.758-7 and shown in Table A2-11 for reference. In Iran, a total of 32 FS stations operating in the frequency range 21.2-23.6 GHz have been registered to the Master of International Frequency Register (MIFR).

TABLE A2-11

Technical and operational characteristics of point-to-point systems operating in the fixed service in the frequency band 21.2-23.6 GHz

Parameters	Units	Values	
Height above ground	m	10, 50	
Transmitter			
Modulation	–	FSK	128-QAM
e.i.r.p. density range	dBW/MHz	7.8 to 10.8	…
Receiver			
Frequency range	GHz	21.2-23.6	
Channel spacing and receiver noise BW	MHz	25	30
NF	dB	11	6
Feeder/multiplexer loss range	dB	0 to 3	…
PSD of receiver noise	dBW/MHz	−133	−138
Normalized Rx input level for 1×10^{-6} BER(1)		−119.6	−108.5
Nominal long-term interference PSD		−133 + *I*/*N*	−138 + *I*/*N*
Antenna gain	dBi	34.8	34.8 (2)
Antenna elevation from the local horizon(3)	degrees	−5 to +5	

(1) BER – Bit error rate.

(2) The antenna gain of FS stations using 128-QAM modulation is not provided in Rec. ITU-R F.758-7 and therefore assumed to be the same as the gain of stations using FSK modulation.

(3) The elevation angle of FS stations operating in the frequency band 21.4-23.6 GHz is assumed to be 0 degree, which is the assumption made in Report ITU-R M.2230-0 that addresses sharing issues between UA transmitters and FS in the frequency range 21.4-23.6 GHz. However, to account for a broader range of configurations, it is assumed that the elevation angle may vary between −5 and 5 degrees.

A2.7.2 Antenna characteristics

Several radiation patterns can be used to model the antenna characteristics of fixed stations in the frequency range 21.2-23.6 GHz, including:

– Recommendation ITU-R F.699-8 is used in single-entry interference analyses;

– Recommendations ITU-R F.1245-3 and ITU-R F.1336-5 provide average side-lobe patterns models that are relevant the FS station receives power from multiple interference sources. Recommendation ITU-R F.1245-3 has been taken as a basis in this Report.

The ratio D/λ, where D denotes the antenna diameter and λ, the wavelength, is used as an input parameter for Recommendation ITU-R F.1245-3. However, Recommendation ITU-R F.758-7 does not provide any information regarding the size of antennas used in FS stations. Nevertheless, D/λ can be evaluated using equation (A2-9), which is an extract from Recommendation ITU-R F.1245-3:

$$\frac{D}{\lambda} \approx (10^{G_{max} - 7.7})^{\frac{1}{20}} \quad \text{(A2-9)}$$

where:

G_{max}: peak gain of the antenna (dBi).

As $G_{max} = 34.8$ dBi from Table A2-11, it follows that $D/\lambda = 22.6$ and therefore the antenna gain $G(\varphi)$ is calculated using *recommends* 2.2.1) in Recommendation ITU-R F.1245-3, see equation (A2-10).

$$G(\varphi) = \begin{cases} G_{max} - 2.5 \cdot 10^{-3} \left(\frac{D}{\lambda}\varphi\right)^2 & \text{for } 0° < \varphi < \varphi_m \\ 39 - 5 \cdot \log_{10}\left(\frac{D}{\lambda}\right) - 25 \cdot \log_{10}(\varphi) & \text{for } \varphi_m \leq \varphi < 48° \\ -3 - 5 \cdot \log_{10}\left(\frac{D}{\lambda}\right) & \text{for } 48° \leq \varphi \leq 180° \end{cases} \quad \text{(A2-10)}$$

where:

φ: off-axis angle (deg)

φ_m: breakpoint computed according to equation (A2-11):

$$\varphi_m = \frac{20\lambda}{D}\sqrt{G_{max} - G_1} \quad \text{(A2-11)}$$

where:

G_1: gain of the first side-lobe computed using equation (A2-12):

$$G_1 = 2 + 15 \cdot \log_{10}\left(\frac{D}{\lambda}\right) \quad \text{(A2-12)}$$

A graphical representation of the radiation pattern is provided in Fig. A2-6.

FIGURE A2-6

Radiation pattern of a fixed station operating in the frequency range 21.2-23.6 GHz, using frequency shift keying modulation (see Table A2-11)

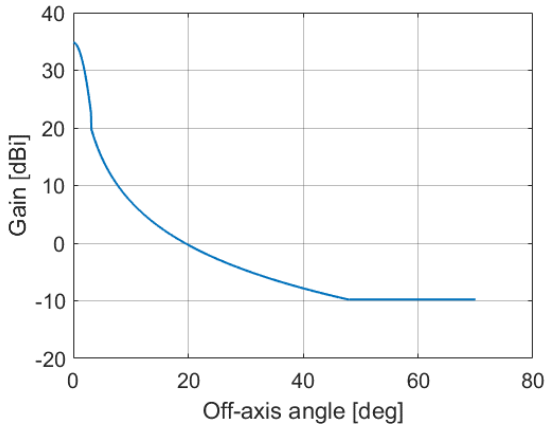

A2.7.3 Long-term protection criteria

The long-term protection criterion of FS to be used in sharing and compatibility studies is $I/N = -10$ dB as specified in Recommendation ITU-R F.758-7 Table 5, which may not be exceeded for more than 20% of the time. In this criterion, I denotes the aggregate interference power at the FS station receiver, and N, the receiver noise power, computed according to the equation (A2-13):

$$N = N_{RX} + 10 \cdot \log_{10}(B) \quad \text{(A2-13)}$$

where:

N_{RX}: Receiver noise power spectral density (dBm/MHz)

B: Receiver Noise bandwidth (MHz).

Typical values used for NRX and B are taken from Table A2-11: $NRX = -133$ dBW/MHz, $B = 25$ MHz.

A2.7.4 Short-term protection criteria

The derivation of short-term protection criteria for the FS is based on the methodology laid out in Annex 1 of Recommendation ITU-R F.1495-2, and described in the following steps:

– The impact of interference onto FS stations is usually accounted for in analysing both the degradation of the Availability Performance Objective (APO) and the Error Performance Objective (EPO). However, the interference produced by AM(OR)S transmitters is fast-varying, as compared to a situation where the interferer would be for instance a GSO satellite. It follows that the predominating effect is the degradation of the EPO. It is further assumed that if the EPO is fulfilled, the APO is also achieved.

– The Fade Margin (FM) of a fixed link operating in the frequency band 21.2-23.6 GHz is computed in Table A2-12 for different values of the BER, the ESR and the SESR;

TABLE A2-12

Computation of the fade margin of a fixed link operating in the frequency range 21.2-23.6 GHz

Parameters	Error metrics	Units	Values
e.i.r.p. (expressed in PSD)	$\underline{\text{BER} = 1 \cdot 10^{-6}}$	dBW/MHz	9.3(1)
Receiver nominal power level (expressed in PSD)	$\underline{\text{BER} = 1 \cdot 10^{-6}}$	dBW/MHz	−119.6(2)
Assumed link length	-	km	10(3)
PL calculated according to Rec. ITU-R P.452-17	-	dB	141.1(4)
FM	$\underline{\text{BER} = 1 \cdot 10^{-6}}$	dB	22.6(5)
FM	$\underline{\text{BER} = 4.8 \cdot 10^{-4}}$	dB	19.6(6)
FM	$\underline{\text{BER} = 1.28 \cdot 10^{-5}}$	dB	21.6(7)
FM	$\underline{\text{ESR} = 4.8 \cdot 10^{-4}}$	dB	**14.6**(8)
FM	$\underline{\text{SESR} = 1.28 \cdot 10^{-5}}$	dB	**16.6**(8)

(1) This represents the average e.i.r.p. PSD for $\text{BER} = 1 \cdot 10^{-6}$ according to Table A2-11.

(2) This value is taken from Table A2-11.

(3) This represents the average length of a fixed link using the frequency band 21.2-23.6 GHz.

(4) In this calculation, it is assumed that both stations are 10 m above ground level, in accordance with Table A2-11.

(5) The FM of the fixed link in the case where $\text{BER} = 1 \cdot 10^{-6}$ is obtained using equation (A2-14) below:

$$FM = \text{EIRP} - \text{RX} - \text{PL} + \text{G}_{\max} \quad \text{(A2-14)}$$

where:

$EIRP$: e.i.r.p. density for $\underline{\text{BER} = 1 \cdot 10^{-6}}$

RX: normalized receiver input level density (dBm/MHz) for $\underline{\text{BER} = 1 \cdot 10^{-6}}$

PL : assumed PL between two FS stations installed 10 m above the ground and at a distance of 10 km.

$\text{G}_{\max}$: peak gain of the FS station.

(6) Using FSK modulation, the FM for $\underline{\text{BER} = 1 \cdot 10^{-6}}$ can be assumed to be 3 dB above the FM for $\underline{\text{BER} = 4.8 \cdot 10^{-4}}$ (see Fig. A2-7).

(7) Using FSK modulation, the FM for $\underline{\text{BER} = 1 \cdot 10^{-6}}$ can be assumed to be 1 dB above the FM for $\underline{\text{BER} = 1.28 \cdot 10^{-4}}$ (see Figure A2-7).

(8) Making the same assumption as in Annex 1 of Rec. ITU-R F.1495-2, the FM for a particular value of the ESR or SESR is 5 dB below the value of the FM for the same value of the BER.

– The allowable degradation of the EPO for a fixed link operating in the frequency band 21.2-23.6 GHz is taken from Recommendation ITU-R F.1565-1 and shown in Table A2-13. The following assumptions are made:

- the considered link is a short-haul inter-exchange network section of 10 km;
- the design is made according to Recommendation ITU-T G.826;
- a medium data rate of 15 to 55 Mbit/s is considered;
- the assumed value of B is 0.08. Indeed, as stated in *recommends* 3 of Recommendation ITU-R F.1565-1, "The value of *B* has provisionally been agreed to be in the range of 0.075 to 0.085". Recommendation ITU-R F.1495-2 has also assumed a value of 0.08;
- errors on a fixed link occur when the interference level rises above the noise level by more than the FM of the link. Therefore, the following apportionment (based on the apportionment proposed in Annex 1 to Recommendation ITU-R F.1495-2) of the EPO degradation is proposed:
  - 20% of the EPO degradation caused by long-term interference
  - 80% of the EPO degradation caused by short-term interference.

TABLE A2-13

Total allowable error performance objective degradation for a fixed link operating in the frequency range 21.2-23.6 GHz

	Total EPO degradation allowable to interference	**Total EPO degradation allowable to short-term interference**
ESR	$6 \cdot 10^{-4}$	$4.8 \cdot 10^{-4}$
SESR	$1.6 \cdot 10^{-5}$	$1.28 \cdot 10^{-4}$

FIGURE A2-7

Bit error rate vs signal to noise ratio for different variants of the frequency shift keying modulation

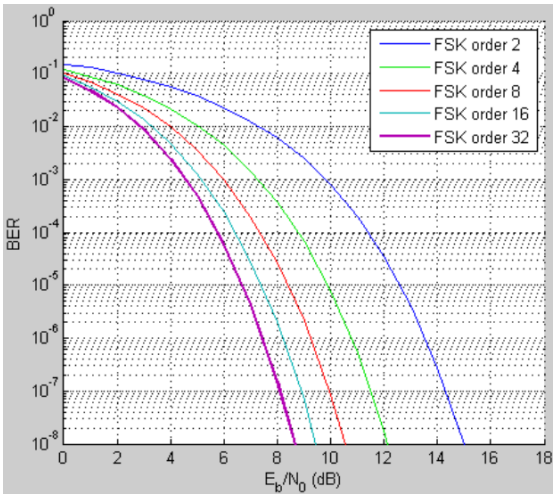

– The two short-term protection criteria are directly derived from the value of the FM for the ESR and SESR) values allowable to short-term interference ($4.8 \cdot 10^{-4}$ and $1.28 \cdot 10^{-5}$ respectively, see Table A2-13):

$$I/N \leq \begin{cases} 14.6 \text{ dB} & \text{for 99.952\% of the time} \\ 16.6 \text{ dB} & \text{for 99.9872\% of the time} \end{cases} \quad \text{(A2-15)}$$

A2.8 Systems operating in the land mobile service in the frequency range 21.4-22.5 GHz

The frequency band 21.4-22.5 GHz is globally allocated to the MS excluding International Mobile Telecommunications (IMT) on a primary basis. Working_Party 5A has identified Recommendation ITU-R M.1825-0 related to the LMS. However, this Recommendation does not provide any specific parameters related to the LMS in this frequency band.

A2.9 Systems operating in the broadcasting- satellite service in the frequency band 21.4-22 GHz

The frequency band 21.4-22 GHz is allocated to the BSS on a primary basis in Regions 1 and 3. This section describes the technical and operational characteristics, as well as antenna characteristics and protection criteria of the earth stations (ES) operating under this allocation.

A2.9.1 Technical and operational characteristics

Technical and operational characteristics of typical ES operating in the BSS in the frequency range 21.4-22 GHz are shown in Table A2-14.

TABLE A2-14

Technical and operational characteristics of an Earth station operating in the broadcasting-satellite service in the frequency band 21.4-22 GHz

Parameter	Notation	Units	Value				
Carrier	–		**1**	**2**	**3**	**4**	**5**
Minimum elevation angle	–	degree	10				
Altitude AGL[(1)]		m	2				
Noise BW	*B*	MHz	1				
System receive noise temperature	*T*	K	275	250		225	

[(1)] The altitude of BSS ES above the ground is arbitrarily chosen equal to 2 m, as this is the lower bound of the application range of Rec. ITU-R P.528-5, which is used to computed the PL between ADTs and BSS ES in sharing studies.

A2.9.2 Antenna characteristics

The radiation pattern of BSS ES proposed in this section is rotationally symmetric around the axis of the peak gain. The radiation pattern depends on the ratio between the antenna diameter *D* and the wavelength λ.

A2.9.2.1 Large antennas

For D/λ values larger than 50, Recommendation ITU-R S.580-6 provides equations for the envelope of the side-lobes. As explained in the Recommendation, the pattern inside the main beam of the antenna can be complemented with Appendix **7**, section 3.2.3, of the RR. In the same way, and the

pattern for high off-axis values is complemented by Recommendation ITU-R S.465-6. This final result is shown in equation (A2-16):

$$G(\varphi) = \begin{cases} G_{a,\max} - 0.0025\left(\frac{D}{\lambda}\cdot\varphi\right)^2 & \text{for } 0 \le \varphi < \varphi_1 \\ G_1 & \text{for } \varphi_1 \le \varphi < \varphi_2 \\ 29 - 25\cdot\log_{10}(\varphi) & \text{for } \varphi_2 \le \varphi < 48° \\ -3.5 & \text{for } 48° \le \varphi < 80° \\ 32 - 25\cdot\log_{10}(\varphi) & \text{for } 80° \le \varphi < 120° \\ -10 & \text{for } 120° \le \varphi \le 180° \end{cases} \quad \text{(A2-16)}$$

where:

φ: off-axis angle (deg.) from the direction of peak gain

$G(\varphi)$: gain of the antenna in the direction φ (dBi)

D: diameter (m) of the antenna

λ: wavelength (m) at the frequency 21.7 GHz

$G_{a,\max}$: peak gain (dBi) of the antenna

φ_1: breakpoint defined in equation (A2-17):

$$\varphi_1 = \frac{20\cdot\lambda}{D}\sqrt{G_{a,\max} - G_1} \quad \text{(A2-17)}$$

φ_2: breakpoint defined in equation (A2-18):

$$\varphi_{\min} = \max\left(1°; 100\frac{D}{\lambda}\right) \quad \text{(A2-18)}$$

G_1: gain value defined in equation (A2-19):

$$G_1 = 2 + 15\cdot\log_{10}\left(\frac{D}{\lambda}\right) \quad \text{(A2-19)}$$

A2.9.2.2 Small antennas

For D/λ values smaller than 50, Recommendation ITU-R S.465-6 applies. The gain inside the main beam is completed in the same way by equations taken from Appendix **7**, section 3.2.3, of the RR, which leads to equation (A2-20):

$$G(\varphi) = \begin{cases} G_{a,\max} - 0.0025\left(\frac{D}{\lambda}\cdot\varphi\right)^2 & \text{for } 0 \le \varphi < \varphi_1 \\ G_1 & \text{for } \varphi_1 \le \varphi < \varphi_2 \\ 32 - 25\cdot\log_{10}(\varphi) & \text{for } \varphi_2 \le \varphi < 48° \\ -10 & \text{for } 48° \le \varphi < 80° \end{cases} \quad \text{(A2-20)}$$

where:

φ_1: breakpoint given in equation (A2-21):

$$\varphi_1 = \max\left(2°; 114\left(\frac{D}{\lambda}\right)^{-1.09}\right) \quad \text{(A2-21)}$$

φ_2: breakpoint defined in equation (A2-17).

The parameters $G_{a,\max}$, D, λ are given in Table A2-15 for the five ES introduced in § A2.9.1. As an example, Fig. A2-8 shows the radiation pattern of the antenna associated to the BSS ES n° 1.

TABLE A2-15

Antenna parameters of five typical Earth stations operating in the BSS in the frequency band 21.4-22 GHz

Parameters	Notation	Units	Values				
Carrier	–		**1**	**2**	**3**	**4**	**5**
Antenna diameter	D	m	0.2	0.45	0.6	0.75	1.2
Wavelength	λ		0.0138				
Ratio D/λ	-		14.5	32.6	43.4	54.3	86.6
Peak gain	$G_{a,\max}$	dBi	31.7	38	41.3	43.2	47.3

FIGURE A2-8

Radiation pattern of the antenna associated to Earth station n°1 operating in the BSS

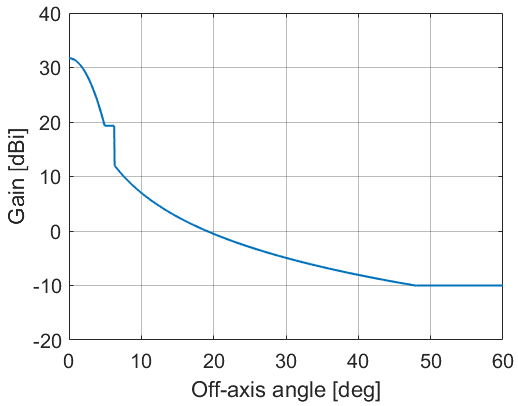

A2.9.3 Protection criteria

The protection criterion of ES receivers operating in the BSS in the frequency band 21.4-22 GHz is the same as the protection criterion of space stations operating in the FSS (Earth-to-space) in the band 15.43-15.63 GHz, which is given in § A2.3.3.

Note that the noise power *N* is computed according to equation (A2-22):

$$N = 10\log_{10}(kTB) + 90 \quad \text{(A2-22)}$$

where:

N: thermal noise (dBm) of the ES receiver

K: Boltzmann's constant $\left(k = 1.38 \cdot 10^{-23}\ W \cdot s/K\right)$

T: receive noise temperature (K)

B: noise BW (MHz).

Numerical values for *T* and the *B* are provided in Table A2-7 for the five BSS ES considered in this Report.

Attachment A
to Annex 2

Modelling of antennas used in radars operating in the radiolocation service in the frequency range 15.4-17.3 GHz

This Attachment provides a reference antenna pattern for RLS System 6 introduced in § A2.1.1, based on the methodology laid out in in section 2.1.3 of Recommendation ITU-R M.1851-1. Input parameters are taken from Recommendation ITU-R M.1730-1 and summarized in Table A2-16. Note that the average pattern is computed rather than the peak pattern because most of the sharing studies performed in this Report have considered the impact of multiple interferers onto RLS radars.

First, a theoretical value of the gain (denoted by $G_{\text{theoretical}}(\theta)$) is computed according to equation (A2-23).

$$G_{\text{theoretical}}(\theta) = F + 20 \cdot \log_{10}\left(\frac{\pi^2}{2\mu}\left[\frac{\cos(\mu)}{\left(\frac{\pi}{2}\right)^2 - \mu^2}\right]\right) \quad \text{(A2-23)}$$

where:

θ: off-axis angle (deg) measured from the main beam direction of the antenna

F: 6.02 dB, normalization constant

μ: parameter (1/deg) computed according to equation (A2-24):

$$\mu(\theta) = \frac{83.2 \cdot \pi \cdot \sin(\theta)}{\theta_3} \quad \text{(A2-24)}$$

where:

θ_3: HPBW (degree) (see Table A2-16).

Equation (A2-23) is applicable for values of θ between 0° and a breakpoint value θ_{bp} which is provided in Table 3 of Recommendation ITU-R M.1851-1. For a cosine square distribution, θ_{bp} is given in equation (A2-25):

$$G_{\text{theoretical}}(\theta_{bp}) = G_{\text{peak}} - 29 \quad \text{(A2-25)}$$

where:

G_{peak}: peak gain of the antenna (dBi) (see Table A2A-1).

The value of θ_{bp} can be determined by replacing $G_{\text{theoretical}}(\theta_{bp})$ in equation (A2-25) by its expression (using equation (A2-23)), and G_{peak} by its numerical value (using the data provided in Table A2A-1), resulting in equation (A2-26):

$$20 \cdot \log_{10}\left(\frac{\pi^2}{2 \cdot \mu}\left[\frac{\cos\left(\frac{83.2\,\pi \sin(\theta_{bp})}{\theta_3}\right)}{\left(\frac{\pi}{2}\right)^2 - \left(\frac{83.2\,\pi \sin(\theta_{bp})}{\theta_3}\right)^2}\right]\right) = -0.02 \quad \text{(A2-26)}$$

Equation (A2-26) can be solved numerically, which leads to $\theta_{bp} = 4.05°$.

For values of θ larger than θ_{bp}, the radiation pattern is given by equation (A2-27), that is taken from Table 3 of Recommendation ITU-R M.1851-1:

$$G_{\text{beyond bp}}(\theta) = -26.882 \cdot \ln\left(1.962 \cdot \frac{|\theta|}{\theta_3}\right) \quad \text{(A2-27)}$$

In equation (A2-27), *ln* denotes the natural logarithm function.

The floor level for this radiation pattern is taken from Table 3 of Recommendation ITU-R M.1851-1 and shown in equation (A2-28):

$$G_{\text{floor}} = G_{\text{peak}} - 60 \quad \text{(A2-28)}$$

A graphical representation of the complete radiation pattern is shown in Fig. A2-9.

TABLE A2-16

Input parameters for the computation of the radiation pattern of system-6 operating in the radiolocation service

Characteristics	Units	Value
Pattern type	-	Rec. ITU-R M.1851-1 cosine square distribution
Polarization		Linear
Peak gain	dBi	35
Vertical HPBW	degree	3.2
Horizontal HPBW		
1st side-lobe level	dBi	3.5 at 5.2°
Radar sweep		
Horizontal scan range	degree	±45 (electronic)
Vertical scan range		+5 to −45 (electronic)
Horizontal scan rate	degree/s	1 to 30
Vertical scan rate		1, 5

FIGURE A2-9

Radiation pattern of system-6 operating in the radiolocation service

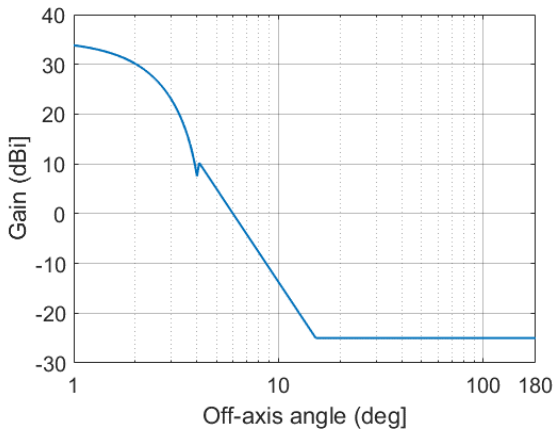

Attachment B
to Annex 2

Modelling of antennas used in the airborne receiver of automatic landing systems operating in the frequency range 15.4-15.7 GHz

The technical characteristics of the horn antenna associated to the airborne receiver of ALS systems described in § A2.2.2 are presented in Table A2-17. They are extracted from the ITU-R Recommendation mentioned in § A2.2 that describes ARNS systems operating in the frequency band 15.4-15.7 GHz.

To compute the complete radiation pattern of this antenna, the general information in Table A2B-1 is complemented by specific parameters shown in Table A2-18. These parameters have been chosen to match the characteristics of Table A2-17 with the best possible precision. Based on these characteristics, the peak gain of the antenna is computed in § A2B.1, and the radiation pattern in § A2B.2.

TABLE A2-17

Antenna characteristics of the airborne receiver of automatic landing systems operating in the frequency range 15.4-15.7 GHz

Parameter	Notation	Units	Value
Type	–		Horn
Placement			Bottom of aircraft
Peak gain	$G_{\max}$	dBi	6
First side lobe	–		>17 dB below peak
Horizontal HPBW		degree	70
Vertical HPBW			36
Polarization	–		Vertical

TABLE A2-18

Specific parameters of the horn antenna used by the airborne receiver of automatic landing systems operating in the frequency range 15.4-15.7 GHz

Parameter	Notation	Units	Value
Width of the aperture of the horn antenna	a	mm	27
Height of the aperture of the horn antenna	b		17
Length of the horn in the H-plane	R_H		70
Length of the horn in the E-plane	R_E		
Aperture efficiency	e_A	∅	0.265

A2B.1 Peak gain

The peak gain $G_{\max}$ of the horn antenna can be computed using equation (A2-29):

$$G_{\max} = 10 \cdot \log_{10}\left(\frac{4\pi \cdot e_A \cdot a \cdot b}{\lambda^2}\right) \quad \text{(A2-29)}$$

where:

e_A: aperture efficiency (Ø)

a, b: width and height (m) of the horn aperture (m)

λ: wavelength (m).

The numeric values assumed for the aperture efficiency, and the width and height of the aperture are provided in Table A2-18.

A2B.2 Radiation pattern

The normalized amplitude $E_A(\mathrm{x};\mathrm{y})$ of the electric field across the opening of the horn is computed using equation (A2-29):

$$E_A(\mathrm{x};\mathrm{y}) = \cos\left(\frac{\pi \cdot \mathrm{x}}{2}\right) \cdot e^{-\mathrm{j}\cdot\frac{\mathrm{k}}{2}\cdot\left(\frac{\mathrm{x}^2}{R_H}+\frac{\mathrm{y}^2}{R_E}\right)}, \qquad -\frac{a}{2} \le x \le +\frac{a}{2}, -\frac{b}{2} \le y \le +\frac{b}{2} \quad \text{(A2-29)}$$

where:

x, y: coordinates along the x- and y-axis (see Fig. A2-10)

j: complex number defined as $j = \sqrt{-1}$

k: wave number defined as $k = 2\pi/\lambda$

R_H, R_E: length (mm) of the horn along the a- and b-dimensions (see Table A2-18).

It follows that the electric field intensity $E(r;\theta;\varphi)$ is given in equation (A2-30):

$$E(r;\theta;\varphi) = \frac{k}{4\pi r}\left(1+\cos(\theta)\right)\int_{-\frac{b}{2}}^{+\frac{b}{2}}\int_{-\frac{a}{2}}^{+\frac{a}{2}} E_A(x;y)\cdot F(x;y;\theta;\varphi)\cdot dx\cdot dy \quad \text{(A2-30)}$$

$$\mathrm{F}(\mathrm{x};\mathrm{y};\theta;\varphi) = \exp\{jk(\mathrm{x}\cdot\sin(\theta)\cdot\cos(\varphi)+y\cdot\sin(\theta)\cdot\sin(\varphi))\}$$

where:

r: absolute distance (m) between the measurement point and the aperture centre

θ: elevation (deg) from the H-plane of the measurement point

φ: off-axis angle (deg) from the (yOz) plane of the measurement point.

The definition of the position parameters r, θ and φ is also shown in Fig. A2-10. The complete radiation pattern of the horn antenna is finally shown in Fig. A2-11.

FIGURE A2-10

Definition of the coordinate system and the dimensions of the horn antenna used for aircraft receivers of automatic landing systems

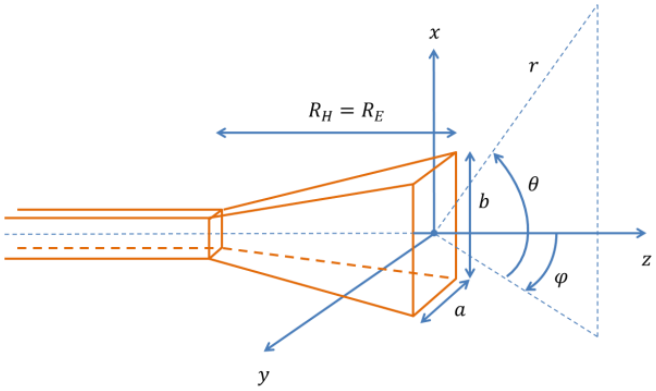

FIGURE A2-11

Horizontal and vertical radiation patterns of the horn antenna used for aircraft receivers of automatic landing systems

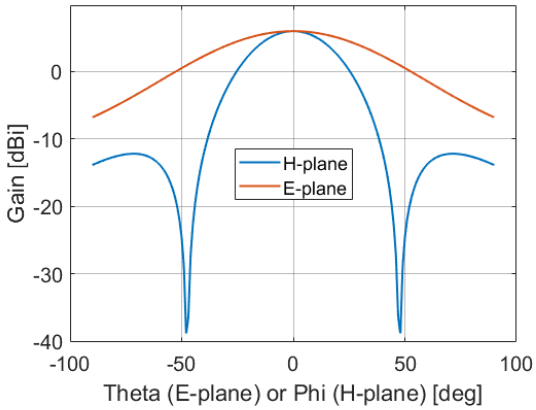

Annex 3

Sharing of the frequency range 15.4-15.7 GHz between radiolocation radars and future non-safety aeronautical mobile (off-route) service systems

TABLE OF CONTENTS

Page

The frequency range 15.4-17.3 GHz is globally allocated to the RLS on a primary basis. This Annex comprises three different studies that have studied the feasibility to share this frequency band with future non-safety AM(OR)S systems planned to operate in the sub-band 15.4-15.7 GHz.

A3.1 Study A

The analysis calculates the interference of AM(OR)S airborne systems 1, 2 and 3 of Table A1-1 to the RLS system. The protection criteria for the RLS is assumed to be $I/N = -6$ dB. The N value can be determined from Recommendation ITU-R M.1461-2. According to the characteristics of Table A2-1, it can be calculated that N is –95 dBm and I is –101 dBm.

Equation (A3-1) can be used to determine if interference to the RLS System 6 (see Table A3-1) receiver from AM(OR)S transmissions is likely to occur and what separation distance is required to eliminate the interference:

$$PL(F,R) = P_{Tx} + G_{Tx} + G_{Rx} - FRD_{IF} - (- 101) \quad \text{(A3-1)}$$

where:

P_{Tx}: power level (dBm) of the interfering system

G_{Tx}: antenna gain (dBi) of the interfering transmitter in the direction of the victim receiver. In this study, only the side-lobe gain of the AM(OR)S antenna is considered and assumed to be 0 dBi

G_{Rx}: antenna gain (dBi) of the victim receiver in the direction of the interfering transmitter. In this study, the peak gain and first side-lobe gain of the RLS antenna are considered

$PL(F,R)$: required propagation attenuation (dB) between transmitting and receiving antennas. In this study, the Recommendation ITU-R P.528-5 propagation model is used for A2A path with the 50% time percentage and different heights for the transmitting and receiving antennas

F: frequency (MHz)

R: required separation distance (km)

FRD_{IF}: frequency dependent rejection (dB) produced by the receiver IF selectivity curve on an unwanted transmitter emission spectrum.

The FDR_{IF} value can be determined from Recommendation ITU-R SM.337-6. Since the radars will operate on a co-frequency basis, only the on-tune rejection (OTR) is considered. OTR for non-coherent chirped pulsed signals is given by equation (A3-2):

$$\mathrm{OTR} = \begin{cases} 10\log_{10}\left({\mathrm{BW_{Tx}}}/{\mathrm{BW_{Rx}}}\right) & \text{for } \mathrm{BW_{Rx}} \le \mathrm{BW_{Tx}} \\ 0 & \text{otherwise} \end{cases} \quad \text{(A3-2)}$$

where:

BW_{Rx}: receiver bandwidth (MHz)

BW_{Tx}: transmitter bandwidth (MHz).

For example, when the transmitting BW are set to be 10, 150 and 200 MHz, the receiving BW to be 25 MHz, and if the transmitter and the receiver have the same centre frequency, FDR_{IF} *is* 0, 7.7 and 9 dB, respectively.

The required propagation attenuation between airborne AM(OR)S system and RLS receivers for different FDR values and different antenna configurations are summarized in Table A3-1.

TABLE A3-1

Required propagation attenuation in dB between systems operating in the aeronautical mobile (off-Route) service and receivers operating in the radiolocation service for different frequency dependent rejection values and different antenna configurations

	AM(OR)S airborne system		
	1	**2**	**3**
FDR = 0 dB			
RLS main lobe (1)	176	161	176
RLS 1st side-lobe (2)	144.5	129.5	144.5
FDR = 7.7 dB			
RLS main lobe	168.3	153.3	168.3
RLS 1st side-lobe	136.8	121.8	136.8
FDR = 9 dB			
RLS main lobe	167	152	167
RLS 1st side-lobe	135.5	120.5	135.5

(1) The peak gain of the RLS antenna is 35 dBi (see Table A2-16).

(2) The first side-lobe gain of the RLS antenna is 3.5 dBi (see Table A2-16).

The separation distances that are required to ensure sharing between the AM(OR)S system and the RLS system are summarized in Tables A3-2 and A3-3.

TABLE A3-2

Required separation distance in km between the airborne aeronautical mobile (off-route) service system and the radiolocation system

	System 1 (airborne)	System 2 (airborne)	System 3 (airborne)
10 000 m height for both the transmitting and receiving antennas			
FDR = 0 dB			
The main lobe of RLS	610	169	610
1st side-lobe level of RLS	26	4.6	26
FDR = 7.7 dB			
The main lobe of RLS	387	70	387
1st side-lobe level of RLS	10.7	1.9	10.7
FDR = 9 dB			
The main lobe of RLS	334	61	334
1st side-lobe level of RLS	9.2	1.6	9.2
5 000 m height for both the transmitting and receiving antennas			
FDR = 0 dB			
The main lobe of RLS	587	328	587
1st side-lobe level of RLS	29	6	29
FDR = 7.7 dB			
The main lobe of RLS	505	129	505
1st side-lobe level of RLS	14	2	14
FDR = 9 dB			
The main lobe of RLS	474	104	474
1st side-lobe level of RLS	12	2	12
3 000 m height for both the transmitting and receiving antennas			
FDR = 0 dB			
The main lobe of RLS	460	281	460
1st side-lobe level of RLS	29	6	29
FDR = 7.7 dB			
The main lobe of RLS	411	126	411
1st side-lobe level of RLS	13	2	13
FDR = 9 dB			
The main lobe of RLS	389	103	389
1st side-lobe level of RLS	12	2	12
1 000 m height for both the transmitting and receiving antennas			
FDR = 0 dB			
The main lobe of RLS	272	209	272
1st side-lobe level of RLS	41	5.3	41
FDR = 7.7 dB			
The main lobe of RLS	268	124	268
1st side-lobe level of RLS	14	3	14
FDR = 9 dB			
The main lobe of RLS	268	98	268
1st side-lobe level of RLS	14	2	14

TABLE A3-3

Required separation distance in km for the airborne aeronautical mobile service system interfering with the radiolocation system, when the heights for the transmitting and receiving antennas are different

	System 1 (airborne)	System 2 (airborne)	System 3 (airborne)
one is 5 000m and the other is 10 000m			
FDR = 0 dB			
The main lobe of RLS	701	355	701
1st side-lobe level of radiolocation system	35	3	35
FDR = 7.7 dB			
The main lobe of radiolocation system	567	141	567
1st side-lobe level of radiolocation system	14	0.1	14
FDR = 9 dB			
The main lobe of radiolocation system	529	122	529
1st side-lobe level of radiolocation system	12	0.1	12
one is 3 000 m and the other is 10 000 m			
FDR = 0 dB			
The main lobe of radiolocation system	638	332	638
1st side-lobe level of radiolocation system	34 km	0.1 km	34
FDR = 7.7 dB			
The main lobe of radiolocation system	513	137	513
1st side-lobe level of radiolocation system	13	0.1	13
FDR = 9 dB			
The main lobe of radiolocation system	482	119	482
1st side-lobe level of radiolocation system	11	0.1	11
one is 1 000 m and the other is 10 000 m			
FDR = 0 dB			
The main lobe of radiolocation system	542	300	542
1st side-lobe level of radiolocation system	32	0.1	32
FDR = 7.7 dB)			
The main lobe of radiolocation system	447	132	447
1st side-lobe level of radiolocation system	13	0.1	13
FDR = 9 dB			
The main lobe of radiolocation system	421	115	421
1st side-lobe level of radiolocation system	10	0.1	10

A3.2 Study B

A3.2.1 Methodology

Study B is a Monte Carlo analysis whose general methodology is laid out in Annex 11 to this Report.

A3.2.2 Results

Results are shown as the ECDF of aggregate *I*/*N* at the RLS receiver in Fig. A3-1A for the four operational scenarios introduced in § 6.2. The interference threshold of RLS (*I*/*N* < −6 dB as per § A2.1.3) is also as a vertical dotted line beside the ECDF plots. Fig. A3-1B shows that in the four considered scenarios, at least 99.999% of the 100 000 simulated snapshots resulted in an aggregate *I*/*N* value at the RLS receiver of less than −12 dB. Besides, the aggregate *I*/*N* value is lower than −50 dB for at least 99.6% of the snapshots in the four scenarios.

FIGURE A3-1A

Empirical cumulative distribution function of aggregate *I/N* at the receiver of the radio location service in the four operational scenarios described in § 6.2

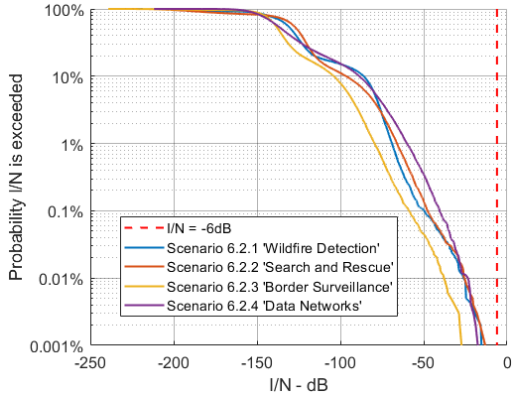

FIGURE A3-1B

Zoom of Fig. A3-1A around 0.1%

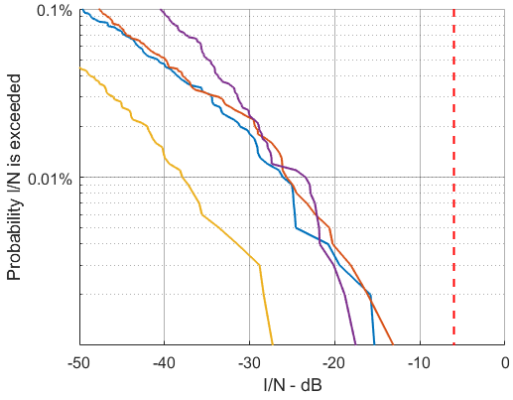

A3.2.3 Mitigation measures

In the cases where interference would occur at the RLS receiver i.e. during less than 0.001% of the time according to the previous section, some specific mitigation measures can be envisaged, further described in the sections below.

A3.2.3.1 Antenna dynamic null steering

This mitigation technique can be used by AM(OR)S systems using dynamically steered antenna arrays (for instance, Systems 1 and 3, see Table A1-2), in order to direct the nulls of the radiation pattern in the direction of the RLS radars when these can be properly detected. The effectiveness of this technique is further increased when large distances separate AM(OR)S systems from RLS radars, in which case the latter appear nearly motionless to the AM(OR)S transmitters. Also note that this technique could require in some circumstances a dynamic geographical reconfiguration of the clusters. Another possible implementation is sector blanking which consists for AM(OR)S stations to create a so-called cone of avoidance around RLS radars detected in the distance.

A3.2.3.2 Dynamic frequency selection

By sensing whether the different channels that they have at their disposal are idle or busy, AM(OR)S systems (and RLS radars) can avoid using channels that are determined to be occupied. This technique however implies that both systems can detect the waveform of each other. Note that this technique,

sometimes also known as sense and avoid (SSA), is also widely used between AM(OR)S systems themselves to cancel or reduce intra-system interference effects.

A3.2.3.3 Reconfiguration of clusters in the aeronautical mobile (off-route) service

The AM(OR)S operational scenarios presented in § 6.2 are flexible in terms of platform location. It means that the relative positioning of the AM(OR)S stations matters little as long as the mission data is transmitted error-free. For instance, in scenario 6.2.2, the central aircraft collecting the data from the different observation aircraft flies 2 600 m above them. In the case where the observation aircraft would detect RLS signals aligned with its own direction of transmission, the central aircraft could change its relative location to avoid interference. Also note in general AM(OR)S missions can tolerate transmission delays of several minutes in the case where real-time forwarding is not desired, for instance if an RLS radar is operating in the vicinity. In the case of scenario 6.2.2, the observation aircraft could first store the data and then forward it to the central aircraft at a later point in time.

A3.2.3.4 Automatic transmit power control adaptation

In the case where RLS transmissions are detected close by, AM(OR)S stations can adapt their ATPC algorithm described in § A11.6.1 to reduce interference, for example by decreasing the SNR target at the receiver, which in turn reduces the TPO. Note however that in this case, more transmission errors occur and therefore more retransmissions are necessary, which ultimately decreases the throughput of mission data.

A3.2.3.5 Signal processing

As explained in § A2.1.3, AM(OR)S signals appear noise-like to RLS receivers. It makes it possible for RLS radars to decrease the impact of AM(OR)S interference by raising the detection threshold.

A3.3 Study C

This section assesses sharing between a single cluster of AM(OR)S stations operating in the frequency band 15.4-15.7 GHz and an RLS system operating in the band 15.4-17.3 GHz. It determines minimum separation zones around the RLS receiver to meet the protection criterion $I/N = -6$ dB.

A3.3.1 Methodology

The study evaluates the aggregate I/N variable at the RLS receiver, and determines the required separation distance to meet the protection criterion. The impact of GDTs (if some are present in a given scenario, for instance 6.2.1 and 6.2.3) is not taken into account. The simulation setup is described in Table A3-3. Two different configurations are envisaged regarding the BW allocated to ADTs (configuration n° 1 and 2). Figures A3-1 through A3-4 depict the sharing scenarios between a single cluster of AM(OR)S and Radiolocation system.

FIGURE A3-2

Sharing study between systems operating in the aeronautical mobile (off-Route) service and radiolocation systems based on the wildfire observation scenario

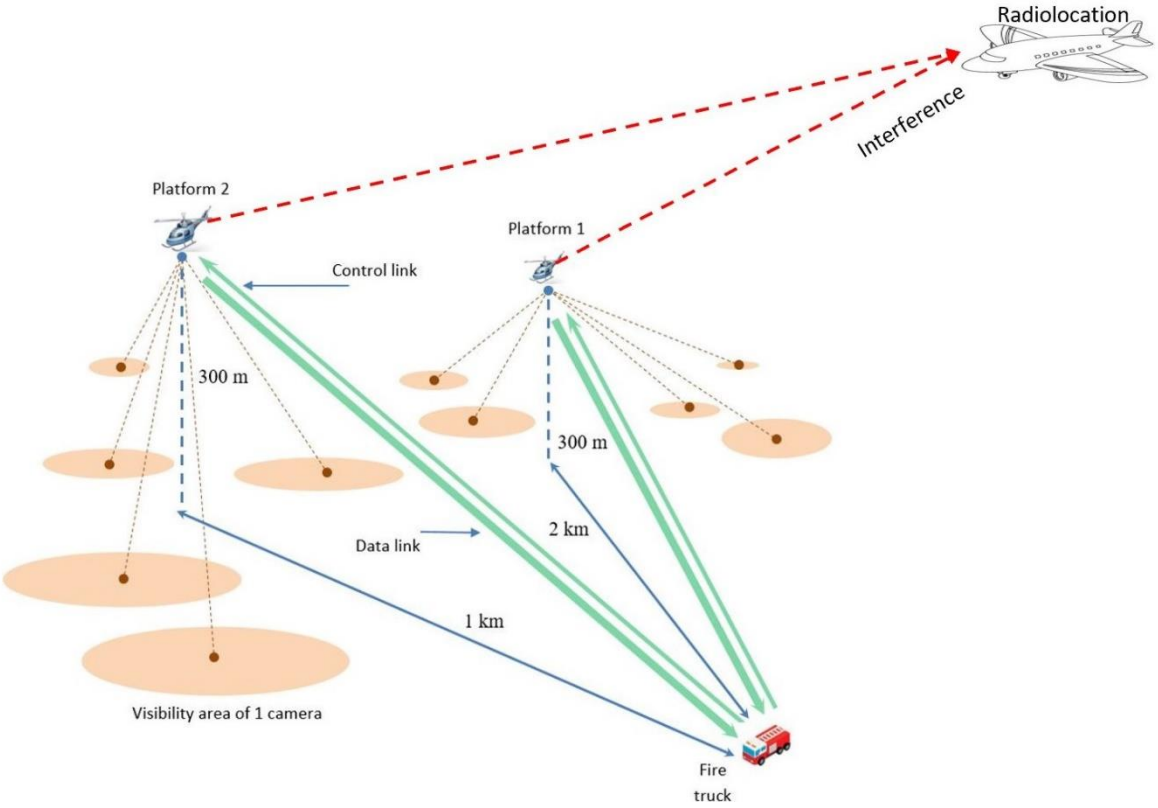

FIGURE A3-3

Sharing study between systems operating in the aeronautical mobile (off-Route) service and radiolocation systems based on the search and rescue scenario

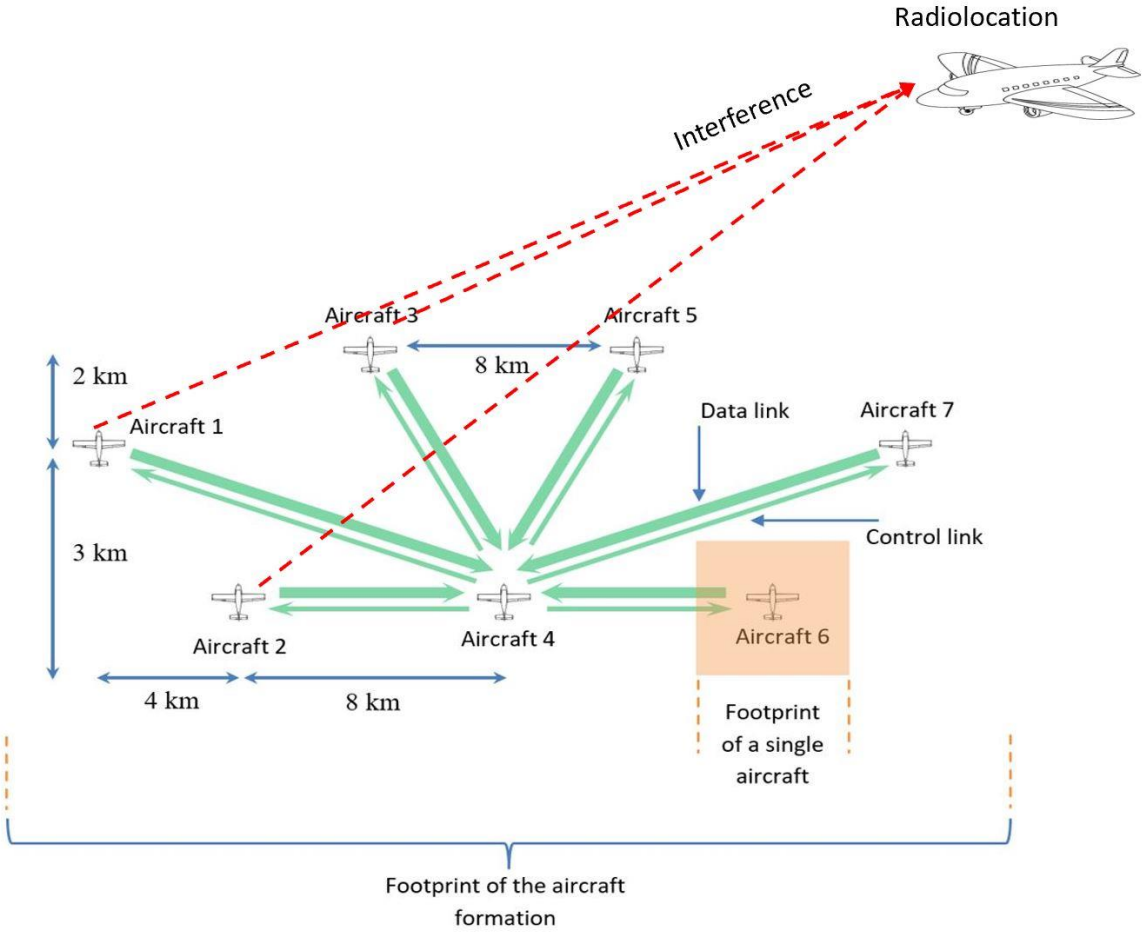

FIGURE A3-4

Sharing study between systems operating in the aeronautical mobile (off-Route) service and radiolocation systems based on the surveillance mission scenario

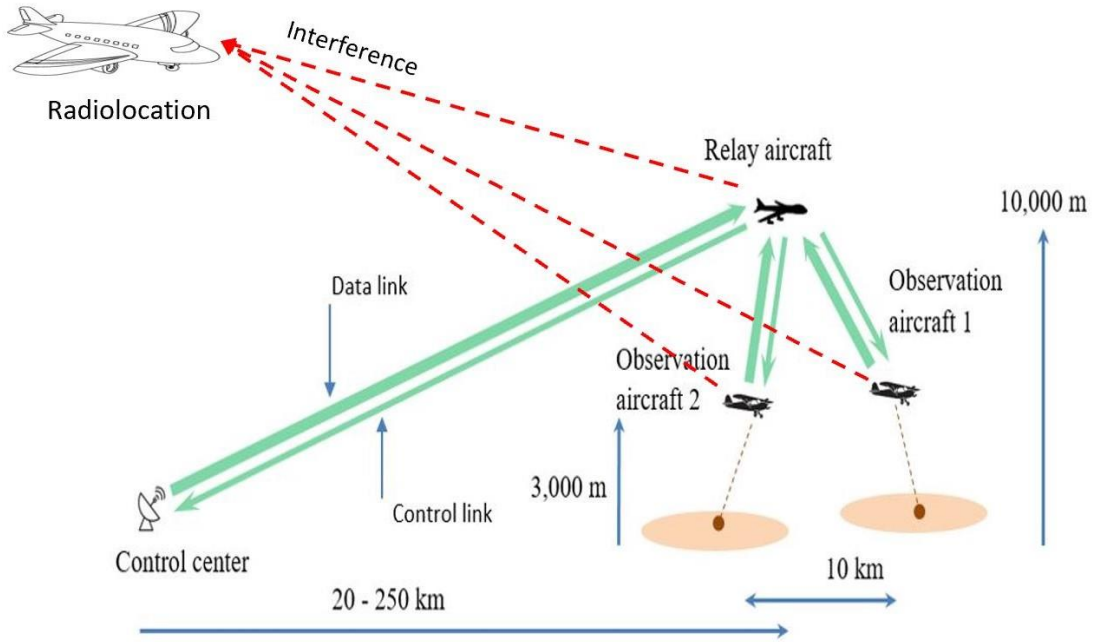

FIGURE A3-5

Sharing study between systems operating in the aeronautical mobile (off-Route) service and radiolocation systems based on the Internet above the cloud's scenario

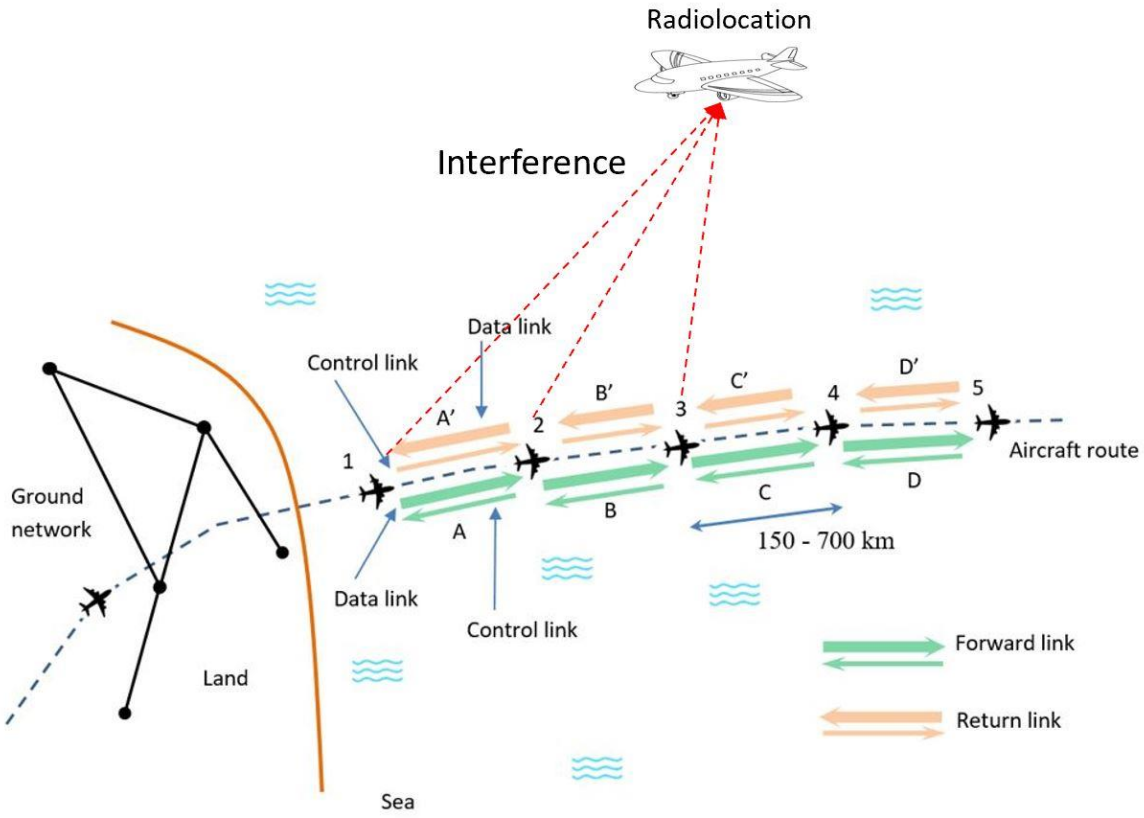

A3.3.2 Results

Figures A3-6 through A3-9 provide the ECDF of *I*/*N* measured at the RLS receiver in the four operational scenarios, in two different configurations of the AM(OR)S clusters. Figures A3-10 to A3-13 repeat the simulation by introducing separation distances indicated in the title of each Figure.

A3.3.3 Summary

Depending on the interference scenario under consideration and the AM(OR)S system characteristics, a separation distance is required between AM(OR)S and RLS stations.

TABLE A3-4

Simulation setup of Study C

		Units	Scenario			
			6.2.1	6.2.2	6.2.3	6.2.4
	Cluster deployment					
	TPO		Maximum power level for all AM(OR)S systems as per Table A1-1			
	Altitude of ADTs AGL	km	According to Table 3			
	Altitude of GDTs AGL					
	ADTs antenna	–	According to § A1.2			
Configuration n° 1	ADT BW	MHz	150	200	200	150
	Interfering ADTs	–	1	1	1 (relay or observation)	1
	ADTs centre frequency	GHz	15.4	15.4	15.4	15.4
	Position of AM(OR)S stations inside a cluster		ADT randomized within 70 km from the fire truck	ADT randomized on a ring of 8 km from the receiver	Relay randomized within 300 km from the control centre	Transmitting ADT randomized within 500 km from its receiver
Configuration n° 2	ADTs BW	MHz	10	10	10 (observation) 10 (relay)	10
	Interfering ADTs	–	2	3	3	3
	ADTs centre frequency	GHz	15.3925, 15.4025	15.3925, 15.4025, 15.4125		
	Position of AM(OR)S stations inside a cluster		ADTs randomized within 70 km from the fire truck	ADTs randomized on rings of 6, 8 and 12 km from the receiver	Same as conf. 1 for the relay; observation aircraft randomized within 5 km from the relay	Transmitting ADTs randomized within 500 km from their receiver

TABLE A3-4 (*end*)

	Units	Scenario			
		6.2.1	**6.2.2**	**6.2.3**	**6.2.4**
Simulation parameters					
Number of snapshots	–	10^6	10^6	10^6	10^6
PL ADTs – RLS	dB	According to Rec. ITU-R P.528-5 (with 5% time)			
Size of the simulation area	km	400 around 1 of the 2 ADTs	800 around 1 of the 7 ADTs	900 around the relay	900 around 1 of the 5 ADTs
RLS receiver deployment					
Location	–	Randomized within the simulation area			
Altitude AGL	km	Uniformly randomized between 0.3 and 13.7, see Table A2-1			
Antenna pointing	–	Uniformly randomized within ±45° in azimuth and between +5° and −45° in elevation as per Table A2A-1			
Protection criterion	–	$I/N = -6$ dB according to § A2.1.3			
RLS antenna	–	According to § A2.1.2 and Attachment A to Annex 2			
RLS centre frequency	GHz	15.4	15.4	15.4	15.4
RLS BW	MHz	25	25	25	25

FIGURE A3-6

Empirical cumulative distribution function (%) of *I*/*N* at the radiolocation receiver in scenario 6.2.1; the protection criterion of the radiolocation system (*I*/*N* = −6 dB) is indicated by a vertical red line; configuration 1 in blue; configuration 2 in black

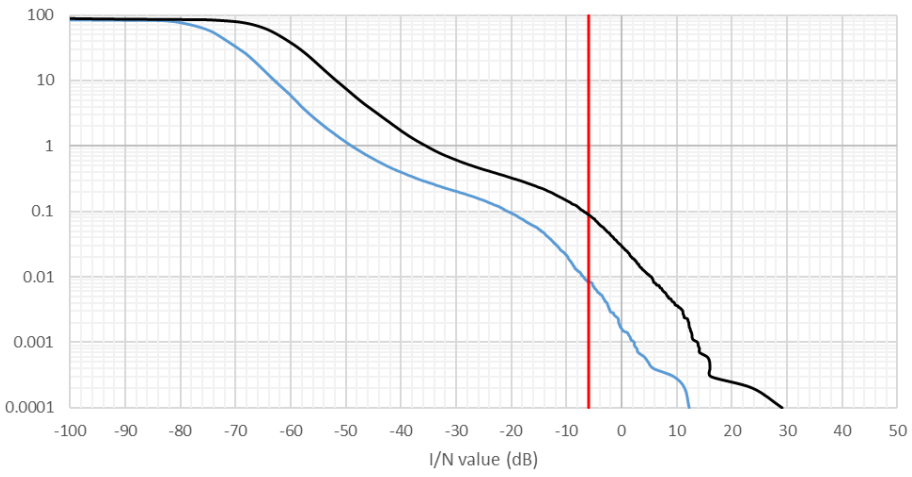

FIGURE A3-7

As in Fig. A3-6, in scenario 6.2.2; configuration 1 in blue; configuration 2 in black

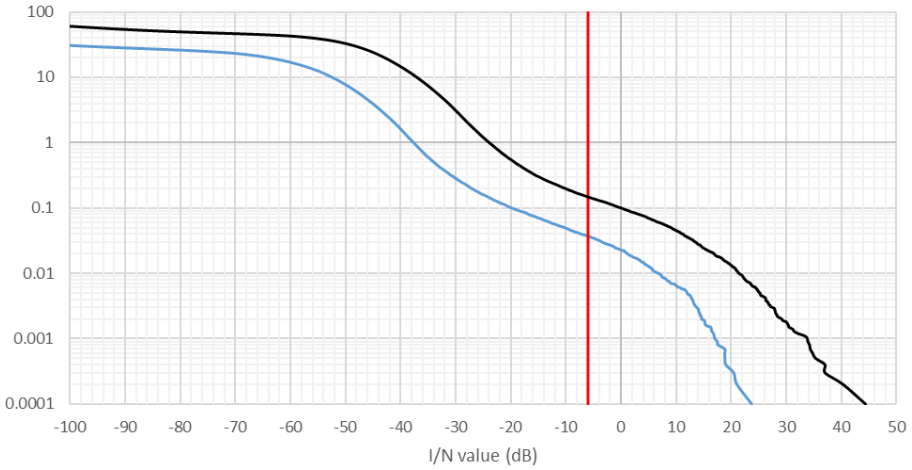

FIGURE A3-8

As in Fig. A3-6, in scenario 6.2.3; configuration 1 in blue if the relay is considered, in yellow if an observation if an airborne data terminal is considered; configuration 2 in black

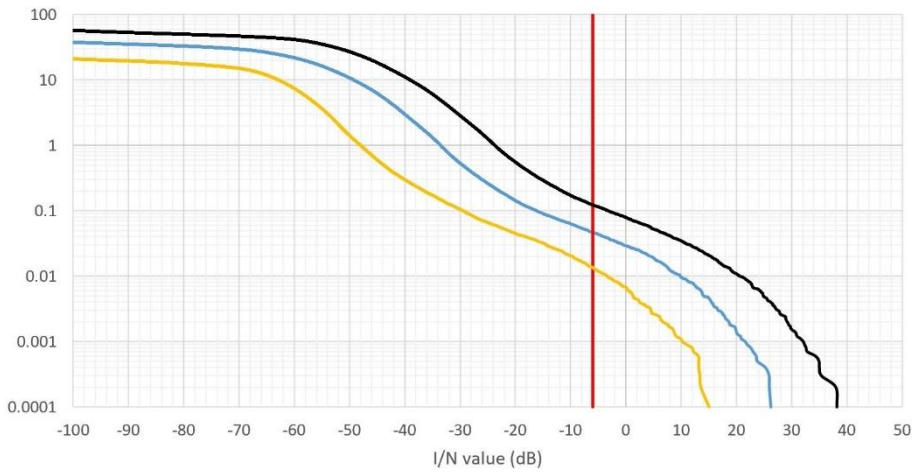

FIGURE A3-9

As in Fig. A3-6, in scenario 6.2.4; configuration 1 in blue; configuration 2 in black

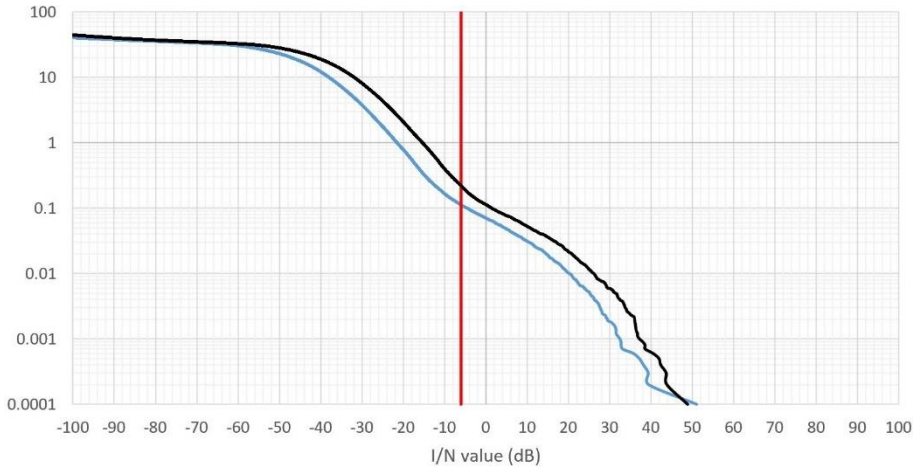

FIGURE A3-10

Empirical cumulative distribution function (%) of *I*/*N* at the radiolocation receiver in scenario 6.2.1; the protection criterion for the radiolocation system is shown as a vertical red line
Configuration 1 (orange): continuous curve for 205 km exclusion around the radiolocation receiver, dashed for 210 km
Configuration 2 (blue): continuous curve for 450 km exclusion around the radiolocation receiver, dashed for 455 km

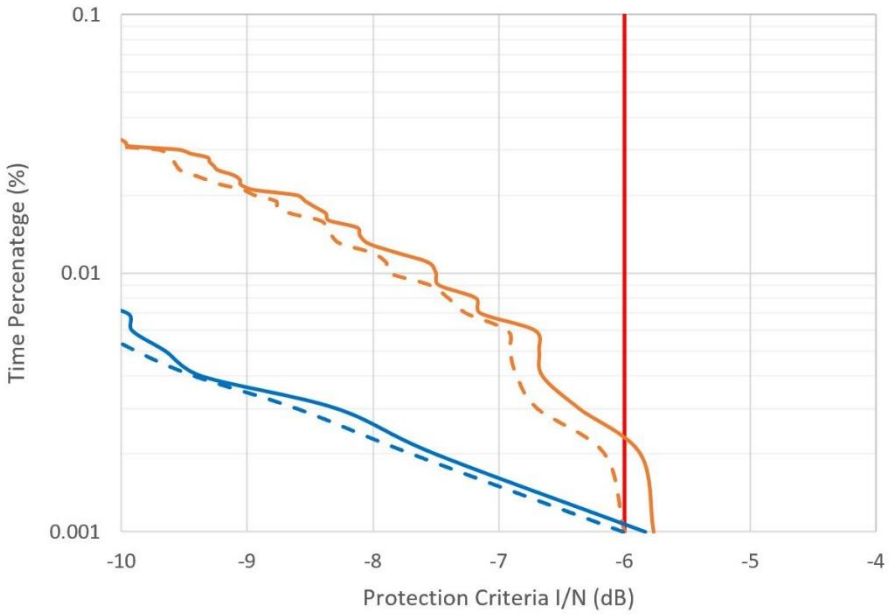

FIGURE A3-11

As in Fig. A3-10, in scenario 6.2.2
Configuration 1 (orange): continuous curve for 705 km exclusion around the radiolocation receiver, dashed for 710 km;
Configuration 2 (blue): continuous curve for 710 km exclusion around the radiolocation receiver, dashed for 715 km

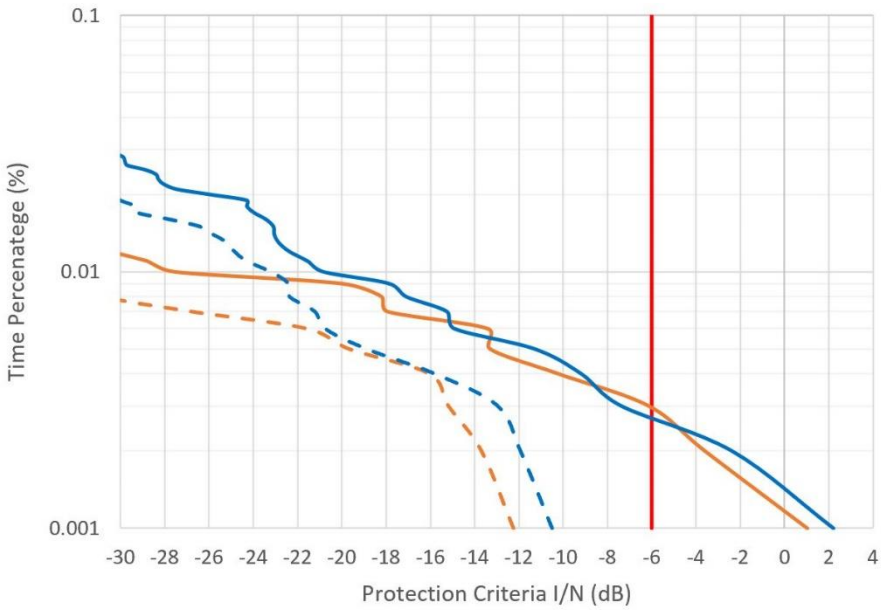

FIGURE A3-12

As in Fig. A3-10, in scenario 6.2.3
Configuration 1 (relay) (orange): plain curve for 880 km exclusion around the radiolocation receiver, dashed for 885 km;
Configuration 1 (observation) (green): plain curve for 610 km exclusion around the radiolocation receiver, dashed for 615 km;
Configuration 2 (blue): plain curve for 880 km exclusion around the radiolocation receiver, dashed for 885 km

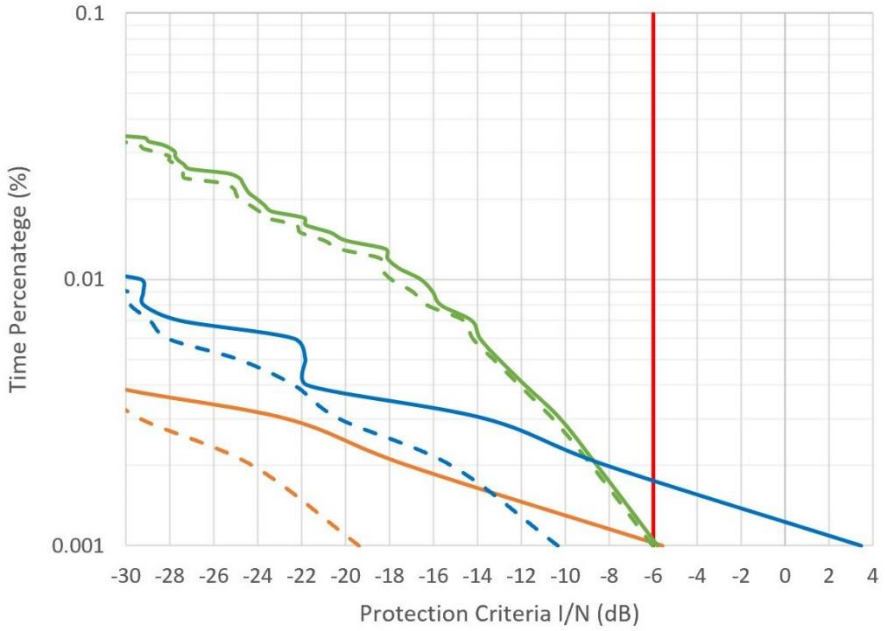

FIGURE A3-13

As in Fig. A3-10, in scenario 6.2.4
Configuration 1 (orange): continuous curve for 880 km exclusion around the radiolocation receiver, dashed for 885 km;
Configuration 2 (blue): continuous curve for 880 km exclusion around the radiolocation receiver, dashed for 885 km

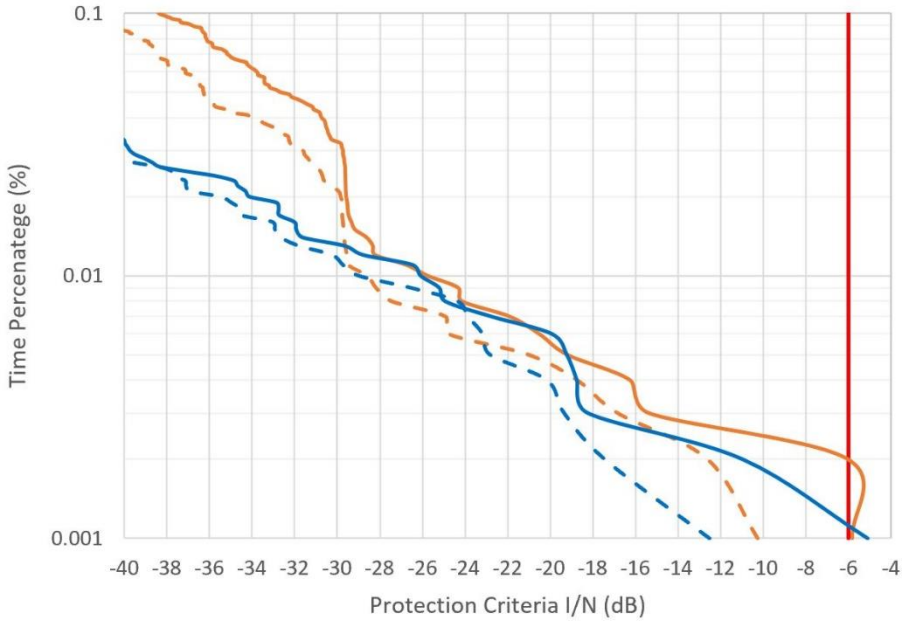

Table A3-5 provides the separation distance between non-safety AM(OR)S and radiolocation.

TABLE A3-5

Separation distance between systems operating in the aeronautical mobile (off-route) service and the radiolocation service

	Non-safety AM(OR)S transmitter bandwidth (MHz)	Non-safety AM(OR)S transmitter e.i.r.p. (dBW)	Separation distance between AM(OR)S and radiolocation (km)
Fig. 4-2 – Wildfire observation scenario	150	–2	210
	10	–2	455
Fig. 4-3 – Search and rescue scenario	200	35	710
	10	35	715
Fig. 4-4 – Surveillance mission scenario	200 (relay)	35	885
	200 (observation)	35	615
	10	35	885
Fig. 4-5 – Data networks	150	48	885
	10	48	885

A3.4 Study D

This section assesses sharing between multiple clusters of AM(OR)S stations operating in the frequency band 15.4-15.7 GHz and an RLS system operating in the band 15.4-17.3 GHz. It determines minimum separation zones around the RLS receiver to meet the protection criterion $I/N = -6$ dB.

A3.4.1 Methodology

The study evaluates the aggregate I/N variable at the RLS receiver and determines the required separation distance to meet the protection criterion. The impact of GDTs (if some are present in a given scenario, for instance 6.2.1 and 6.2.3) is not taken into account. The simulation setup is described in Table A3-6. Figs. A3-14 through A3-17 depicts the sharing scenarios between multiple clusters of AM(OR)S and radiolocation.

A3.4.2 Results

Figs. A3-18 through A3-21 provide the ECDF of I/N measured at the RLS receiver in the four operational scenarios, in two different configurations of the AM(OR)S clusters. Figs. A3-22 to A3-25 repeat the simulation by introducing separation distances indicated in the title of each figure.

A3.4.3 Summary

Depending on the interference scenario under consideration and the AM(OR)S system characteristics, a separation distance is required between AM(OR)S and RLS stations.

TABLE A3-6

Simulation setup of Study D

	Units	Scenario			
		6.2.1	**6.2.2**	**6.2.3**	**6.2.4**
Clusters deployment					
Number of clusters	–	5	3	4	8
Location		All clusters randomized within 254 km from the centre of the simulation area	All clusters randomized within 467 km from the centre of the simulation area	All clusters randomized within 484 km from the centre of the simulation area	All clusters randomized within 332 km from the centre of the simulation area
AM(OR)S stations deployment within a cluster					
Position of AM(OR)S stations inside a cluster	–	ADTs randomized within 70 km from the GDT	According to Table 3	Relay ADT randomized 300 km from the GDT; observation ADTs randomized within 5 km from the relay ADT	ADT#3 is fixed; ADT#2 and ADT#4 are randomized within 500 km from ADT#3; ADT#1 within 500 km from ADT#2; ADT#5 within 500 km from ADT#4
Altitude of AM(OR)S stations AGL	km	According to Table 3			
TPO	dBm	Adapt the ATPC algorithm described in § A11.6.1			
Antennas of AM(OR)S stations	–	According to § A1.2			
ADTs BW	MHz	10	10	10	10
GDTs BW		10	–	10	–
AM(OR)S stations centre frequency	GHz	Randomized in 15.4-15.7			
Simulation parameters					
Simulation area radius	km	400	800	900	1500
PL ADTs – RLS	dB	According to Rec. ITU-R P.528-5 (with 5% time)			
PL AM(OR)S Tx – AM(OR)S Rx	dB	According to Rec. ITU-R P.528-5 (with 95% time)			
Number of snapshots	–	10^6	10^6	10^6	10^6
RLS receiver deployment					
Location	–	Randomized within the simulation area			
Altitude AGL	km	Uniformly randomized between 0.3 and 13.7, see Table A2-1			
Antenna pointing	–	Uniformly randomized within ±45° in azimuth and between +5° and −45° in elevation as per Table A2A-1			
Protection criterion	–	$I/N = -6$ dB according to § A2.1.3			
Antenna	–	According to § A2.1.2 and Attachment A to Annex 2			
Centre frequency	GHz	Randomized in 15.4-15.7			
BW	MHz	25	25	25	25

FIGURE A3-14

Sharing study between multiple clusters operating in the aeronautical mobile (off-route) service and radiolocation systems based on the wildfire observation scenario

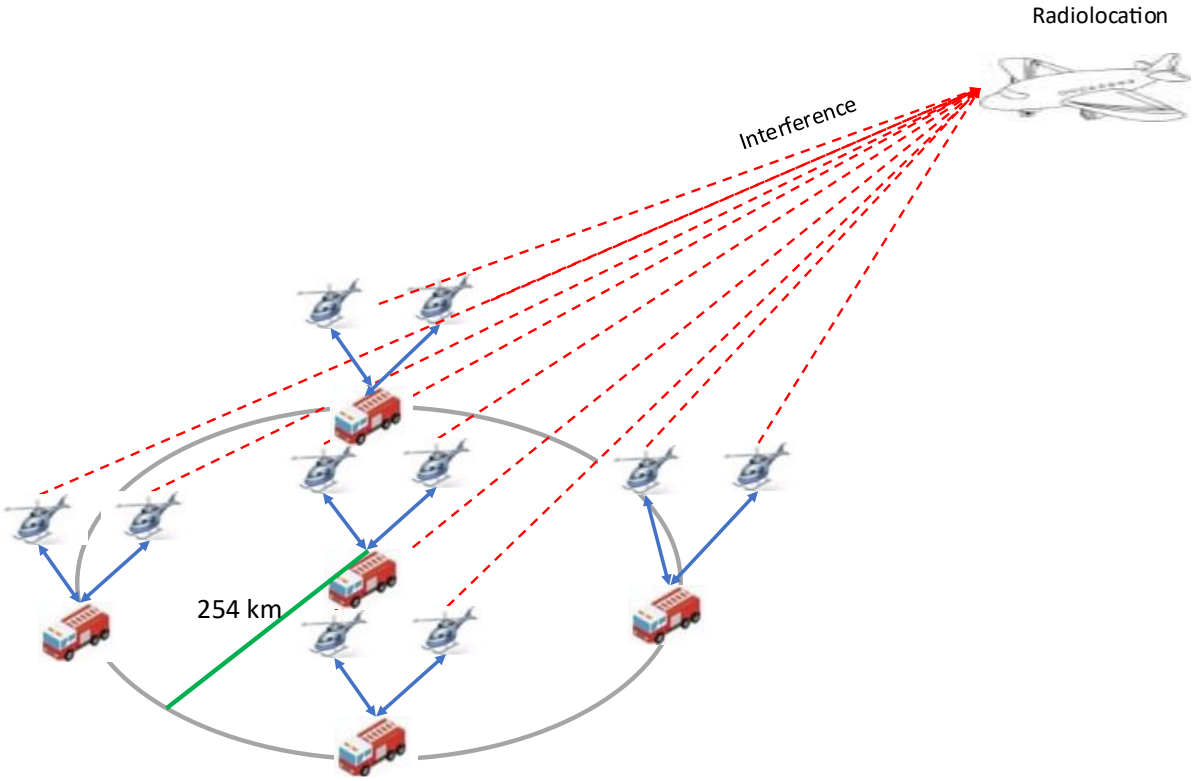

FIGURE A3-15

Sharing study between multiple clusters operating in the aeronautical mobile (off-route) service and radiolocation systems based on the search and rescue scenario

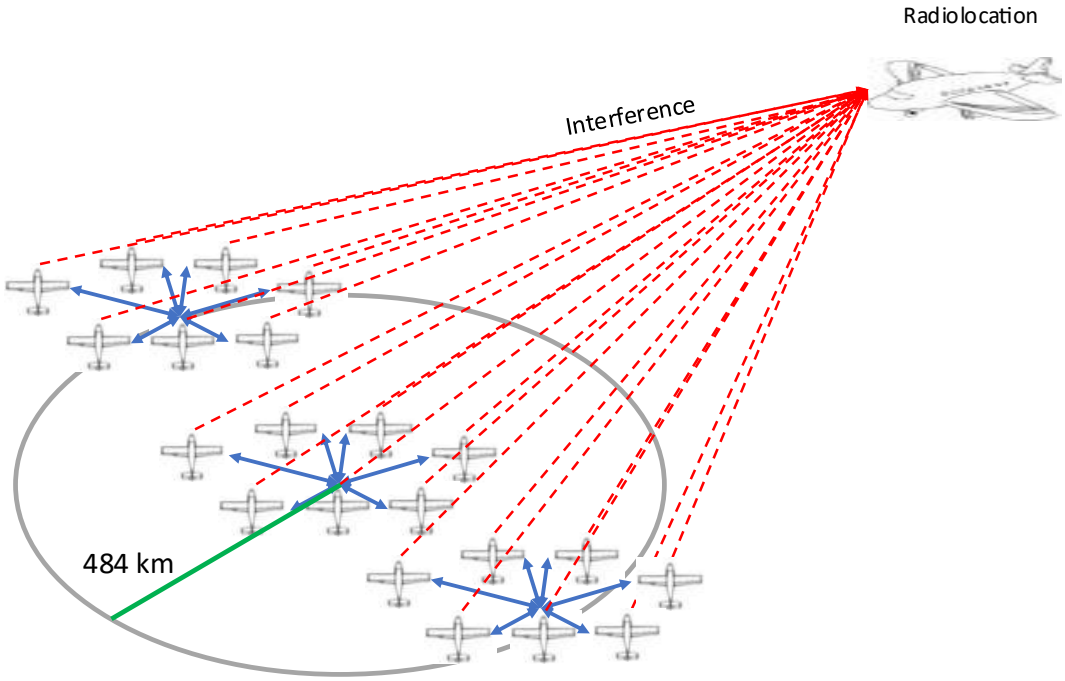

FIGURE A3-16

Sharing study between multiple clusters operating in the aeronautical mobile (off-route) service and radiolocation systems based on the surveillance mission scenario

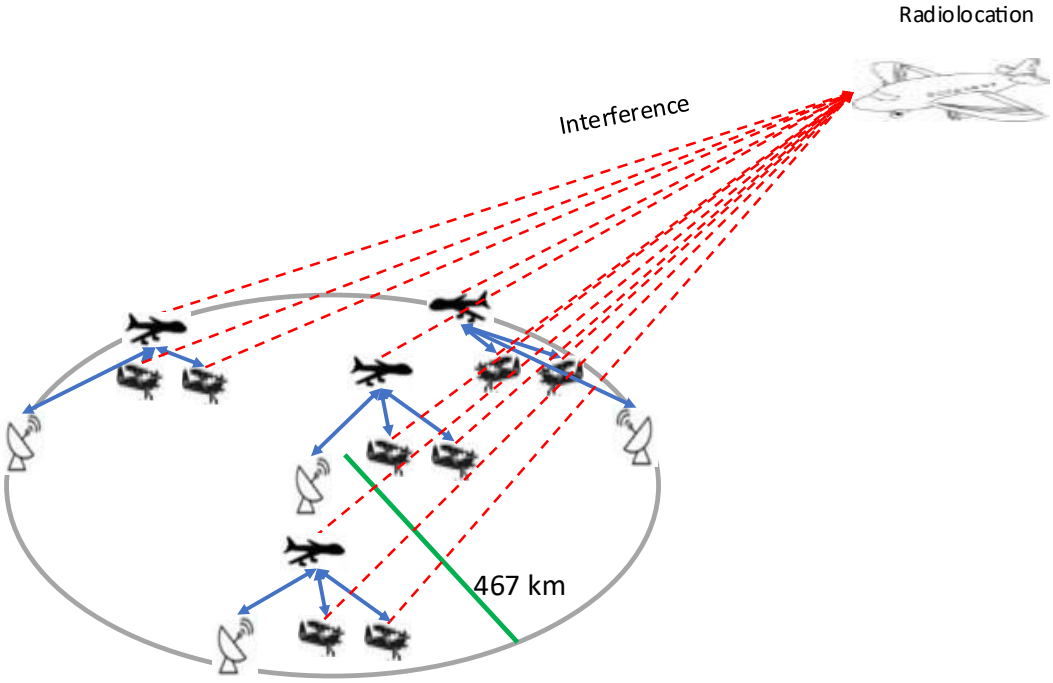

FIGURE A3-17

Sharing study between multiple clusters operating in the aeronautical mobile (off-route) service and radiolocation systems based on the Internet above the clouds scenario

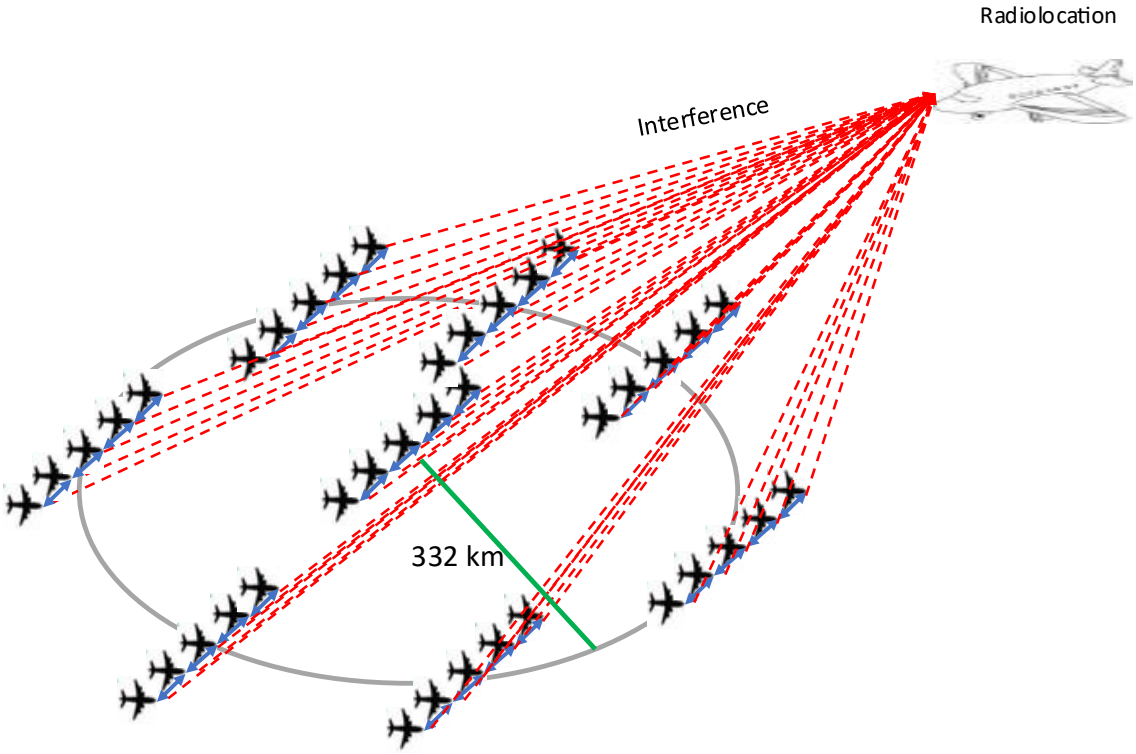

FIGURE A3-18

Empirical cumulative distribution function (%) of *I/N* at the radiolocation receiver in scenario 6.2.1; the protection criterion of radiolocation systems (*I/N* = −6 dB) is indicated by a vertical red line; the left figure is without automatic transmit power control, and the right figure is with automatic transmit power control

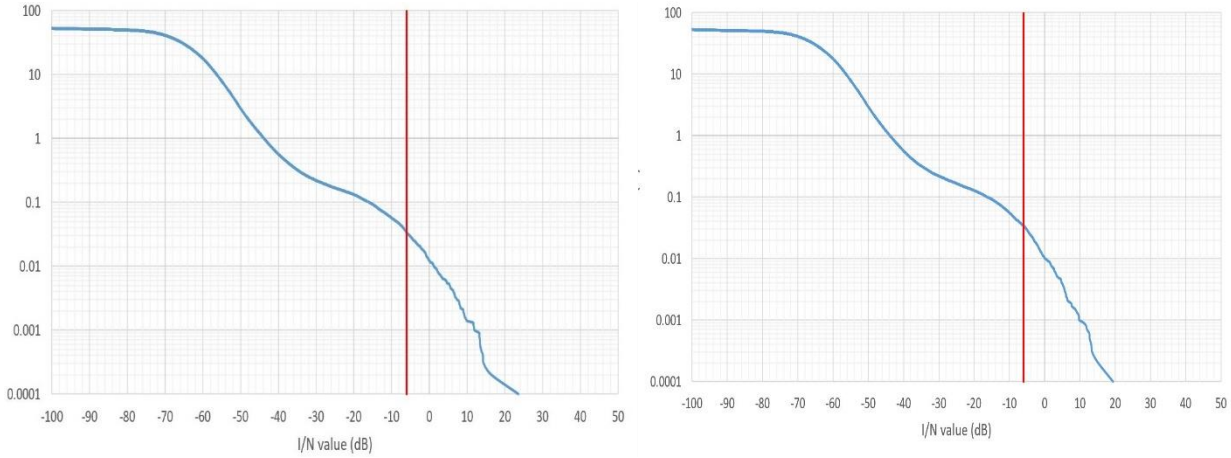

FIGURE A3-19

As in Fig. A3-18, in scenario 6.2.2

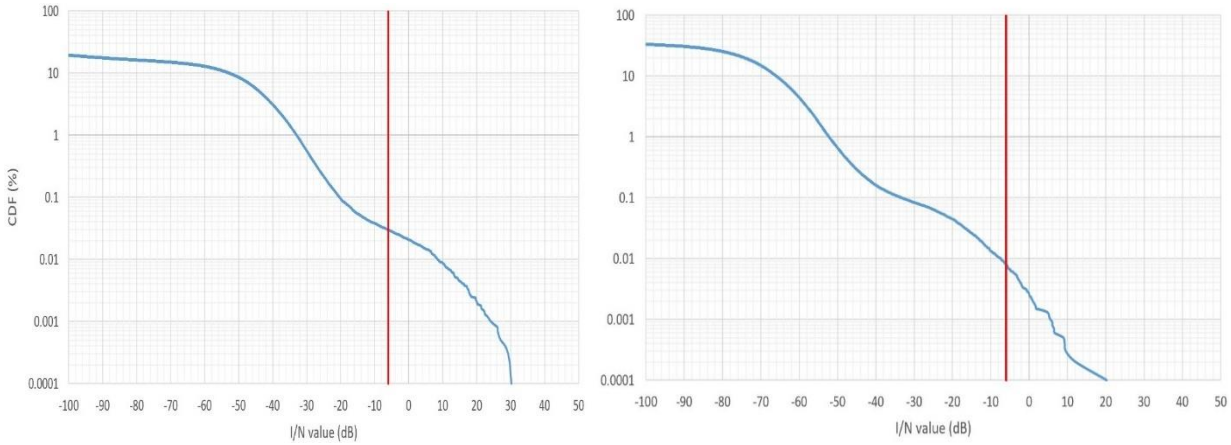

FIGURE A3-20

As in Fig. A3-18, in scenario 6.2.3

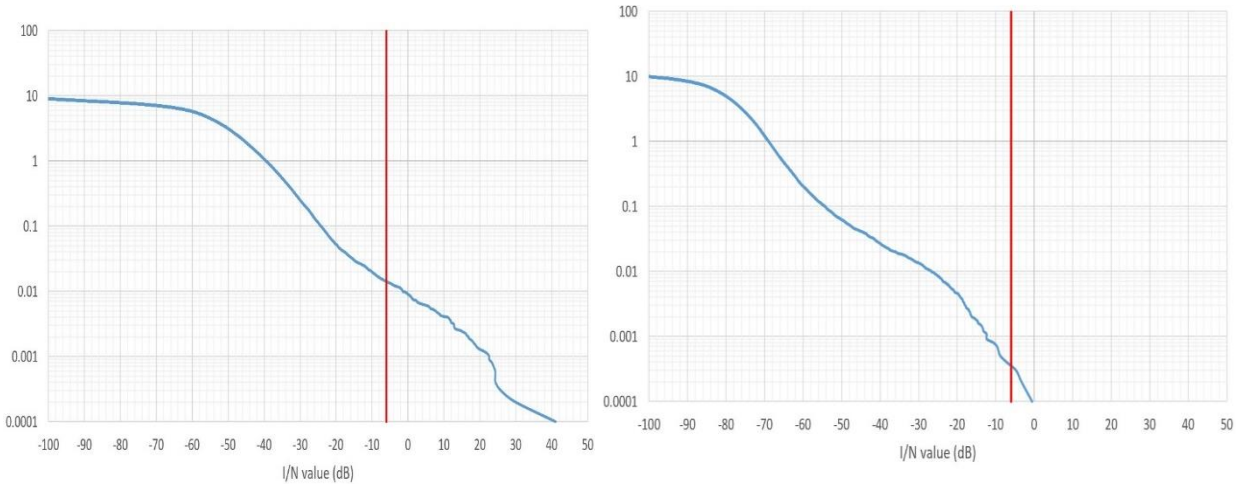

FIGURE A3-21

As in Fig. A3-18, in scenario 6.2.4

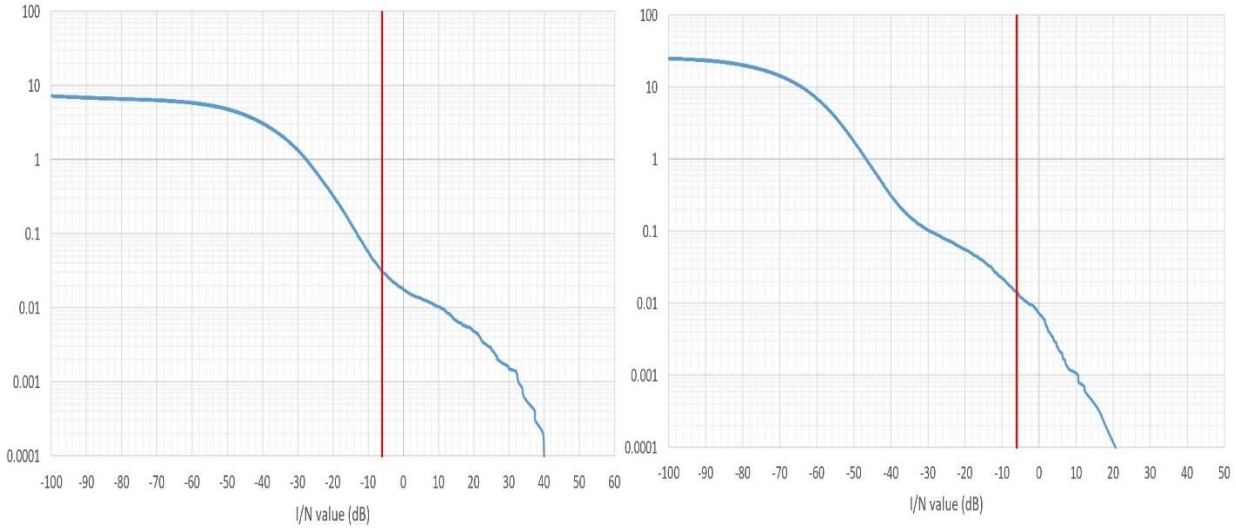

FIGURE A3-22

Empirical cumulative distribution function (%) of *I/N* at the radiolocation receiver in scenario 6.2.1; the protection criterion for the radiolocation system is shown as a vertical red line; in the left figure 560 km exclusion zone in green and 565 km in blue; in the right figure, 555 km exclusion zone in green and 560 km in blue

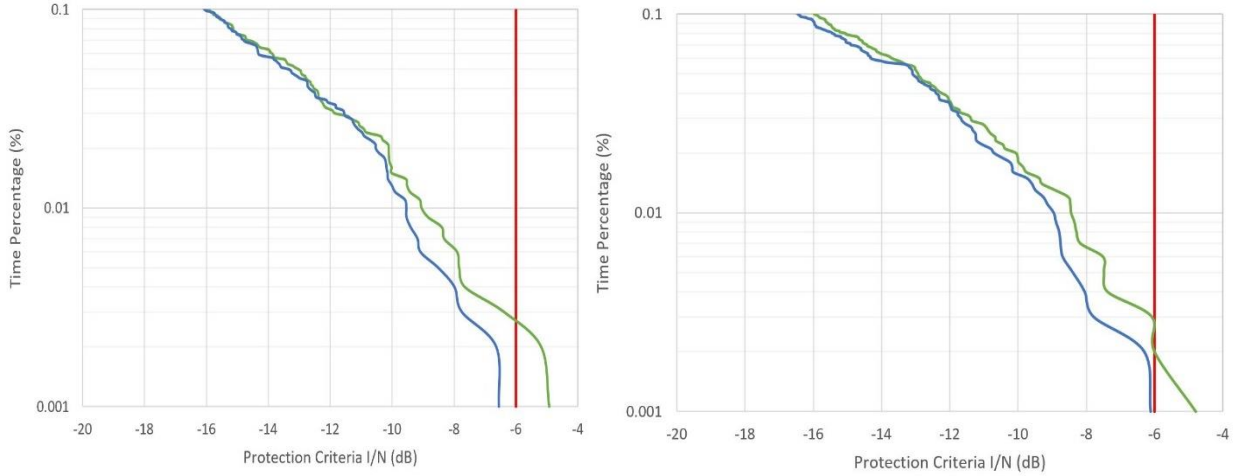

FIGURE A3-23

As in Fig. A3-22, in scenario 6.2.2; in the left figure, 1 200 km exclusion zone in green and 1 205 km in blue; in the right figure, 1 005 km exclusion zone in green and 1 010 km in blue

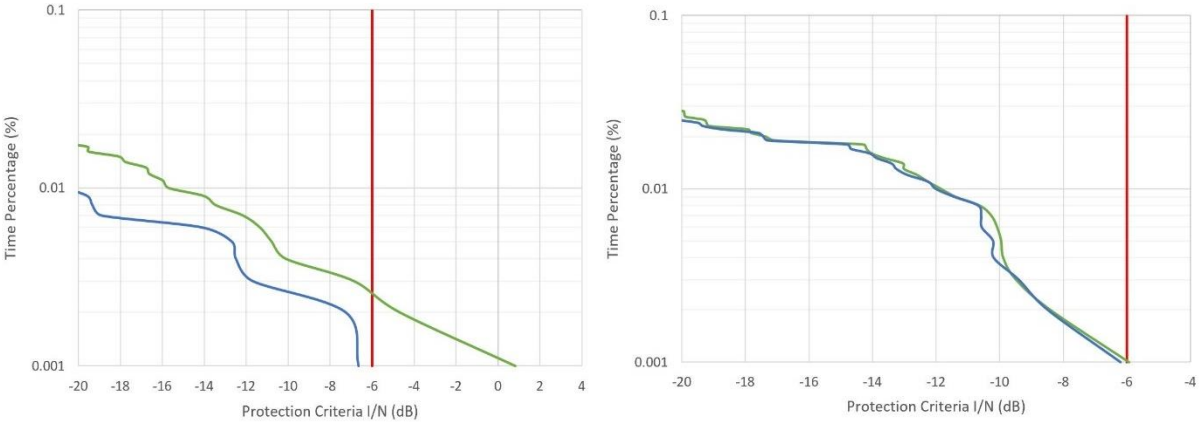

FIGURE A3-24

As in Fig. A3-22, in scenario 6.2.3; in the left figure, 875 km exclusion zone in green and 880 km in blue; in the right figure, 715 km exclusion zone in green and 720 km in blue

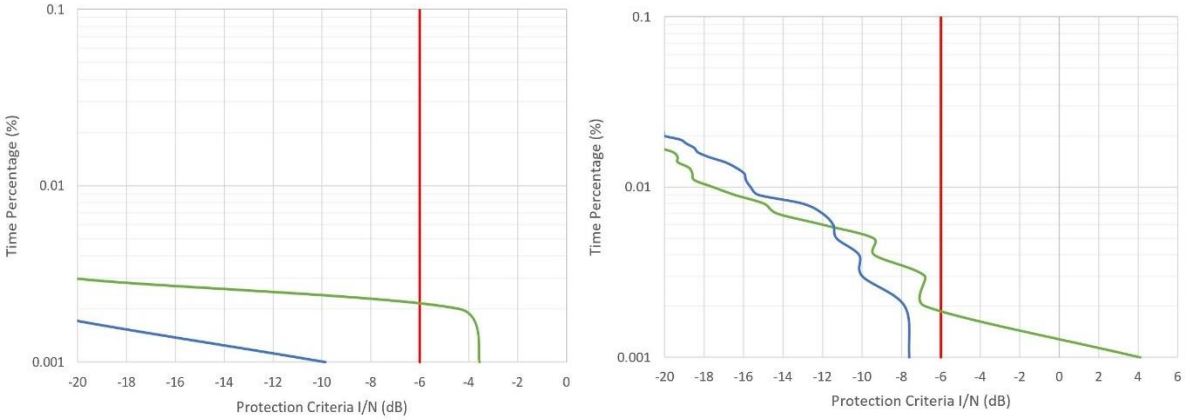

FIGURE A3-25

As in Fig. A3-22, in scenario 6.2.4; in the left figure, 1 435 km exclusion zone in green and 1 440 km in blue; in the right figure, 1 330 km exclusion zone in green and 1 335 km in blue

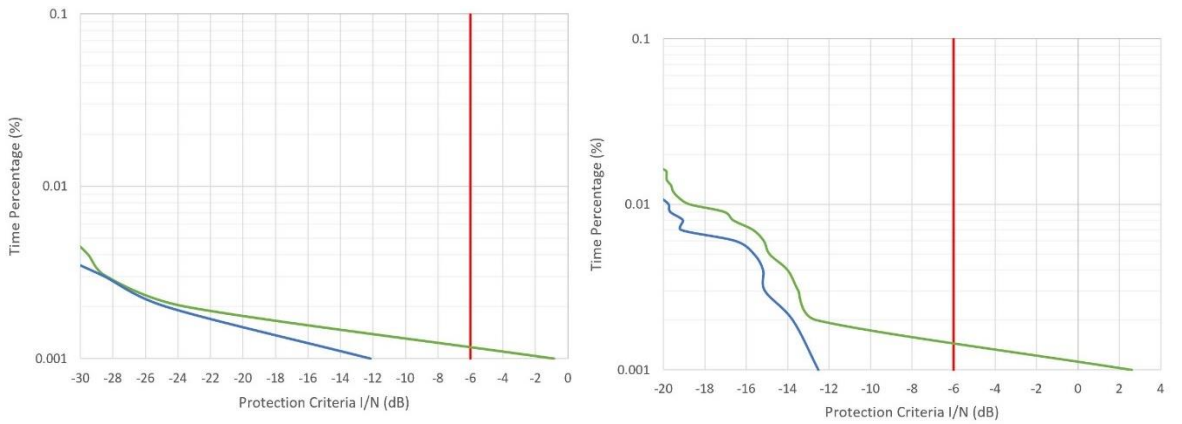

Table A3-7 provides the separation distance between non-safety AM(OR)S and radiolocation.

TABLE A3-7

Separation distance in km between systems operating in the aeronautical mobile service (off-route) and radiolocation service

	Separation distance between Radiolocation and the centre of non-safety AM(OR)S cluster deployment without ATPC feature	**Separation distance between Radiolocation and the centre of non-safety AM(OR)S cluster deployment with ATPC feature**
Figure 4-2 – Wildfire observation scenario	565	560
Figure 4-3 – Search and rescue scenario	1 205	1 010
Figure 4-4 – Surveillance mission scenario	880	720
Figure 4-5 – Internet above the clouds scenario	1 440	1 335

A3.5 Study E

A3.5.1 Introduction

This section analyses the time variation of the *I*/*N* variable at the RLS receiver in an ADT-RLS encounter.

A3.5.2 Methodology

The setup represented graphically in Fig. A3-26 is used for the simulation. It is assumed that an ADT and an aircraft equipped with RLS travel with constant bearing in the direction of each other. The main beam of the AM(OR)S is in the direction of flight i.e. in the direction of the RLS. However, the RLS antenna main beam moves over time according to the scanning behaviour described for System-6 in Recommendation ITU-R M.1730-1.

FIGURE A3-26

Simulation setup for Study D

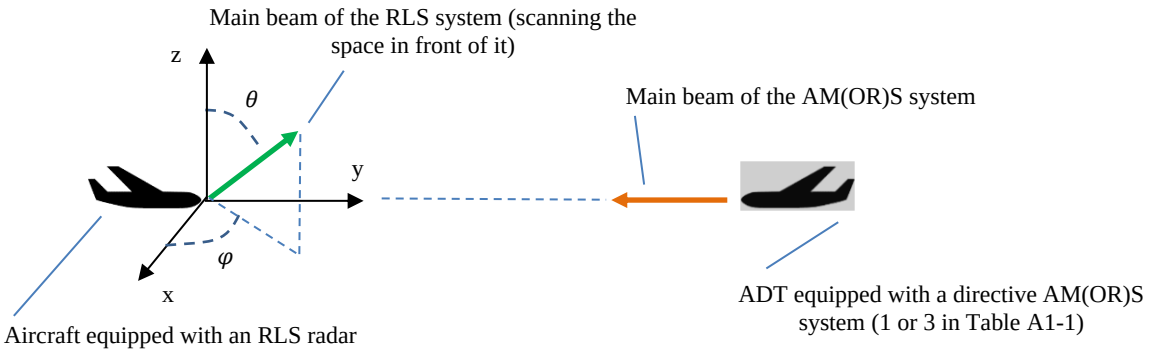

The orientation of the RLS antenna changes over time within a sector in front of the aircraft according to the scanning behaviour described in Table A2-16. By making the assumption that at $t = 0$ s, the

antenna is in the bottom left corner of this sector (from the perspective of Fig. A3-26), the spherical coordinates of the antenna direction are given in equation (A3-3):

$$\theta(t) = 100\left|\frac{t\cdot s_v}{100} - \left\lfloor\frac{t\cdot s_v}{100} + \frac{1}{2}\right\rfloor\right| + 85 \quad \text{(A3-3)}$$

where:

t: time in seconds from the start of the simulation

s_v: vertical scanning speed (degrees/sec) of the RLS radar

$\lfloor x \rfloor$: integer part of x.

In the same way:

$$\varphi(t) = 180\left|\frac{t\cdot s_h}{180} - \left\lfloor\frac{t\cdot s_h}{180} + \frac{1}{2}\right\rfloor\right| + 45 \quad \text{(A3-4)}$$

where:

t: time in seconds from the start of the simulation

s_h: horizontal scanning speed (degrees/sec.) of the RLS radar.

The angle α between the [Oy) axis and the antenna main beam is given in equation (A3-5):

$$\alpha(t) = \operatorname{acos}\left(\sin(\theta)\cdot\sin(\varphi)\right) \quad \text{(A3-5)}$$

The variation of θ and φ and α is shown in Fig. A3-27.

FIGURE A3-27

Variation of θ and φ over time for $s_v = s_h = 1$ degree/sec

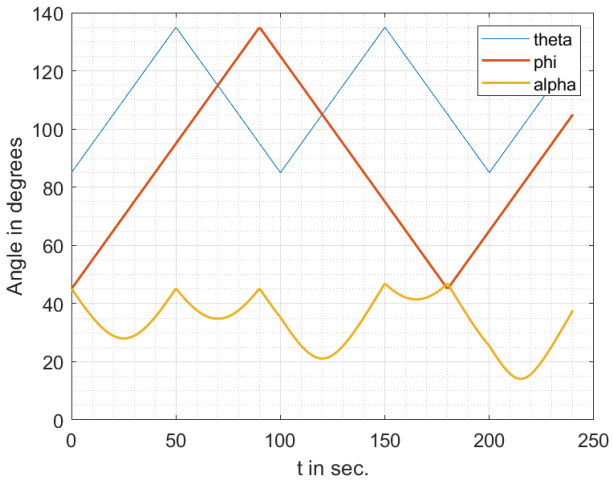

Using the FSPL model for propagation, the *I/N* at the RLS receiver is given in equation (A3-6), where the assumed frequency is 15 400 MHz.

$$I/N = -21.2 + P_{AM(OR)S} + G_{AM(OR)S} + G_{RLS(\alpha)} - 20\cdot\log_{10}(D_o - (v\cdot t/1\,800)) \quad \text{(A3-6)}$$

where:

$P_{AM(OR)S}$: peak power (dBm) of AM(OR)S

$G_{AM(OR)S}$: peak gain (dBi) of AM(OR)S

$G_{RLS(\alpha)}$: gain (dBi) of the RLS system in the direction of the AM(OR)S station, calculated according to § A2.1.2

D_o: initial distance (km) between RLS and AM(OR)S

v: speed (km/h) of RLS and AM(OR)S.

Figure A3-28 shows the variation of the interference over time for typical RLS and AM(OR)S parameters. In this configuration, the interference occurs 4 times in 30 minutes and each interference event last for approximately 6 seconds.

FIGURE A3-28

Variation of I/N over 30 min for $s_V = s_H$ =1 degree/sec, $P_{AM(OR)S}$ = 40 dBm, $G_{AM(OR)S}$ = 25 dBi, D_0 = 500 km, and v = 400 km/h

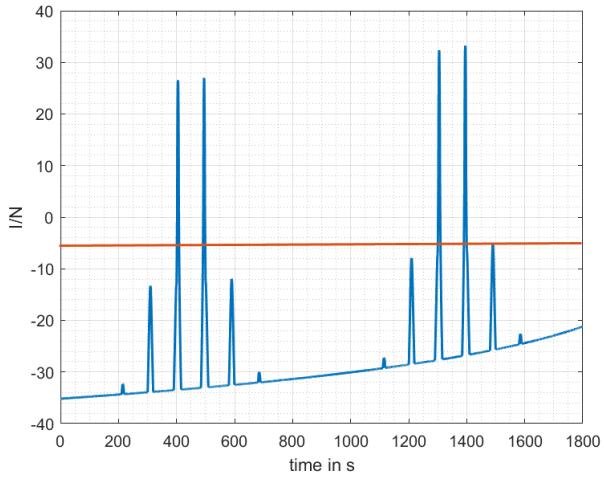

A3.5.3 Summary

This study has shown that, even if interference events can happen in rare configurations (for instance when the AM(OR)S station and the RLS station are flying towards each other) for extended periods of time, the interference occurs 4 times in 30 minutes and each interference event last for approximately 6 seconds.

Annex 4

Sharing between systems operating in the aeronautical mobile (off-route) service (interferer) and automatic landing system operating in the aeronautical radionavigation service in the frequency band 15.4-15.7 GHz

TABLE OF CONTENTS

Page

The frequency band 15.4-15.7 GHz is globally allocated to the ARNS on a primary basis. ALS are operated in this band under the ARNS allocation. This Annex contains a study that assesses the feasibility of sharing this frequency band between non-safety AM(OR)S and ALS.

A4.1 Methodology

The study presented in this Annex is a Monte Carlo analysis whose general methodology is laid out in Annex 11 to this Report.

A4.2 Results

Results are shown in Figs A4-1 to A4-4 for the four scenarios considered in § 6 of this Report. A zoom of the figures for low percentages of time is also provided next to each of these Figures. In scenarios 6.2.1, 6.2.2 and 6.2.3, at least 99.99% of the 100 000 simulated snapshots resulted in aggregate *I*/*N* lower than −30 dB at the ALS airborne receiver. In scenario 6.2.4, at least 99.99% of the 100 000 simulated snapshots produced an aggregate *I*/*N* value lower than −20 dB. Finally, in the four operational scenarios, none of the snapshots exceeded −10 dB.

A4.3 Summary

The results presented in § A4.2 lead to the conclusion that the sharing of the frequency band 15.4-15.7 GHz between future non-safety AM(OR)S systems and ARNS ALS is possible without particular mitigation techniques.

FIGURE A4-1A

Empirical cumulative distribution function of aggregate interference-to-noise ratio at the automatic landing system receiver in scenario 6.2.1

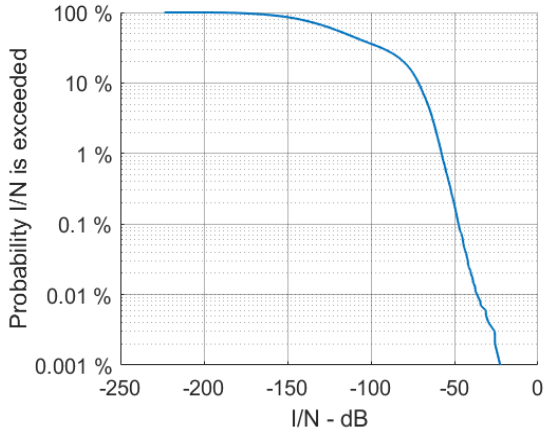

FIGURE A4-1B

Zoom of Fig. A4-1A for low time percentages

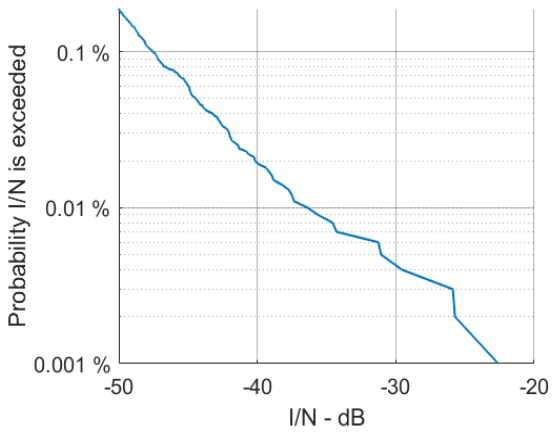

FIGURE A4-2A

Empirical cumulative distribution function of aggregate *I*/*N* at the automatic landing system receiver in scenario 6.2.2

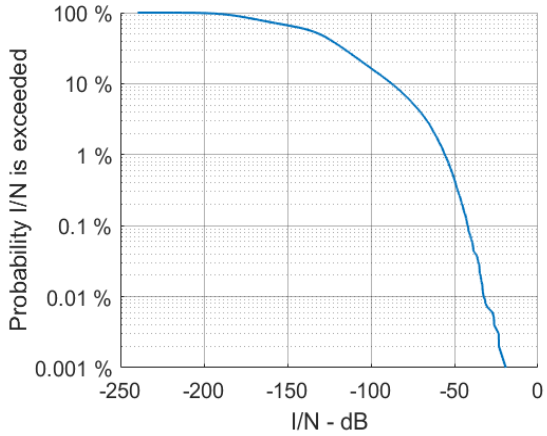

FIGURE A4-2B

Zoom of Fig. A4-2A for low time percentages

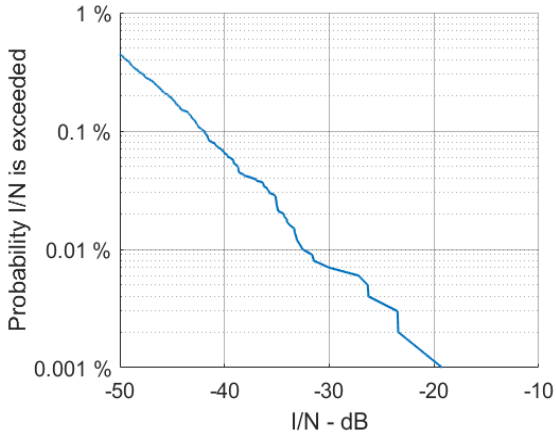

FIGURE A4-3A

Empirical cumulative distribution function of aggregate *I*/*N* at the automatic landing system receiver in scenario 6.2.3

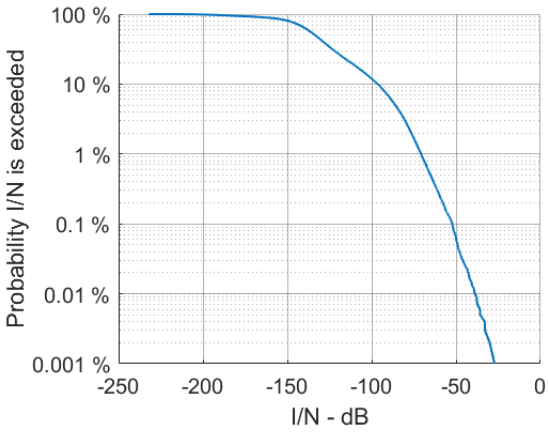

FIGURE A4-3B

Zoom of Fig. A4-3A for low time percentages

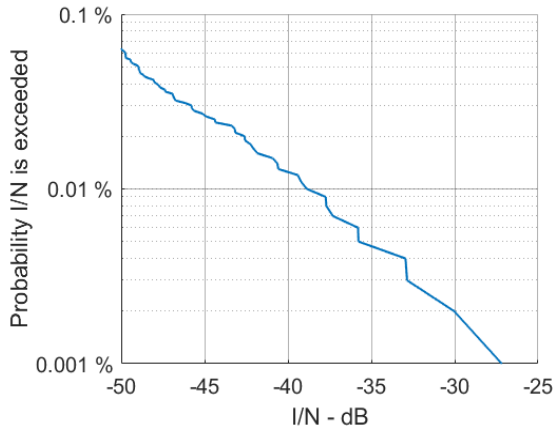

FIGURE A4-4A

Empirical cumulative distribution function of aggregate *I*/*N* at the automatic landing system receiver in scenario 6.2.4

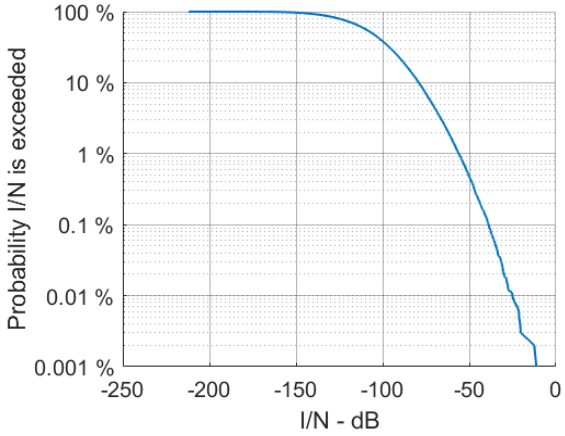

FIGURE A4-4B

Zoom of Fig. A4-4A for low time percentages

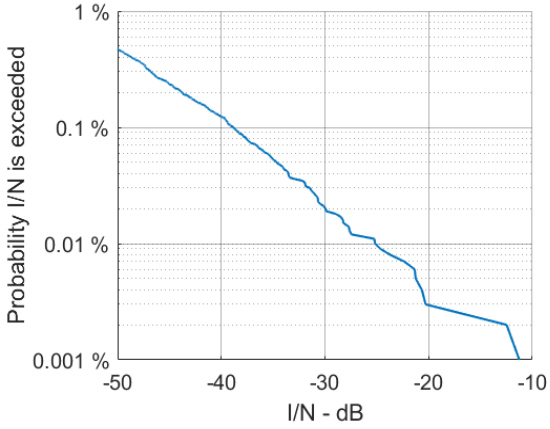

Annex 5

Sharing of the frequency band 15.4-15.7 GHz between detect and avoid radars and future systems operating in the non-safety aeronautical mobile (off-route) service

TABLE OF CONTENTS

The frequency band 15.4-15.7 GHz is globally allocated to the ARNS on a primary basis. DAA radars are operated in this band under the ARNS allocation. This Annex contains two studies (A and B) that assess the feasibility of sharing this frequency band between non-safety AM(OR)S and DAA radars.

A5.1 Study A

A5.1.1 Methodology

The study presented in this section is a Monte Carlo analysis whose general methodology is laid out in Annex 11 to this Report.

A5.1.2 Results

Results are shown in Figs A5-1 to A5-4 for the four DAA radars introduced in § A2.2.1.1 of this Report, and for the four scenarios considered in § 6.2. A zoom on the Figures for low percentages of time is also provided.

These plots show that in scenarios 6.2.1 and 6.2.3 (Figs A5-1 and A5-3), the aggregate I/N at the DAA receiver is lower than −10 dB in at least 99.99% of the 100 000 simulated snapshots. In scenarios 6.2.2 and 6.2.4 (Figs A5-2 and A5-4), the aggregate I/N is lower than −10 dB in at least 99.9% of the snapshots. While still acceptably low, these percentages could be further reduced by applying some specific mitigation measures described in § A3.2.2 of this Report (sharing between new non-safety AM(OR)S systems and RLS in the frequency band 15.4-15.7 GHz).

A5.1.3 Summary

The results presented in § A5.2 lead to the conclusion that the sharing of the frequency band 15.4-15.7 GHz between future non-safety AM(OR)S systems and ARNS DAA radars is possible, optionally with some specific mitigations measures.

FIGURE A5-1A

Empirical cumulative distribution function of aggregate *I*/*N* at the detect and avoid radars in scenario 6.2.1

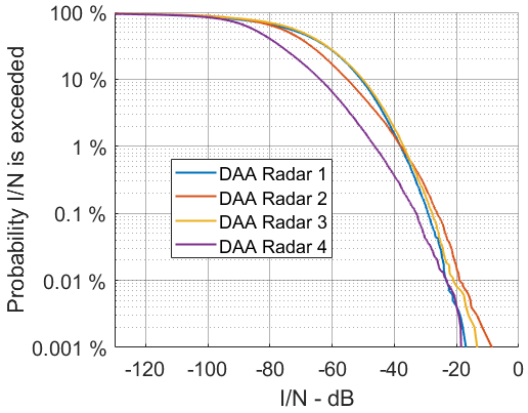

FIGURE A5-1B

Zoom of Fig. A5-1A around 1%

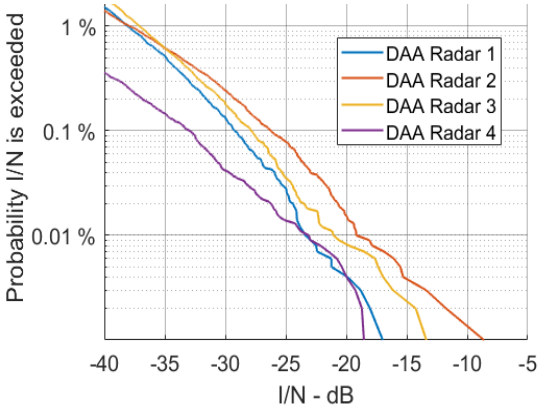

FIGURE A5-2A

Empirical cumulative distribution function of aggregate *I*/*N* at the detect and avoid radars in scenario 6.2.2

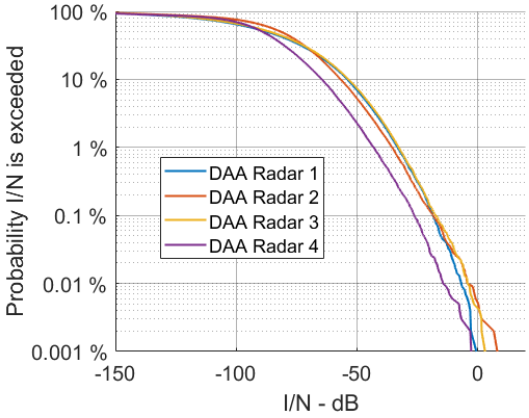

FIGURE A5-2B

Zoom of Fig. A5-2A around 1%

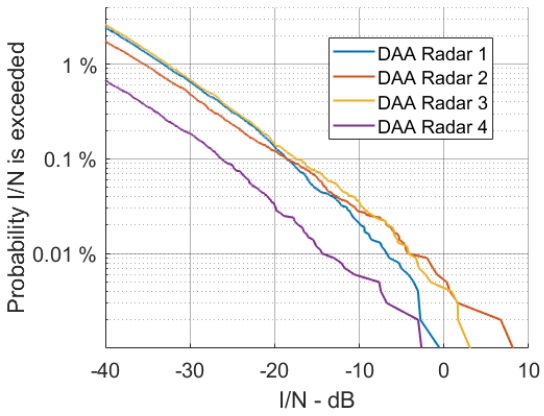

FIGURE A5-3A

Empirical cumulative distribution function of aggregate *I*/*N* at the detect and avoid radars in scenario 6.2.3

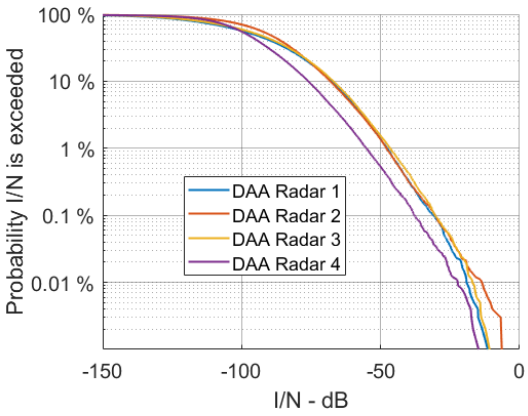

FIGURE A5-3B

Zoom of Fig. A5-3A around 1%

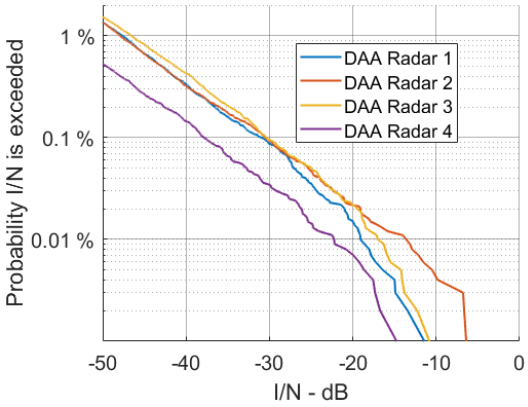

FIGURE A5-4A

Empirical cumulative distribution function of aggregate *I*/*N* at the detect and avoid radars in scenario 6.2.4

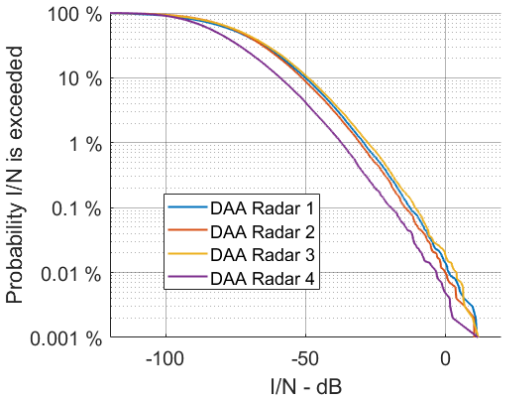

FIGURE A5-4B

Zoom of Fig. A5-4A around 1%

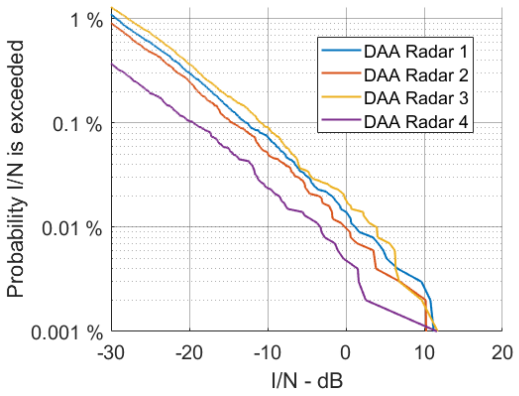

A5.2 Study B

The analysis calculates the interference of AM(OR)S airborne systems (Systems 1, 2 and 3 of Table A1-1) to the DAA system (Table A2-2).

The protection criteria for the DAA is assumed to be $I/N = -10$ dB. We assume that the antenna side-lobe gain of AM(OR)S and DAA are both 0 dB. The separation distances are calculated between the AM(OR)S system and the DAA system and the results are summarized in Tables A5-1 and A5-2.

Equation (A5-1) can be used to determine if interference to the DAA systems receiver from AM(OR)S transmissions is likely to occur and what separation distance is required to eliminate the interference.

$$PL = P_{Tx} + G_{Tx} + G_{Rx} - FDR_{IF} - (N - 10) \quad \text{(A5-1)}$$

where:

P_{Tx}: power level (dBm) of the AM(OR)S system

G_{Tx}: antenna gain (dBi) of the interfering transmitter in the direction of the victim receiver, In this study, only the side-lobe gain of the AM(OR)S antenna is considered and assumed to be 0 dBi

G_{Rx}: antenna gain (dBi) of the victim receiver in the direction of the interfering transmitter. In this study, the peak gain and side-lobe gain of the DAA system antenna are considered

PL: required propagation attenuation (dB) between transmitting and receiving antennas. In this study, the Recommendation ITU-R P.528-5 propagation model is used for air-to-air path with the 50% time percentage and 10 000 m heights for both the transmitting and receiving antennas

F: frequency (MHz)

R: required separation distance (km)

FDR_{IF}: frequency dependent rejection (dB) produced by the receiver IF selectivity curve on an unwanted transmitter emission spectrum

N: noise power of DAA system receivers in Table A2-2 (dBm).

The FDR_{IF} value can be determined from Recommendation ITU-R SM.337-6. Since the radars will operate on a co-frequency basis, only the on-tune rejection (OTR) is considered. OTR for non-coherent chirped pulsed signals is given by equation (A5-2):

$$OTR = \begin{cases} 10\log_{10}\left({\mathrm{BW_{Tx}}}/{\mathrm{BW_{Rx}}}\right) & \text{for } \mathrm{BW_{Rx}} \le \mathrm{BW_{Tx}} \\ 0 & \text{otherwise} \end{cases} \quad \text{(A5-2)}$$

where:

BW_{Rx}: receiver bandwidth (MHz), 15, 160, 15, 200 for System 1 to System 4 respectively as depicted in Table A2-2

BW_{Tx}: transmitter bandwidth (MHz), 10-200, 10-150, 10-150 for System 1 to System 3 respectively as depicted in Table A1-1.

The required propagation attenuation between airborne AM(OR)S system and the ARNS DAA radars for different bandwidth of AM(OR)S systems and different antenna configurations are summarized in Table A5-1.

TABLE A5-1

Required propagation attenuation between systems operating in the aeronautical mobile (off-Route) service and detect and avoid radars for different bandwidth of systems operating in the aeronautical mobile (off-Route) service and different antenna configurations

	Required propagation attenuation (dB)(1)		
	AM(OR)S System 1 (airborne)	**AM(OR)S System 2 (airborne)**	**AM(OR)S System 3 (airborne)**
The main lobe of DAA System 1	151.5-162.7	137.7-147.7	152.7-162.7
The side lobe of DAA System 1	139.5-150.7	125.7-135.7	140.7-150.7
The main lobe of DAA System 2	164.5-165.5	150.5	165.5

TABLE A5-1 (*end*)

	Required propagation attenuation (dB)[1]		
	AM(OR)S System 1 (airborne)	**AM(OR)S System 2 (airborne)**	**AM(OR)S System 3 (airborne)**
The side lobe of DAA System 2	139.5-140.5	125.5	140.5
The main lobe of DAA System 3	154.5-165.7	140.7-150.7	155.7-165.7
The side lobe of DAA System 3	139.5-150.7	125.7-135.7	140.7-150.7
The main lobe of DAA System 4	180.0	165.0	180.0
The side lobe of DAA System 4	153.0	138.0	153.0

[1] The ranges of the propagation attenuations in the table correspond to the Min. data link bandwidth to Max. data link bandwidth ranges of AM(OR)S systems as depicted in Table A1-1.

The separation distances that are required to ensure sharing between the AM(OR)S system and the ARNS DAA radars are summarized in Table A5-2.

TABLE A5-2

The separation distance between systems operating in the aeronautical mobile (off-route) service interfering with detect and avoid radars (side-lobe to main-lobe, side-lobe to side-lobe)

	Required separation distance (km)[1]		
	AM(OR)S System 1 (airborne)	**AM(OR)S System 2 (airborne)**	**AM(OR)S System 3 (airborne)**
The main lobe of DAA System 1	57-205	12-37	66-205
The side lobe of DAA System 1	14-52	3-9	17-52
The main lobe of DAA System 2	251-282	51	282
The side lobe of DAA System 2	14-16	3	16
The main lobe of DAA System 3	81-288	17-52	93-288
The side lobe of DAA System 3	14-52	3-9	17-52
The main lobe of DAA System 4	720	266	720
The side lobe of DAA System 4	68	12	68

[1] The ranges of the separation distances in the Table correspond to the Min. data link bandwidth to Max. data link bandwidth ranges of AM(OR)S systems as depicted in Table A1-1.

Annex 6

Sharing of the frequency band 15.43-15.63 GHz between systems operating in the fixed-satellite service (Earth-to-space) and future systems operating in the non-safety aeronautical mobile (off-route) service planned to operate in 15.4-15.7 GHz

TABLE OF CONTENTS

The frequency band 15.43-15.63 GHz is globally allocated to the FSS (Earth-to-space) on a primary basis. This annex contains a study that assesses the feasibility of sharing this frequency band between FSS (Earth-to-space) and non-safety AM(OR)S planned to operate in the frequency band 15.4-15.7 GHz.

A6.1 Methodology

The sharing study presented in this Annex is a multiple-entry Monte Carlo analysis that evaluates the impact of AM(OR)S systems onto FSS (Earth-to-space) space borne receivers in the four operational scenarios described in § 6.2 of this Report. The general methodology is highlighted in Annex 11. For definiteness, the three FSS carriers considered in § A2.3.1 were studied separately.

A6.2 Results

Results are shown in Figs A6-1 to A6-4 for the three different FSS carriers and in the four operational scenarios described in § 6.2 of this Report. The long- and short-term protection criteria of FSS space borne receivers as highlighted in § A2.3.3 are also shown in the Figures.

FIGURE A6-1

Empirical cumulative distribution function of aggregate *I*/*N* at the spaceborne receiver operating in the fixed satellite service (Earth-to-space) spaceborne receiver (Carrier 1: red, Carrier 2: blue, Carrier 3: yellow, long-term protection criterion: red dot, short-term protection criteria: blue and green dots) in scenario 6.2.1

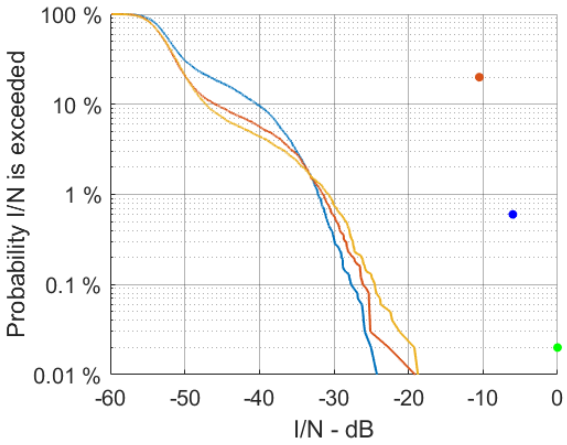

FIGURE A6-2

As in Fig. A6-1, in scenario 6.2.2

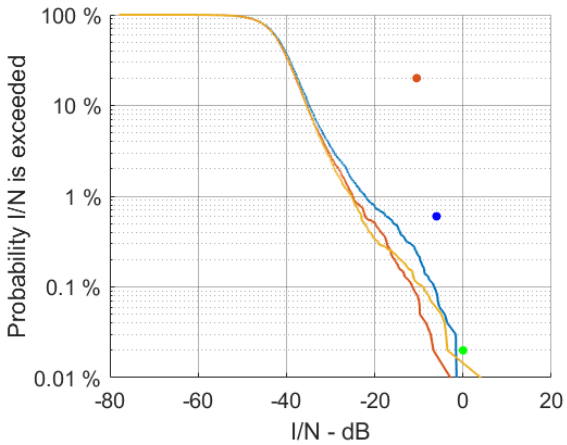

FIGURE A6-3

As in Fig. A6-1, in scenario 6.2.3

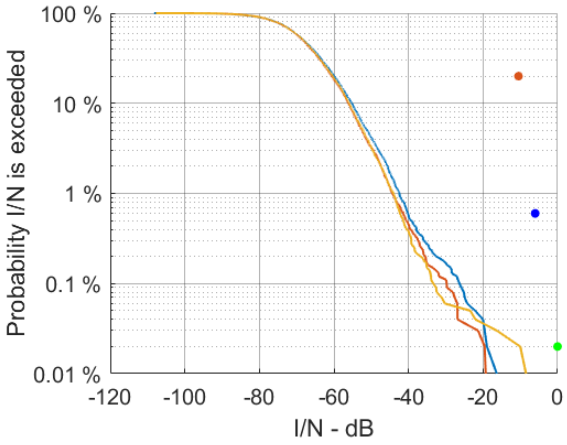

FIGURE A6-4

As in Fig. A6-1, in scenario 6.2.4

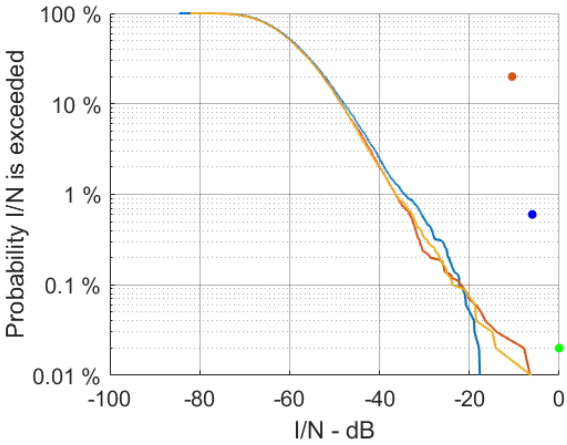

Scenario 6.2.1 ‘Wildfire Detection’ (Fig. A6-1) has the least impact onto FSS (Earth-to-space), whilst scenarios 6.2.2 ‘Search and Rescue’ (Fig. A6-2), 6.2.3 ‘Border Surveillance’ (Fig. A6-3) and 6.2.4 ‘Data Networks’ (Fig. A6-4) provide less margin with the different protection criteria, while still meeting them. Scenario 6.2.1 indeed only uses ‘downwards WBLOSDL’ (in the sense of the definition given in § 5.5), whereas the three other scenarios use ‘horizontal (scenario 6.2.4) or upwards WBLOSDL’ (scenarios 6.2.2 and 6.2.3) that have more severe impact on space borne receivers.

A6.3 Summary

The results presented in § A6.2 indicate that sharing of the frequency band 15.43-15.63 GHz between FSS (Earth-to-space) and non-safety AM(OR)S is possible without any specific protection measures to be implemented.

Annex 7

Compatibility studies between future systems operating in the non-safety aeronautical mobile (off-route) service planned to operate in frequency bands 15.4-15.7 GHz and 22-22.21 GHz and radio astronomy stations operating in 15.35-15.4 GHz and 22.21-22.5 GHz

TABLE OF CONTENTS

The frequency bands 15.35-15.4 GHz and 22.21-22.5 GHz are allocated to the RAS and other passive services on a primary basis and 15.35-15.4 GHz is subject to RR No. **5.340**. This Annex is composed of four studies (A to D) that address different aspects of the compatibility between future AM(OR)S systems planned to operate in the frequency bands 15.4-15.7 GHz and 22-22.21 GHz and RAS operating in the frequency bands 15.35-15.4 GHz and 22.21-22.5 GHz.

A7.1 Study A

A7.1.1 General description

Radio telescopes are sited in remote locations, often at appreciable altitude, with a clear horizon down to elevation angles of a few degrees rendering aircraft visible in LOS at large distances. Site characteristics have little influence on the study results presented here but, for definiteness, this study took as an example a radio telescope operating at an elevation of 7 000 feet AMSL like the Karl Jansky very large array (VLA) in New Mexico, USA. The VLA is shown in Fig. A7-1. It is registered at a single central coordinate in the MIFR.

FIGURE A7-1

A radio telescope operating at 15.4 and 22.4 GHz, the Jansky VLA in New Mexico, USA

Compatibility is affected by many factors: the TPO and the frequency channel of the transmitting ADT; the situation of the RAS station in the antenna beam pattern of the ADT; the height of the ADT (determining the RHD) and the distance between the ADT nadir and the RAS station.

This study calculated the OOB attenuation required of an ADT transmitting in the adjacent frequency bands 15.4-15.7 GHz and 22-22.21 GHz. The distance between the ADT nadir and the RAS station was varied between 0 km and the RHD in a spherical Earth geometry for ADT at altitudes of 10 000, 30 000 and 50 000 ft[17] AGL. Tables A7-1 through A7-3 show the RAS operating characteristics and protection threshold, the ADT characteristics, and the assumed propagation model, respectively.

TABLE A7-1

RAS stations operating characteristics and protection thresholds

RAS parameters	Value	Reference
Site altitude AMSL (km)	2.13	Karl Jansky VLA (USA)
Allocated frequency bands (GHz)	15.35-15.4 GHz 22.21-22.5 GHz	RR No. **5.340**
Antenna gain (dBi)	0	Rec. ITU-R RA.769-2
Pfd threshold (dB(W/(m^2 · Hz)))	−233 in 15.35-15.4 GHz −231 in 22.21-22.5 GHz	Rec. ITU-R RA.769-2, Table 1
Maximum data loss (%)	2	Rec. ITU-R RA.1513-2

[17] 10 000 ft = 3 048 km.

TABLE A7-2

ADT characteristics

Parameters	Value or description	Reference in Annex 1
Considered altitude AGL (ft.)	10 000, 30 000, 50 000	Table A1-1
OOB emission relative to emission in the necessary band (dB)	See Fig. A1-1	Numerical integration of the SEM in Fig. A1-1
Power applied at antenna port in the necessary band (dBm)	40, 25 and 40 for AM(OR)S systems 1, 2 and 3 in 15.4 GHz - - - 40, 25 and 50 for AM(OR)S systems 1, 2 and 3 in 22 GHz	See Table A1-1
Antenna gain (dBi)	See § A1.2	-

TABLE A7-3

Propagation characteristics assumed in Study A

Propagation loss	Value or description	Reference
FSPL	Inverse square law	Rec. ITU-R P.525-4
Atmospheric attenuation	Numerical integration of 0.013 dB/km · $e^{(-h/6\ km)}$ at height h along slant path to RAS station	Rec. ITU-R P.619-5 Rec. ITU-R P.676-12 Rec. ITU-R P.835-6

A7.1.2 Unwanted emissions falling in the measurement band

The SEM shown in Fig. A1-1 was numerically integrated across the RAS measurement band to produce the results shown in Fig. A7-2A for an ADT operating in the frequency band 15.4-15.7 GHz and Fig. A7-2B for an ADT operating in the frequency band 22-22.21 GHz. In these Figures, the attenuation of unwanted emissions relative to the wanted emission is shown as a function of lower band edge frequency for four different ADTs transmitter BW.

In the frequency band 15.4-15.7 GHz (Fig. A7-2A), the curves for BW of 100 and 200 MHz are limited by the 300 MHz BW of the transmitting band 15.4-15.7 GHz. In the frequency band 22-22.21 GHz (Fig. A7-2B), the curves for BW of 100 MHz and 200 MHz are severely limited by the 210 MHz BW of the transmitting band 22-22.21 GHz.

Figures A7-2A and A7-2B can be used in conjunction with Figs A7-3A and A7-3B to determine the band use that is compatible with the geometry of an aircraft-RAS station encounter.

FIGURE A7-2A

Attenuation of unwanted emissions with respect to wanted emissions for an ADT operating at 15.4 GHz, for different channel bandwidths and lower edge of the channel

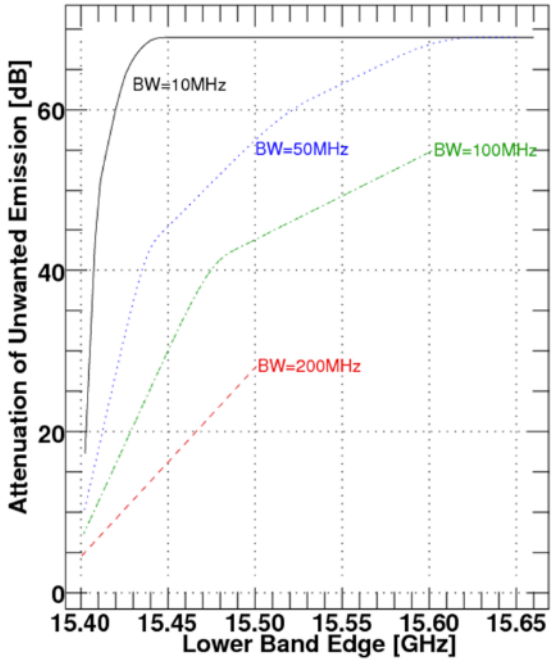

FIGURE A7-2B

Attenuation of unwanted emissions with respect to wanted emissions for an airborne data terminal operating at 22 GHz, for different channel bandwidths and lower edge of the channel

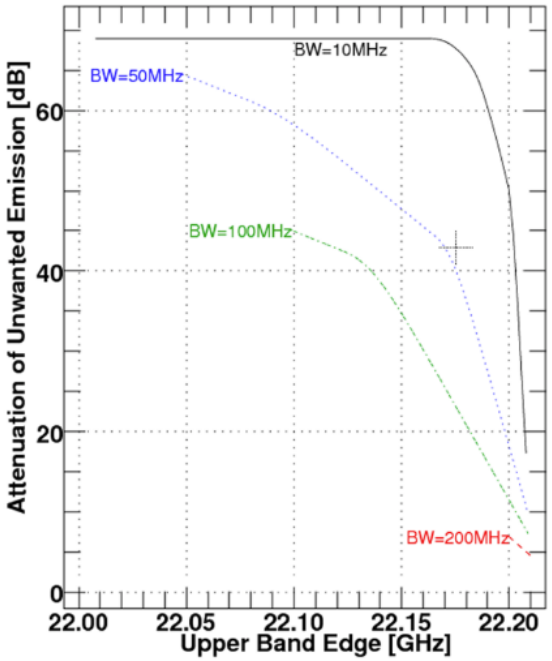

A7.1.3 Airborne data terminal antenna beam

A description of the ADT antenna beam for airborne AM(OR)S Systems 1 and 3 using active antenna arrays and for System 2 using an omnidirectional antenna is given in Attachment A to Annex 1 and § A1.2.2, respectively. In Attachment A to Annex 1, the half-wavelength antenna element spacing refers to in-band operation: the actual antenna pattern is very slightly modified when computed in the centre of the adjacent RAS band.

A7.1.4 Use case 1

Shown in Figs A7-3A and A7-3B is the required attenuation for an ADT flying with azimuth bearing toward a RAS station and with an antenna pointed in the direction of flight i.e. an A2A application. The TPO for each system is given in Table A7-2. The incident pfd values were computed for Systems 1 and 3 and System 2 using an omnidirectional antenna, and these were differenced with the RAS protection threshold to produce the results shown.

The angle between the antenna boresight and the RAS station is very nearly equal to the apparent elevation angle of the ADT as seen on the ground at the RAS station. This increases as the ADT nears, lowering the ADT antenna gain in the direction of the RAS station while the distance decreases in parallel, and the PL diminishes. The net result is that the incident pfd and required attenuation tend to remain constant. This implies that the geometric accumulation of interferers at large distances will dominate a calculation of aggregate interference.

FIGURE A7-3A

Attenuation needed for an Airborne data terminal operating at 15.4 GHz and transmitting in the horizontal plane with azimuth bearing toward a radio astronomy station, to reduce the incident mean pfd in the adjacent frequency band 15.35-15.4 GHz to −233 dB(W/(m² · Hz))

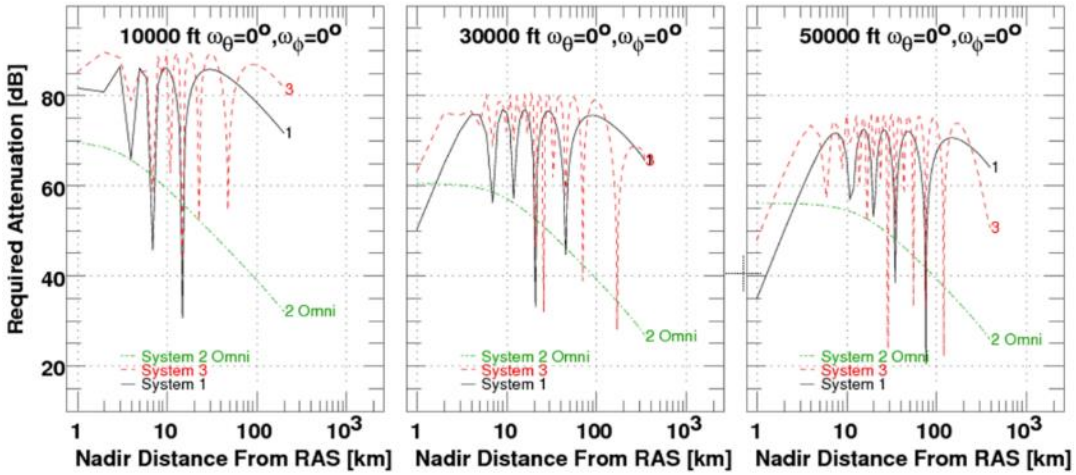

FIGURE A7-3B

Attenuation needed for an airborne data terminal operating at 22 GHz and transmitting in the horizontal plane with azimuth bearing toward a radio astronomy station, to reduce the incident mean pfd in the adjacent frequency band 15.35-15.4 GHz to −231 dB(W/(m² · Hz))

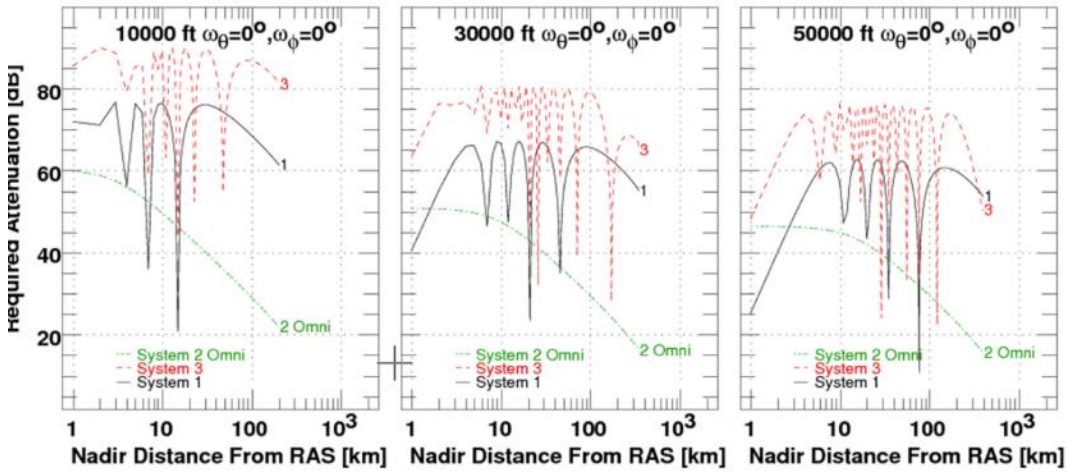

The conditions that foster compatibility can be inferred from a comparison with Figs A7-2A and A7-2B:

– In 15.4-15.7 GHz, for an ADT using System 1 at a nadir distance of 100 km and height of 30 000 ft., the required attenuation is 65 dB. According to Fig. A7-2A, this is attainable for 10 MHz BW centred at 15.43 GHz i.e. with 25 MHz guard band relative to the upper edge of the RAS measurement band. However, compatibility with the use of wider BW would require a reduction in power below the maximum of 40 dBm. With 20 dBm TPO, a 45 dB attenuation would be achievable with 50 MHz BW at the very upper end of the band 15.4-15.7 GHz, and only barely achievable with a 100 MHz BW.

– In 22-22.21 GHz, the same situation requires 75 dB attenuation that is not attainable for any BW-guard band configuration according to Fig. A7-2B. Use of a lower power, 20 dBm is compatible with 50 or 100 MHz BW when suitably displaced from the upper edge of the RAS band.

A7.1.5 Use case 2

The use of beam steering was also considered. Shown in Figs A7-4A and A7-4B is the case where the beam is steered downward by 30 degrees.

FIGURE A7-4A

As in Fig. A7-3A but with the beam also steered 30 degrees downward

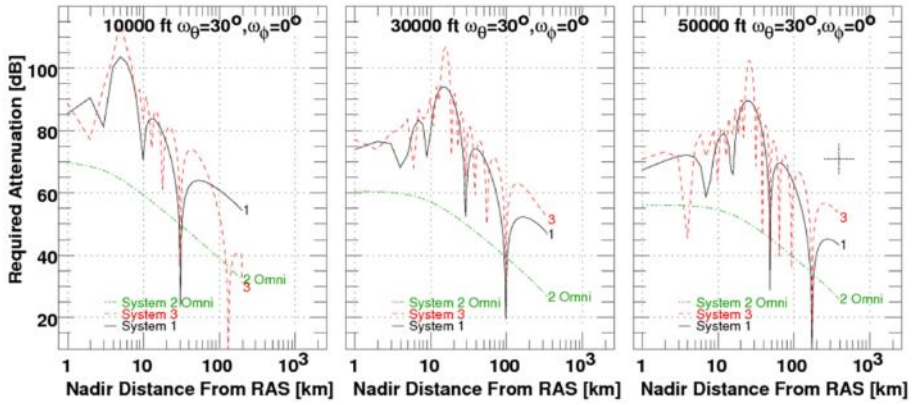

FIGURE A7-4B

As in Fig. A7-3B but with the beam also steered 30 degrees downward

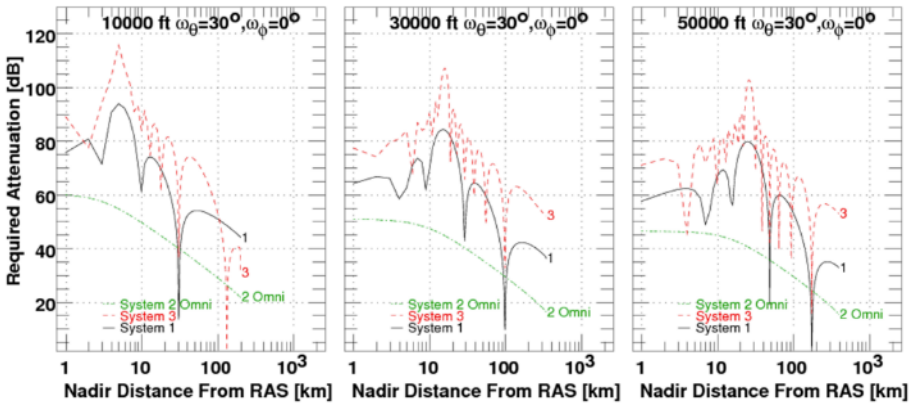

At large nadir distances the decrease in the incident pfd is just as expected from the antenna patterns illustrated in Fig. A1A-2 but at smaller separations the ADT antenna pattern is deflected toward the RAS station and more radiation is received. Therefore, the placement of GDTs will have to take into account the location of RAS stations in order to avoid drawing directional ADT antenna patterns too near the direction of the RAS stations.

A7.1.6 Use case 3

Avoiding illumination of the RAS site is likely to be an important element in achieving compatibility and the use of beam-steering is illustrated in Fig. A7-5. The solid curve shows the normalized ADT antenna gain of the two steerable AM(OR)S systems (Systems 1 and 3) when the beam is steered azimuthally away from the direction of RAS station by an angle ω_ϕ[18]. Also shown as a dashed curve is the effect of averaging over the full ±60° steering range of the antenna, while simultaneously excluding steering the beam within an azimuthal angle range $\pm\omega_\phi$ about the RAS station. Avoiding

[18] The definition of the angles ω_θ and ω_ϕ is provided in equation (A1A-5).

steering the beam in azimuth within 10-20° of the RAS station can provide 20-30 dB of isolation. Limiting the aggregate interference could require managing a network of distant ADTs.

FIGURE A7-5

Effects avoiding azimuthal beam steering toward the radio astronomy station for an airborne data terminal using Systems 1 and 3 operating in the aeronautical mobile (off-route) service in the frequency bands 15.4-15.7 GHz and 22-22.21 GHz

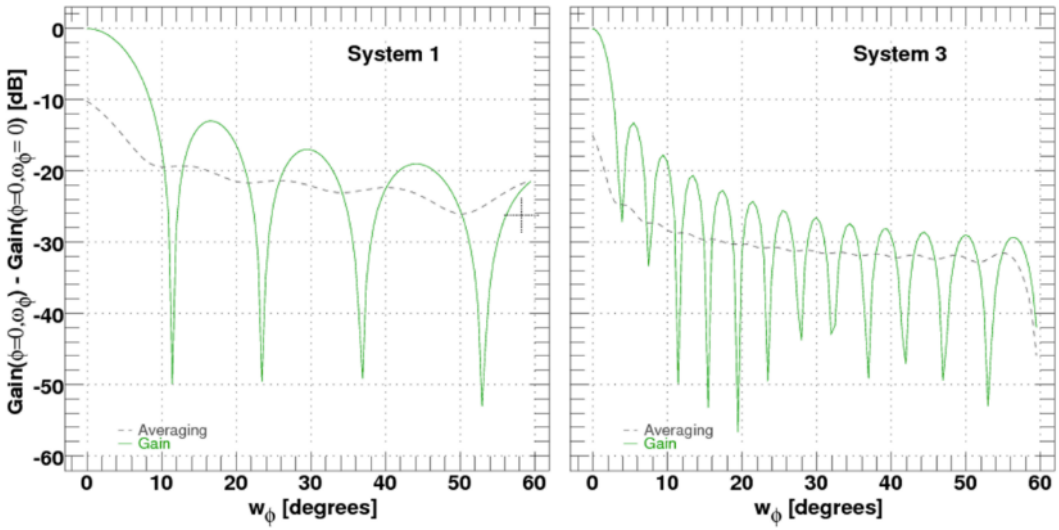

A7.1.7 Mitigation

Mitigating the negative margins shown in Figs A7-3A and A7-3B may take several forms:

– lowering the TPO or excluding transmission within some distance of a RAS station;

– choosing an appropriate channel BW for the ADTs;

– for AM(OR)S systems using directional antennas, avoiding pointing or steering the beam toward the RAS station, including when linking to GDTs.

A7.1.8 Summary

Study A shows that AM(OR)S use of the frequency bands 15.4-15.7 GHz and 22-22.21 GHz presents challenges to achieve compatibility with RAS operating in the adjacent bands 15.35-15.4 GHz and 22.21-22.5 GHz. Compatible operation of the ADT requires simultaneous consideration of many factors:

– the TPO of the ADT and the frequency channel use by the ADT;

– the situation of the RAS station in the antenna beam pattern of the ADT;

– the altitude of the ADT (also determining the RHD to the RAS station);

– the placement of GDTs receiving data from the ADT;

– the number of ADTs in LOS. In that case, the aggregate incident power will be dominated by ADTs at large nadir distances and steering of directional ADT antennas should avoid the direction of the RAS station. Therefore, limiting the aggregate interference could require managing a network of distant ADTs.

A7.2 Study B

A7.2.1 Methodology

Study B is a Monte Carlo analysis that evaluates the impact of future AM(OR)S systems planned to operate in the frequency bands 15.4-15.7 GHz and 22-22.21 GHz onto RAS stations performing CO in the adjacent bands 15.35-15.4 GHz and 22-22.21 GHz. The basic methodology, similar to a large extent to other Monte Carlo studies performed throughout this Report, is highlighted in Annex 16 to this Report.

However, Monte Carlo studies made with the RAS must also account for the integration time of CO measurements (2 000-s as highlighted in § A3.4.3). Therefore, instead of considering the statistical distribution of the aggregate received power over independent snapshots i.e. with a completely new deployment of AM(OR)S stations and a new configuration of the RAS station (including a new pointing of the antenna), snapshots are grouped in series of 100 to reproduce effective trajectories of AM(OR)S stations in the vicinity of RAS stations over the 2 000-s integration time[19]. The azimuth bearing of the clusters is supposed to not change over the whole trajectory.

The approach described above is equivalent to introducing a spatial and frequency correlation between snapshots in the same trajectory because the location of the next snapshot in the trajectory is determined from the location of the previous depending on the azimuth bearing and the assumed ground speed. On the other hand, the 100 snapshots in a given trajectory are considered to not change their channel allocation to best reproduce a real use case.

In summary, instead of considering 100 000 independent snapshots, 1 000 independent trajectories of AM(OR)S clusters around a RAS station are observed, each having a fixed configuration of the RAS station and a fixed channel allocation of AM(OR)S channels in the frequency bands 15.4-15.7 GHz and 22-22.21 GHz. In a second step, the average aggregate power received by the RAS station over each trajectory is compared against the detrimental thresholds of -172 dBm/50 MHz in the band 15.35-15.4 GHz and −165 dBm/290 MHz in the band 22.21-22.5 GHz highlighted in §§ A3.4.3 and A4.3.3. By convention, a RAS measurement is considered lost if the average power level over the integration period exceeds this detrimental threshold.

As explained in Annex 11, the four operational scenarios of AM(OR)S described in § 6.2 are taken as a basis for the study, together with the reference densities calculated in § 6.5. In particular, according to Table A11-5, one cluster is deployed around the RAS station in scenarios 6.2.1, 6.2.2 and 6.2.3, and two in scenario 6.2.4. In the latter case, one RAS measurement can potentially be disturbed by two clusters of AM(OR)S stations on simultaneous trajectories.

The specificities of the eight RAS sites introduced in § A3.4 and listed in Table A2-8 are also duly taken into consideration. In particular, the altitude of the RAS sites AMSL (which is represented by an altitude AGL in the smooth Earth model used in this study) and their antenna characteristics which can vary from one site to another, are taken into account.

Finally, the 100 000 snapshots (= 1 000 independent trajectories or groups of trajectories if several clusters are deployed per snapshot like in scenario 6.2.4) are repeated for different ranges of elevation angles at the RAS station, and to each elevation interval is associated a percentage of erroneous measurements which is compared against the maximum average over the whole sky of 2% indicated in § A2.4.3.

The methodology laid out in Recommendation ITU-R S.1586-1 divides the observable sky in rings of constant elevation offset and further divides each of these rings into a number of cells so that the

[19] If AM(OR)S clusters are assumed to move with constant nadir speed, a snapshot would therefore reflect the interference situation at the RAS station for a duration of 20 s.

area of each cell measured on the half-sphere over the RAS station is constant. This method is well adapted to study cases where an azimuth dependency is expected, for instance when the interferer is an non-GSO satellite network, for which Recommendation ITU-R S.1586-1 was originally developed. However, in this study, AM(OR)S clusters are uniformly distributed in azimuth around the RAS station, and therefore the results should not exhibit any azimuth dependency. It follows that the sole influence of the elevation is assessed. The half-sphere over the RAS station is therefore divided into 14 rings of equal area according to equation (A7-1):

$$\begin{cases} \theta_1 = \theta_{min} \\ \theta_{i+1} = \text{asin}\left(\frac{1}{N+1} + \sin(\theta_i)\right) \text{ for } 1 \le i \le 14 \end{cases} \quad \text{(A7-1)}$$

where:

θ_i: elevation angle (deg.) at the RAS station towards the bottom of the i-th ring

θ_{min}: minimum elevation angle i.e. 5 degrees according to note (3) under Table A2-8.

Note that the 14th ring does not have the same surface area, which should be taken into account when calculating the average percentage of erroneous measurements over the complete half-sphere over the RAS station.

A7.2.2 Simple study cases

To illustrate the methodology described in the previous section, shown in Figs A7-6 and A7-7 below are two particular trajectories of AM(OR)S clusters in scenario 6.2.1, in the band in the frequency bands 15.4-15.7 GHz. In this scenario, as explained in §§ A11.3 and A11.4, a single AM(OR)S cluster is deployed around the RAS station, and the radius of the spherical cap representing the simulation area is 254 km.

FIGURE A7-6

1 trajectory of stations operating in the aeronautical mobile (off-route) service in scenario 6.2.1 in the frequency band 15.4-15.7 GHz

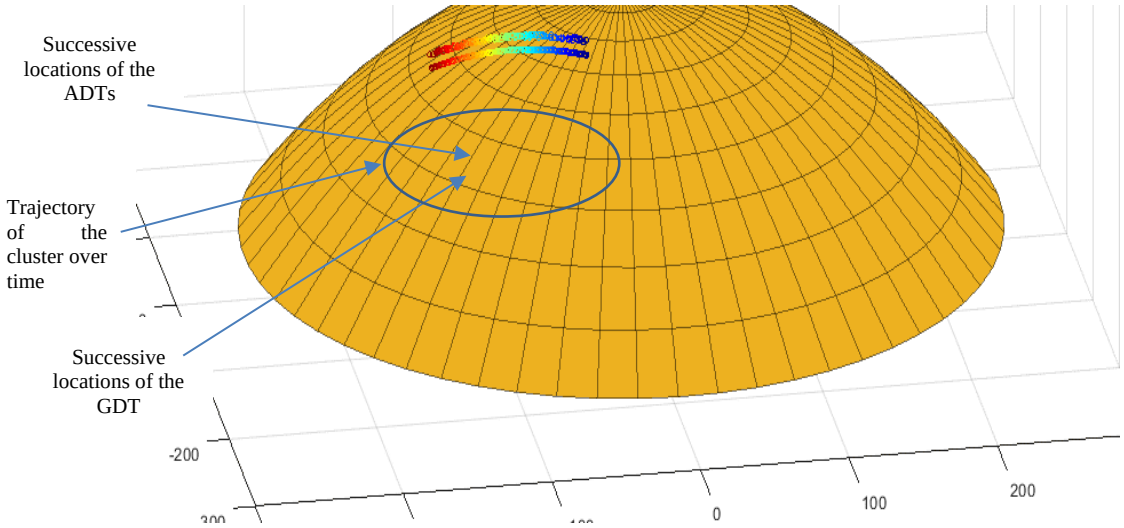

Note to Fig. A7-6: Distances are indicated in km and the Earth curvature is deliberately exaggerated. The radio astronomy station (blue dot in the middle of the simulation area) is assumed to have the characteristics of the Effelsberg site (in particular the altitude above mean sea level is 369 m as per Table A2-8. The antenna boresight (blue arrow) is 5 degrees above the local horizon. Successive positions of the cluster are shown with

different colours (blue at t = 0 s, red at t = 2 000 s). The nadir cluster speed is 200 km/h according to Table 3. The two airborne data terminals flying 300 m above the ground data terminal are not discernible in the swarm.

FIGURE A7-7

As in Fig. A7-6 using a different trajectory

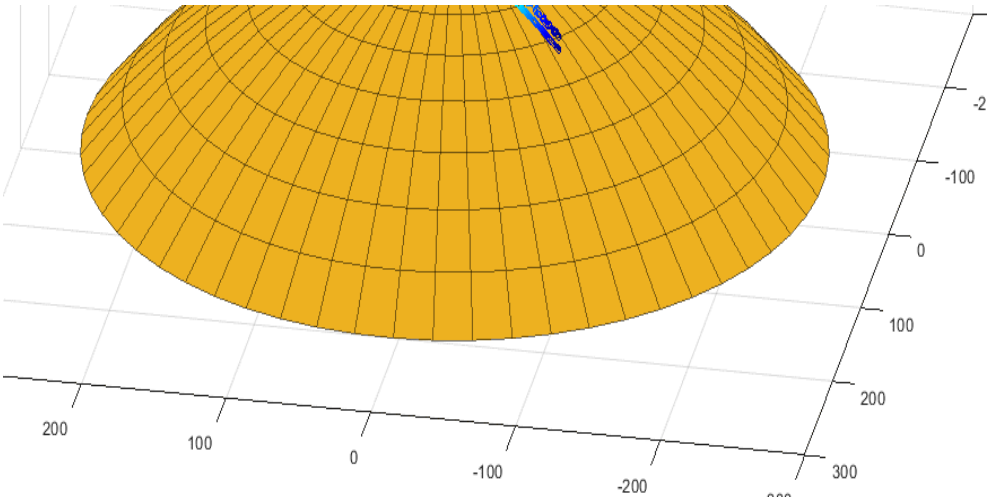

Figures A7-8 and A7-9 respectively show the instantaneous aggregate power received over the integration time by the RAS station in the two cases illustrated in Figs A7-6 and A7-7. In Fig. A7-8, the power is decreasing as the cluster is moving away from the RAS station. In Fig. A7-9, the power is increasing for the opposite reason. Over these two trajectories, the aggregate power level never exceeds the detrimental threshold of −172 dBm/50 MHz and therefore the RAS measurements are considered valid. This favourable situation can be explained by the fact that both trajectories are opposed in azimuth to the boresight of the RAS antenna and therefore are 'seen' with low gain values.

FIGURE A7-8

Instantaneous aggregate power (in dBm) received by the radio astronomy station over the trajectory shown in Fig. A7-6

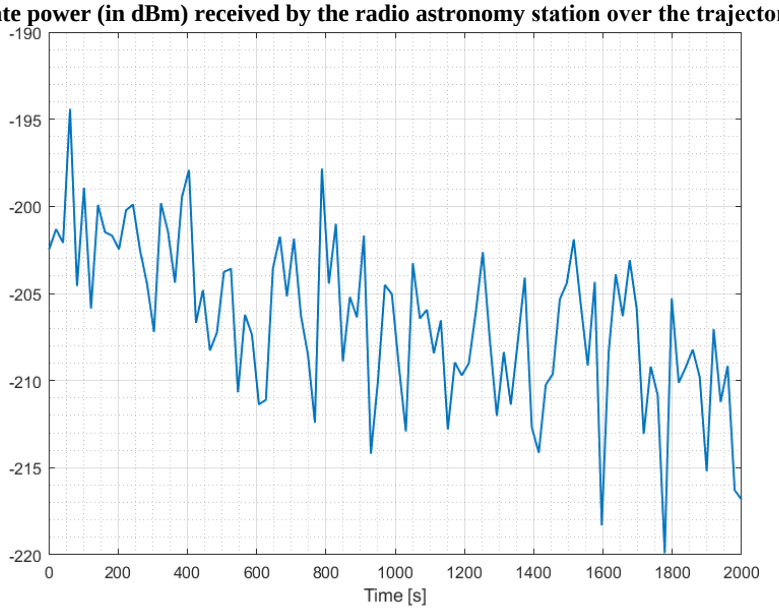

FIGURE A7-9

Instantaneous aggregate power (in dBm) received by the radio astronomy station over the trajectory shown in Fig. A7-7

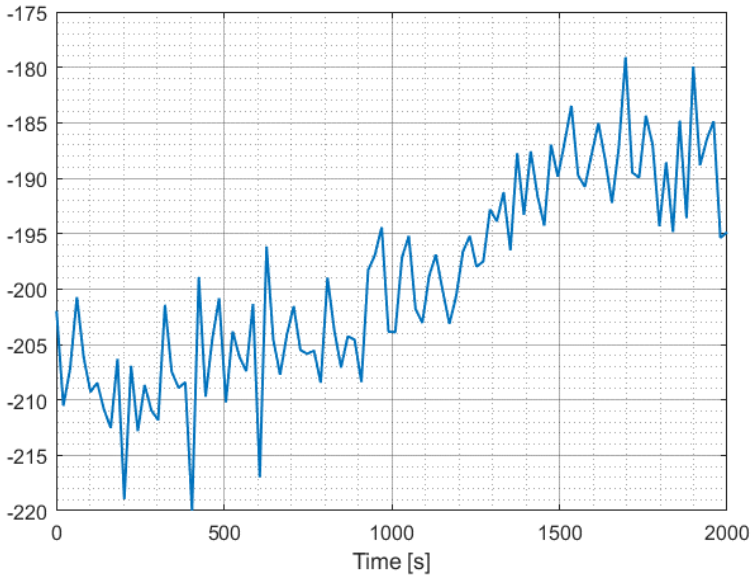

Figures A7-10 and A7-11 show the ground track of 1 000 different cluster trajectories around the Effelsberg RAS station. Figure A7-12 shows the power levels averaged over the 2 000-s integration time of RAS measurements for the 1 000 snapshots. In this example, the probability to have an erroneous measure because of interference corresponds to the ratio of points above the detrimental threshold. This is about 11.3% or equivalently 113 measurements out of a total of 1 000 (value underlined in Table A7-4).

FIGURE A7-10

Top view of 1 000 ground tracks of the ground data terminal (fire truck) around the Effelsberg site in scenario 6.2.1, elevation of the radio astronomy station is between 5 and 8.85 degrees, distances are indicated in km, assumed nadir cluster speed = 200 km/h according to Table 3

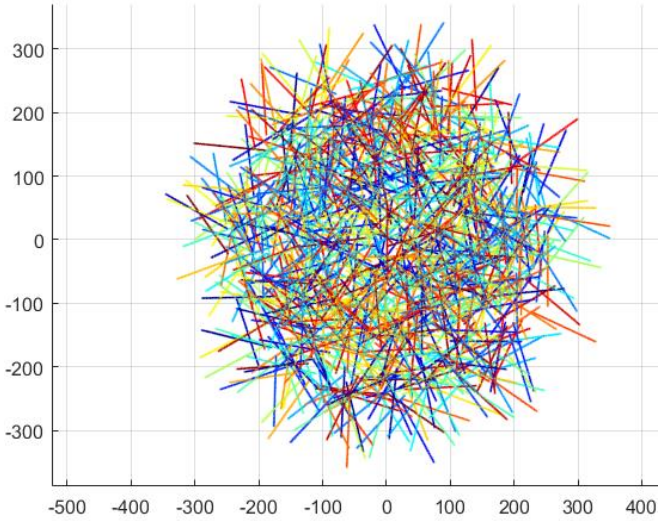

FIGURE A7-11

As in Fig. A7-10, side view

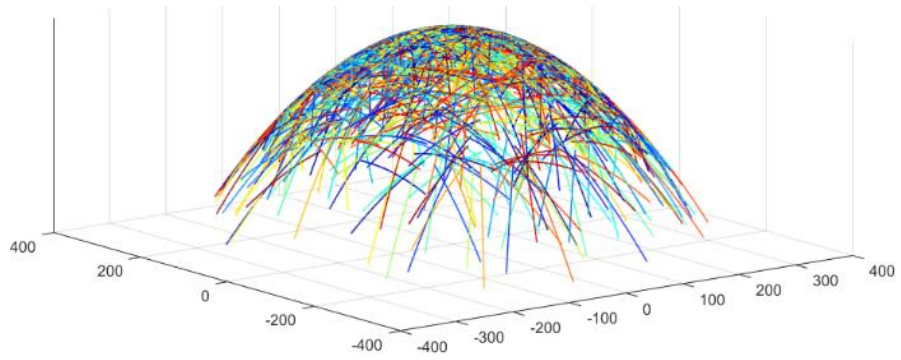

FIGURE A7-12

Average aggregate power at the Effelsberg radio astronomy station (blue dots) for 1 000 different trajectories, the configuration is as in Fig. A7-10, the detrimental interference level is indicated as a red line

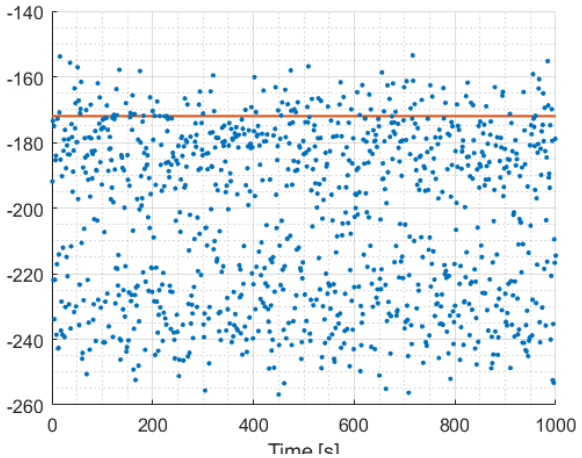

Snapshot

A7.2.3 Results

Intermediate results, for instance, the FDR between AM(OR)S channels and the RAS measurement band, antenna gains and so on are provided in Attachment A to this Annex. The complete set of results is shown in Tables A7-4 to A7-7 below for the four scenarios. These Tables indicate the number of erroneous measurements (out of a total of 1 000) for different ranges of elevation angles and for the eight RAS stations listed in § A2.4.1. Each cell contains in the upper part the result for RAS measurements in the frequency band 15.35-15.4 GHz, and in the lower part, for measurements in the band 22.21-22.5 GHz. Cells highlighted in green show less than 10 erroneous measurements (i.e. less than 1%), in orange between 10 and 20 (i.e. between 1% and 2%), and in red, above 20 (i.e. above 2%).

The average number of erroneous measurements over all elevation angles for each RAS is also calculated using equation (A7-2) and indicated under each Table. Finally, Fig. A7-13 shows the ECDF of the average aggregate power level over 1 000 RAS measurements in the four scenarios.

In scenario 6.2.1 (Table A7-4), in the band 15.35-15.4 GHz, the average number of erroneous measurements is higher than 2% in all considered RAS stations. In the band 22.21-22.5 GHz, it is between 0 and 1% for all sites, except the GBT and the Tianma station, which can be explained by the fact that these two sites have the lowest altitude and therefore have higher sensitivity to low altitude ADTs (ADTs fly at an altitude of 300 m AGL in this scenario as per Table 3).

In scenario 6.2.2, three RAS stations (Jansky VLA, Nobeyama and Plateau de Bure) have returned more that 2% of erroneous measurements in the band 15.35-15.4 GHz, the situation being more favourable in the band 22.21-22.5 GHz.

In scenario 6.2.3, no measurement was found erroneous in any of the RAS site for any elevation angle, except for 1 measurement at the Bure station between 8.85 and 12.7 degrees.

In scenario 6.2.4, no elevation range in any of the eight RAS stations has produced more than 2% of erroneous measurements.

One can also note that less measurements are lost when RAS measurements are performed in the band 15.4-15.7 GHz (i.e. when AM(OR)S stations are operating in the frequency band 15.4-15.7 GHz) as compared to 22.21-22.5 GHz (i.e. when AM(OR)S stations are operating in the frequency band 22-22.21 GHz), which can be explained as follows:

– the frequency band 22-22.21 GHz is higher in frequency than in the frequency band 15.4-15.7 GHz, which increases the PL between ADTs and the RAS station, hence improving the coexistence situation;

– the measurement band adjacent to the frequency band 15.4-15.7 GHz is smaller than the band adjacent to the frequency band 22-22.21 GHz, which relaxes the protection criterion according to equation (3) in Recommendation ITU-R RA.769-2;

– in general, the model used in this Report makes RAS antennas slightly more directive when the frequency increases (one can compare the antenna characteristics provided in Table A2-8 for the frequency band 15.4-15.7 GHz with the equivalent characteristics for the frequency band 22-22.21 GHz in Table A2-4). In general, more directive antennas at the RAS site improves the coexistence situation with active services.

Figure A7-13 shows in three dimensions the percentage of lost measurements in the band 15.35-15.4 GHz at the Effelsberg RAS station as a function of the elevation angle, i.e. the first column (in bold) in Table A7-4.

Figure A7-14 finally show the ECDF of the average power level at the RAS station over the complete measurement range 5 to 90 degrees.

$$\begin{cases} N_{\text{average}} = \dfrac{1}{\mathrm{A}_{\text{total}}} \displaystyle\sum_{n=1}^{14} A_n \cdot N_i = \dfrac{1}{A_{\text{total}}} \cdot \left(A_{1-13} \cdot \displaystyle\sum_{n=1}^{13} N_i + \mathrm{A}_{14} \cdot N_{14} \right) \\ A_{1-13} = \frac{2\pi}{15} \text{ and } A_{1-13} = 2\pi\left(1 - \sin(72.5°)\right) \text{ using equation (A7-1)} \\ A_{\text{total}} = 2\pi\left(1 - \sin(\theta_{\min})\right) \end{cases} \quad \text{(A7-2)}$$

where:

N_{average}: average number of erroneous measurements for a given RAS station over all possible elevation angle from θ_{min} to 90°, rounded to the closest integer

A_{total}: total area of the measurement unit hemisphere over the RAS station

A_n: area of the n-th ring of the unit hemisphere over the RAS station.

FIGURE A7-13

Simulated percentage of erroneous measurements at the Effelsberg radio astronomy station in the frequency band 15.35-15.4 GHz

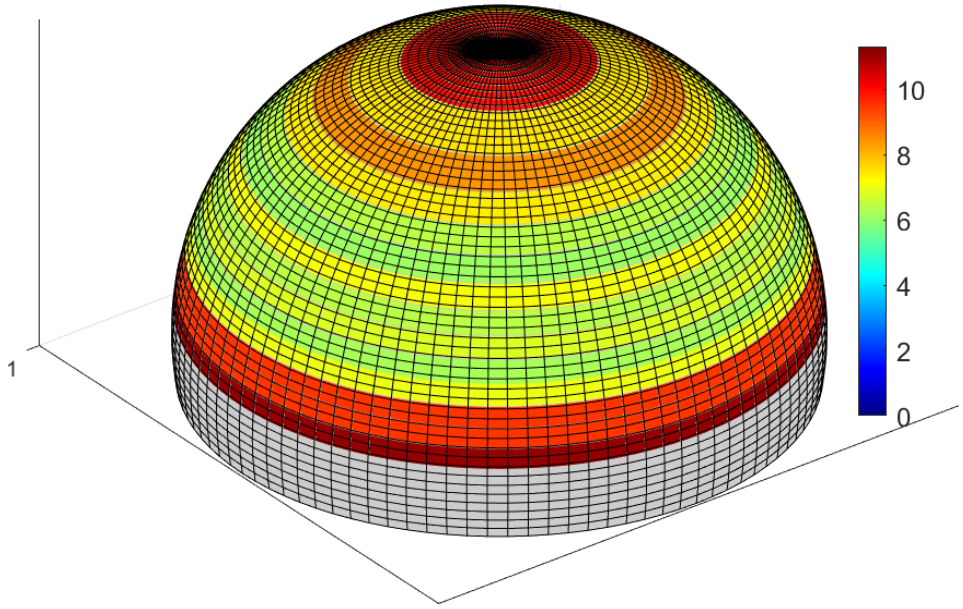

Note to Fig. A7-13: The data are taken from the first column in Table A7-4; no measurements are performed in the grey area, which corresponds to elevation angles below the minimum of 5 degrees.

FIGURE A7-14

Empirical cumulative distribution function of the average measured interference level over the 2 000 s integration time (example of the Effelsberg radio astronomy station in the frequency band 22.21-22.5 GHz in scenario 6.2.1)

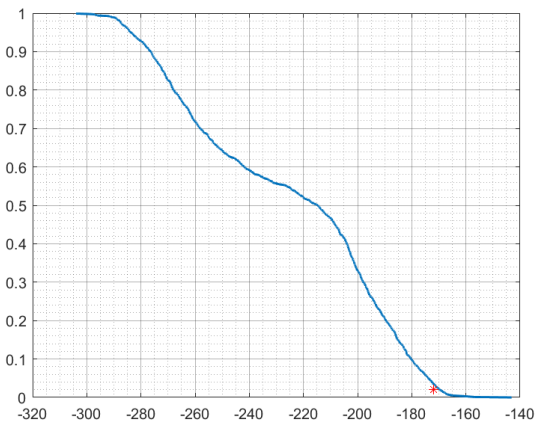

TABLE A7-4

Percentage of erroneous measurements at the radio astronomy station in the frequency band 15.35-15.4 GHz as a function of the elevation angle in scenario 6.2.1

	Effelsberg	MeerKAT	GBT	Jansky VLA	Parkes	Tianma	Nobeyama	Bure
5°-8.85°	11%	8.8%	9.4%	7.6%	11%	6.5%	8.0%	5.1%
8.85°-12.7°	7.6%	5.5%	10%	4.8%	10%	7.0%	5.2%	3.2%
12.7°-16.7°	9.2%	3.8%	7.6%	3.1%	7.5%	5.6%	4.0%	3.1%
16.7°-20.7°	6.8%	4.3%	7.4%	2.7%	7.6%	5.6%	3.3%	2.7%
20.7°-24.9°	6.7%	3.2%	7.6%	3.4%	6.6%	7.2%	2.0%	2.6%
24.9°-29.2°	5.7%	3.7%	6.0%	1.9%	6.3%	5.6%	2.0%	2.5%
29.2°-33.6°	6.5%	2.1%	7.4%	1.6%	6.4%	5.4%	2.4%	1.6%
33.6°-38.4°	5.1%	2.3%	6.9%	2.6%	6.7%	6.1%	1.6%	2.1%
38.4°-43.4°	5.8%	2.4%	7.2%	2.7%	6.6%	5.0%	2.4%	2.8%
43.4°-49°	6.0%	2.5%	6.0%	2.3%	5.3%	6.3%	2.1%	2.0%
49°-55.1°	6.7%	1.6%	6.4%	1.8%	5.7%	5.2%	2.3%	2.4%
55.1-62.5°	6.7%	2.3%	7.6%	2.7%	8.6%	6.0%	2.7%	2.8%
62.5°-72.5°	7.5%	3.0%	9.4%	3.6%	8.3%	6.8%	2.7%	2.6%
72.5°-90°	10%	4.0%	8.6%	4.3%	9.5%	7.1%	3.8%	2.8%
Average	**6.7%**	**3.5%**	**7.7%**	**3.2%**	**7.5%**	**6.1%**	**3.2%**	**2.7%**

TABLE A7-5

Percentage of erroneous measurements at the radio astronomy station in the frequency band 22-22.21 GHz as a function of the elevation angle in scenario 6.2.1

	Effelsberg	MeerKAT	GBT	Jansky VLA	Parkes	Tianma	Nobeyama	Bure
5°-8.85°	0.90%	0.40%	1.6%	1.0%	0.70%	1.3%	0.20%	0.40%
8.85°-12.7°	0.90%	0.90%	2.3%	0.80%	1.2%	2.4%	1.0%	0.50%
12.7°-16.7°	1.7%	2.0%	2.8%	0.70%	0.60%	3.1%	0.60%	0.60%
16.7°-20.7°	1.0%	1.0%	1.4%	0.60%	0.80%	1.5%	0.70%	0.20%
20.7°-24.9°	0.80%	0.40%	2.0%	0.00%	0.90%	1.7%	0.40%	0.80%
24.9°-29.2°	0.90%	1.1%	0.60%	0.40%	0.80%	1.4%	0.50%	0.50%
29.2°-33.6°	0.60%	0.40%	1.3%	0.40%	0.90%	1.1%	0.70%	0.20%
33.6°-38.4°	0.70%	0.30%	1.6%	0.40%	0.70%	1.3%	0.30%	0.10%
38.4°-43.4°	0.40%	0.40%	2.5%	0.20%	0.60%	1.2%	0.30%	0.60%
43.4°-49°	0.60%	0.30%	1.7%	0.50%	0.60%	1.8%	0.30%	0.70%
49°-55.1°	0.40%	0.50%	1.3%	0.70%	0.40%	1.5%	0.50%	0.10%
55.1-62.5°	0.60%	0.50%	1.9%	0.30%	1.1%	1.9%	0.80%	0.50%
62.5°-72.5°	0.90%	0.60%	2.1%	0.80%	0.50%	1.5%	1.2%	0.90%
72.5°-90°	0.80%	0.80%	1.6%	0.80%	0.60%	1.9%	0.90%	0.50%
Average	**0.80%**	**0.55%**	**1.8%**	**0.54%**	**0.75%**	**1.7%**	**0.59%**	**0.47%**

TABLE A7-6

Percentage of erroneous measurements at the radio astronomy station in the frequency band 15.35-15.4 GHz as a function of the elevation angle in scenario 6.2.2

	Effelsberg	MeerKAT	GBT	Jansky VLA	Parkes	Tianma	Nobeyama	Bure
5°-8.85°	1.7%	2.0%	2.1%	2.4%	1.9%	1.3%	2.3%	3.3%
8.85°-12.7°	1.8%	2.3%	2.2%	2.4%	2.5%	1.4%	1.4%	3.2%
12.7°-16.7°	1.1%	1.8%	1.6%	3.3%	2.0%	0.80%	1.6%	1.9%
16.7°-20.7°	2.2%	2.0%	1.1%	1.8%	1.4%	1.2%	1.8%	2.0%
20.7°-24.9°	1.1%	1.4%	1.0%	1.6%	2.0%	1.4%	1.8%	1.8%
24.9°-29.2°	2.0%	1.9%	1.7%	1.4%	1.2%	2.0%	1.5%	2.8%
29.2°-33.6°	1.4%	1.6%	1.4%	1.9%	2.4%	1.0%	1.6%	2.1%
33.6°-38.4°	1.7%	2.0%	1.3%	1.4%	1.3%	1.4%	1.8%	1.8%
38.4°-43.4°	1.4%	1.8%	1.2%	2.1%	1.5%	0.80%	1.5%	1.5%
43.4°-49°	1.5%	1.4%	0.90%	2.8%	1.4%	1.3%	0.90%	1.6%
49°-55.1°	1.5%	1.8%	1.2%	1.7%	1.6%	1.0%	1.2%	1.7%
55.1-62.5°	1.8%	1.6%	1.4%	1.6%	1.0%	1.5%	1.7%	1.6%
62.5°-72.5°	1.6%	1.6%	0.90%	2.4%	1.8%	1.5%	2.9%	2.0%
72.5°-90°	1.8%	1.9%	1.4%	2.6%	2.7%	1.7%	2.4%	2.1%
Average	**1.6%**	**1.8%**	**1.4%**	**2.1%**	**1.7%**	**1.3%**	**1.7%**	**2.1%**

TABLE A7-7

Percentage of erroneous measurements at the radio astronomy station in the frequency band 22-22.21 GHz as a function of the elevation angle in scenario 6.2.2

	Effelsberg	**MeerKAT**	**GBT**	**Jansky VLA**	**Parkes**	**Tianma**	**Nobeyama**	**Bure**
5°-8.85°	0.20%	0.10%	0.10%	0.20%	0.20%	0.20%	0.30%	0.20%
8.85°-12.7°	0.30%	0.10%	0.10%	0.30%	0.20%	0.10%	0.10%	0.10%
12.7°-16.7°	0.0%	0.10%	0.0%	0.30%	0.10%	0.0%	0.30%	0.20%
16.7°-20.7°	0.20%	0.40%	0.20%	0.20%	0.10%	0.10%	0.0%	0.40%
20.7°-24.9°	0.0%	0.10%	0.0%	0.20%	0.20%	0.10%	0.20%	0.0%
24.9°-29.2°	0.0%	0.0%	0.10%	0.10%	0.10%	0.20%	0.10%	0.30%
29.2°-33.6°	0.0%	0.20%	0.10%	0.20%	0.0%	0.0%	0.10%	0.40%
33.6°-38.4°	0.30%	0.0%	0.10%	0.10%	0.0%	0.10%	0.10%	0.10%
38.4°-43.4°	0.10%	0.10%	0.0%	0.20%	0.10%	0.0%	0.10%	0.20%
43.4°-49°	0.0%	0.10%	0.10%	0.20%	0.10%	0.0%	0.0%	0.0%
49°-55.1°	0.20%	0.20%	0.0%	0.0%	0.0%	0.0%	0.10%	0.40%
55.1-62.5°	0.10%	0.10%	0.0%	0.0%	0.10%	0.0%	0.10%	0.0%
62.5°-72.5°	0.10%	0.30%	0.10%	0.40%	0.10%	0.10%	0.0%	0.30%
72.5°-90°	0.10%	0.10%	0.10%	0.20%	0.10%	0.20%	0.20%	0.10%
Average	**0.11%**	**0.14%**	**0.071%**	**0.19%**	**0.10%**	**0.076%**	**0.12%**	**0.19%**

TABLE A7-8

Percentage of erroneous measurements at the radio astronomy station in the frequency band 15.35-15.4 GHz as a function of the elevation angle in scenario 6.2.3

	Effelsberg	**MeerKAT**	**GBT**	**Jansky VLA**	**Parkes**	**Tianma**	**Nobeyama**	**Bure**
5°-8.85°	0.0%	0.0%	0.0%	0.0%	0.0%	0.0%	0.0%	0.0%
8.85°-12.7°	0.0%	0.0%	0.0%	0.0%	0.0%	0.0%	0.0%	0.0%
12.7°-16.7°	0.0%	0.0%	0.0%	0.0%	0.0%	0.0%	0.0%	0.0%
16.7°-20.7°	0.0%	0.0%	0.0%	0.0%	0.0%	0.0%	0.0%	0.0%
20.7°-24.9°	0.0%	0.0%	0.0%	0.0%	0.0%	0.0%	0.0%	0.0%
24.9°-29.2°	0.0%	0.0%	0.0%	0.0%	0.0%	0.0%	0.0%	0.0%
29.2°-33.6°	0.0%	0.0%	0.0%	0.0%	0.0%	0.0%	0.0%	0.0%
33.6°-38.4°	0.0%	0.0%	0.0%	0.0%	0.0%	0.0%	0.0%	0.0%
38.4°-43.4°	0.0%	0.0%	0.0%	0.0%	0.0%	0.0%	0.0%	0.0%
43.4°-49°	0.0%	0.0%	0.0%	0.0%	0.0%	0.0%	0.0%	0.0%
49°-55.1°	0.0%	0.0%	0.0%	0.0%	0.0%	0.0%	0.0%	0.0%
55.1-62.5°	0.0%	0.0%	0.0%	0.0%	0.0%	0.0%	0.0%	0.0%
62.5°-72.5°	0.0%	0.0%	0.0%	0.0%	0.0%	0.0%	0.0%	0.0%
72.5°-90°	0.0%	0.0%	0.0%	0.0%	0.0%	0.0%	0.0%	0.0%
Average	**0.0%**	**0.0%**	**0.0%**	**0.0%**	**0.0%**	**0.0%**	**0.0%**	**0.0%**

TABLE A7-9

Percentage of erroneous measurements at the radio astronomy station in the frequency band 22-22.21 GHz as a function of the elevation angle in scenario 6.2.3

	Effelsberg	**MeerKAT**	**GBT**	**Jansky VLA**	**Parkes**	**Tianma**	**Nobeyama**	**Bure**
5°-8.85°	0.0%	0.0%	0.0%	0.0%	0.0%	0.0%	0.0%	0.0%
8.85°-12.7°	0.0%	0.0%	0.0%	0.0%	0.0%	0.0%	0.0%	0.0%
12.7°-16.7°	0.0%	0.0%	0.0%	0.0%	0.0%	0.0%	0.0%	0.0%
16.7°-20.7°	0.0%	0.0%	0.0%	0.0%	0.0%	0.0%	0.0%	0.0%
20.7°-24.9°	0.0%	0.0%	0.0%	0.0%	0.0%	0.0%	0.0%	0.0%
24.9°-29.2°	0.0%	0.0%	0.0%	0.0%	0.0%	0.0%	0.0%	0.0%
29.2°-33.6°	0.0%	0.0%	0.0%	0.0%	0.0%	0.0%	0.0%	0.0%
33.6°-38.4°	0.0%	0.0%	0.0%	0.0%	0.0%	0.0%	0.0%	0.0%
38.4°-43.4°	0.0%	0.0%	0.0%	0.0%	0.0%	0.0%	0.0%	0.0%
43.4°-49°	0.0%	0.0%	0.0%	0.0%	0.0%	0.0%	0.0%	0.0%
49°-55.1°	0.0%	0.0%	0.0%	0.0%	0.0%	0.0%	0.0%	0.0%
55.1-62.5°	0.0%	0.0%	0.0%	0.0%	0.0%	0.0%	0.0%	0.0%
62.5°-72.5°	0.0%	0.0%	0.0%	0.0%	0.0%	0.0%	0.0%	0.0%
72.5°-90°	0.0%	0.0%	0.0%	0.0%	0.0%	0.0%	0.0%	0.0%
Average	**0.0%**	**0.0%**	**0.0%**	**0.0%**	**0.0%**	**0.0%**	**0.0%**	**0.0%**

TABLE A7-10

Percentage of erroneous measurements at the radio astronomy station in the frequency band 15.35-15.4 GHz as a function of the elevation angle in scenario 6.2.4

	Effelsberg	**MeerKAT**	**GBT**	**Jansky VLA**	**Parkes**	**Tianma**	**Nobeyama**	**Bure**
5°-8.85°	0.50%	1.0%	0.90%	0.40%	0.90%	0.70%	1.7%	1.1%
8.85°-12.7°	0.30%	0.80%	1.3%	1.1%	1.3%	0.70%	0.70%	0.70%
12.7°-16.7°	0.90%	0.90%	1.1%	1.2%	0.50%	0.70%	0.90%	1.0%
16.7°-20.7°	0.50%	0.50%	0.40%	0.60%	0.80%	0.80%	1.0%	0.40%
20.7°-24.9°	1.0%	1.1%	0.60%	1.6%	0.80%	0.80%	1.2%	1.5%
24.9°-29.2°	0.70%	0.90%	0.90%	0.80%	0.10%	0.40%	1.1%	0.20%
29.2°-33.6°	0.30%	0.80%	0.70%	0.60%	0.40%	0.40%	1.3%	0.80%
33.6°-38.4°	1.0%	0.50%	0.70%	1.2%	1.0%	0.40%	1.0%	1.2%
38.4°-43.4°	0.90%	0.60%	0.90%	0.70%	0.20%	0.30%	0.40%	0.50%
43.4°-49°	0.60%	1.2%	0.40%	1.1%	1.0%	0.70%	0.60%	1.4%
49°-55.1°	0.90%	0.80%	0.40%	1.2%	0.50%	0.80%	1.0%	0.70%
55.1-62.5°	0.60%	0.70%	0.60%	0.80%	0.30%	0.60%	0.90%	0.70%
62.5°-72.5°	1.0%	0.80%	0.30%	0.50%	1.2%	0.50%	1.2%	1.4%
72.5°-90°	1.0%	1.2%	1.2%	0.90%	1.0%	0.70%	1.1%	0.80%
Average	**0.72%**	**0.83%**	**0.73%**	**0.91%**	**0.71%**	**0.61%**	**1.0%**	**0.89%**

TABLE A7-11

Percentage of erroneous measurements at the radio astronomy station in the frequency band 22-22.21 GHz as a function of the elevation angle in scenario 6.2.4

	Effelsberg	**MeerKAT**	**GBT**	**Jansky VLA**	**Parkes**	**Tianma**	**Nobeyama**	**Bure**
5°-8.85°	0.20%	0.10%	0.20%	0.10%	0.10%	0.00%	0.10%	0.10%
8.85°-12.7°	0.00%	0.00%	0.00%	0.30%	0.10%	0.20%	0.10%	0.00%
12.7°-16.7°	0.20%	0.40%	0.00%	0.10%	0.10%	0.00%	0.00%	0.40%
16.7°-20.7°	0.00%	0.00%	0.00%	0.10%	0.00%	0.10%	0.40%	0.40%
20.7°-24.9°	0.20%	0.20%	0.30%	0.10%	0.00%	0.00%	0.30%	0.40%
24.9°-29.2°	0.10%	0.20%	0.00%	0.10%	0.20%	0.00%	0.20%	0.10%
29.2°-33.6°	0.00%	0.20%	0.10%	0.40%	0.00%	0.00%	0.10%	0.30%
33.6°-38.4°	0.10%	0.00%	0.00%	0.10%	0.00%	0.00%	0.10%	0.20%
38.4°-43.4°	0.10%	0.00%	0.10%	0.00%	0.30%	0.10%	0.10%	0.40%
43.4°-49°	0.10%	0.00%	0.10%	0.10%	0.30%	0.40%	0.20%	0.40%
49°-55.1°	0.00%	0.00%	0.00%	0.20%	0.10%	0.20%	0.10%	0.40%
55.1-62.5°	0.10%	0.10%	0.30%	0.00%	0.00%	0.10%	0.10%	0.10%
62.5°-72.5°	0.00%	0.00%	0.10%	0.20%	0.00%	0.10%	0.10%	0.30%
72.5°-90°	0.10%	0.30%	0.00%	0.20%	0.10%	0.20%	0.10%	0.50%
Average	**0.085%**	**0.10%**	**0.088%**	**0.14%**	**0.093%**	**0.098%**	**0.14%**	**0.28%**

A7.2.4 Summary

Study B has shown that coexistence between future AM(OR)S systems planned to operate in the frequency bands 15.4-15.7 GHz and 22-22.21 GHz and RAS in the adjacent bands 15.35-15.4 GHz and 22.21-22.5 GHz is in general improved if directive antennas are used (for instance in scenarios 6.2.2, 6.2.3 and 6.2.4 as compared to scenario 6.2.1). In that case, the percentage of erroneous measurements is in general below 2%, with a few exceptions (3 RAS stations in scenario 6.2.2 have returned slightly more than 2% of erroneous measurements). Moreover, coexistence is more easily achieved in the upper band 22-22.21 GHz than in the lower band 15.4-15.7 GHz.

If omnidirectional antennas are used for AM(OR)S, for instance in scenario 6.2.1, the percentage of erroneous measurements can raise above 2%. Therefore, mitigation techniques shall be tested in study C and D to reduce this percentage.

A7.3 Study C

A7.3.1 Introduction

Study B has shown that the protection criteria of RAS can be exceeded in the band 15.35-15.4 GHz in some scenarios where omnidirectional antennas are used (for instance scenario 6.2.1), and in some other configurations where directive antennas are used (scenario 6.2.2 for 3 RAS configurations). Therefore, some mitigation measures must be considered to reduce the power captured by the RAS station from AM(OR)S transmissions.

The power emitted in the RAS measurement band 15.35-15.4 GHz by an AM(OR)S transmitter (measured at the antenna port of the AM(OR)S system) is given in equation (A7-3):

$$P_{RAS} = P_{Tx} - FDR_{RAS} \quad \text{(A7-3)}$$

where:

P_{RAS}: power level (dBm) emitted by the AM(OR)S station in the RAS band 15.35-15.4 GHz, measured at the antenna port

P_{Tx}: TPO (dBm) of the AM(OR)S station

FDR_{RAS}: FDR (dB) between the AM(OR)S channel inside the tuning range 15.4-15.7 GHz and the RAS band 15.35-15.4 GHz.

As explained in § A2.4.1 of this Report, RAS stations are assumed to filter all emissions outside of their measurement band. It results that FDR_{RAS} is simply obtained by integrating the SEM of AM(OR)S stations (provided in Table A1-1) over the RAS band 15.35-15.4 GHz. Consequently FDR_{RAS} only depends on the guard band between the AM(OR)S channel and the RAS frequency band. On the other hand P_{RAS} can also be reduced by decreasing P_{Tx}. These two mitigation techniques are studied independently in the following subsections.

A7.3.2 Guard band

One leverage to decrease P_{RAS} in equation (A7-1) is to increase FDR_{RAS} by using a guard band with the RAS measurement band ending at 15.4 GHz. Tables A7-8 to A7-11[20] show the effect of this guard band on the percentage of erroneous measurements at the RAS station and can be compared against Tables A7-4 to A7-7 in Study B where no such mitigation measure was applied. One can see that this guard band is sufficient to meet the protection criterion at all RAS stations considered.

A7.3.3 Capacity reduction

Another way of reducing P_{Tx} is to decrease the necessary BW of AM(OR)S stations and hence the WBLOSDL capacity. The effect of this measure has not been assessed in this Report, but it is thought to be similar to the introduction of a guard band with the RAS measurement band.

A7.3.4 Summary

In AM(OR)S configuration where the RAS protection criteria is exceeded (for instance, as shown in Study B, when omnidirectional antennas are used), introducing a 10 MHz guard band with the RAS measurement band or equivalently reducing the capacity of WBLOSDL in the vicinity of the RAS station is an efficient measure to reduce interference to an acceptable level.

---

[20] The effect of a 10 MHz guard ban is studied in the four scenarios 6.2.1 to 6.2.4 and in the two frequency bands 15.4-15.7 GHz and 22-22.21 GHz even though Study B shows that such mitigation technique is not always necessary.

TABLE A7-12

Percentage of erroneous measurements at the radio astronomy station in the frequency band 15.35-15.4 GHz as a function of the elevation angle in scenario 6.2.1. A guard band of 10 MHz at 15.4-15.41 GHz is used

	Effelsberg	**MeerKAT**	**GBT**	**Jansky VLA**	**Parkes**	**Tianma**	**Nobeyama**	**Bure**
5°-8.85°	3.0%	2.0%	2.9%	0.80%	2.3%	3.3%	3.9%	2.5%
8.85°-12.7°	1.2%	0.20%	3.1%	0.50%	1.6%	1.9%	2.0%	s
12.7°-16.7°	1.5%	0.60%	2.3%	0.50%	1.5%	2.1%	1.7%	1.6%
16.7°-20.7°	1.1%	0.30%	1.7%	0.30%	0.60%	1.6%	1.1%	1.3%
20.7°-24.9°	0.80%	0.60%	2.1%	0.60%	0.60%	2.1%	1.0%	1.4%
24.9°-29.2°	0.30%	0.20%	0.90%	0.00%	0.20%	1.9%	1.0%	1.2%
29.2°-33.6°	0.50%	0.20%	1.1%	0.50%	0.30%	1.8%	1.2%	0.8%
33.6°-38.4°	0.70%	0.20%	1.7%	0.80%	0.30%	1.5%	0.8%	1.0%
38.4°-43.4°	0.50%	0.10%	1.7%	0.10%	0.50%	1.4%	1.2%	1.5%
43.4°-49°	0.20%	0.20%	1.1%	0.50%	0.40%	1.8%	1.0%	0.9%
49°-55.1°	0.50%	0.50%	1.2%	0.00%	0.80%	1.1%	1.1%	1.1%
55.1-62.5°	0.60%	0.40%	1.6%	0.60%	0.70%	1.3%	1.3%	1.2%
62.5°-72.5°	0.80%	0.60%	2.1%	0.60%	0.50%	2.6%	1.5%	1.3%
72.5°-90°	1.2%	0.50%	1.6%	0.40%	1.3%	2.2%	2.0%	1.5%
Average	**0.72%**	**0.47%**	**1.7%**	**0.44%**	**0.82%**	**1.9%**	**1.5%**	**1.4%**

TABLE A7-13

Percentage of erroneous measurements at the RAS station in the frequency band 22-22.21 GHz as a function of the elevation angle in scenario 6.2.1. A guard band of 10 MHz at 22.2-22.21 GHz is used

	Effelsberg	**MeerKAT**	**GBT**	**Jansky VLA**	**Parkes**	**Tianma**	**Nobeyama**	**Bure**
5°-8.85°	0.10%	0.00%	0.20%	0.20%	0.10%	0.10%	0.00%	0.00%
8.85°-12.7°	0.00%	0.10%	0.30%	0.10%	0.20%	0.20%	0.10%	0.10%
12.7°-16.7°	0.30%	0.00%	0.40%	0.00%	0.10%	0.30%	0.00%	0.20%
16.7°-20.7°	0.10%	0.20%	0.20%	0.00%	0.00%	0.20%	0.00%	0.00%
20.7°-24.9°	0.20%	0.00%	0.30%	0.00%	0.20%	0.20%	0.00%	0.20%
24.9°-29.2°	0.20%	0.20%	0.00%	0.00%	0.10%	0.20%	0.00%	0.10%
29.2°-33.6°	0.10%	0.00%	0.20%	0.00%	0.20%	0.10%	0.00%	0.10%
33.6°-38.4°	0.30%	0.00%	0.20%	0.00%	0.10%	0.20%	0.00%	0.00%
38.4°-43.4°	0.00%	0.00%	0.30%	0.00%	0.00%	0.20%	0.10%	0.00%
43.4°-49°	0.00%	0.00%	0.10%	0.00%	0.00%	0.30%	0.00%	0.00%
49°-55.1°	0.00%	0.00%	0.10%	0.00%	0.00%	0.20%	0.00%	0.00%
55.1-62.5°	0.00%	0.00%	0.20%	0.00%	0.10%	0.20%	0.00%	0.00%
62.5°-72.5°	0.10%	0.10%	0.20%	0.10%	0.00%	0.10%	0.10%	0.10%
72.5°-90°	0.10%	0.20%	0.10%	0.20%	0.00%	0.20%	0.10%	0.00%
Average	**0.11%**	**0.054%**	**0.20%**	**0.039%**	**0.080%**	**0.19%**	**0.027%**	**0.058%**

TABLE A7-14

Percentage of erroneous measurements at the radio astronomy station in the frequency band 15.35-15.4 GHz as a function of the elevation angle in scenario 6.2.2. A guard band of 10 MHz at 15.4-15.41 GHz is used

	Effelsberg	**MeerKAT**	**GBT**	**Jansky VLA**	**Parkes**	**Tianma**	**Nobeyama**	**Bure**
5°-8.85°	0.30%	0.40%	0.40%	0.40%	0.40%	0.20%	0.50%	0.70%
8.85°-12.7°	0.20%	0.30%	0.40%	0.50%	0.50%	0.20%	0.20%	0.60%
12.7°-16.7°	0.10%	0.20%	0.30%	0.60%	0.30%	0.00%	0.20%	0.20%
16.7°-20.7°	0.20%	0.30%	0.20%	0.40%	0.20%	0.10%	0.30%	0.40%
20.7°-24.9°	0.20%	0.30%	0.30%	0.30%	0.60%	0.20%	0.40%	0.30%
24.9°-29.2°	0.30%	0.30%	0.40%	0.30%	0.20%	0.40%	0.10%	0.40%
29.2°-33.6°	0.20%	0.20%	0.20%	0.40%	0.40%	0.00%	0.10%	0.30%
33.6°-38.4°	0.40%	0.10%	0.30%	0.20%	0.20%	0.20%	0.10%	0.50%
38.4°-43.4°	0.30%	0.30%	0.40%	0.30%	0.20%	0.10%	0.20%	0.20%
43.4°-49°	0.20%	0.20%	0.10%	0.60%	0.10%	0.10%	0.10%	0.10%
49°-55.1°	0.20%	0.20%	0.10%	0.20%	0.10%	0.00%	0.00%	0.30%
55.1-62.5°	0.40%	0.30%	0.30%	0.30%	0.20%	0.30%	0.30%	0.20%
62.5°-72.5°	0.30%	0.20%	0.00%	0.50%	0.40%	0.20%	0.50%	0.40%
72.5°-90°	0.20%	0.30%	0.30%	0.50%	0.50%	0.10%	0.40%	0.40%
Average	**0.25%**	**0.26%**	**0.26%**	**0.38%**	**0.30%**	**0.15%**	**0.24%**	**0.36%**

TABLE A7-15

Percentage of erroneous measurements at the radio astronomy station in the frequency band 22-22.21 GHz as a function of the elevation angle in scenario 6.2.2. A guard band of 10 MHz at 22.2-22.21 GHz is used

	Effelsberg	**MeerKAT**	**GBT**	**Jansky VLA**	**Parkes**	**Tianma**	**Nobeyama**	**Bure**
5°-8.85°	0.00%	0.00%	0.00%	0.00%	0.10%	0.00%	0.00%	0.00%
8.85°-12.7°	0.00%	0.00%	0.00%	0.00%	0.00%	0.00%	0.00%	0.00%
12.7°-16.7°	0.00%	0.10%	0.00%	0.00%	0.00%	0.00%	0.10%	0.00%
16.7°-20.7°	0.00%	0.10%	0.10%	0.10%	0.00%	0.00%	0.00%	0.00%
20.7°-24.9°	0.00%	0.10%	0.00%	0.00%	0.00%	0.00%	0.00%	0.00%
24.9°-29.2°	0.00%	0.00%	0.00%	0.00%	0.10%	0.00%	0.00%	0.00%
29.2°-33.6°	0.00%	0.00%	0.00%	0.00%	0.00%	0.00%	0.10%	0.00%
33.6°-38.4°	0.00%	0.00%	0.10%	0.00%	0.00%	0.00%	0.00%	0.00%
38.4°-43.4°	0.00%	0.00%	0.00%	0.00%	0.00%	0.00%	0.00%	0.00%
43.4°-49°	0.00%	0.00%	0.00%	0.00%	0.00%	0.00%	0.00%	0.10%
49°-55.1°	0.00%	0.00%	0.00%	0.00%	0.00%	0.00%	0.00%	0.00%
55.1-62.5°	0.00%	0.00%	0.00%	0.00%	0.00%	0.00%	0.00%	0.00%
62.5°-72.5°	0.00%	0.00%	0.00%	0.10%	0.00%	0.00%	0.00%	0.00%
72.5°-90°	0.00%	0.00%	0.00%	0.00%	0.00%	0.00%	0.00%	0.00%
Average	**0.00%**	**0.022%**	**0.015%**	**0.015%**	**0.015%**	**0.0073%**	**0.015%**	**0.0073%**

TABLE A7-16

Percentage of erroneous measurements at the radio astronomy station in the frequency band 15.35-15.4 GHz as a function of the elevation angle in scenario 6.2.3. A guard band of 10 MHz at 15.4-15.41 GHz is used

	Effelsberg	**MeerKAT**	**GBT**	**Jansky VLA**	**Parkes**	**Tianma**	**Nobeyama**	**Bure**
5°-8.85°	0.0%	0.0%	0.0%	0.0%	0.0%	0.0%	0.0%	0.0%
8.85°-12.7°	0.0%	0.0%	0.0%	0.0%	0.0%	0.0%	0.0%	0.0%
12.7°-16.7°	0.0%	0.0%	0.0%	0.0%	0.0%	0.0%	0.0%	0.0%
16.7°-20.7°	0.0%	0.0%	0.0%	0.0%	0.0%	0.0%	0.0%	0.0%
20.7°-24.9°	0.0%	0.0%	0.0%	0.0%	0.0%	0.0%	0.0%	0.0%
24.9°-29.2°	0.0%	0.0%	0.0%	0.0%	0.0%	0.0%	0.0%	0.0%
29.2°-33.6°	0.0%	0.0%	0.0%	0.0%	0.0%	0.0%	0.0%	0.0%
33.6°-38.4°	0.0%	0.0%	0.0%	0.0%	0.0%	0.0%	0.0%	0.0%
38.4°-43.4°	0.0%	0.0%	0.0%	0.0%	0.0%	0.0%	0.0%	0.0%
43.4°-49°	0.0%	0.0%	0.0%	0.0%	0.0%	0.0%	0.0%	0.0%
49°-55.1°	0.0%	0.0%	0.0%	0.0%	0.0%	0.0%	0.0%	0.0%
55.1-62.5°	0.0%	0.0%	0.0%	0.0%	0.0%	0.0%	0.0%	0.0%
62.5°-72.5°	0.0%	0.0%	0.0%	0.0%	0.0%	0.0%	0.0%	0.0%
72.5°-90°	0.0%	0.0%	0.0%	0.0%	0.0%	0.0%	0.0%	0.0%
Average	**0.0%**	**0.0%**	**0.0%**	**0.0%**	**0.0%**	**0.0%**	**0.0%**	**0.0%**

TABLE A7-17

Percentage of erroneous measurements at the radio astronomy station in the frequency band 22-22.21 GHz as a function of the elevation angle in scenario 6.2.3. A guard band of 10 MHz at 22.2-22.21 GHz is used

	Effelsberg	**MeerKAT**	**GBT**	**Jansky VLA**	**Parkes**	**Tianma**	**Nobeyama**	**Bure**
5°-8.85°	0.0%	0.0%	0.0%	0.0%	0.0%	0.0%	0.0%	0.0%
8.85°-12.7°	0.0%	0.0%	0.0%	0.0%	0.0%	0.0%	0.0%	0.0%
12.7°-16.7°	0.0%	0.0%	0.0%	0.0%	0.0%	0.0%	0.0%	0.0%
16.7°-20.7°	0.0%	0.0%	0.0%	0.0%	0.0%	0.0%	0.0%	0.0%
20.7°-24.9°	0.0%	0.0%	0.0%	0.0%	0.0%	0.0%	0.0%	0.0%
24.9°-29.2°	0.0%	0.0%	0.0%	0.0%	0.0%	0.0%	0.0%	0.0%
29.2°-33.6°	0.0%	0.0%	0.0%	0.0%	0.0%	0.0%	0.0%	0.0%
33.6°-38.4°	0.0%	0.0%	0.0%	0.0%	0.0%	0.0%	0.0%	0.0%
38.4°-43.4°	0.0%	0.0%	0.0%	0.0%	0.0%	0.0%	0.0%	0.0%
43.4°-49°	0.0%	0.0%	0.0%	0.0%	0.0%	0.0%	0.0%	0.0%
49°-55.1°	0.0%	0.0%	0.0%	0.0%	0.0%	0.0%	0.0%	0.0%
55.1-62.5°	0.0%	0.0%	0.0%	0.0%	0.0%	0.0%	0.0%	0.0%
62.5°-72.5°	0.0%	0.0%	0.0%	0.0%	0.0%	0.0%	0.0%	0.0%
72.5°-90°	0.0%	0.0%	0.0%	0.0%	0.0%	0.0%	0.0%	0.0%
Average	**0.0%**	**0.0%**	**0.0%**	**0.0%**	**0.0%**	**0.0%**	**0.0%**	**0.0%**

TABLE A7-18

Percentage of erroneous measurements at the radio astronomy station in the frequency band 15.35-15.4 GHz as a function of the elevation angle in scenario 6.2.4. A guard band of 10 MHz at 15.4-15.41 GHz is used

	Effelsberg	**MeerKAT**	**GBT**	**Jansky VLA**	**Parkes**	**Tianma**	**Nobeyama**	**Bure**
5°-8.85°	0.10%	0.20%	0.00%	0.00%	0.00%	0.00%	0.00%	0.10%
8.85°-12.7°	0.00%	0.10%	0.00%	0.10%	0.10%	0.00%	0.10%	0.20%
12.7°-16.7°	0.00%	0.10%	0.00%	0.10%	0.00%	0.10%	0.00%	0.00%
16.7°-20.7°	0.00%	0.00%	0.10%	0.00%	0.00%	0.00%	0.10%	0.00%
20.7°-24.9°	0.00%	0.00%	0.00%	0.00%	0.10%	0.00%	0.00%	0.00%
24.9°-29.2°	0.00%	0.10%	0.00%	0.00%	0.00%	0.10%	0.00%	0.00%
29.2°-33.6°	0.10%	0.00%	0.00%	0.00%	0.00%	0.00%	0.00%	0.00%
33.6°-38.4°	0.00%	0.00%	0.00%	0.00%	0.00%	0.00%	0.00%	0.00%
38.4°-43.4°	0.00%	0.10%	0.00%	0.00%	0.00%	0.00%	0.00%	0.00%
43.4°-49°	0.00%	0.00%	0.00%	0.10%	0.00%	0.00%	0.00%	0.00%
49°-55.1°	0.00%	0.10%	0.00%	0.00%	0.00%	0.00%	0.00%	0.00%
55.1-62.5°	0.00%	0.00%	0.00%	0.00%	0.10%	0.00%	0.00%	0.00%
62.5°-72.5°	0.00%	0.10%	0.00%	0.10%	0.00%	0.10%	0.10%	0.10%
72.5°-90°	0.00%	0.10%	0.00%	0.10%	0.00%	0.00%	0.00%	0.10%
Average	**0.015%**	**0.063%**	**0.0073%**	**0.034%**	**0.022%**	**0.022%**	**0.022%**	**0.034%**

TABLE A7-19

Percentage of erroneous measurements at the radio astronomy station in the frequency band 22-22.21 GHz as a function of the elevation angle in scenario 6.2.4. A guard band of 10 MHz at 22.2-22.21 GHz is used

	Effelsberg	MeerKAT	GBT	Jansky VLA	Parkes	Tianma	Nobeyama	Bure
5°-8.85°	0.00%	0.00%	0.00%	0.00%	0.00%	0.00%	0.00%	0.10%
8.85°-12.7°	0.00%	0.10%	0.10%	0.10%	0.00%	0.00%	0.00%	0.10%
12.7°-16.7°	0.00%	0.10%	0.00%	0.10%	0.00%	0.00%	0.00%	0.00%
16.7°-20.7°	0.00%	0.00%	0.00%	0.00%	0.00%	0.00%	0.10%	0.00%
20.7°-24.9°	0.00%	0.00%	0.00%	0.00%	0.10%	0.00%	0.00%	0.00%
24.9°-29.2°	0.00%	0.10%	0.00%	0.00%	0.00%	0.10%	0.00%	0.10%
29.2°-33.6°	0.00%	0.00%	0.00%	0.00%	0.00%	0.00%	0.00%	0.00%
33.6°-38.4°	0.00%	0.00%	0.00%	0.00%	0.00%	0.00%	0.00%	0.00%
38.4°-43.4°	0.00%	0.10%	0.00%	0.10%	0.00%	0.00%	0.00%	0.00%
43.4°-49°	0.00%	0.00%	0.00%	0.10%	0.00%	0.00%	0.00%	0.00%
49°-55.1°	0.00%	0.10%	0.00%	0.00%	0.00%	0.00%	0.00%	0.00%
55.1-62.5°	0.00%	0.00%	0.00%	0.10%	0.00%	0.00%	0.10%	0.10%
62.5°-72.5°	0.00%	0.00%	0.00%	0.10%	0.00%	0.00%	0.00%	0.00%
72.5°-90°	0.00%	0.10%	0.00%	0.10%	0.00%	0.00%	0.00%	0.10%
Average	**0.00%**	**0.042%**	**0.0073%**	**0.049%**	**0.0073%**	**0.0073%**	**0.00%**	**0.027%**

A7.4 Study D

A7.4.1 Introduction

Study B has shown that some scenarios of non-safety AM(OR)S do not meet the protection criterion of RAS if no protection measures are considered. This is particularly clear if omnidirectional antennas are used. Some protection measures have been envisaged in Study C to resolve the issue, like a guard band with the RAS measurement band, or a capacity reduction.

However, Studies B and C take a pure Monte Carlo approach and make the assumption of a smooth Earth. Whilst this methodology is well adapted to scenarios with high-altitude ADTs (for instance scenarios 6.2.2, 6.2.3, and 6.2.4) where the Earth's terrain influence on the wave propagation is negligible, this might lead to inaccuracies in scenarios with low-altitude ADTs (typically scenario 6.2.1). In the latter case, the relief of the Earth around the RAS station becomes the driving factor of compatibility. Hence, a reduction of the WBLOSDL capacity or a possible guard band with the RAS measurement band should be based on site-specific rather than "smooth Earth" calculations.

Therefore, this Study D intends to complement and confirm the conclusions of Study C, by taking into account the exact terrain profile around each of the eight RAS stations listed in Table A2-8. For the sake of brevity, the analysis is limited to the frequency band 15.4-15.7 GHz.

A7.4.2 Methodology

This study is a minimum coupling loss (MCL) analysis that considered a single ADT in scenario 6.2.1 equipped with the omnidirectional AM(OR)S System 2 and operating in the frequency band 15.4-15.7 GHz. In this scenario, the ADT operates at a low altitude of 300 m AGL according to Table 3, which gives prominence to the terrain model surrounding the RAS station.

The analysis determines the maximum e.i.r.p. of this ADT inside the RAS measurement band 15.35-15.4 GHz so that the interference power level received by the RAS station does not exceed the detrimental threshold of -172 dBm measured in 50 MHz (see § A4.4.3). This study being a pure MCL analysis, the 2%-time percentage associated to this threshold and highlighted in Recommendation ITU-R RA.1513-2 is left out of consideration. Moreover, it is assumed that most of the power is received through the side-lobes of the RAS station as the ADT is flying at low altitude and therefore a constant gain of 0 dBi is assumed as in Recommendation ITU-R RA.769-2.

The propagation model used in this study is taken from Recommendation ITU-R P.452-17 instead of Recommendation ITU-R P.528-5 as in Study B and C, because the latter model does not account for site-specific parameters and only considers smooth-Earth diffraction effects. Table A7-12 below shows the configuration parameters associated to Recommendation ITU-R P.452-17 that will be used for each of the eight RAS stations studied.

TABLE A7-20

Input parameters of Recommendation ITU-R P.452-17 for site-specific coexistence studies between aeronautical mobile (off-route) systems operating in the frequency band 15.4-15.7 GHz and radio astronomy stations performing measurement in the adjacent frequency band 15.35-15.4 GHz

Notation	f	p	d, h	z	h_{tg}	h_{rg}	φ_t	φ_r	G_t	G_r	pol	d_{ct}	d_{cr}	Δ_N	N_0	P	T
Units	GHz	%	km, m	ø	m				dBi		ø	km			N-units	hPa	°C
Note	(1)	(2)	(3)	(4)	(5)		(6)		(7)	(8)	(9)	(10)		(11)	(12)	(13)	
Effelsberg	15.38	50	SRTM database (3 arc second)	1 (inland) over the whole path	300	2	Computed for each position of the ADT	50.5	3	0	2	250		50	330	1 013	15
MeerKAT	15.38	50			300	2		−30.7	3	0	2	330		50	330	1 013	15
Green Bank Telescope	15.38	50			300	2		38.4	3	0	2	320		40	360	1 013	15
Jansky VLA	15.38	50			300	2		34.2	3	0	2	630		30	320	1 013	15
Parkes	15.38	50			300	2		−33	3	0	2	290		30	330	1 013	15
Tianma	15.38	50			300	2		31.1	3	0	2	44		60	380	1 013	15
Nobeyama	15.38	50			300	2		35.9	3	0	2	90		50	380	1 013	15
Plateau de Bure	15.38	50			300	2		44.6	3	0	2	150		50	330	1 013	15

(1) f is defined in Table 1 in Rec. ITU-R P.452-17 and denotes the frequency, which is chosen to be the middle of the measurement band 15.35-15.4 GHz.

(2) p is defined in Table 1 in Rec. ITU-R P.452-17 and denotes the percentage of time when the computed PL value is not exceeded and is arbitrarily chosen to be 50%, which means that the median of the propagation loss is calculated.

(3) d, h denote the path profile vector of nadir distance and height AMSL on the way between the ADT and the RAS station. This data is extracted from the Shuttle Radar Topography Mission (SRTM) database. SRTM is terrain map of the world up covering the surface of the Earth up to latitudes of about 60°. The default precision is 3 arc second, which corresponds to a granularity of approximately 90 m on the surface of the Earth. This database is freely available on the Internet, for instance on the following website of the U.S. government: https://www.usgs.gov/centers/eros/science/usgs-eros-archive-digital-elevation-shuttle-radar-topography-mission-srtm-1.

(4) z is defined in Table 2 in Rec. ITU-R P.452-17 and denotes the terrain vector on the way between the ADT and the RAS station (1=land). For the sake of simplicity, it is assumed that the path between the ADT and the RAS station does not cross a lake or a sea;

(5) h_{tg} and h_{tr} are defined in Table 1 in Rec. ITU-R P.452-17 and respectively denote the antenna centre height AGL of the ADT and the RAS station. In scenario 6.2.1, the altitude of ADTs is 300 m AGL as per Table 3. The altitude of RAS stations is arbitrarily chosen to be 2 m AGL.

(6) φ_t and φ_r are defined in Table 1 in Rec. ITU-R P.452-17 and respectively denote the latitude of the ADT and the RAS station, which is indicated in Table A2-8 in § A3.4 for the different sites considered.

(7) G_t is defined in Table 1 in Rec. ITU-R P.452-17 and denotes the antenna gain of the ADT in the direction of the horizon along the great-circle interference path toward the RAS station. In scenario 6.2.1, the ADTs are equipped with AM(OR)S System 2 (as per Table 3), which uses an omnidirectional antenna (as per Table A1-2) further described in § A1.2.2.

(8) G_r is defined in Table 1 in Rec. ITU-R P.452-17 and denotes the antenna gain of the RAS station in the direction of the horizon along the great-circle interference path toward the ADT. In scenario 6.2.1, as ADTs are flying at low altitude above the ground, and as the RAS is in general higher in altitude than the surrounding area, it is assumed that the interference is received from the side lobes of the RAS antenna, to which a gain of 0 dBi is associated in accordance with § 1.3 of Rec. ITU-R RA.769-2.

(9) *pol* is defined in Table 1 in Rec. ITU-R P.452-17 and denotes the wave polarization, 1 for horizontal, and 2 for vertical polarization.

(10) d_{ct} and $\mathrm{d_{cr}}$ are defined in Table 3 in Rec. ITU-R P.452-17 and respectively denote the distance over land from the ADT and the RAS station to the coast along the great-circle interference path. For the sake of simplicity, it is assumed that the distances d_{ct} and d_{ct} are the same for the RAS station and the ADT in its vicinity.

(11) Δ_N is defined in Step 3 in Rec. ITU-R P.452-17 and denotes the average radio-refractivity lapse-rate through the lowest 1 km of the atmosphere. Numerical values have been determined using Fig. 5 in Rec. ITU-R P.453-7 (monthly mean values in the month of August).

(12) N_0 is defined in Step 3 in Rec. ITU-R P.452-17 and denotes the sea-level surface refractivity. Numerical values have been determined using Fig. 2 in Rec. ITU-R P.453-7 (monthly mean values in the month of August).

(13) *P* and *T* are defined in Table 5 in Rec. ITU-R P.452-17 and respectively denote the surface pressure and temperature. Default values are taken from this Table 5.

A7.4.3 Results

Results are shown for the Effelsberg RAS site in Figs A7-15A, A7-15B and A7-15C that respectively show the location of the RAS station (*source*: Google Earth), the topography around it, and the maximum permissible e.i.r.p. of the ADT in the RAS measurement band 15.35-15.4 GHz. Equivalent results are provided in Attachment B to this Annex for the seven other sites referenced in Table A2-8.

Building upon Fig. A7-15C, Fig. A7-16 shows the necessary guard band between the ADT channel and the RAS band, assuming a maximum TPO of 25 dBm. It shows that when the ADT is operating in the valley northwest of the Effelsberg site, it would need to implement a 40 MHz guard band when the distance to the RAS site is less than about 150 km. When the distance is less than about 40 km, the guard band should be 70 MHz. Figure A7-16 shows that the operation of the ADT is possible at maximum TPO even when very close to the RAS site (in that case a 180 MHz guard band would be necessary).

The difference in the necessary guard band that was found in this Study as compared to Study C (in which 10 MHz were found, see § A7.3.4) is due to the fact that Study D is based on an MCL analysis that does not consider any time percentage associated with the RAS protection criterion.

A7.4.4 Summary

Study D has shown the paramount influence of the terrain surrounding a RAS station on the coexistence between AM(OR)S stations using omnidirectional antenna and flying at low altitude. It demonstrated that the choice of an appropriate guard band should be based on site-specific considerations rather than computations made with a “smooth Earth” model.

FIGURE A7-15A

Location of the Effelsberg radio astronomy station (white cross) and deployment zone of the airborne data terminal (red area)

FIGURE A7-15B

Topography around the Effelsberg site (black dot), *Source*: Shuttle Radar Topography Mission (3 arc second precision)

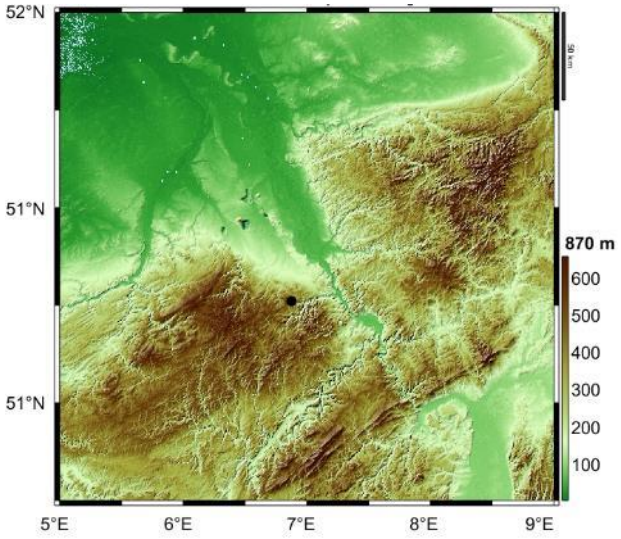

FIGURE A7-15C

Maximum permissible e.i.r.p. (in dBm) inside the radio astronomy station measurement band 15.35-15.4 GHz of the airborne data terminal (altitude = 300 m AGL) using the aeronautical mobile (off-route) System 2 and operating in the frequency band 15.4-15.7 GHz around the Effelsberg site (black dot)

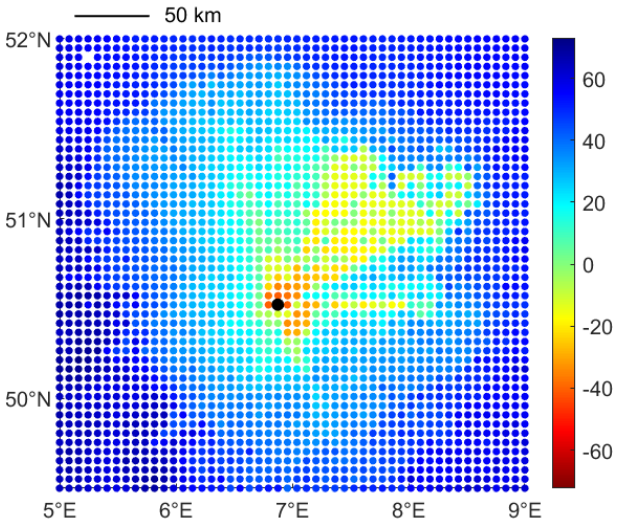

FIGURE A7-16

Necessary guard band (in MHz) for the airborne data terminal in scenario 6.2.1 around the Effelsberg site (black dot) if the maximum transmit power output of 25 dBm is used, so that the detrimental interference threshold of 172 dBm/50 MHz is not exceeded for 100% of the time

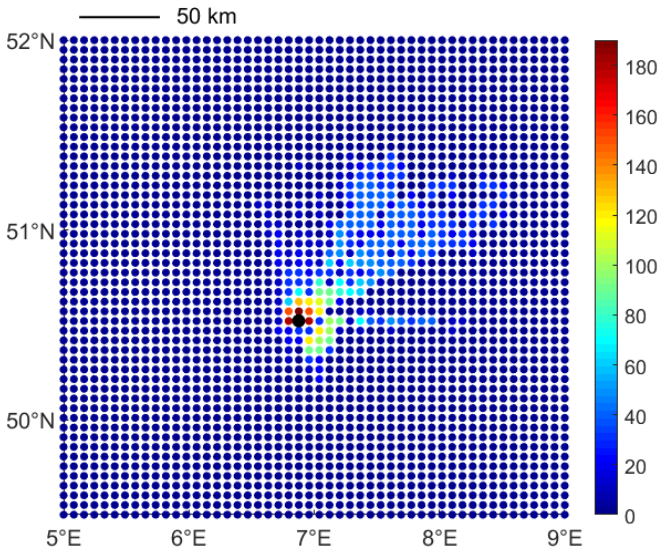

Attachment A
to Annex 7

Calculation details related to Study B

This Attachment provides intermediate results of Study B in Annex 9. It shows and comments on the statistical distribution of the intermediate variables that were needed to obtain the final results of the study in terms of received aggregate power at the RAS station. For the sake of clarity, and because results are similar to a large extent for the eight RAS sites listed in § A2.4.1, this attachment will focus on the Effelsberg site, using the measurement band 22.21-22.5 GHz and an elevation angle between 5 and 8.85°. Moreover, only scenario 6.2.1 "Wildfire detection" is presented for brevity.

A7A.1 Setup of the simulation area

The methodology to set up the simulation area around the RAS station is explained in a generic way in Annex 11 to this Report (see in particular §§ A11.1 to A11.4). In summary, the RAS site is deployed according to the parameters highlighted in § A2.4.1. The elevation above the local horizontal of the RAS antenna is chosen with uniform probability distribution between 5 and 8.85 degrees once for each group of 100 successive snapshots (that represent a trajectory or a group of trajectories of AM(OR)S clusters around the RAS station).

The simulation area around the RAS site has a radius of 254 km in scenario 6.2.1, 484 km in scenario 6.2.2, 467 km in scenario 6.2.3 and 469 km in scenario 6.2.4 (see Table A11-7). One cluster will be deployed in this simulation area in scenarios 6.2.2, 6.2.2 and 6.2.3, whereas two clusters will be deployed in scenarios 6.2.4 (see Table A11-5).

A7A.2 Deployment of aeronautical mobile (off-route) stations

A7A.2.1 Centre frequency

As explained in § A11.5.2, the centre frequency of AM(OR)S stations is chosen uniformly within the frequency bands 15.4-15.7 GHz and 22-22.21 GHz in such a way that the necessary BW is totally included inside the band. This is reflected in Fig. A11-1 that shows for instance the ECDF of the centre frequency in scenario 6.2.1. One can see that the upper and lower edges of the tuning range 22-22.21 GHz are separated from the maximum and minimum centre frequency by half the BW of the channel.

FIGURE A7-17

Empirical cumulative distribution function of the centre frequency of the aeronautical mobile (off-route) systems (System 4 in red has a bandwidth of 0.55 MHz and System 2 in blue has a bandwidth of 55 MHz according to Table 5)

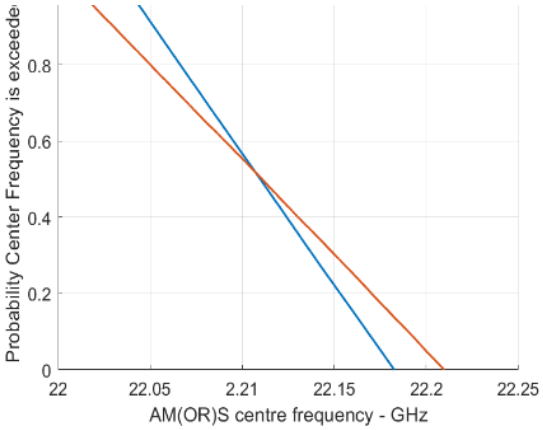

A7A.2.2 Transmit power output

As explained in § A11.6.1 of this Report, TPO of AM(OR)S stations inside a cluster is determined using an ATPC algorithm that does not depend on the interfered-with system (IWS) under study. Refer to Figs A11-7 to A11-10 in Annex 11 that show the ECDF of the TPO of AM(OR)S stations in the different scenarios.

A7A.3 Antenna gains

Gain values at the AM(OR)S systems in the direction of the RAS site and at the RAS site in the direction of AM(OR)S systems are computed using the methodology laid out in § A11.6.2. They are addressed separately in the subsequent paragraphs.

A7A.3.1 Gain of aeronautical mobile (off-route) systems

The gain of the AM(OR)S systems toward the RAS station is shown in Fig. A7-18 for scenario 6.2.1. Approximately 50% of ADTs “see” the RAS station with a negative elevation angle with respect to their local horizon (in which case the gain is −3 dBi) and 50% with positive elevation angles (in which case the gain is 3 dBi). The gain of the GDT in the direction of the RAS station takes only two discrete values: −30 dBi in approximately 90% of the cases, and 14 dBi in approximately 10% of the cases.

FIGURE A7-18

Empirical cumulative distribution function of the gain of the aeronautical mobile (off-route) systems (System 4 in red and System 2 in blue) towards the radio astronomy station

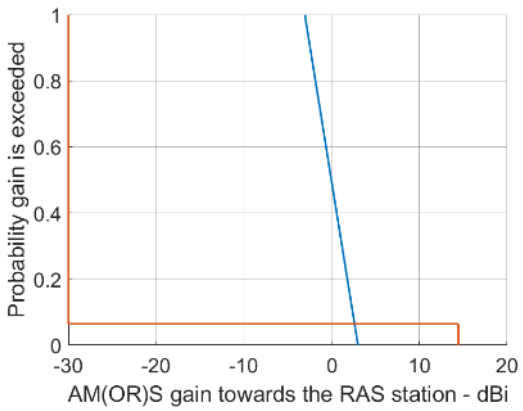

A7A.3.2 Radio astronomy antenna gain

Shown in Fig. A7-19 is the ECDF of the gain at the RAS station in the direction of the ADTs in scenario 6.2.1. The gain in the direction of the GDT is not shown in this figure. From Fig. A7-19, the maximum gain over all the snapshots is approximately 10 dBi. This maximum value can be found by analysing the elevation at the RAS station in the direction of an ADT in scenario 6.2.1 as a function of the nadir distance. This angle is represented in Fig. A7-20 and shows a maximum of −0.25 dBi at a nadir distance of 30 km. This value is the result of equation (A2-5) with a peak gain G_0 of 82.6dBi, a HPBW φ_0 of 0.004 6° (see Table A2-8), and an off-axis angle φ of 5.25 degrees i.e. the addition of the minimum elevation angle 5 degrees at the RAS station and the maximum elevation angle at the RAS station in the direction of the ADT (0.25 degrees below the local horizon).

FIGURE A7-19

Empirical cumulative distribution function of the gain of the radio astronomy station in the direction of the airborne data terminals

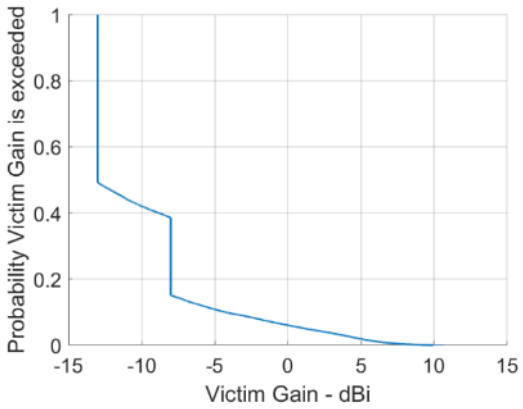

FIGURE A7-20

Elevation angle at the radio astronomy station in the direction of an airborne data terminal as a function of the nadir distance

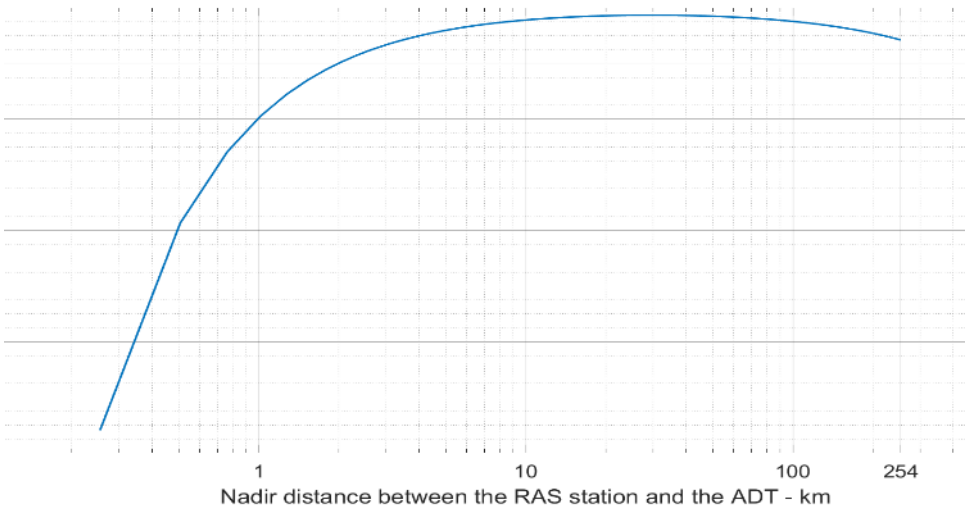

A7A.4 Path loss

As explained in § A11.6.3 of this Report, the PL between AM(OR)S and RAS stations is computed using Recommendation ITU-R P.528-5, together with a uniformly distributed time percentage. This

leads to Fig. A7-21 that shows the ECDF of the PL in scenario 6.2.1 between the RAS station and the AM(OR)S stations. One can note that both curves have an inflection point that separates LOS and BLOS PL values. The fact that some ADT can be beyond the RHD in some snapshots is due to the travelling of the clusters.

FIGURE A7-21

Empirical cumulative distribution function of the path loss between the radio astronomy station and the airborne data terminals (blue) and between the radio astronomy station and the ground data terminals (red)

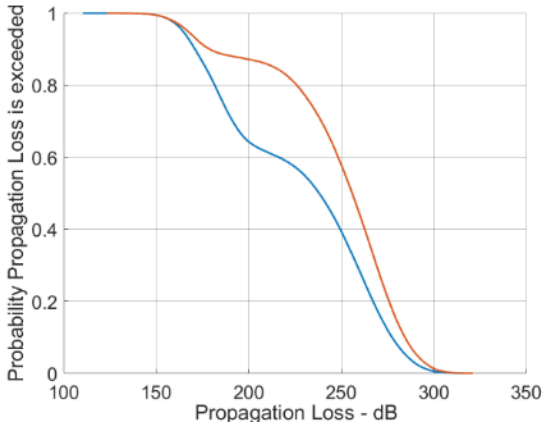

A7A.5 Frequency dependent rejection

Figure A7-22 shows the FDR between AM(OR)S channels and the RAS measurement band 22.21-22.5 GHz in scenario 6.2.1. As the RF filter of the RAS station is supposed to be perfect (see § A3.4.1), the FDR is simply obtained by integrating the SEM of the AM(OR)S systems (provided in Table A1-1) over the frequency band 22.21-22.5 GHz.

FIGURE A7-22

Empirical cumulative distribution function of the frequency dependent rejection between the airborne data terminals channels and the radio astronomy measurement band (blue) and between the ground data terminals channels and the radio astronomy measurement band (red)

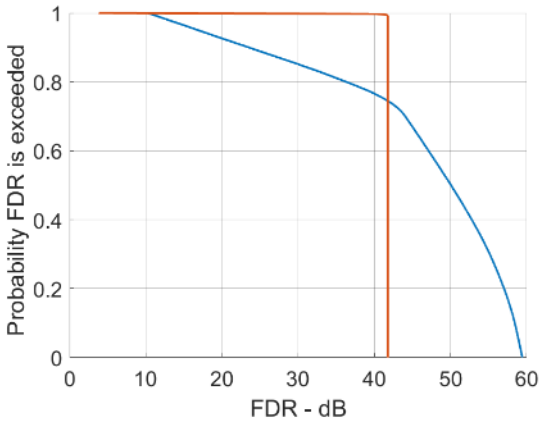

System 4 used by the GDT has a constant FDR of about 41 dB. Indeed, as System 4 uses a narrowband channel of 0.55 MHz (see Table 5), the RAS measurement band 22.21-22.5 GHz is almost always in the spurious domain of the AM(OR)S emission. The exact value of the FDR is obtained using the calculation below, replacing $RPSD_{RAS}$ by 69 dB, which is the RPSD in the spurious domain according to Table A1-1, $BW_{AM(OR)S}$ by 0.55 MHz, and BW_{RAS} by 290 MHz.

Following the same methodology, the maximum value of the FDR for System 2 i.e. 60 dB is obtained when the RAS measurement band is contained in the spurious domain. The same calculation as above can be used, replacing $BW_{AM(OR)S}$ by 55 MHz, which is the necessary BW in this scenario as shown in Table 6.

$$\begin{aligned} \text{FDR} &= P_{AM(OR)S} - P_{RAS} \\ &= \left[PSD_{\max} + 10\log_{10}\left(BW_{AM(OR)S}\right)\right] \\ &\quad - \left[PSD_{RAS} + 10\log_{10}\left(BW_{RAS}\right)\right] \\ &= \left[PSD_{\max} - PSD_{RAS}\right] + 10\log_{10}\left(\frac{BW_{AM(OR)S}}{BW_{RAS}}\right) \\ &= RPSD_{RAS} + 10\log_{10}\left(\frac{BW_{AM(OR)S}}{BW_{RAS}}\right) \end{aligned}$$

where:

FDR_{RAS}: FDR (dB) between the AM(OR) channel and the RAS measurement band 22.21-22.5 GHz

$P_{AM(OR)S}$: TPO (dBm) of the AM(OR)S channel

P_{RAS}: integrated power level (dBm) created by the AM(OR)S channel inside the RAS measurement band 22.21-22.5 GHz

$PSD_{\max}$: PSD (dBm/MHz) of the AM(OR)S channel inside the necessary BW

PSD_{RAS}: PSD (dBm/MHz) of the AM(OR)S channel in the RAS measurement band 22.21-22.5 GHz

$BW_{control}$: necessary BW (MHz) of the AM(OR)S channel

BW_{RAS}: BW (MHz) of the RAS measurement band 22.21-22.5 GHz i.e. 290 MHz

$RPSD_{RAS}$: RPSD inside the RAS measurement band 22.21-22.5 GHz, i.e. −53 dB as per Table A1-1 if the RAS band is in the spurious domain of AM(OR)S emission.

A7A.6 Power flux density

The power flux-density (pfd) measured in the 290 MHz between 22.21 and 22.5 GHz, created at the RAS station by AM(OR)S stations in scenario 6.2.1 is shown in Fig. A7-23.

FIGURE A7-23

Empirical cumulative distribution function of the power flux-density produced at the radio astronomy station by airborne data terminals (blue) and by the ground data terminals (red)

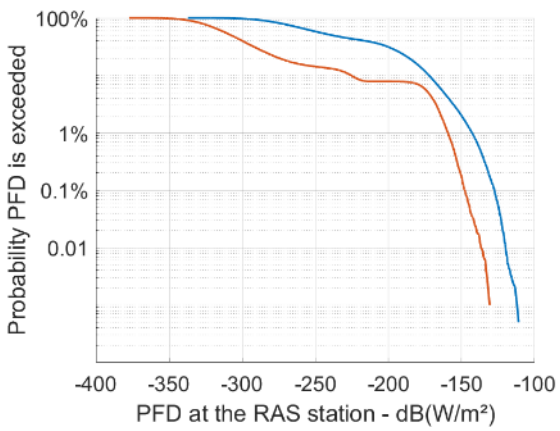

Attachment B
to Annex 7

Complementary results of Study D

A7B.1 MeerKAT (South Africa)

FIGURE A7-24

Location of the MeerKAT radio astronomy station and deployment zone of the airborne data terminals (red area)

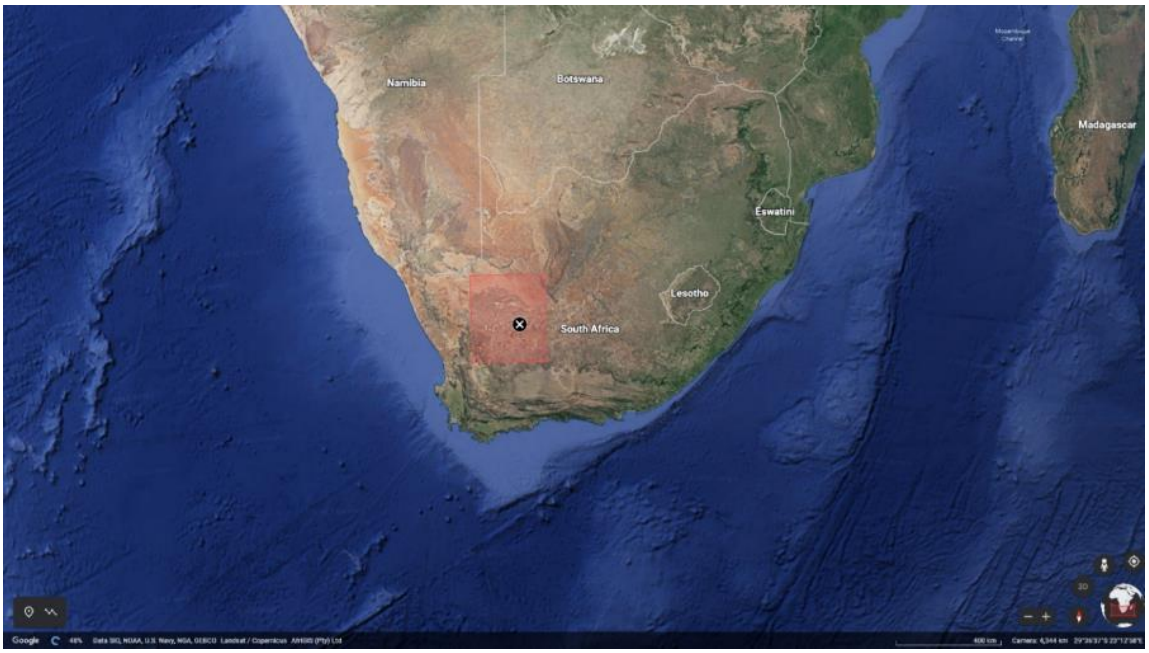

FIGURE A7-25

Topography around the MeerKAT site (black dot), *Source*: Shuttle Radar Topography Mission (3 arc second precision)

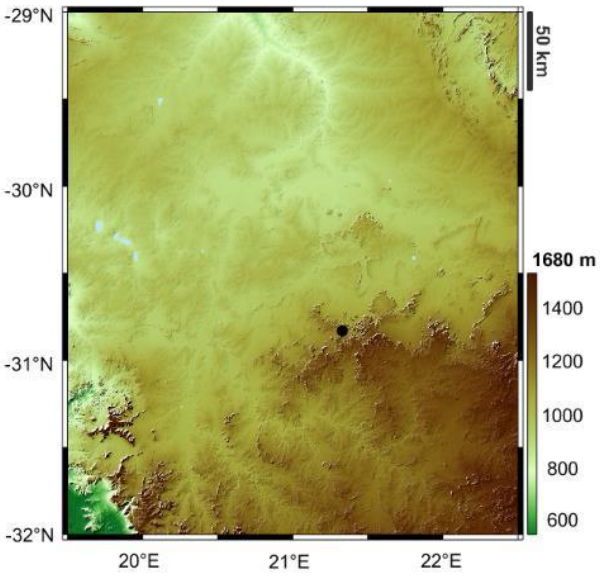

FIGURE A7-26

Maximum permissible e.i.r.p. (in dBm) inside the radio astronomy measurement band 15.35-15.4 GHz of the airborne data terminal (altitude = 300 m AGL) using aeronautical mobile (off-route) System 2 and operating in the frequency band 15.4-15.7 GHz around the MeerKAT site (black dot)

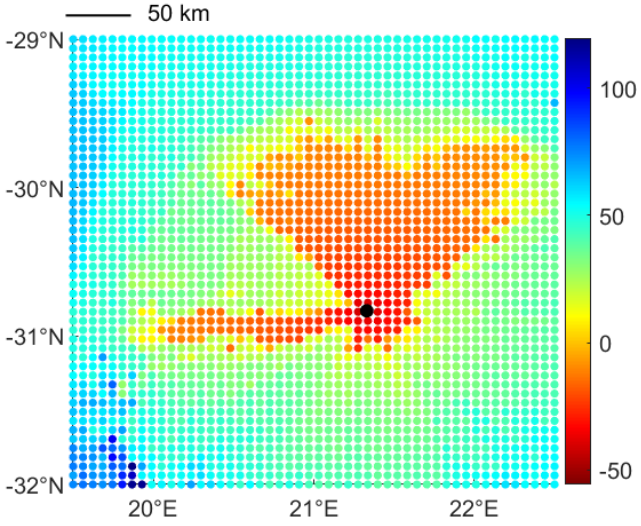

A7B.2 Green Bank telescope (USA)

FIGURE A7-27

Location of the Green Bank telescope radio astronomy station and deployment zone of the airborne data terminals (red area)

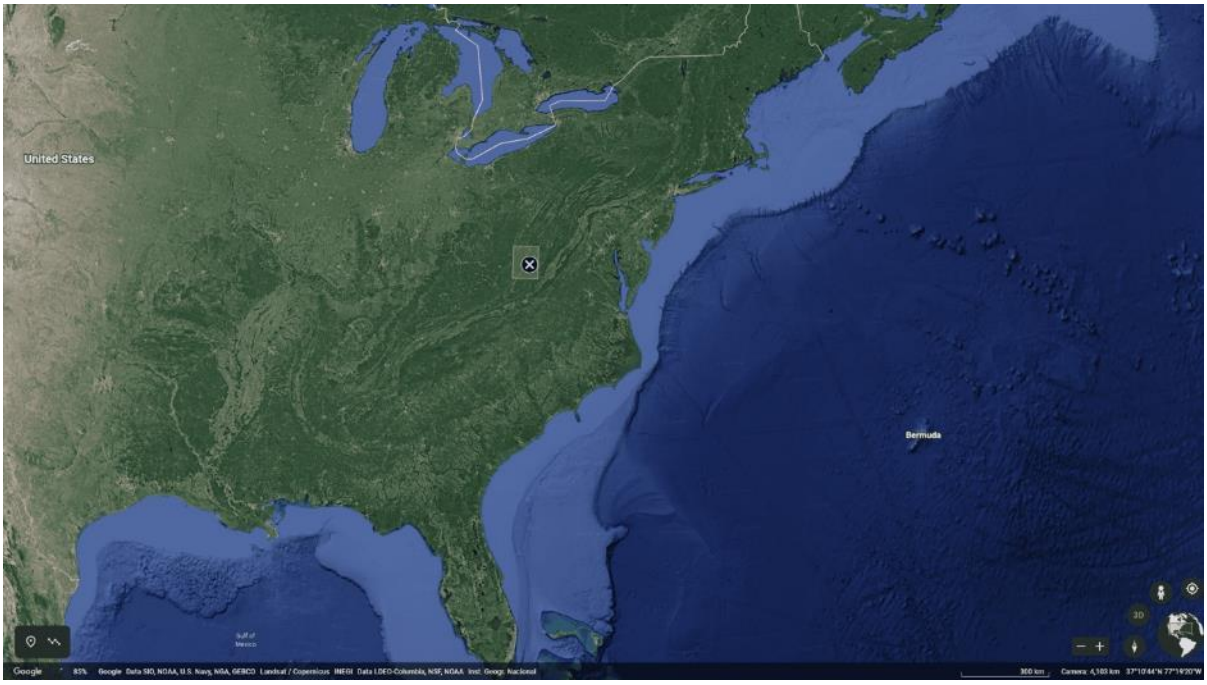

FIGURE A7-28

Topography around the Green Bank telescope site (black dot),
***Source*: Shuttle Radar Topography Mission**
(3 arc second precision)

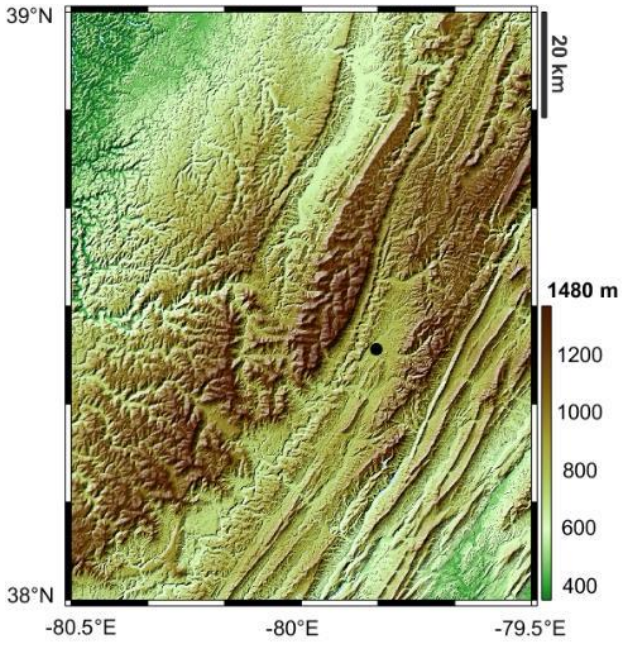

FIGURE A7-29

Maximum permissible e.i.r.p. (in dBm) inside the radio astronomy measurement band 15.35-15.4 GHz of the airborne data terminal (altitude = 300 m AGL) using aeronautical mobile (off-route) System 2 and operating in the frequency band 15.4-15.7 GHz around the Green Bank telescope site (black dot)

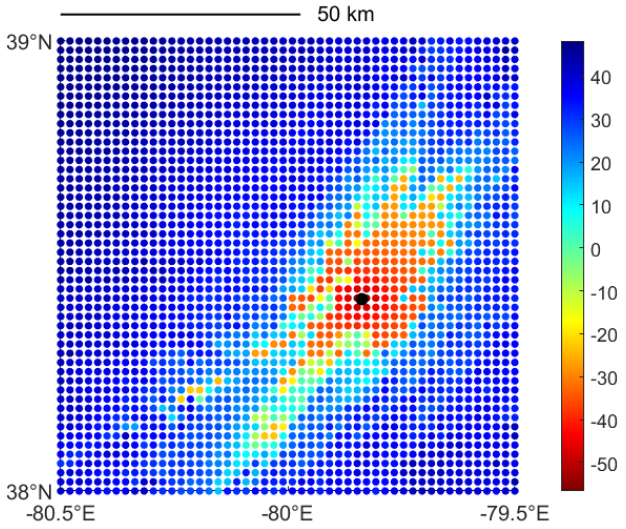

A7B.3 Jansky very large array (USA)

FIGURE A7-30

Topography around the Jansky very large array site (white cross) and deployment zone of the airborne data terminal (red area)

FIGURE A7-31

Topography around the Jansky very large array site (black dot)
***Source*: Shuttle Radar Topography Mission (3 arc second precision)**

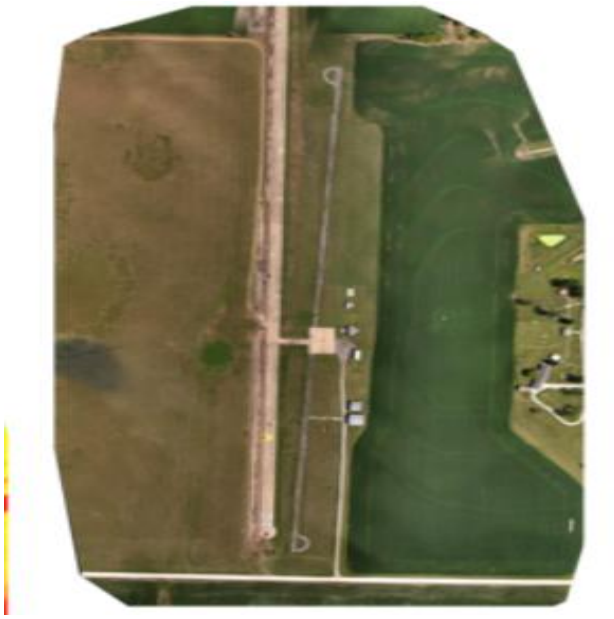

FIGURE A7-32

Maximum permissible e.i.r.p. (in dBm) in the radio astronomy frequency band 15.35-15.4 GHz of the aeronautical mobile (off-route) System 2 (alt = 300 m AGL) around the Green Bank telescope site (black dot)

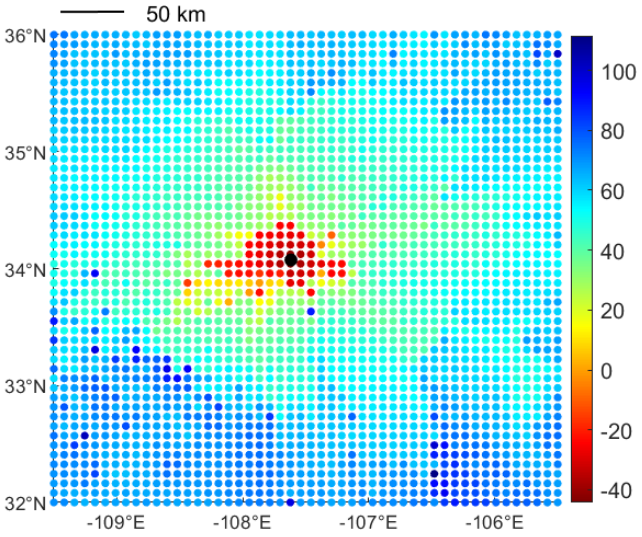

A7B.4 Parkes (Australia)

FIGURE A7-33

Topography around the Parkes site (white cross) and deployment zone of the airborne data terminal (red area)

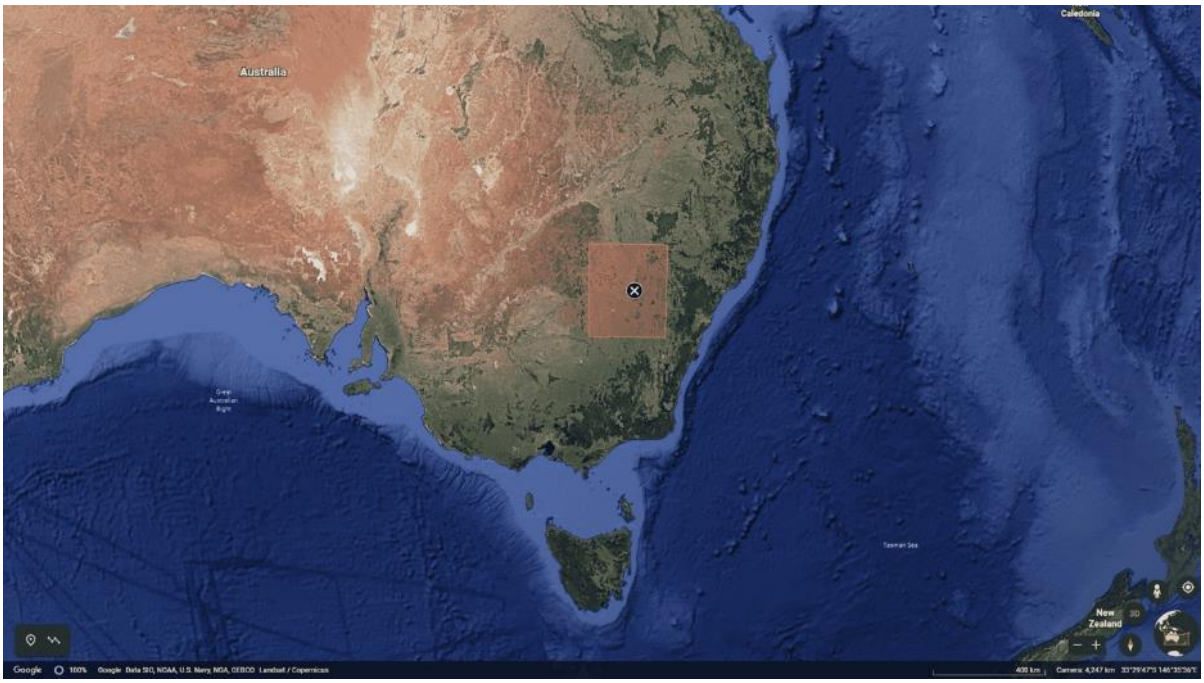

FIGURE A7-34

Topography around the Parkes site (black dot)
***Source*: Shuttle Radar Topography Mission (3 arc second precision)**

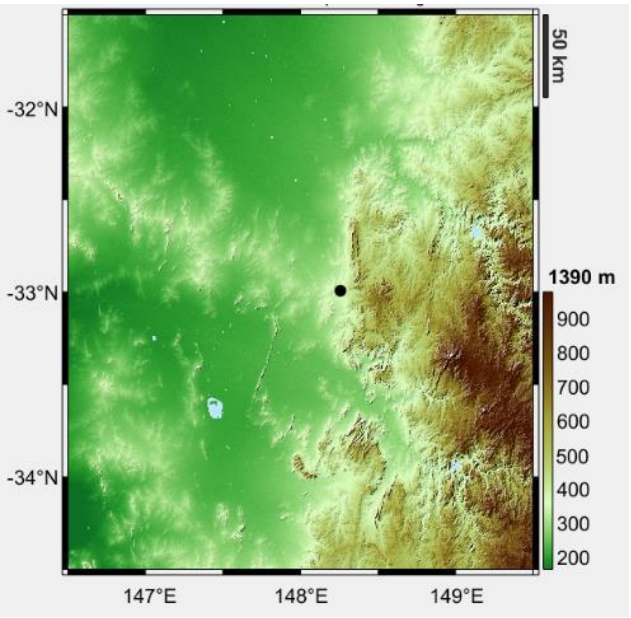

FIGURE A7-35

Maximum permissible e.i.r.p. (in dBm) in the radio astronomy frequency band 15.35-15.4 GHz of the aeronautical mobile (off-route) System 2 (alt = 300 m AGL) around the Parkes site (black dot)

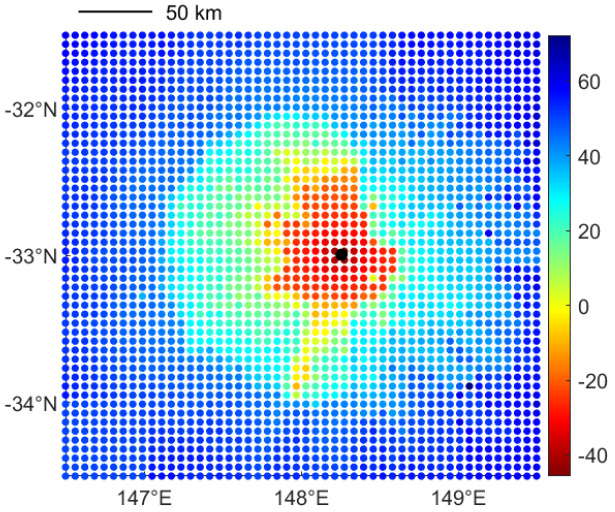

A7B.5 Tianma (China)

FIGURE A7-36

Topography around the Tianma site (black dot) and deployment zone of the airborne data terminal (red area)

FIGURE A7-37

Topography around the Tianma site (black dot)
***Source*: Shuttle Radar Topography Mission**
(3 arc second precision)

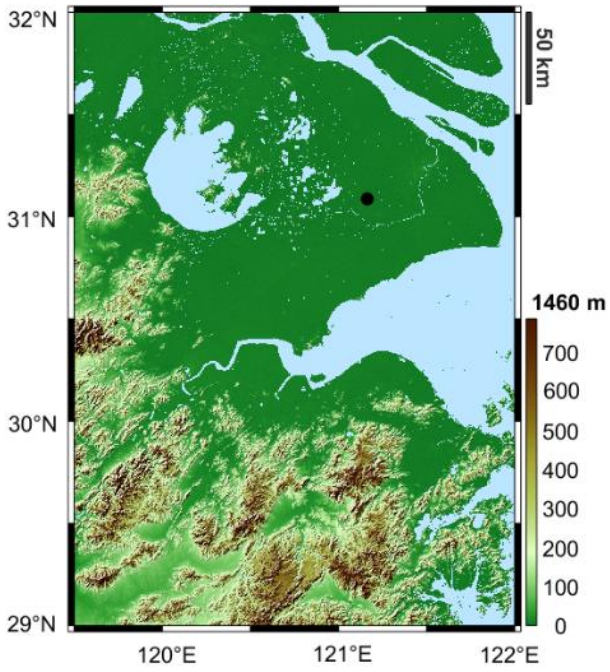

FIGURE A7-38

Maximum permissible e.i.r.p. (in dBm) in the radio astronomy frequency band 15.35-15.4 GHz of the aeronautical mobile (off-route) System 2 (alt = 300 m AGL) around the Tianma site (black dot)

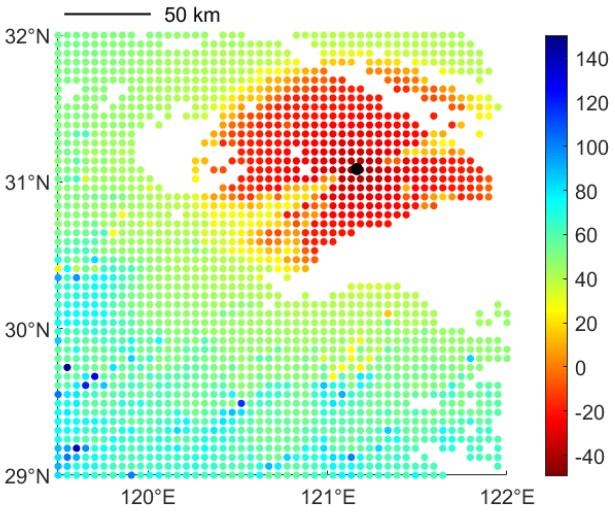

A7B.6 Nobeyama (Japan)

FIGURE A7-39

Topography around the Nobeyama site (black dot) and deployment zone of the airborne data terminal (red area)

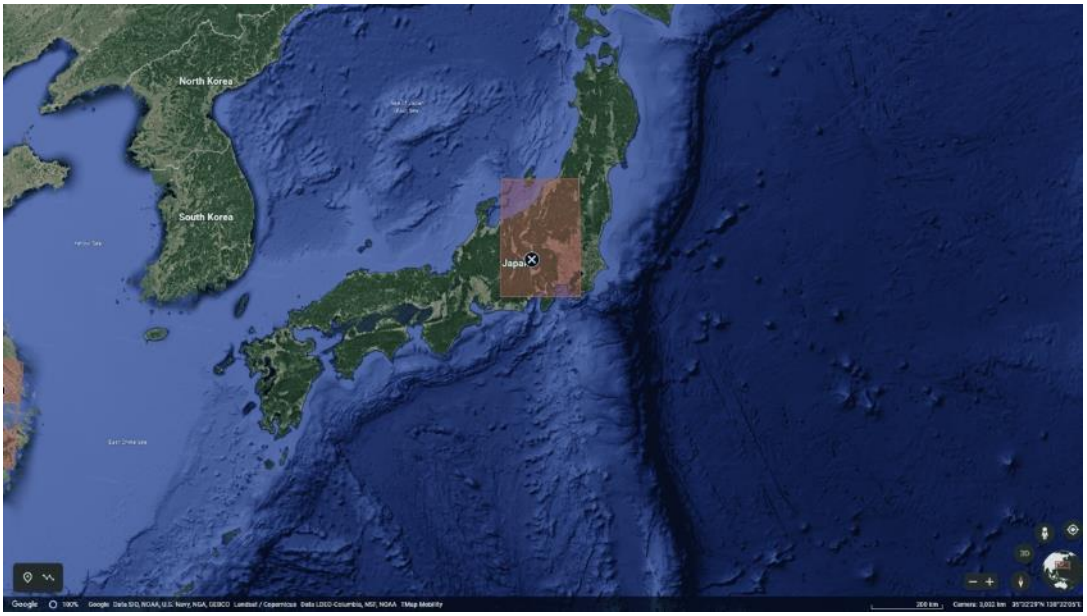

FIGURE A7-40

Topography around the Nobeyama site (black dot)
***Source*: Shuttle Radar Topography Mission**
(3 arc second precision)

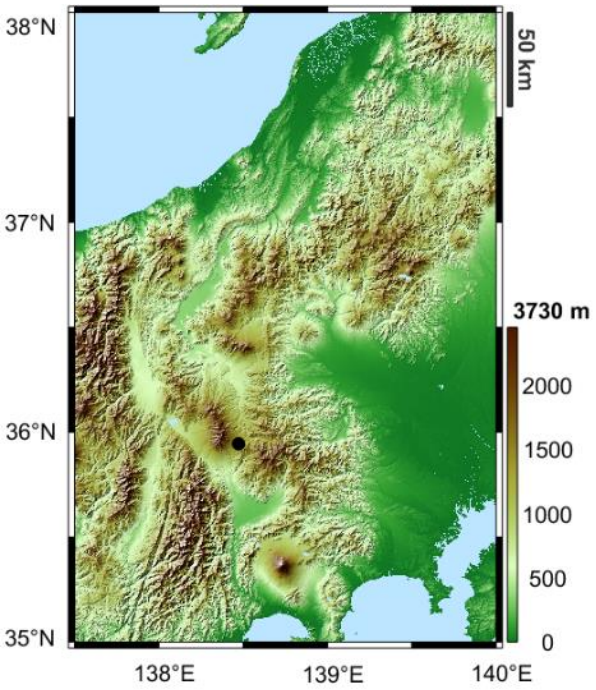

FIGURE A7-41

Maximum permissible e.i.r.p. (in dBm) in the radio astronomy frequency band 15.35-15.4 GHz of the aeronautical mobile (off-route) System 2
(alt = 300 m AGL) around the Nobeyama site (black dot)

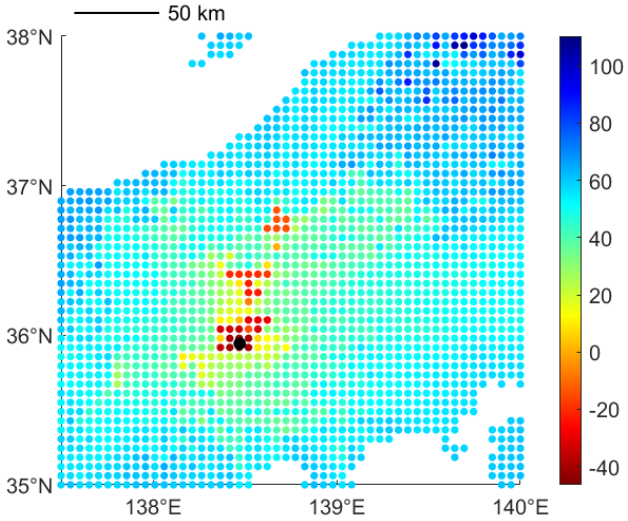

A7B.7 Plateau de Bure (France)

FIGURE A7-42

Topography around the Plateau de Bure site (black dot) and deployment zone of the airborne data terminal (red area)

FIGURE A7-43

Topography around the Plateau de Bure (black dot)
***Source*: Shuttle Radar Topography Mission (3 arc second precision)**

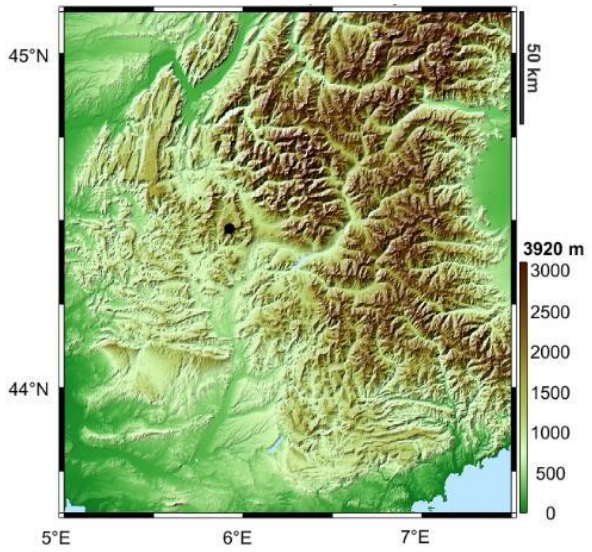

FIGURE A7-44

Maximum permissible e.i.r.p. (in dBm) in the radio astronomy frequency band 15.35-15.4 GHz of the aeronautical mobile (off-route) System 2 (alt = 300 m AGL) around the Plateau de Bure site (black dot)

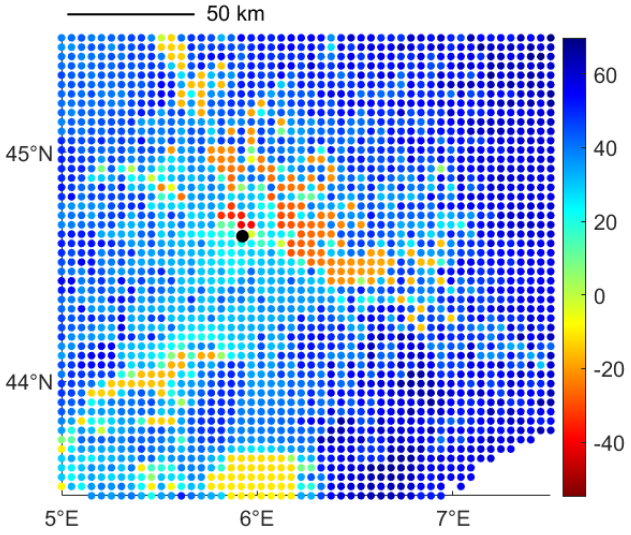

Annex 8

Sharing of the frequency band 22-22.21 GHz between future systems operating in the non-safety aeronautical mobile (off-route) service and the fixed service

TABLE OF CONTENTS

The frequency band 21.2-23.6 GHz is globally allocated to the FS. This annex comprises three different studies (A, B and C) that address different aspects of the sharing of the frequency band 22-22.21 GHz with future non-safety AM(OR)S systems planned to operate in this frequency band.

A8.1 Study A

Three different aspects have been addressed in Study A. In § A8.1.1, an elementary study case is studied using the MCL approach. Sections A8.1.2 and A8.1.3 assess more complex situations using the Monte Carlo analysis.

A8.1.1 Dynamic study case

A8.1.1.1 Simulation setup

The considered scenario is shown in Fig. A8-1. It is assumed that an ADT is providing A2A or A2G links. The aim is to determine the maximum PSD of the e.i.r.p. for this ADT in the direction of an FS station deployed in the same area. The value is computed using equation (A8-1):

$$EIRP_{\max}(\theta, \mathrm{h}) = N_{RX} + \frac{\mathrm{I}}{\mathrm{N}} - G_{FS}(\theta) + L(\theta, h) \qquad \text{(A8-1)}$$

where:

$EIRP_{\max}(\theta)$: maximum PSD of the e.i.r.p. of the ADT in the direction of the FS station

N_{RX}: receiver noise PSD in the FS receiver according to Table A2-11 i.e. −138 dBW/MHz for 128-QAM modulation

$\frac{I}{N}$: long-term interference threshold of the FS i.e. −10 dB according to § A4.1.3

$G_{FS}(\theta)$: FS antenna gain in the direction of the ADT. A maximum gain of 34.8 dBi is assumed according to Table A4-1 and the radiation pattern is calculated using Recommendation ITU-R F.699-8 as seen in § A4.1.2

$L(\theta, h)$: PL calculated using Recommendation ITU-R P.528-5 according to § 8.2. A time percentage of 20% is assumed to model the time variability of the propagation model.

A8.1.1.2 Results

Results are shown in Figs A8-2 to A8-4 for different heights of the ADT and different tilt angles at the FS station. In these Figures, the x-axis shows the elevation angle at the FS station in the direction of the ADT, which is calculated from the altitude AGL of the ADT.

FIGURE A8-1

Interference scenario for the single minimum coupling loss study

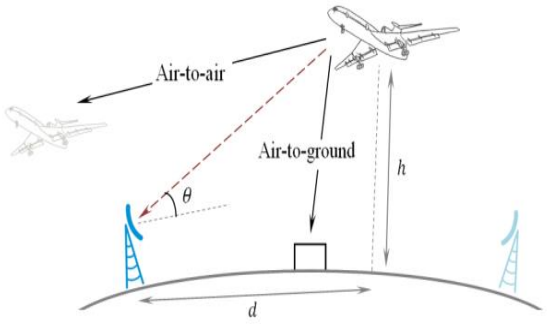

FIGURE A8-2

Maximum permissible e.i.r.p. of the airborne data terminal in the direction of the fixed station (the tilt angle at the fixed station is 5 degrees below the local horizontal)

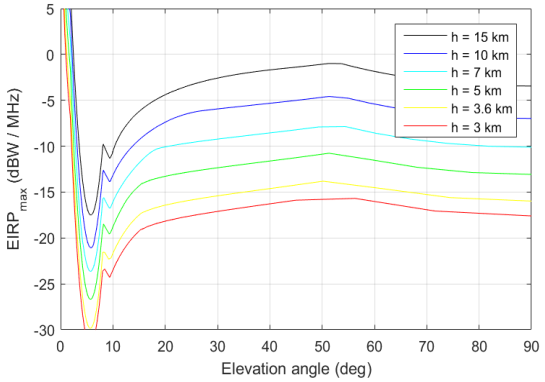

FIGURE A8-3

Maximum permissible e.i.r.p. of the airborne data terminal in the direction of the fixed station (the tilt angle at the fixed station is 0 degrees)

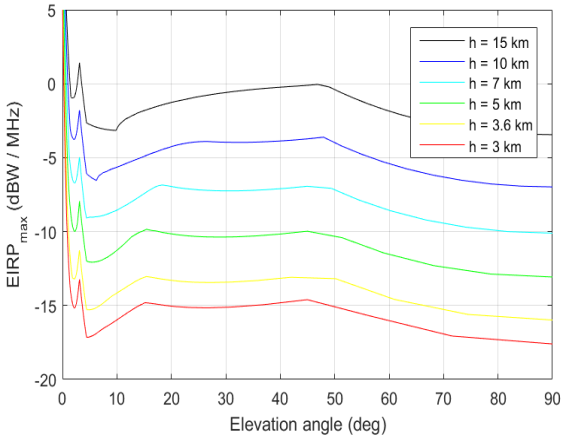

FIGURE A8-4

Maximum permissible e.i.r.p. of the airborne data terminal in the direction of the fixed station (the tilt angle at the fixed station is 5 degrees above the local horizontal)

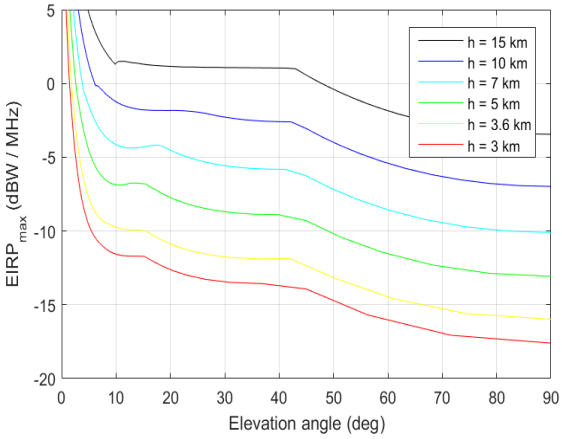

A8.1.1.3 Summary

While comparing the results presented in Figs. A8-2 to A8-4 with Table A2-11 in Annex 2 it can be seen that the long-term interference threshold of FS may be exceeded in some cases.

A8.1.2 Monte Carlo analysis for a single cluster

This section evaluates the impact of a single ADT inside a single cluster onto an FS station, using the Monte Carlo methodology.

A8.1.2.1 Simulation setup

The following setup is used for the simulation:

– The simulation area is limited by the LOS distance between the ADT and the FS station, considering their respective altitudes.

– The FS station is located in the centre of the simulation area. The height above the ground is 10 m or 50 m as per Table A2-11 and the tilt angle is 0°.

– Only one WBLOSDL is working co-channel with the FS station and therefore only one cluster is deployed in the simulation area. The deployment of the cluster (in particular the distance between ADTs and GDTs and their respective altitudes) inside the simulation area is made in accordance with Table 3 in § 6.3. The parameters of the ADT are taken from Table A1-2. ATPC is taken into account and calculations are performed for different values of the margins above the minimum power needed to close the link (0 dB, 5 dB, 10 dB and 15 dB). As an illustration, Figs A8-5 to A8-8 below show the ECDF of the PSD of the ADTs' TPO in the four scenarios. In these Figures, a power margin of 0 dB is considered.

– The BW of the FS station is 112 MHz (maximum value provided in Recommendation ITU-R F.758-7 for FS stations operating in the frequency range 21.2-23.6 GHz). The unique interfering ADT has the same centre frequency as the FS station and has a BW of 100 MHz.

– The propagation model is Recommendation ITU-R P.528-5, and the percentage of time associated to this model is a random value with uniform distribution between 1% and 99%.

– The pattern used to model the FS station antenna is Recommendation ITU-R F.1245-2.

FIGURE A8-5

Empirical cumulative distribution function of the transmit power output of the airborne data terminals in scenario 6.2.1 (aeronautical mobile (off-route) system 2 is transmitting)

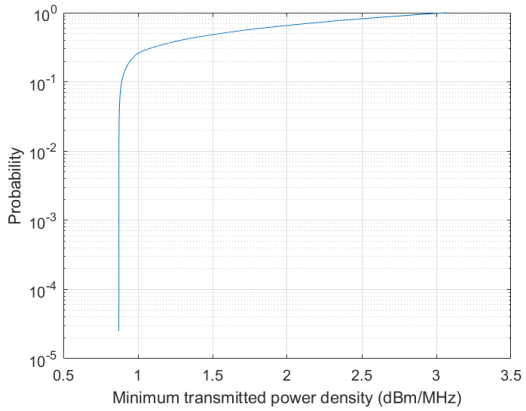

FIGURE A8-6

Empirical cumulative distribution function of the transmit power output of observation airborne data terminals in scenario 6.2.2 (aeronautical mobile (off-route) system 1 is transmitting)

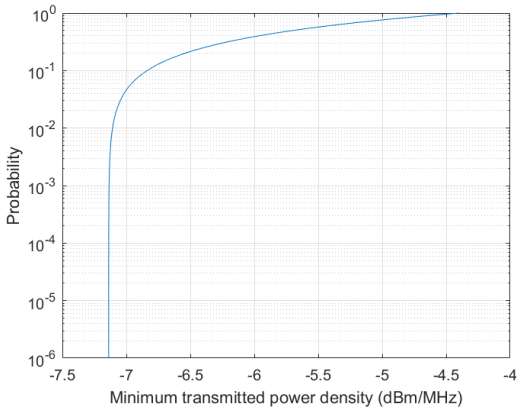

FIGURE A8-7

Empirical cumulative distribution function of the total power output of the relay airborne data terminals in scenario 6.2.3 (aeronautical mobile (off-route) system 1 is transmitting)

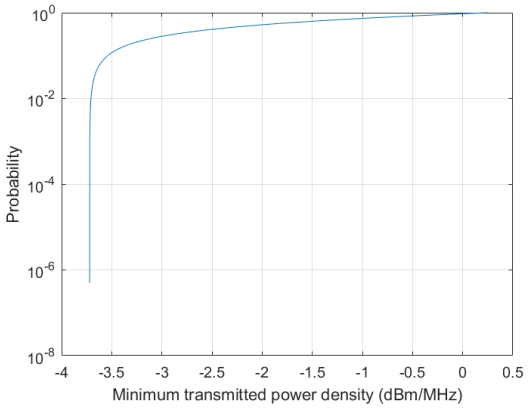

FIGURE A8-8

Empirical cumulative distribution function of the total power output of observation airborne data terminals in scenario 6.2.3 (aeronautical mobile (off-route) system 1 is transmitting)

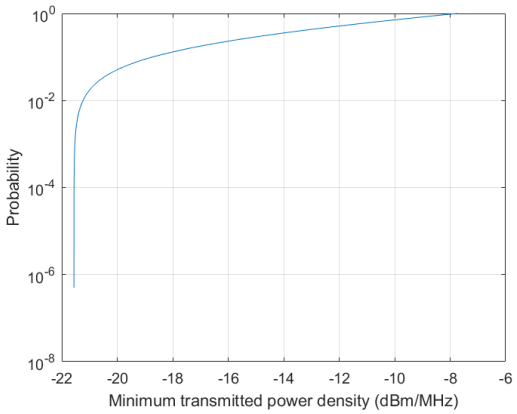

A8.1.2.2 Results

Figures A8-9 to A8-16 below show the ECDF of the variable *I*/*N* at the FS station. Small crosses on the graphs indicate the long- and short-term protection criteria of the FS as highlighted in §§ A2.7.3 and A2.7.4 of this Report.

FIGURE A8-9

Empirical cumulative distribution function of *I*/*N* at the fixed station in scenario 6.2.1 (aeronautical mobile (off-route) system 2 is transmitting); the fixed station is at 50 m above the ground

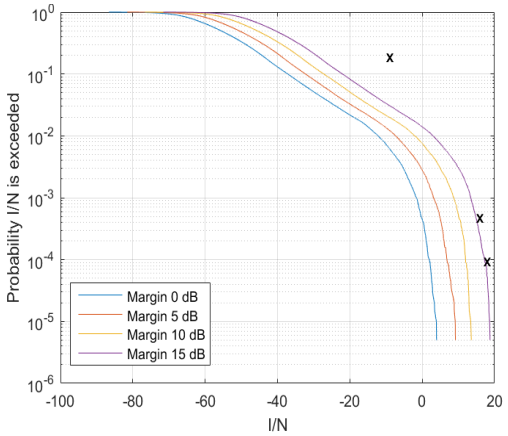

FIGURE A8-10

Empirical cumulative distribution function of *I*/*N* at the fixed station in scenario 6.2.2 (aeronautical mobile (off-route) system 2 is transmitting); the fixed station is at 10 m above the ground

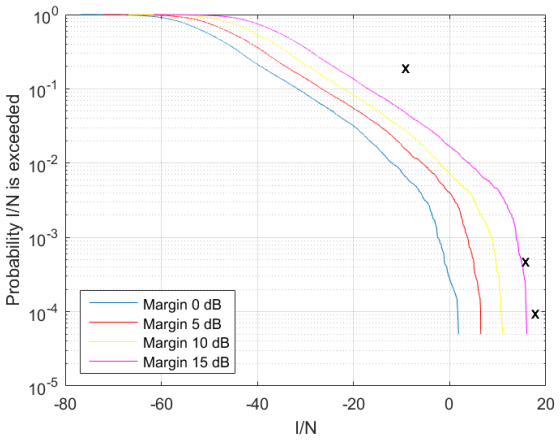

FIGURE A8-11

Empirical cumulative distribution function of *I*/*N* at the fixed station in scenario 6.2.2 (aeronautical mobile (off-route) system 1 is transmitting); the fixed station is at 50 m above the ground

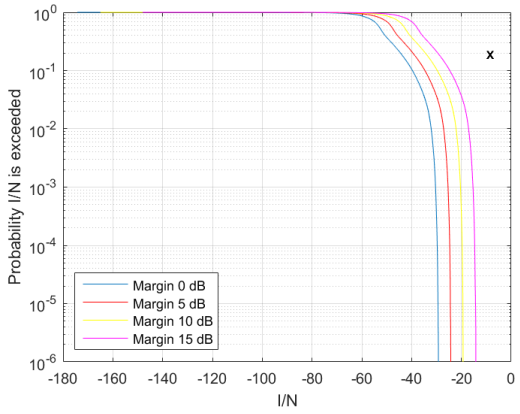

FIGURE A8-12

Empirical cumulative distribution function of *I*/*N* at the fixed station in scenario 6.2.2 (aeronautical mobile (off-route) system 1 is transmitting); the fixed station is at 10 m above the ground

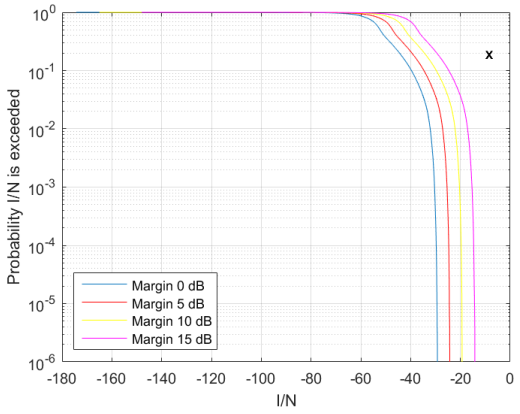

FIGURE A8-13

Empirical cumulative distribution function of *I*/*N* at the fixed station caused by A2A links in scenario 6.2.3 (aeronautical mobile (off-route) system 2 is transmitting); the fixed station is at 50 m above the ground

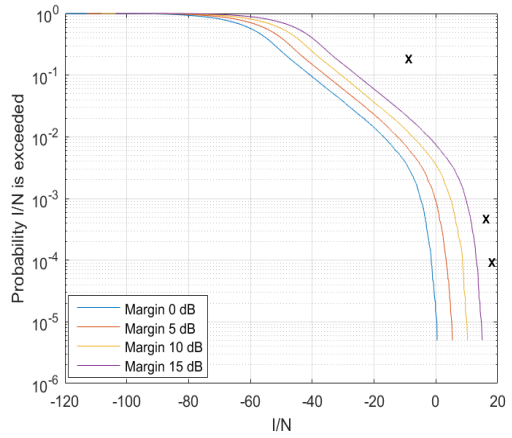

FIGURE A8-14

Empirical cumulative distribution function of *I*/*N* at the fixed station caused by A2A links in scenario 6.2.3 (aeronautical mobile (off-route) system 2 is transmitting); the fixed station is at 10 m above the ground

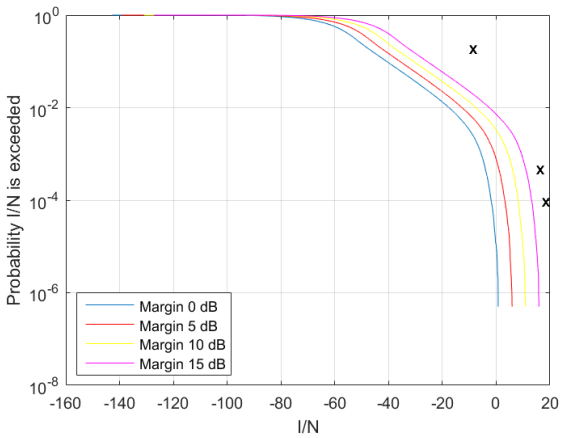

FIGURE A8-15

Empirical cumulative distribution function of *I*/*N* at the fixed station caused by A2G links in scenario 6.2.3 (aeronautical mobile (off-route) system 1 is transmitting); the fixed station is at 50 m above the ground

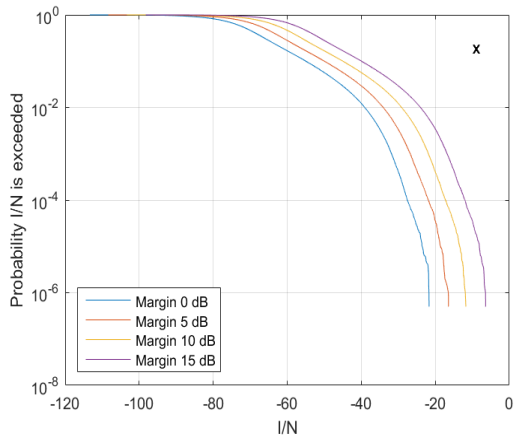

FIGURE A8-16

Empirical cumulative distribution function of *I*/*N* at the fixed station caused by A2G links in scenario 6.4 (aeronautical mobile (off-route) system 1 is transmitting); the fixed station is at 10 m above the ground

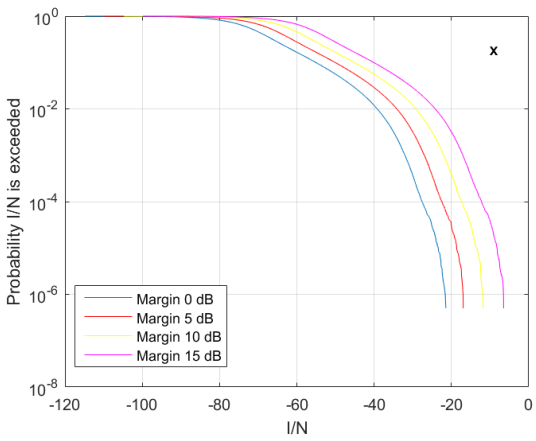

A8.1.2.3 Summary

From Figs A8-10 to A8-15, a conclusion may be drawn that the long- and short-term protection criteria of FS are not exceeded when AM(OR)S systems are working with directive antennas and ATPC.

However, omnidirectional or other wide beam antennas have a more severe impact onto the operation of FS, the analysis has shown that scenario 6.2.1 exceeds the short-term criteria when the SNR margin is 15 dB, see Fig. A8-9.

It should also be taken into account that these single-entry Monte Carlo simulations underestimate possible interference issues as most of the time AM(OR)S systems operate outside of the main beam of the FS station. However it may happen that the operating area lies near the boresight of the FS station for some time. The next section investigates this particular case.

A8.1.3 Monte Carlo analysis for multiple clusters

The next step is to consider the impact of multiple ADTs operating in the visibility of an FS station. The scenario where this is likely to happen is scenario 6.2.1. Wildfires may indeed happen in extended forest areas. In that case, the AM(OR)S stations participating in the mission would not be uniformly distributed around the FS station but rather concentrated within a limited angular sector of the FS station.

A8.1.3.1 Simulation setup

The simulation setup is the same as in § A8.1.2.1 for the single-entry analysis, with the difference that the simulation area is limited to an angular sector of the FS station and several AM(OR)S clusters are uniformly deployed within this sector. For the sake of simplicity, all ADTs use the same 100 MHz frequency channel which is centred on the channel used by the FS station. Furthermore, the link margin of AM(OR)S systems is assumed to be 0 dB.

A8.1.3.2 Results

The results for different sectors and different number of clusters distributed uniformly inside the sector are shown in Fig. A8-17. It can be seen that the long-term protection criteria is exceeded when 6 clusters (i.e. 12 ADTs) are deployed within a 30° sector of the FS station.

FIGURE A8-17

Empirical cumulative distribution function of the aggregate *I*/*N* at the fixed station in scenario 6.2.1 (aeronautical mobile (off-route) system 2 is transmitting); clusters are deployed within an angular sector of the fixed station; the fixed station is 10 m above the ground

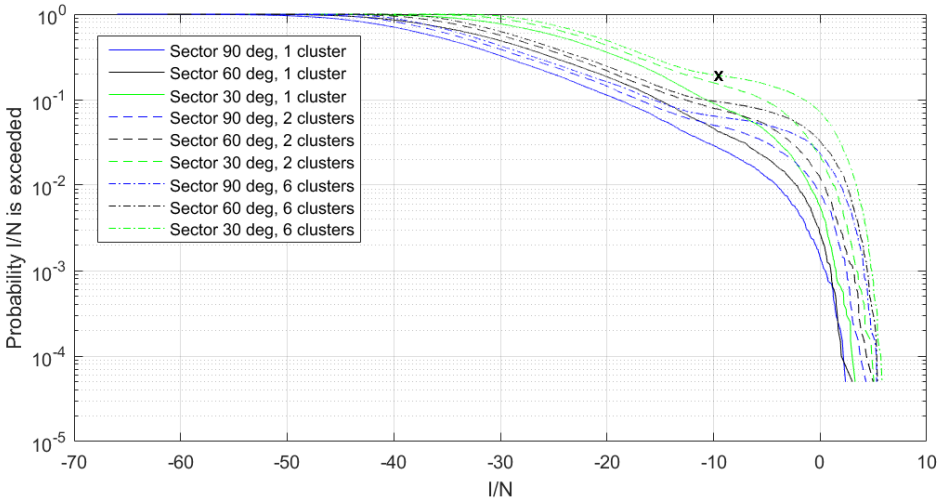

A8.1.4 Summary

Study A has first demonstrated in § A8.1.1 that the long-term interference threshold of the FS may be exceeded in some situations. However, it could not be determined the percentage of time during which this threshold is exceeded.

In a second time, it is shown in § A8.1.2 that, for a single cluster of AM(OR)S stations, both the long- and the short-term protection criteria of the FS are met when AM(OR)S systems are working with ATPC and use directive antennas. However, when omnidirectional or other wide beams antennas are used, the short-term protection criteria are exceeded in some cases where an additional link margin is needed for WBLOSDL. This relates to the additional power needed by omnidirectional AM(OR)S systems to obtain the required SNR at the receiver. It should also be taken into account that this single-cluster analysis underestimates the interference level as most part of the time AM(OR)S system is outside of the main beam of FS station but in real life it may happen that the area, where AM(OR)S system performs its mission, is near the boresight of FS station for some time.

The last part of the study (§ A2.1.3) further investigates the effect of multiple AM(OR)S clusters onto FS stations and shows that under certain circumstances, the long-term protection criterion of the FS is exceeded, for instance when massive deployments of AM(OR)S stations take place in a limited area close to an FS station. In the context of scenario 6.2.1 ‘Wildfire Observation’, this situation can be typical for large forest areas in summertime.

Study C will investigate three possible pfd masks to protect FS stations and address the issues mentioned above.

A8.2 Study B

A8.2.1 Methodology

Study B is a multiple-entry Monte Carlo analysis that evaluates the impact of AM(OR)S systems onto FS station in the four operational scenarios described in § 6.2 of this Report. The general methodology, which is common to other Monte Carlo studies performed throughout this Report, is highlighted in Annex 11. The study was performed assuming first FSK modulation and then 128-QAM modulation at the FS station.

A8.2.2 Results

Results are shown in Figs A8-18 to A8-21 for the four different scenarios as a set of ECDF curves of the variable *I/N* measured at the FS station. In each figure, different modulation schemes, altitude and tilting are considered at the FS station. The protection criteria (both short-term and long-term as described in §§ A2.7.3 and A2.7.4 of this Report) are also plotted in the Figures.

Results are in general better when FSK modulation is used at the FS station than 128-QAM, which is due to the lower noise PSD in the latter case (see Table A2-11 in § A2.7.1). In addition, sharing is improved as the tilt of the FS station under the local horizon increases and as the height of the station above ground decreases.

In scenarios 6.2.2, 6.2.3 and 6.2.4 (Figs A8-19, A8-20 and A8-21), the long- and short-term protection criteria of the FS are met, whilst in scenario 6.2.1 (Fig. A8-18), the short-term protection criteria is exceeded for some configurations. In this scenario, if FSK modulation is assumed, one configuration was found (tilt of the FS station = +5° and height AGL = 10 m) where the second short-term protection criterion ($I/N < 16.6$ dB for at least 99.9872% of the time, see equation (A2-15)) is exceeded. If 128-QAM modulation is assumed, all the tested configurations exceeded this second short-term criterion and the first short-term criterion ($I/N < 14.6$ dB for at least 99.952% of the time, see equation (A2-15)) is exceeded for two configurations (tilt of the FS station = +5° or 0° and height AGL = 50 m).

FIGURE A8-18

Empirical cumulative distribution function of *I/N* at the fixed station in scenario 6.2.1, for different modulation schemes, altitudes of the fixed station above ground and tilt angles of the fixed antenna

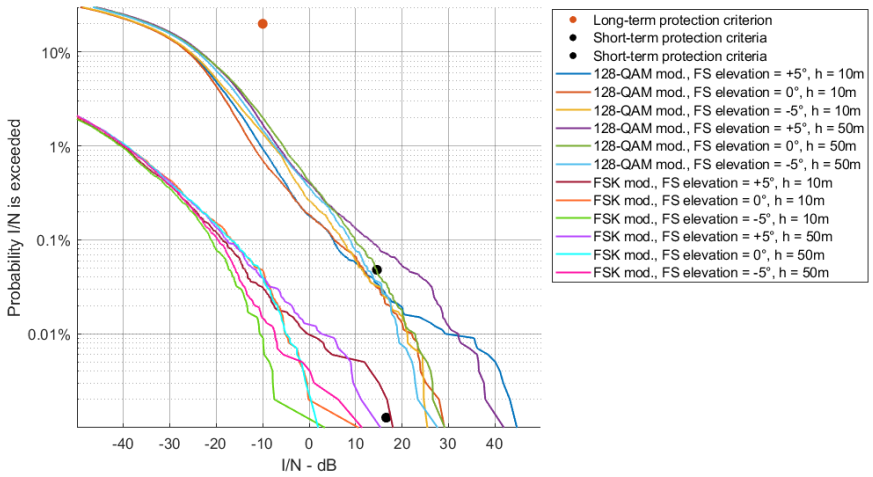

FIGURE A8-19

As in Fig. A8-18, in scenario 6.2.2

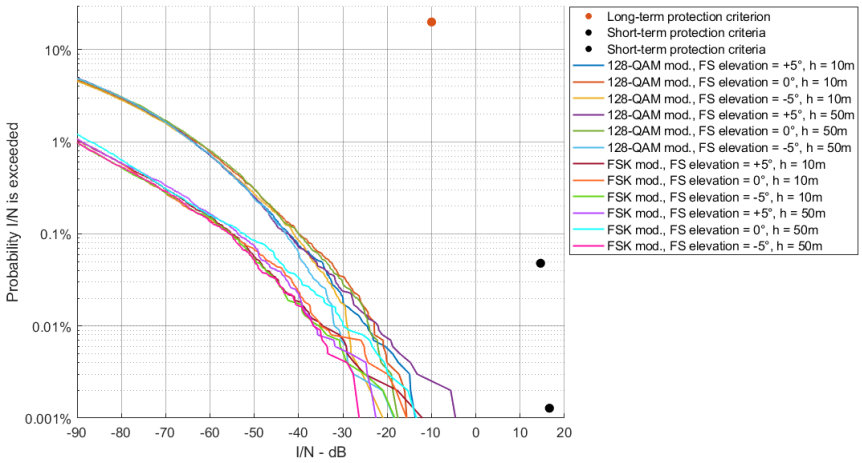

FIGURE A8-20

As in Fig. A8-18, in scenario 6.2.3

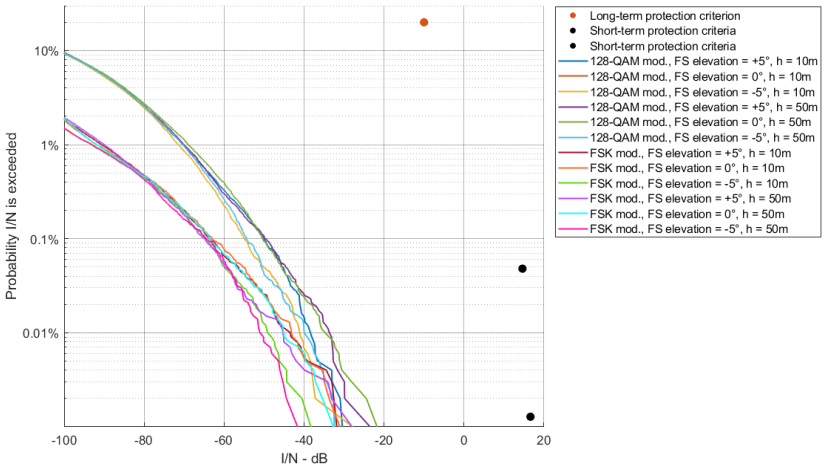

FIGURE A8-21

As in Fig. A8-18, in scenario 6.2.4

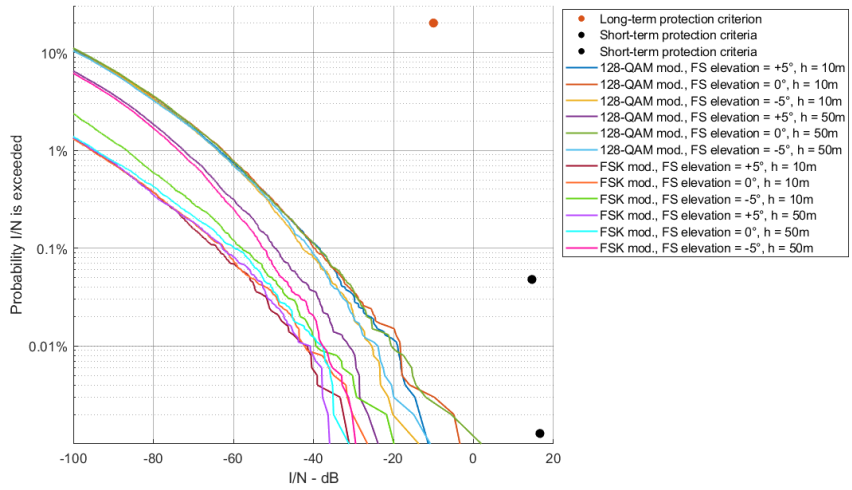

A8.2.3 Summary

Study B has shown that the sharing of the band 22-22.21 GHz between FS and directive AM(OR)S systems (Systems 1 and 3) is in general possible without mitigation measures (Figs A8-19, A8-20 and A8-21). Omnidirectional (System 2) or other wide beam AM(OR)S systems (Fig. A8-18) can in some situations exceed the short-term protection criteria of the FS. Study C addresses some protection measures to implement in this case.

A8.3 Study C

A8.3.1 Introduction

Studies A and B in §§ A8.1 and A8.2 have shown that the long- and/or short-term protection criteria of the FS are exceeded in some AM(OR)S scenarios, especially when ADTs use omnidirectional antennas. Protection measures should be envisaged independently of the considered scenario to provide protection in every situation to the FS stations. This is why a pfd mask is thought to be the best option as it provides sufficient protection and leaves some flexibility to the AM(OR)S operator as to how to comply with the pfd mask.

Two methodologies are highlighted in §§ A8.3.1 and A8.3.2, which leads to different pfd masks. Section A8.3.3 compares the protection level provided by these two masks.

A8.3.2 Power flux-density mask option 1

The following assumptions were taken to find a suitable pfd mask:

– FS tilt angles are randomized in the range ±5 degrees according to Table A2-11;

– the PSD of the noise floor at the FS station is −138 dBW/MHz as in Table A2-11;

– ADTs are assumed to be uniformly deployed in azimuth and elevation on the hemisphere above the FS station.

Results are shown in Fig. A8-22 with blue-yellow points. Permissible pfd values are shown on the horizontal axis, and elevation angles in the direction of the ADT are shown on the vertical axis. Colours show probabilities that this pdf value is exceeded. Blue colour is when the probability tends to 1, yellow colour, when the probability tends to 0.

FIGURE A8-22

Power flux-density vs elevation angle and probability

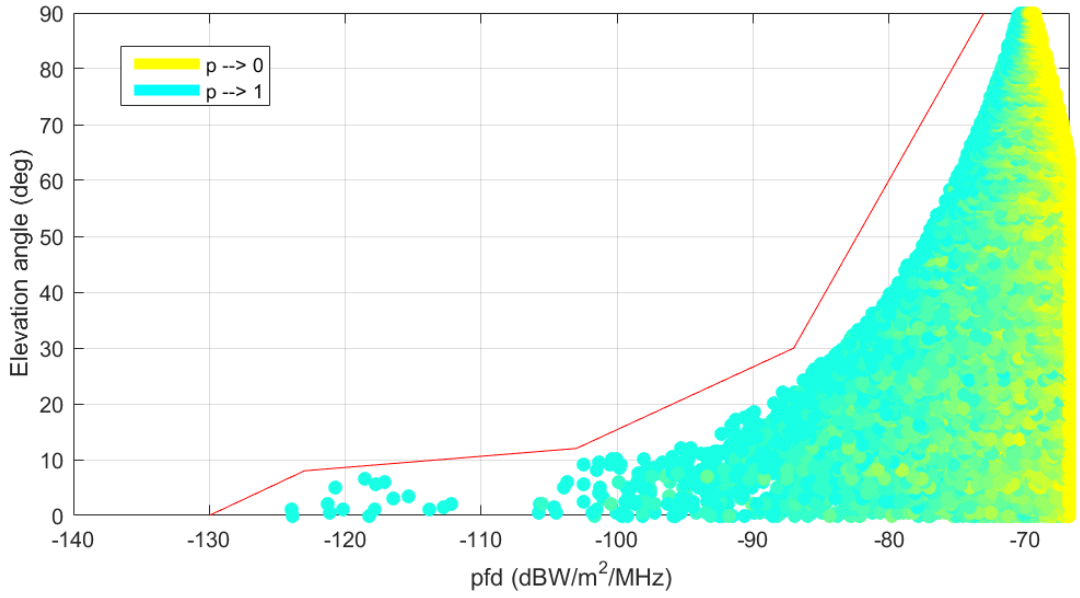

Based on Fig. A8-22 the following pfd mask at the surface of the Earth above the horizontal plane is obtained (shown with red line in Fig. A8-22):

$$PFD_{\max} = \begin{cases} 0.875 \cdot \theta - 130 & \text{for } 0 \leq \theta \leq 8 \\ 5 \cdot \theta - 163 & \text{for } 8 < \theta \leq 12 \\ 0.89 \cdot \theta - 113.68 & \text{for } 12 < \theta \leq 30 \\ 0.233 \cdot \theta - 93.99 & \text{for } 30 < \theta \leq 90 \end{cases} \quad \text{(A8-1)}$$

where:

θ: elevation angle (degree) at the FS station

$PFD_{\max}$: maximum allowable spectral pfd for ADTs, measured at the FS station in the frequency band 22-22.21 GHz (dB(W/(m^2 · MHz))).

This pfd mask should be used to ensure protection of FS stations.

A8.3.3 Power flux-density mask option 2

The mask proposed in this section is defined in equation (A8-2) below and shown in Fig. A8-23. The mask defined in § A8.3.2 is also indicated in the figure for reference.

$$PFD_{\max} = \begin{cases} A & \text{for } 0° \leq \theta < 10° \\ 50\log_{10}\left(\frac{\theta}{10}\right) + A & \text{for } 10° \leq \theta < 30° \\ 50\log_{10}(3) + A & \text{for } 30° \leq \theta \leq 90° \end{cases} \quad \text{(A8-2)}$$

where:

θ: elevation angle (degrees) at the FS station

$PFD_{\max}$: maximum allowable spectral pfd for ADTs, measured at the FS station in the frequency band 22-22.21 GHz (dB(W/(m^2 · MHz))).

$$A = -110 + MOD + FDR + L$$

where:

MOD: constant depending on the modulation scheme used by the FS station, 0 dB for 128-QAM and 5 dB for FSK modulation

FDR: constant depending on the BW of the FS station (BW_{FS}) and on the BW $BW_{AM(OR)S}$ of the AM(OR)S stations, i.e. 0 dB if $BW_{AM(OR)S} \leq BW_{FS}$, and $10\log_{10}\left(\frac{BW_{AM(OR)S}}{BW_{FS}}\right)$ otherwise. BW_{FS} is 25 MHz if FSK modulation is used at the FS station, and 30 MHz if 128-QAM is used

L: feeder loss (FL) at the FS station that lies between 0 and 3 dB.

FIGURE A8-23

Proposed power flux-density masks (option 1 in blue and 2 in red assuming frequency shift keying modulation, L = 3 dB and $BW_{AM(OR)S}$ = 200 MHz) to protect fixed stations from interference caused by systems operating in aeronautical mobile (off-route) service

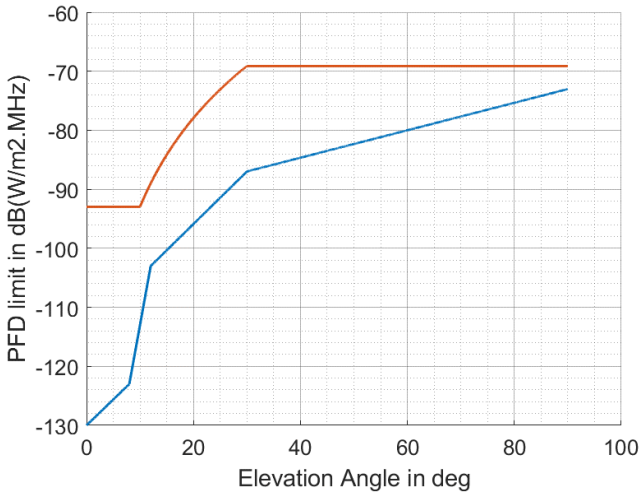

A8.3.4 Comparison of Option 1 and Option 2 power flux-density masks

This section evaluates and compares the protection offered to an FS station by the masks presented in §§ A8.3.1 and A8.3.2 of this Report (Option 1 and Option 2).

A8.3.4.1 Methodology

The approach followed in this section is explained in the steps below:

– Deploy a single FS station in the middle of the simulation area, using worst case assumptions[21] in terms of deployment according to the Table A2-11, i.e. the elevation of the FS station above the ground is chosen as 50 m, the tilt angle as +5° above the local horizon, and the modulation as 128-QAM. Therefore, if mask Option 2 is used, the following parameters are assumed: MOD = 0 dB, L = 0 dB, and FDR = 0 dB. The simulation is in principle agnostic to the azimuth direction of the FS antenna which is therefore assumed to be eastwards.

– Decide about the minimum and maximum altitude of ADTs. According to Table A1-1 in Annex 1, they are respectively 300 m and 15 km. The maximum altitude determines the visibility area of the FS station and hence the size of the simulation area. Using equation (A11-1) in Annex 11, the simulation area has a great circle radius of approximately 462 km.

– Compute the number of points within the simulation area that represent the possible positions of ADTs. The number of points to simulate is given in Table A8-1 and should be in compliance with the densities associated to each scenario as provided in § 6.5.

– Spread these points in the simulation area with uniform probability distribution.

– Compute the elevation angle at the FS station in the direction of all these points.

– Compute the corresponding pfd values using one of the mask provided in §§ A8.3.1 and A8.3.2.

– Compute the off-axis angle between the direction of maximum gain of the FS station and the lines joining the FS station to the selected points. From there, deduce the gain values at the FS station using Recommendation ITU-R F.1245-3 (see § A2.7.2).

---

[21] Worst-case assumptions are chosen for the parameters of the FS station because the mask under test has to offer protection to all FS stations operating in this frequency band, independently of their configuration.

– Compute the effective area for all the selected points using equation (A8-3):

$$A_{eff} = \frac{\lambda^2}{4\pi} 10^{\frac{G}{10}} \quad \text{(A8-3)}$$

where:

G: gain (dBi) of the FS antenna in the direction of the selected point

λ: wavelength (m)

A_{eff}: effective area (m²) of the FS antenna corresponding to the gain *G*.

– Multiply the effective area associated with all selected points by the corresponding pfd value, which produces a power level at the FS receiver.

– Aggregate for all the selected points and compute *I*/*N*. It is assumed that the deployed ADTs and the FS station operate using the same channel BW and the same centre frequency. Therefore, all calculations are performed using spectral power levels.

– Repeat all the steps above until statistical significance is achieved. 1 000 000 iterations were found to be sufficient to check the long- and short-term protection criteria of the FS and achieve sufficiently narrow confidence intervals.

– Compare the obtained ECDF of *I*/*N* with the long- and short-term protection criteria of the FS as highlighted in §§ A2.1.3 and A2.1.4 of this Report.

– Conclude whether the selected mask provides a sufficient protection level to the FS station.

TABLE A8-1

Number of airborne data terminals to simulate in order to reproduce reference densities in each scenario

	Scenario			
	6.2.1	**6.2.2**	**6.2.3**	**6.2.4**
Radius in km of the circle in which 1 cluster is expected(1)	254	484	467	332
Number of transmitting ADTs per cluster(2)	2	6	3	4
Number of ADTs to simulate in this section(3)	≈ 7	≈ 5	≈ 3	≈ 8

(1) See Table 4.

(2) See Table 5.

(3) The number of ADTs i.e. of points to consider in this simulation, is obtained using equation (A8-4). The 02round () function approximates to the closest integer.

$$N_{ADT,\ \text{simulation}} = \text{Round}\left(N_{ADT,\ \text{scenario}} \left(\frac{R_{\text{scenario}}}{R_{\text{simulation}}}\right)^2\right) \quad \text{(A8-4)}$$

where:

$N_{ADT,\ \text{simulation}}$: number of ADTs to deploy in the simulation area

$N_{ADT,\ \text{scenario}}$: number of ADTs per cluster in a given scenario

R_{scenario}: radius (km) of the circle in which one cluster is expected at any point in time in a given scenario

$R_{\text{simulation}}$: radius of the simulation area i.e. 462 km as per § A8.3.3.1.

A8.3.4.2 Results

Figures A8-24 and A8-25 below show the ECDF of the aggregate *I*/*N* value at the FS station as a function of the ADT density and the pfd mask. Table A8-1 shows the number of ADTs to simulate to reproduce the density values associated to typical scenarios introduced in § 6.5. The range of heights of AMS stations for each curves are from 300 m to 15 km.

FIGURE A8-24

Empirical cumulative distribution function of *I*/*N* at the fixed station considering mask option 1 for different densities of airborne data terminals in a simulation area of 462 km radius

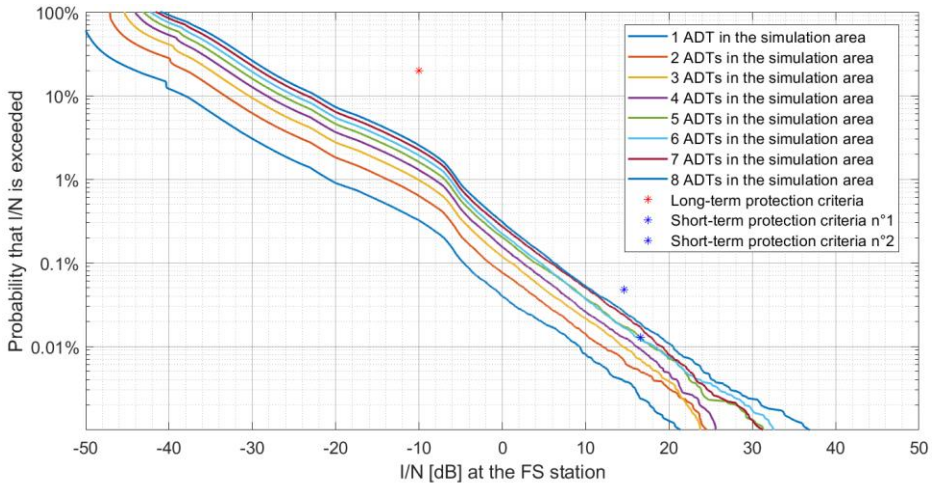

FIGURE A8-25

Empirical cumulative distribution function of *I*/*N* at the fixed station considering mask option 2 for different densities of airborne data terminals in a simulation area of 462 km radius

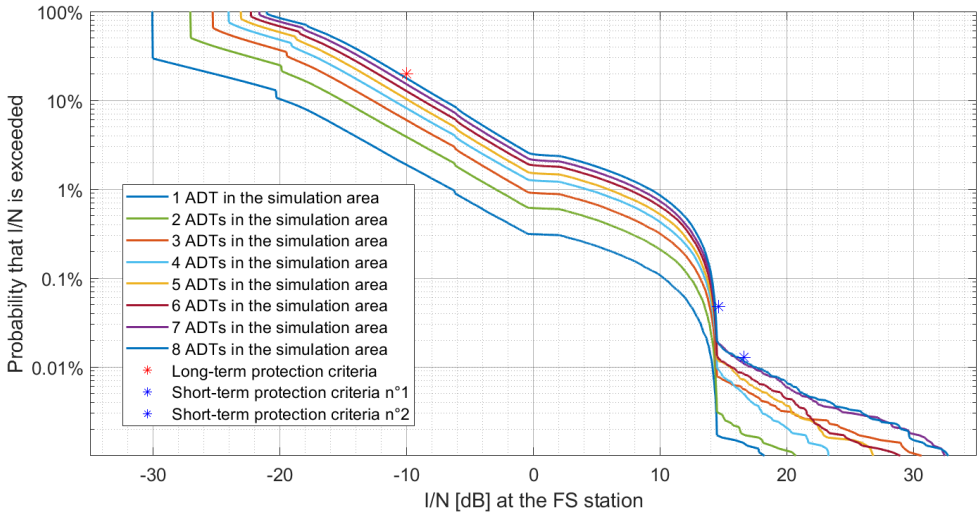

A8.3.4.3 Summary

From Figs A8-24 and A8-25, one can conclude that the two masks presented in §§ A8.3.1 and A8.3.2 ensure that the long-term protection criterion of FS stations is met when deployment densities of AM(OR)S stations are comparable to the values referenced in § 6.5 of this Report. However, mask option 1 seems more restrictive as it provides a significant margin in this simulation approach. The analysis has also shown that both masks are roughly equivalent for meeting the short-term protection

criteria of FS. These masks must also be revised if deployment densities significantly differ from the typical values provided in § 6.5 of this Report.

A8.3.5 Power flux-density mask option 3

In this section another comparison of pfd masks from Option 1 and Option 2 was performed and a new pfd mask was developed based on these results.

The first step to compare Option 1 and Option 2 pfd masks may be to calculate ECDF of *I*/*N* at the FS station if the AM(OR)S stations compile with one of the masks, but without taking into account propagation conditions (or considering it as a free space). The location of AM(OR)S stations is a random value, the number of simultaneously working in the simulation volume AM(OR)S stations is a constant value for each ECDF curve. The number of AM(OR)S stations for different scenarios was taken as in Table A8-1 and is as follows:

– Scenario from § 6.2.1 – 7 AM(OR)S stations;
– Scenario from § 6.2.2 – 5 AM(OR)S stations;
– Scenario from § 6.2.3 – 3 AM(OR)S stations;
– Scenario from § 6.2.4 – 8 AM(OR)S stations.

There is a problem what is the range of altitudes of AM(OR)S stations for the simulations. The analysis included in § A8.3.4.2 assumes a uniform distribution of AM(OR)S stations from 300 m to 15 km. But four scenarios of AM(OR)S deployment (from §§ 6.2.1 to 6.2.4) are for some more restricted ranges of heights. As the heights are interrelated with elevation angles of the incident signals at the FS station, the shapes of ECDF curves differ.

The following heights were considered in this section based on the operational scenarios:

– Scenario from § 6.2.1 – 300 m;
– Scenario from § 6.2.2 – from 1 to 3.6 km;
– Scenario from § 6.2.3 – from 3 to 10 km;
– Scenario from § 6.2.4 – 10 km.

As a “general” scenario like in § A8.3.4.2 (heights between 300 m and 15 km) is denoted, the maximum AM(OR)S station number is 8.

The results of calculations for Option 1 and Option 2 masks are presented on Figs A8-26 and A8-27, respectively. The dashed lines are for only one AM(OR)S station in the visibility of FS station and solid lines of the same colour are for maximum number of AM(OR)S stations as provided above.

It should be taken into account that AM(OR)S station cannot have information on type of modulation, working channel and feeder losses of the FS station in each moment of time so only a pfd mask with constant parameters may be used. In the later calculations and comparisons variables MOD, FDR and L for Option 2 mask were taken as zeros.

FIGURE A8-26

Empirical cumulative distribution function of *I*/*N* at the fixed station for power flux-density mask option 1 without taking into account propagation

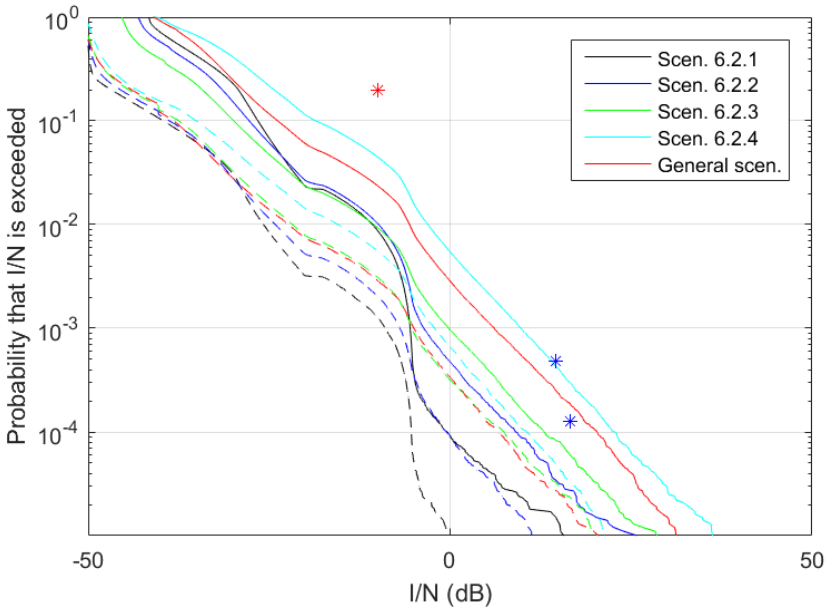

FIGURE A8-27

Empirical cumulative distribution function of *I*/*N* at the fixed station for power flux-density mask option 2 without taking into account propagation

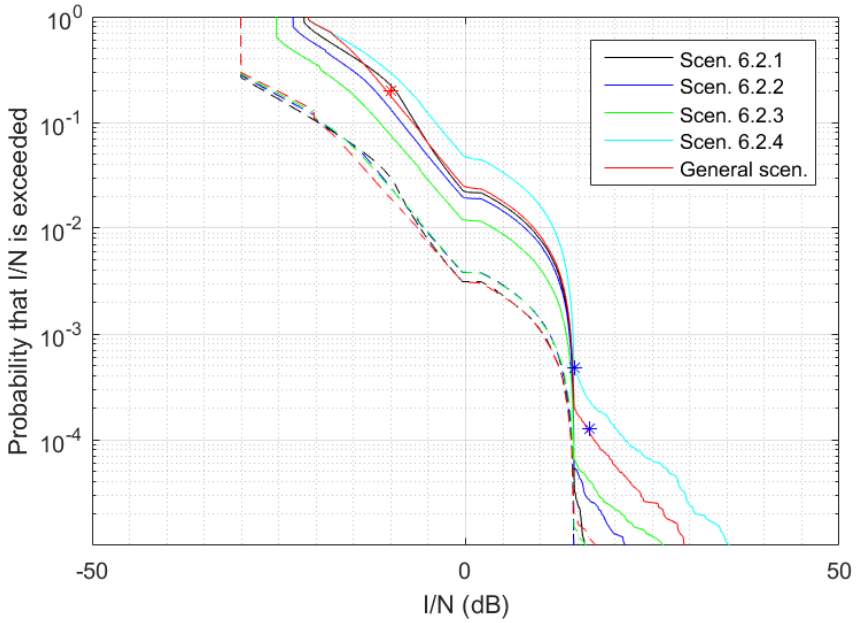

It can be concluded from these figures it can be concluded that Option 1 provides certain margin for long-term protection criteria, and it leads to exceedance of short-term protection criteria in some extreme cases for eight AM(OR)S stations. Option 2 mask gives *I*/*N* very "close" to all protection criteria and all protection criteria can be exceeded in some configurations (scenarios 6.2.1 and 6.2.4 – long-term protection criteria, scenario 6.2.4 – short-term protection criteria) for maximum number of AM(OR)S stations.

The next step to assess the pfd masks is to include propagation effects. If the AM(OR)S station will compile with some pfd mask on the surface of the Earth, then these values should be recalculated to the e.i.r.p. at the AM(OR)S station. And then the signal will propagate in real propagation

environment towards the Earth. The propagation model is from Recommendation ITU-R P.528-5 with random percentages of time.

The ECDFs of *I*/*N* at the FS station for this more realistic case are shown for Option 1 and Option 2 masks on Figs A8-28 and A8-29. The scenarios remain the same as in Figs A8-26 and A8-27, the number of AM(OR)S stations were taken as maximum values provided above (7, 5, 3, 8 and 8, respectively).

FIGURE A8-28

Empirical cumulative distribution function of *I*/*N* at the fixed station for power flux-density mask option 1 with propagation according to Rec. ITU-R P.528

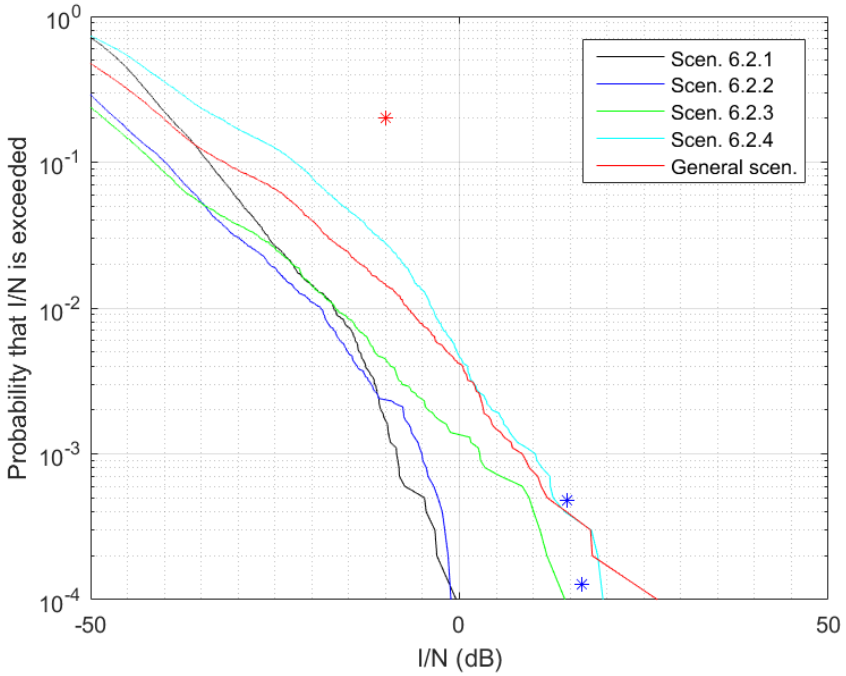

FIGURE A8-29

Empirical cumulative distribution function of *I*/*N* at the fixed station for power flux-density mask option 2 with propagation according to Rec. ITU-R P.528

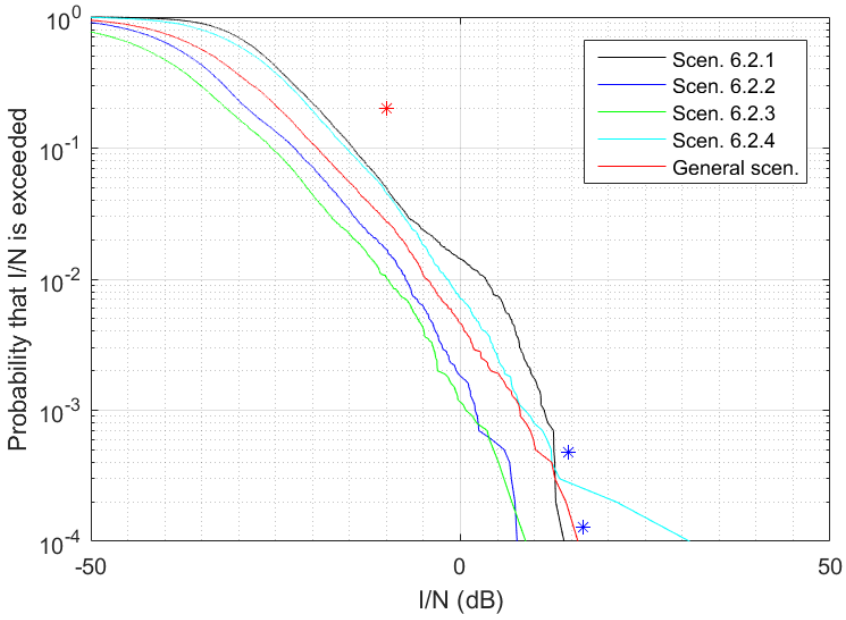

The shape of the curves has changed comparing with Figs A8-26 and A8-27, this is due to the fact that the interference level in Figs A8-26 and A8-27 was impacted only by FS antenna radiation pattern, but here different propagation effects on different elevation angles and different distances impact the results. It should also be noted that for very small percentages of time the basic transmission loss according to Recommendation ITU-R P.528-5 may give in some cases lower losses than Recommendation ITU-R P.525 – free space basic transmission loss.

According to these Figures it may be concluded that Option 1 and Option 2 masks may lead to exceedance of short-term protection criteria if several AM(OR)S stations are deployed in the visibility of FS station.

So a new pfd mask (Option 3) is proposed based on Option 1 pfd mask, it is shown on Fig. A8-30 with black dashed line:

$$PFD_{\max} = \begin{cases} 0.88 \cdot \theta - 130 & \text{for} \quad 0° \le \theta \le 8° \\ 2.86 \cdot \theta - 146 & \text{for} \quad 8° < \theta \le 15° \\ 0.87 \cdot \theta - 116 & \text{for} \quad 15° < \theta \le 30° \\ 0.067 \cdot \theta - 92 & \text{for} \quad 30° < \theta \le 90° \end{cases}$$

FIGURE A8-30

pfd masks from options 1, 2 and 3

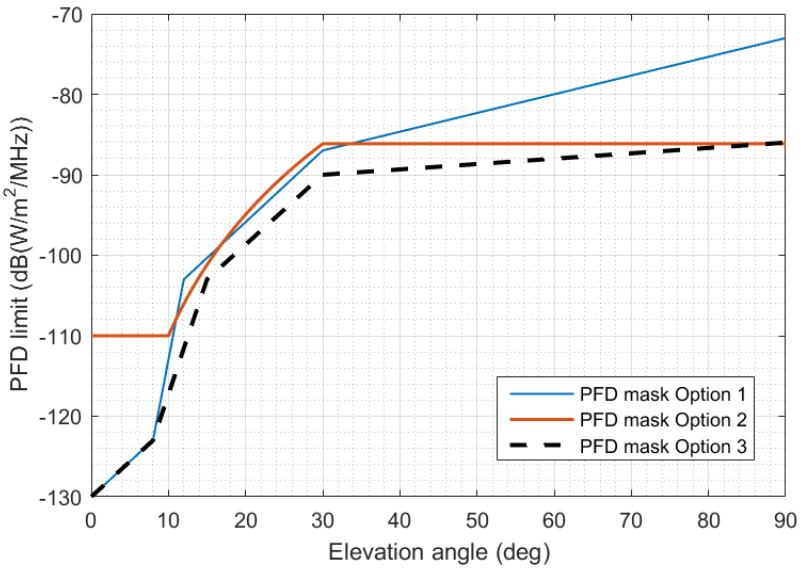

ECDF of *I*/*N* for this pfd mask is shown in Figs A8-31 and A8-32 without taking into account propagation conditions and with propagation conditions, respectively.

FIGURE A8-31

Empirical cumulative distribution function of *I*/*N* at the fixed station for pfd mask Option 3 without taking into account propagation

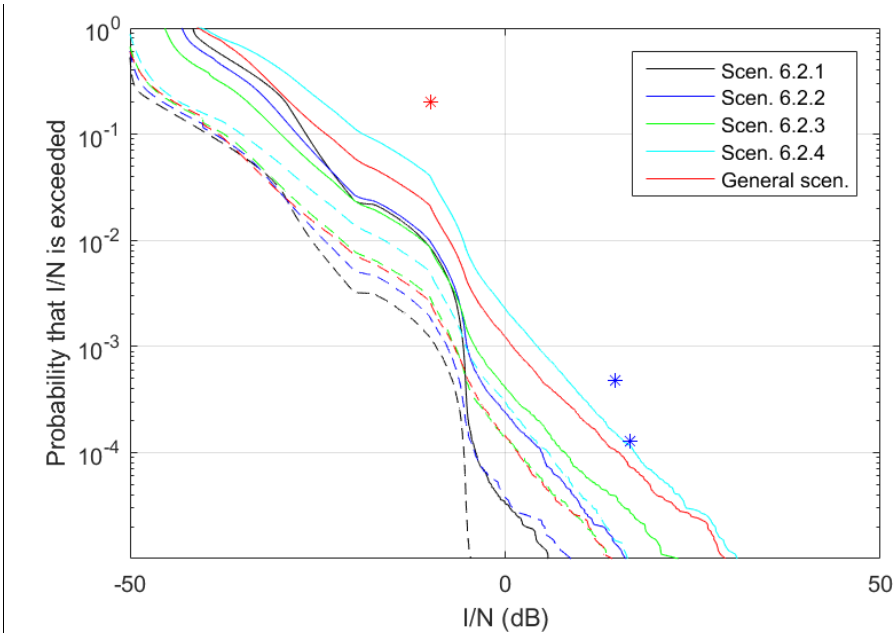

FIGURE A8-32

Empirical cumulative distribution function of *I*/*N* at the fixed station for pfd mask option 3 with propagation according to Rec. ITU-R P.528

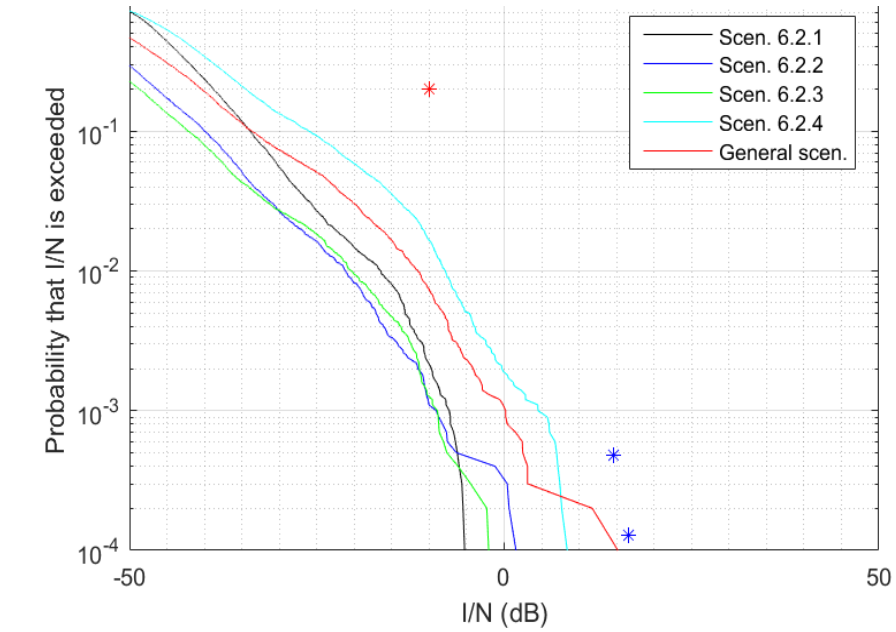

Based on Figs A8-31 and A8-32 it can be concluded that all protection criteria are met for the considered configurations of AM(OR)S stations for Option 3 mask.

Annex 9

Compatibility studies between future aeronautical mobile (off-route) systems planned to operate in 22-22.21 GHz and Earth exploration-satellite (passive) systems operating in the adjacent frequency band 22.21-22.5 GHz

TABLE OF CONTENTS

The frequency band 22.21-22.5 GHz is globally allocated to the EESS (passive) on a primary basis. This annex contains two studies that evaluate the maximum unwanted emission limits in this band of AM(OR)S stations planned to operate in the adjacent band 22-22.21 GHz.

A9.1 Study A

A9.1.1 Methodology

A9.1.1.1 Introduction

The unwanted emissions characteristics of future AM(OR)S systems planned to operate in 22-22.21 GHz are provided in Table A1-1 and graphically represented in Fig. A1-1 in Annex 1. The study takes a Monte Carlo approach whose general methodology is laid out in Annex 11 to this Report with some specificities highlighted in the following sections.

A9.1.1.2 Earth exploration-satellite service (passive) characteristics

A typical EESS (passive) space borne sensor (sensor R1) operating in the frequency band 22.21-22.31 GHz i.e. at the lower edge of the EESS (passive) band is described in Table A2-10 of this Report. It is considered representative of other sensors operating under the same allocation and will therefore be taken as a basis for this study.

According to Table A2-10, the satellite operating the sensor R1 travels on a retrograde circular orbit with 98.6° inclination and 833 km altitude AGL. The longitude of the ascending node at the beginning of the simulation has no influence on the results of the study but for definiteness, it is chosen as 0 degree. The study considers a complete revolution of the satellite around the Earth. Considering

the orbital parameters, the revolution has a duration of 101 min 25 s according to the standard Keplerian model highlighted in the equation below:

$$T_0 = \frac{\pi}{30}\sqrt{\frac{(R_e+h)^3}{\mu}} \quad \text{(A9-1)}$$

where:

T_0: duration (min) of a complete revolution around the Earth

R_e: mean radius (km) of the Earth (Re = 6 371 km)

h: altitude (km) of the satellite AGL

μ: Kepler's constant (μ = 3.986005 × km^3/s^2).

Figure A9-1 shows the successive positions of the satellite over a complete revolution in the Earth-centred Earth-fixed (ECDF) coordinate system, where the equatorial plane is (xOy) and the Earth rotation axis is (Oz). Figure A9-2 further shows the successive positions of the sub-satellite point in a projected map of the Earth.

According to the Table A2-10 in Annex 2, the sensor R1 uses a conical scanning method whose principle is explained in § 4.2 of Recommendation ITU-R RS.1861-1 and highlighted in § A2.5.1 of this Report. $(\vec{u};\vec{v};\vec{w})$ denotes the local direct orthonormed coordinate system attached to the satellite, where $\vec{u}$ is colinear to the speed vector, $\vec{v}$ is colinear to the centripetal force vector, and $\vec{w} = \vec{u} \times \vec{v}$. The relevant parameters of the scanning procedure are:

– The swath width W = 1 707 km;

– The time ρ needed for the sensor R1 to sweep from one end of the swath to the other (called beam dynamics in Table A2-10). ρ = 1.9 s.

– The off-nadir angle β = 45° i.e. the angle in the plane $(\vec{u};\vec{v})$ between the projection of the antenna boresight in this plane and the vector $\vec{v}$. This angle is constant over time.

– The angle $\alpha(t)$ in the plane $(\vec{u};\vec{w})$ between the projection of the antenna boresight in this plane and the vector $\vec{u}$. This angle varies overtime between a minimum value $-|\alpha_{max}|$ and a maximum value $+|\alpha_{max}|$. The numerical value of α_{max} is determined from the parameters h, β and W, which results in $\alpha_{max} = 60.3°$. $\alpha(t)$ is essential to model the scanning behaviour of the sensor R1 and varies according to equation (A9-2):

$$\alpha(t) = \frac{2\alpha_{max}}{\rho}\left|60t - 2\rho\left\lfloor\frac{30t}{\rho}\right\rfloor - \rho\right| - \alpha_{max} \quad \text{(A9-2)}$$

where:

t: time elapsed (min) since the beginning of the simulation

$\lfloor x \rfloor$: biggest integer number smaller than x.

Figure A9-3 shows the antenna orientation over a complete revolution of the satellite around the Earth. Note that between each position represented in this Figure, the antenna sweep several times from one end of the swath to the other. Figure A9-4 shows the points successively observed by the sensor on the surface of the Earth, and Fig. A9-5 shows these points on a projected map. The swath on the surface of the Earth is composed of the union of all the points successively observed.

The antenna pattern associated to the sensor R1 is provided in § A2.5.2 of this Report and graphically represented in Fig. A2-5 in Annex 2.

The satellite can be assumed to perform measurements over the complete surface of the Earth. However, for compatibility studies, Recommendation ITU-R RS.2017-0 prescribes to perform analysis over a 10 000 000 km^2 Mission Area of Interest (MAI). Equation (A9-3) approximates the time interval Δt needed by the satellite to cover an area A (km^2):

$$\Delta t = \frac{A \times T_0}{2\pi(R_e + h)W} \quad \text{(A9-3)}$$

where:

Δt: time (min) needed by the satellite to scan an area A

T_0: Keplerian revolution time as defined in equation (A9-1)

h: altitude (m) of the satellite AGL

W: swath width (km) of the satellite.

It results that Δt = 13 min 8 s. The choice of the 10 000 000 km² MAI has no practical influence on the results, but for definitiveness, it was chosen over Europe, between t_{start} = 10 min and $t_{end} = t_{start} + \Delta t$. Figure A9-6 shows the successive positions of the satellite between t_{start} and t_{end} as well as the points observed by the sensor R1.

FIGURE A9-1

Assumed trajectory in the coordinate system of the satellite operating the sensor R1 over a complete revolution; the time stamp (in mins) associated to each position of the satellite is read from the attached colour bar

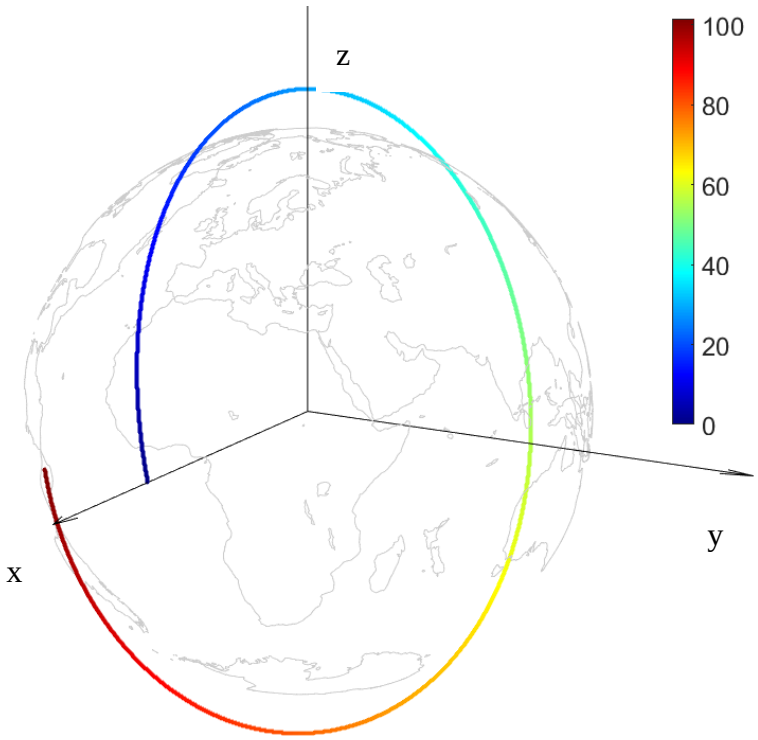

FIGURE A9-2

As in Fig. A9-1 but showing the position of the sub-satellite point in a projected map

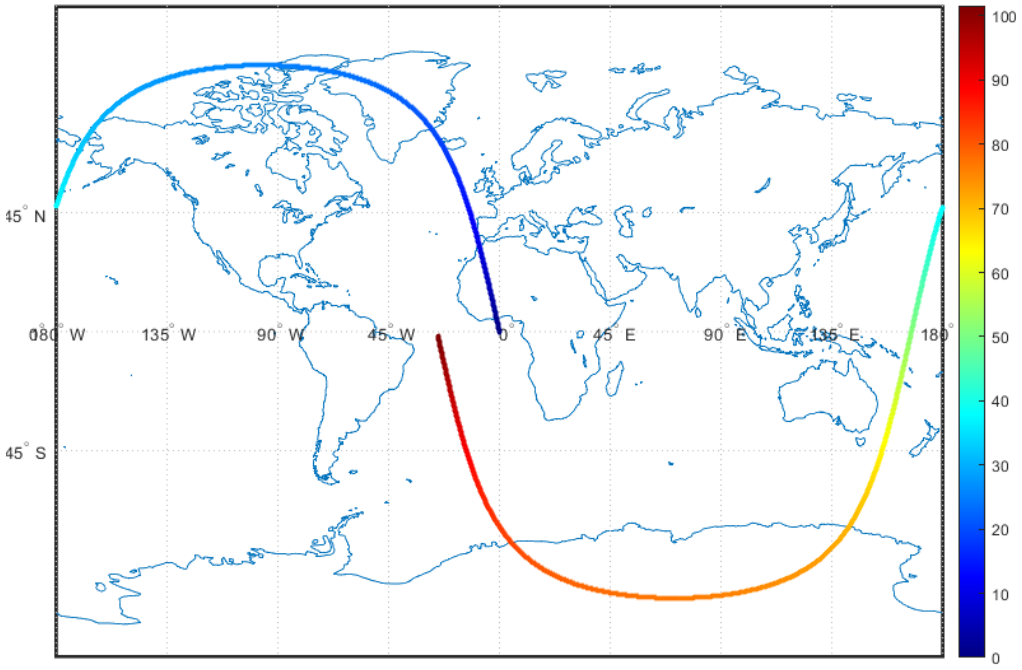

FIGURE A9-3

Successive orientation of the antenna boresight associated to the sensor R1 over a complete revolution of the satellite around the Earth

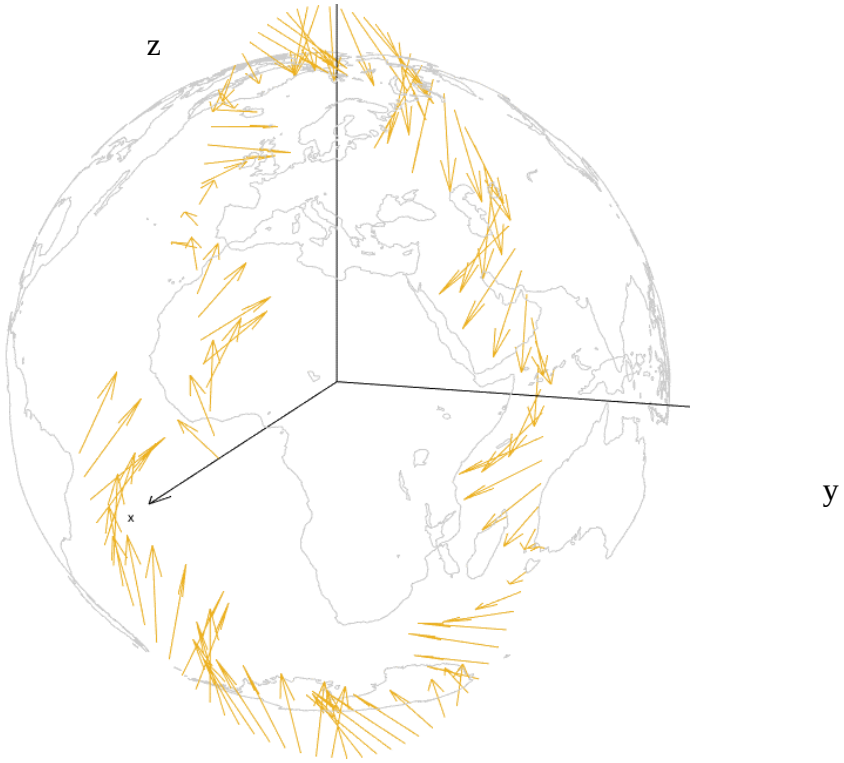

FIGURE A9-4

Successive points on the surface of the Earth observed by the sensor R1 over a complete revolution of the satellite around the Earth (the time stamp of each point in mins is indicated by the associated colourbar)

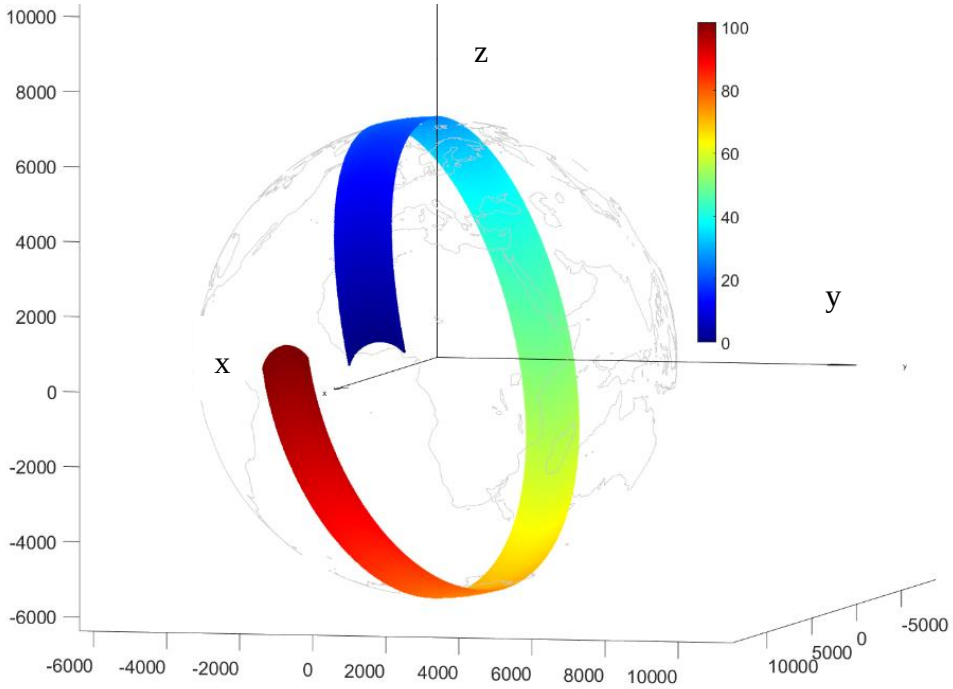

FIGURE A9-5

Successive points on the surface of the Earth observed by the sensor R1 over a complete revolution of the satellite around the Earth (the time stamp of each point in mins is indicated by the associated colourbar)

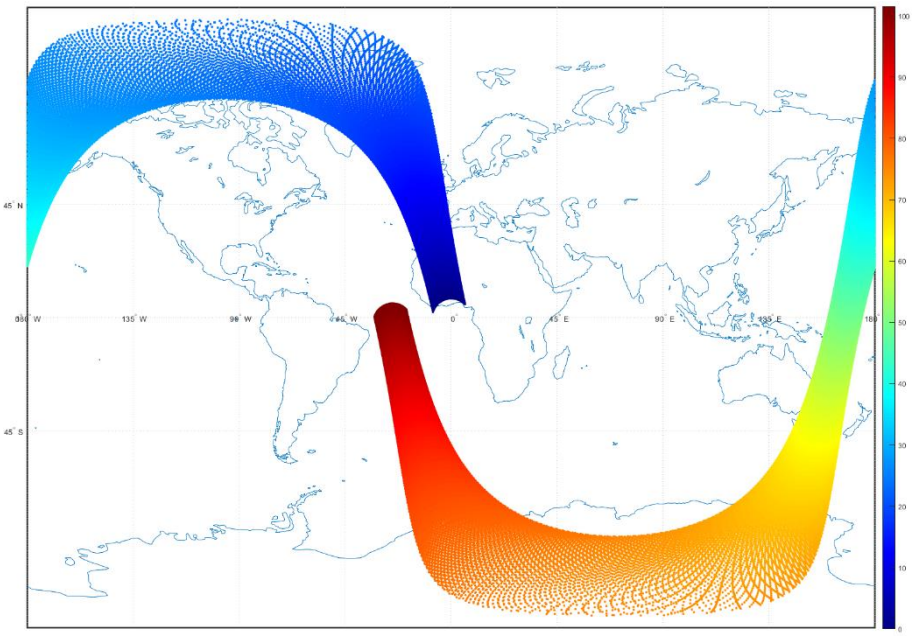

FIGURE A9-6

Successive positions of the satellite (in yellow) between t_{start} = 10 min and t_{end} = 24 min 8s, and successive points observed by the sensor R1 on the surface of the Earth (in violet)

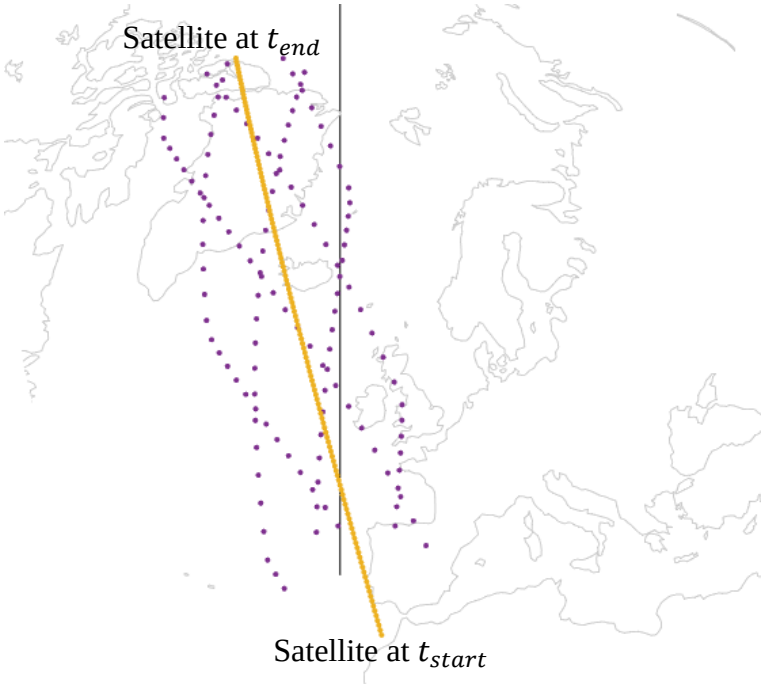

A9.1.1.3 Characteristics of the systems operating in the aeronautical mobile (off-route) service

While some other Monte Carlo sharing and compatibility studies in this Report have considered independent snapshots i.e. iterations of the simulation with new deployments of the interferer and the victim, this study has reproduced the actual cruising of aircraft over the surface of the Earth.

Also, while other studies in this Report have considered the four operational scenarios described in § 6.2, this study has taken a more generic approach by considering independent ADTs flying at a ground speed of 900 km/h with a random but constant azimuth bearing at a constant altitude of 10 km AGL (the exact altitude value having little to no influence on the results).

The initial position of the ADTs is chosen with uniform distribution within a deployment area encompassing the 10 000 000 km^2 MAI mentioned in § A1.1.2 and extending over this area so that each point in this deployment area is visible from the satellite over its trajectory from t_{start} to t_{end}. The area $A_{deployment}$ of the deployment area is based on the radio horizon distance (RHD) (see equation (A11-1) in Annex 11) and given in equation (A9-4):

$$A_{deployment} = \frac{A \times R_e}{W}\left(\cos^{-1}\left(\frac{R_e}{R_e+h}\right) + \cos^{-1}\left(\frac{R_e}{R_e+h_{ADTs}}\right)\right) \quad \text{(A9-4)}$$

where:

A : area of MAI i.e. 10_000_000_km^2

W : swath width i.e. 1 707 km

h : altitude (km) of the satellite AGL

h_{ADTs} : altitude (km) of the ADTs AGL i.e. 10 km

R_e : radius of the Earth (km) i.e. 6 371_km.

It results that $A_{deployment}$ = 20 215 751 km^2. The number of ADTs deployed in this area is chosen equal to the maximum density of clusters over the four scenarios introduced in § 6.2, i.e. one cluster in each disk of radius 254_km, which is reached in scenario 6.1 (see Table 4 in § 6.4). Therefore, the number of ADTs (denoted by N_{ADT}) is given in equation (A9-5):

$$N_{ADTs} = \frac{A_{deployment}}{\pi \times 254^2} \approx 100 \quad \text{(A9-5)}$$

Figure A9-7 shows the successive location of a number of ADTs[22] deployed around the MAI as explained above and travelling at a constant altitude of 10 km AGL, a constant ground speed of 900 km/h, and a randomized but constant azimuth bearing.

The ADTs are each equipped with one of the three airborne AM(OR)S systems characterized in Table A1-1 in Annex 1, i.e. two systems using directive antennas (systems 1 and 3), and one system using an omnidirectional antenna (system 2). The azimuthal direction of the antenna boresight is in the direction of flight, and different ranges of elevation above the local horizontal will be considered for the directive systems 1 and 3.

The ADTs are transmitting with a constant power level and a flat SEM in the same band as the sensor R1 is receiving i.e. in the band 22.21-22.31 GHz. Choosing the transmit band of ADTs in this manner (although ADTs are operating in the band 22-22.21 GHz according to Table A1-1) allows one to compute the maximum permissible unwanted emission level of ADTs in order to protect the sensor R1 operating in the band 22.21-22.31 GHz.

FIGURE_A9-7

Successive locations of a few ADTs (each ADT is assigned a colour) deployed around the MAI (i.e. the area scanned by the sensor R1 between t_{start} and t_{end}) and travelling at 900 km/h during a 101 mins revolution of the EESS satellite; the interference with the sensor R1 is considered between t_{start} and t_{end}

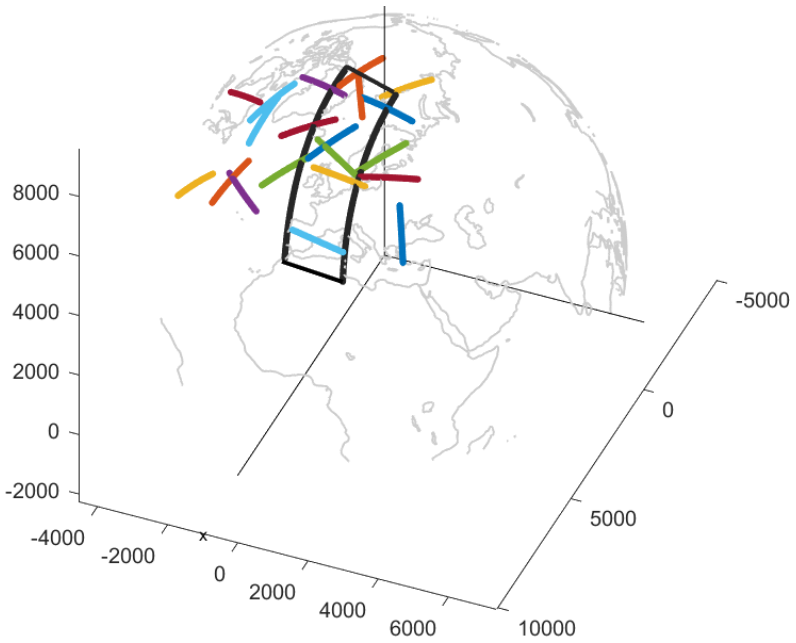

A9.1.1.4 Calculation principle

The variable S (in dB) highlighted in equation (A9-6) is calculated for all successive positions of the satellite when flying over the MAI i.e. between t_{start} and t_{end}.

$$S = 10\log_{10}\left(\sum_{k=1}^{N_{ADTs}} 10^{\frac{G_k + G'_k + L_k}{10}}\right) \quad \text{(A9-6)}$$

where:

G_k: gain (dBi) of the k-th ADT in the direction of the satellite

[22] For the sake of readability, only a subset of the 100 ADTs to deploy are shown in Fig. A9-7.

G'_k: gain (dBi) of the sensor R1 in the direction of the *k*-th ADT

L_k: PL (dB) between the satellite and the *k*-th ADT.

The complete satellite revolution around the Earth is divided in 10 000 sample points that are evenly spread in time[23]. Therefore, the flight over the MAI is bounded by the 990-th and the 2 290-th sample points[24] and 1 301 values of the variable S can be generated during each revolution of the satellite. In order to achieve statistical significance, the simulation is repeated 50 times, so that 50 sets of aggregate interference values at the sensor R1 are generated, each containing 1 301 samples. The value of the variable S during the r-th simulated revolution ($1 \leq r \leq 50$) at the j-th sample point ($990 \leq j \leq 2\,290$) is computed according to equation (A9-7):

$$S_{r,j} = 10\log_{10}\left(\sum_{k=1}^{N_{ADTs}} 10^{\frac{(G_k)_{r,j}+(G'_k)_{r,j}+(L_k)_{r,j}}{10}}\right)_{\substack{1\leq r\leq 50 \\ 990\leq j\leq 2290}} \quad \text{(A9-7)}$$

where:

$(G_k)_{r,j}$: gain (dBi) of the *k*-th ADT in the direction of the satellite at the *j*-th sample point during the *r*-th revolution

$(G'_k)_{r,j}$: gain (dBi) of the sensor R1 in the direction of the *k*-th ADT at the *j*-th sample point during the *r*-th revolution

$(L_k)_{r,j}$: PL (dB) between the satellite and the *k*-th ADT at the *j*-th sample point during the *r*-th revolution.

Therefore, the complete set $\{S_{r,j}\}_{\substack{1\leq r\leq 50 \\ 990\leq j\leq 2290}}$ is composed of 65 050 values that are computed according to equation (A9-7) for each airborne AM(OR)S system and each range of elevation angle. Note that the choice of the system and the elevation solely impacts the variable G in equation (A9-6). The ECDF of this variable S is then drawn and the 999-th 1 000-ile (denoted by S_{999}) is extracted from these plots. For instance, Fig. A9-8 shows the ECDF of the variable S for different ranges of elevation angles when the airborne AM(OR)S system 1 is used. The value of S_{999} can be read from the x-value of the points A, B and C in this Figure (i.e. −153 dB, −172 dB and −174 dB, respectively). In the same manner, S_{999} can be computed for the two other systems which results in the values provided in Table A9-1. Note that this table only contains three ranges of elevation values, but the final results in § A9.1.2 include the full range from −90° to +90° above the local horizontal.

[23] The assumed trajectory of the satellite being circular, these sample points are also evenly spread on a circular orbit.

[24] Considering the respective values of T_0 (see equation (A9-1)), t_{start} and t_{end} (see § A9.1.1.2).

FIGURE A9-8

Aeronautical mobile (off-route) system 1

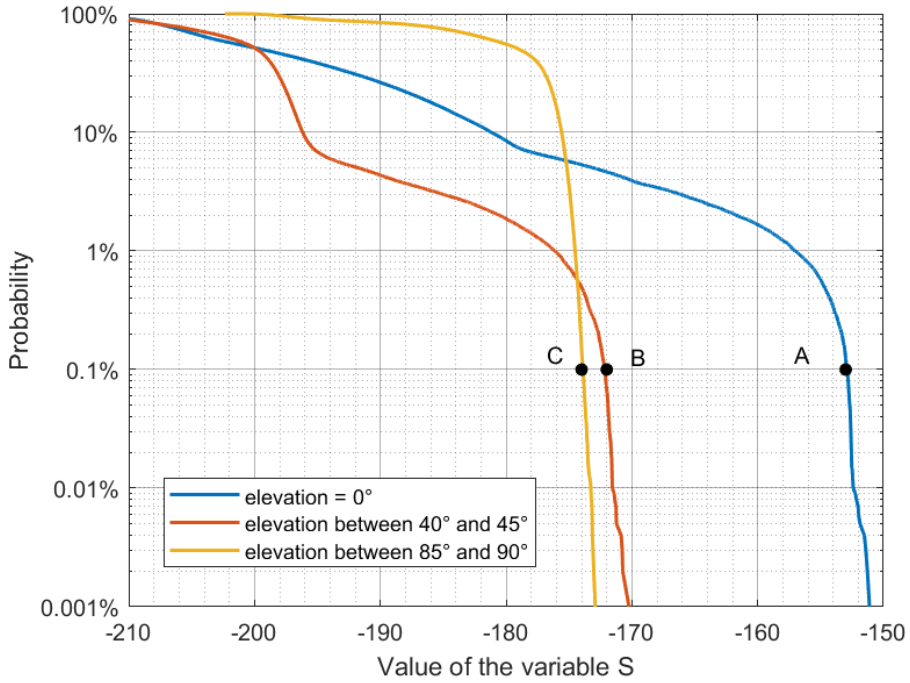

TABLE A9-1

999th 1 000-ile of the variable *S* in dB for different airborne aeronautical mobile (off-route) systems and different ranges of elevation angles above the local horizontal

	Airborne AM(OR)S system		
	1	**2**	**3**
0° elevation	−153	−148	−141
Between 40° and 45°	−172		−170
Between 85° and 90°	−174		−171

The maximum power level of the ADTs (which equals the maximum power level of unwanted emissions in the band 22.21-22.31 GHz for ADTs operating in the adjacent band 22-22.21 GHz) can therefore be computed from equation (A9-8):

$$(P_{ADTs})_{max} = I_{max} - S_{999} - 30 \text{ dB} \quad \text{(A9-8)}$$

where:

$(P_{ADTs})_{max}$: maximum power level in dB(W/100 MHz) of unwanted emissions in the band 22.21-22.31 GHz for ADTs operating in the adjacent band 22-22.21 GHz

I_{max}: interference threshold in dB(W/100 MHz) of the sensor R1. According to § A2.5.3, I_{max} = −139 dB(W/100 MHz)

S_{999}: value in dB computed further above.

As an example, and taking the values of S_{999} provided in Table A9-1, equation (A9-8) yields the values given in Table A9-2.

TABLE A9-2

Maximum power level of unwanted emissions in the frequency band 22.21-22.31 GHz for ADTs operating in the adjacent frequency band 22-22.21 GHz

	Airborne AM(OR)S system		
	1	**2**	**3**
0° elevation	−16	–21	−28
Between 40° and 45°	+3		+1
Between 85° and 90°	+5		+2

A9.1.2 Results

Following the methodology highlighted in § A9.1.1, the results shown in Fig. A9-8 are obtained for the three airborne AM(OR)S systems over the complete range of elevation angles from −90° to +90°. For the system 2, which uses an omnidirectional antenna, the limit is −21 dB(W/100 MHz) independently of the elevation angle. For the systems 1 and 3, which use a directive antenna, the most stringent limit is obtained when the stations are transmitting towards the horizon. This limit is −16 dB(W/100 MHz) and −28 dB(W/100 MHz) for system 1 and system 3, respectively. The OOB limit is relaxed when the elevation angle is increased, as the offset angle relative to the ADTs' boresight in the direction of the sensor R1 increases on average. It should also be noted that the limits for systems 1 and 3 highlighted in Fig. A9-9 are not symmetrical for positive and negative elevation angles.

In order to make results independent of the specific AM(OR)S system under study, the envelope in equation (A9-9) is proposed to limit unwanted emission of directive AM(OR)S systems (i.e. systems 1 and 3) in the frequency band 22.21-22.31 GHz. This generic limit is shown in Fig. A9-8.

$$P_{max}(\theta) = \begin{cases} -28 & \text{if } |\theta| \leq 1° \\ -28\left(1 - \dfrac{\log_{10}(|\theta|)}{\log_{10}(45)}\right) & \text{if } 1° \leq |\theta| \leq 45° \\ 0 & \text{if } |\theta| \geq 45° \end{cases} \quad \text{(A9-9)}$$

where:

θ: elevation angle (degree) above the local horizontal (positive values above the horizon)

P_{max}: maximum permissible unwanted emissions dB(W/100 MHz) in the frequency band 22.21-22.31 GHz of directive AM(OR)S systems operating in the frequency band 22-22.21 GHz.

FIGURE A9-9

Permissible unwanted emissions in the frequency range 22.21-22.31 GHz from airborne aeronautical mobile (off-route) stations operating in the adjacent frequency band 22-22.21 GHz. The power level is measured at the antenna connector of the aeronautical mobile (off-route) system

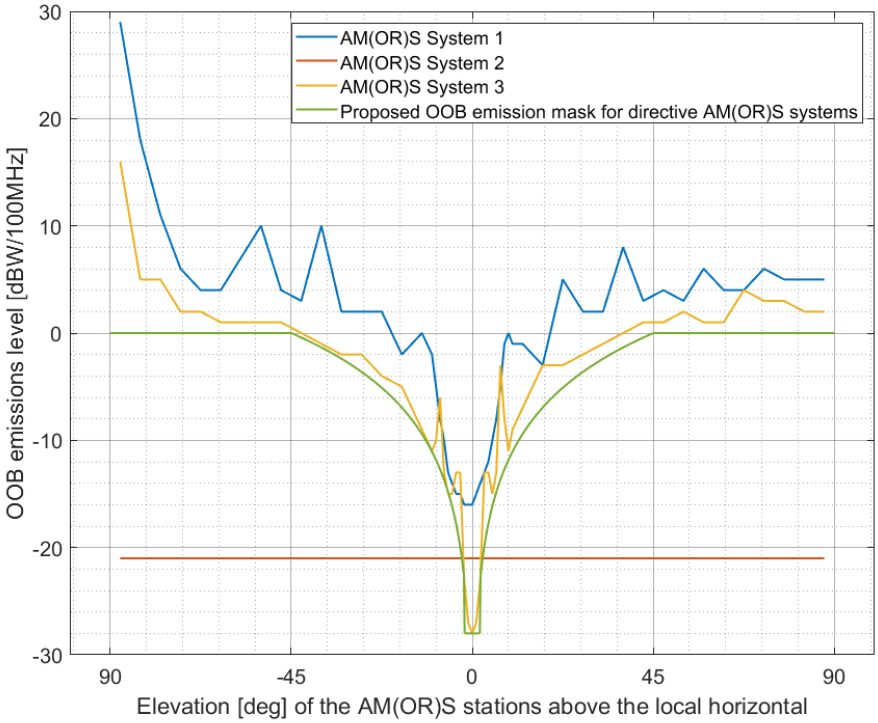

Figures A9-10 to A9-13 show the unwanted emission level of AM(OR)S channels in the band 22.21-22.31 GHz for a 10 MHz, 50 MHz, 100 MHz and 200 MHz channel, as a function of the guard band with the lower edge at 22.21 GHz. These Figures are obtained by integrating the SEM provided in Table A1-1 over the band 22.21-22.31 GHz.

FIGURE A9-10

Unwanted emissions (measured at the antenna connector) in the frequency band 22.21-22.31 GHz as a function of the transmit output power and the guard band between the upper edge of the channel of the aeronautical mobile (off-route) service and the lower edge of the passive frequency band 22.21-22. GHz, for a 10 MHz channel

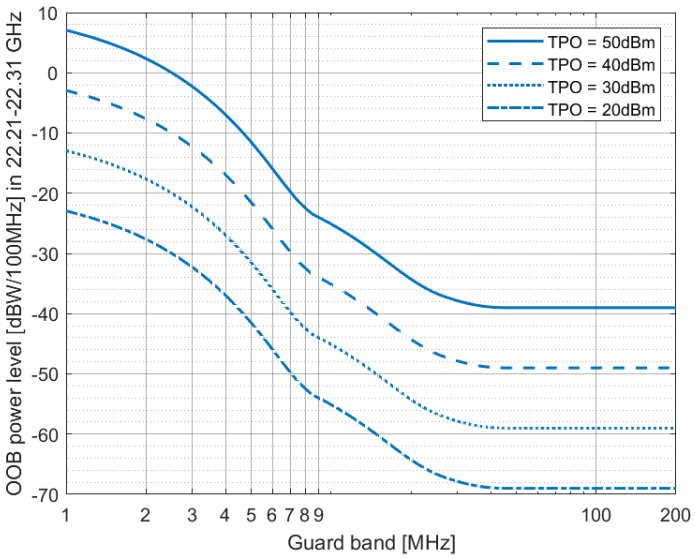

FIGURE A9-11

As in Fig. A9-10, using a 50 MHz channel

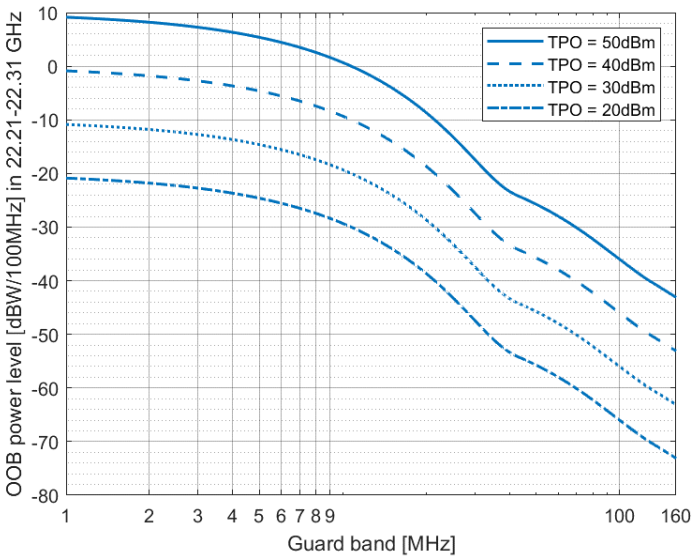

FIGURE A9-12

As in Fig. A9-10, using a 100 MHz channel

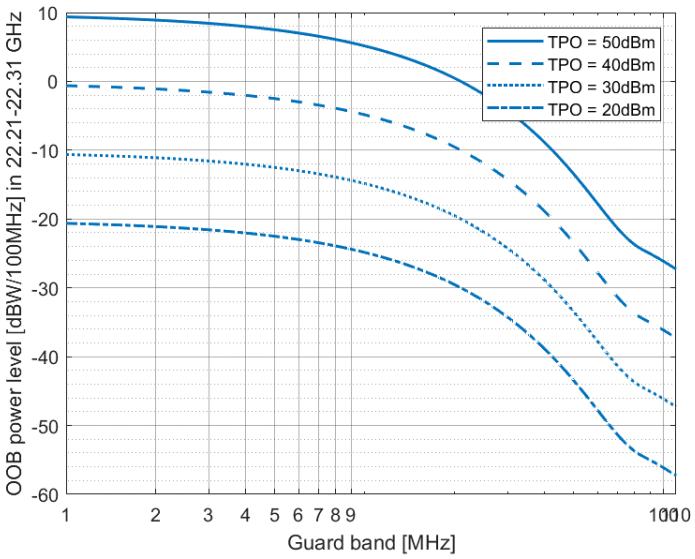

FIGURE A9-13

As in Fig. A9-10, using a 200 MHz channel

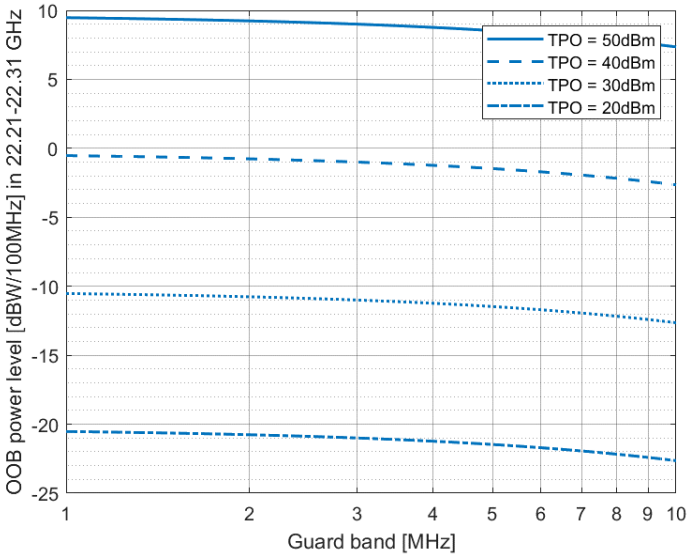

Figures A9-10 to A9-13 can be compared against Fig. A9-9 to determine the necessary guard band. Some exemplary results are shown in Tables A9-2 and A9-3. In these Tables, N/A indicates that the unwanted emissions limit cannot be achieved due to the constraint *BW + Guard Band ≤ 210 MHz*.

TABLE A9-3

Necessary guard band (MHz) for directive aeronautical mobile (off-route) systems operating in 22-22.21 GHz to comply with the limit laid out in equation (A9-2)

AM(OR)S TPO	AM(OR)S channel BW	0°	5°	45°
50 dBm	10 MHz	12.7	6.07	2.50
	100 MHz	N/A	56.3	20.9
	200 MHz			41.3
40 dBm	10 MHz	6.52	3.83	0.376
	100 MHz	60.7	34.2	0
	200 MHz	N/A		
30 dBm	10 MHz	4.22	1.70	
	100 MHz	38.0	12.9	
	200 MHz	N/A		
20 dBm	10 MHz	2.08	0	
	100 MHz	16.7		
	200 MHz	N/A		

TABLE A9-4

As in Table A9-3, for omnidirectional aeronautical mobile (off-route) systems

AM(OR)S TPO	AM(OR)S channel BW	
25 dBm	10 MHz	1.65
	100 MHz	12.4
	200 MHz	24.3
20 dBm	10 MHz	0.591
	100 MHz	1.79
	200 MHz	3.01
10 dBm	10 MHz	0
	100 MHz	
	200 MHz	
0 dBm	10 MHz	
	100 MHz	
	200 MHz	

As seen in Table A9-2, the constraint *BW + Guard Band ≤ 210 MHz* limits the operational range of directive AM(OR)S systems operating in 22-22.21 GHz. For example, using 100 MHz BW and 50 dBm TPO is not practically achievable if transmissions are near the horizon i.e. with 0° elevation above the local horizontal. Figure A9-14 therefore shows the permissible operational points of

AM(OR)S systems operating in 22-22.21 GHz and transmitting towards the horizon. The omnidirectional system 2 is not constrained as the full range of power levels and BW is available. On the contrary, the directive systems 1 and 3 cannot access all their theoretical operational range.

FIGURE A9-14

Permissible operational range of (power, bandwidth) for airborne aeronautical mobile (off-route) systems operating in the frequency band 22-22.21 GHz and transmitting with 0° elevation above the local horizontal. (system 1 in blue, system 2 in red, system 3 in yellow)

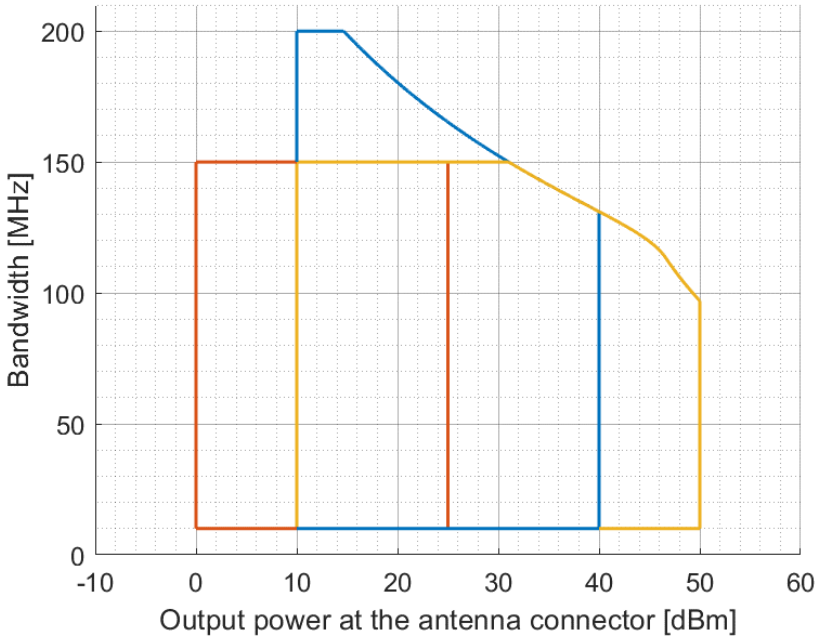

A9.1.3 Summary

Study A is a Monte Carlo analysis that assessed the impact of airborne AM(OR)S stations operating in the band 22-22.21 GHz onto the space-borne EESS (passive) sensor R1 introduced in § A2.5.1 of this Report and operating in the adjacent band 22.21-22.5 GHz. The effective trajectory of the spacecraft around the Earth was simulated according to the orbital parameters introduced in Table A2-10. The scanning behaviour of the sensor was also considered according to the information available in Table A2-10. The trajectory of AM(OR)S stations within the MAI was computed according to a random but constant azimuth bearing, a constant altitude of 10 000 m AGL and a constant ground speed of 900 km/h. A typical deployment density of 50 WBLOSDLs inside the 10 000 000 km^2 was assumed throughout the study.

The study has determined that the maximum power level of unwanted emissions in 22.21-22.31 GHz for AM(OR)S stations operating in the MAI and in the adjacent frequency band 22-22.21 GHz is −21 dB(W/100 MHz) for omnidirectional systems, and according to equation (A9-10) for directive AM(OR)S systems:

$$P_{max}(\theta) = \begin{cases} -28 & \text{if } |\theta| \leq 1° \\ -28\left(1 - \dfrac{log_{10}(|\theta|)}{log_{10}(45)}\right) & \text{if } 1° \leq |\theta| \leq 45° \\ 0 & \text{if } |\theta| \geq 45° \end{cases} \quad \text{(A9-10)}$$

where:

θ: elevation angle (deg) above the local horizontal (positive values above the horizon)

P_{max}: maximum permissible unwanted emissions dB(W/100 MHz) in the frequency band 22.21-22.31 GHz of directive AM(OR)S systems operating in the frequency band 22-22.21 GHz.

Complying with these limits may require the introduction of a guard band between the AM(OR)S channels and the lower edge of the passive band 22.21-22.5 GHz, depending of the necessary BW and the TPO of AM(OR)S stations.

A9.2 Study B

The objective of this study is to determine the maximum allowable density of WBLOSDLs operating in a particular region of the Earth to protect the EESS (passive) R1 sensor characterized in § A2.5 of this Report. In addition, it may be necessary to limit in some specific situations, the unwanted emissions in the adjacent band 22.21-22.5 GHz of AM(OR)S stations. The aggregate interference from non-safety AM(OR)S systems into the R1 sensor is analysed by a Monte Carlo dynamic simulation.

A9.2.1 Calculation of aggregate interference

During the simulation, only a subset of all the collected sample points are relevant to analyse interference effects from AM(OR)S sources. A sample is considered relevant when the R1 sensor points its antenna towards the MAI and makes measurements from within the MAI. The complete set of time steps contains $N_{samples}$ = 687 549 points[25] and is denoted by $\{t_j\}_{1 \le j \le 687\,549}$. The number of relevant time steps $N_{relevant}$ is given in equation (A9-11):

$$N_{relevant} = \frac{N_{samples} \times A}{4\pi \times R_e^2} \quad \text{(A9-11)}$$

where:

A: area of the MAI i.e. 10 000 000 km^2

R_e: radius of the Earth i.e. 6 371 km

Equation (A9-4) yields $N_{relevant}$ = 13 480 samples.

At each relevant time step, the simulation computes the directional vectors from each AM(OR)S source within the MAI to the spacecraft and then computes the gain of the transmit and receive antennas using their respective antenna patterns.

The interfering signal power level, $I_{i,n}$ (W), received by a spaceborne radiometer at the n^{th} time step from the i^{th} active transmitter is calculated from:

$$I_{i,n} = \frac{P_{TX\,i,n} G_{TX\,i,n}\, G_{RX\,i,n}}{L_{a\,i,n}\, L_{FSPL\,i,n}\, L_{pol\,i,n}} \quad \text{(A9-12)}$$

where:

$P_{TX\,i,n}$: i^{th} AM(OR)S source transmitter power (W) in the EESS (passive) band, adjusted for power control as described in § A11.6.1

$G_{TX\,i,n}$: i^{th} AM(OR)S source antenna gain towards spaceborne sensor

$G_{RX\,i,n}$: spaceborne receive antenna gain towards i^{th} AM(OR)S source

$L_{a\,i,n}$: attenuation due to atmospheric absorption between i^{th} AM(OR)S source and space borne sensor

25 $\frac{25\ days \times 24\ hours \times 3{,}600\ seconds}{1 \times \pi\ seconds}$

$L_{FSPL\ i,n}$: FSPL between i^{th} AM(OR)S source and space borne sensor

$L_{pol\ i,n}$: losses (dB) due to polarization mismatch between i^{th} AM(OR)S source and spaceborne sensor.

The aggregate interference at the n[th] timestep, $AggI_n$ (W), is calculated by the summation of the received interference from active AM(OR)S stations within line of sight of EESS (passive):

$$AggI_n = \sum_i I_{i,n} = \sum_i \frac{P_{TX\ i,n}\ G_{TX\ i,n}\ G_{RX\ i,n}}{L_{a\ i,n}\ L_{FSPL\ i,n}\ L_{pol\ i,n}} \quad \text{(A9-13)}$$

Thus, the aggregate interference can be represented in the logarithmic domain as:

$$AggI_{n|\text{dB}} = \left(\sum_i \frac{P_{TX\ i,n}\ G_{TX\ i,n}\ G_{RX\ i,n}}{L_{a\ i,n}\ L_{FSPL\ i,n}\ L_{pol\ i,n}}\right)_{|\text{dB}} \quad \text{(A9-14)}$$

Based on time series values for the interfering signal power level, a CCDF curve will be generated in order to assess if the result exceeds the recommended performance and interference criteria that are defined in Recommendation ITU-R RS.2017-0. The criteria will be used as a metric to assess the impact that the non–safety AM(OR)S allocation would have on the EESS (passive) systems operating in the 22.21-22.5 GHz band. From Recommendation ITU-R RS.2017-0, outlined in § A4.4.3 of this Report, the following is prescribed for the frequency range 22.21-22.5 GHz:

– reference bandwidth: 100 MHz;

– maximum interference level: −169 dBW;

– percentage of area or time permissible interference level may be exceeded: 0.1%;

– the area analyzed should be 10 000 000 km^2.

The selection of the simulation area will be chosen to reflect the operational area of sensors operating in the 22.21-22.5 GHz band.

Determination of OOB limit

The methodology is applied for each scenario described in § 6.2 and taking into account the calculation scheme previously described in this section but also including out-of-band attenuation characteristics from § A1.1:

1) Determine the simultaneous apparent value of antenna gain coupling between one EESS (passive) system and one AM(OR)S system at 0.1% of occurrence. This value is subsequently the sum of antenna gains between a pair of active systems (EESS + AM(OR)S for a given unitary event as simulated according to § A9.2.3. This value is denoted parameter α.

2) Determine the value of RF propagation loss according to § 8.2 between one EESS (passive) system and one AM(OR)S system at 0.1% of occurrence. Again as in 1), this value is taken from the simulation statistics between paired systems. This value is denoted parameter β.

3) Determine the maximum number of AM(OR)S systems that can operate under the simulation parameters described in § A9.2.3 under the condition of not exceeding the protection limit −169 dB(W/100 MHz) at 0.1%. This value is denoted parameter γ.

4) The out-of-band limit for a single AM(O)RS system under a given scenario is computed as

$$OOBL\ \text{dB(W/100 MHz)} = -169\ \text{dB(W/100 MHz)} - \alpha - \beta + \gamma \quad \text{(A9-15)}$$

A9.2.2 Simulation parameters for aeronautical mobile (off-route) systems

The AM(OR)S OOB emissions inside the target range 22.21-22.31 GHz was calculated from Fig. A1-1 in Annex 1.

AM(OR)S system selection as well as operational altitude, and horizontal link distances for each scenario are selected from guidance by Table 3 as well as antenna characteristics via Table A1-2.

The 22.21-22.5 GHz EESS (passive) analysis of this study will focus on current available representative characteristics of AM(OR)S systems within this frequency range. If the deployment densities are significantly different from the values referenced in § 6.4 of this Report, the simulation will need an update to verify co-existence potential. The calculation methodology from § A9.1.1 is inherited for consideration of aggregated emission reception.

The simulation consists in deploying a number of AM(OR)S clusters within the MAIs introduced in § A9.2.1.1 and to analyse the potential impact onto the operation of the R1 sensor collecting data from these MAIs. According to the definition in § 6.2 of this Report, a cluster denotes a group of AM(OR)S stations operating together in a particular scenario. More specifically, the four scenarios introduced in § 6.2 are considered separately. In a given scenario, the selection of the AM(OR)S system, the operational altitude of the ADTs, and the horizontal link distances are selected from the Table 3 in § 6.3. Also note that AM(OR)S clusters are deployed in a region extending by 1 degree in each direction beyond the boundaries of the MAIs. This is to take into account AM(OR)S sources that could contribute to the aggregate interference received by the R1 sensor while being outside of the MAI.

Table A9-5 shows the deployment of AM(OR)S stations within the MAIs and the associated densities. Figures A9-20 and A9-21 show an exemplary deployment of the AM(OR)S stations in the configuration n°1 (corresponding to the operational scenario 6.2.1).

TABLE A9-5

Deployment of the aeronautical mobile (off-route) systems clusters inside mission areas of interest

	AM(OR)S configuration			
	1	**2**	**3**	**4**
Reference scenario in § 6.2	6.2.1	6.2.2	6.2.3	6.2.4
Deployment of the clusters				
MAI(s) (see Figs A9-16 and A9-17) where the clusters are deployed	MAI n°1			MAI n°1 and 2
Number of AM(OR)S clusters deployed within the MAI (1)	Variable between 2 and 32	Variable between 2 and 128	Variable between 2 and 32	Variable between 2 and 16 in MAI n°1, and between 4 and 128 in MAI n°2

TABLE A9-5 (*end*)

	AM(OR)S configuration			
	1	**2**	**3**	**4**
Movement of the clusters over the simulation time	Not moving	The centre of the clusters moves according to a random walk [2]	Not moving	According to navigational routes in Fig. A9-22 for the MAI n°1 and Figs A9-23 and A9-24 for the MAI n°2 [3]
Ground speed of the ADTs [4]		400 km/h		900 km/h
Deployment of the ADTs and GDTs inside a cluster				
Number of ADTs and GDTs in each cluster and establishment of links	See § 6.2.1	See § 6.2.3	See § 6.2.4	See § 6.2.5
Links BW [6]	50 MHz	30 MHz	10 MHz or 20 MHz [5]	80 MHz
Channel allocation	In a particular scenario, only the part of the operating range 22–22.21 GHz composed of the two channels closest to the lower band edge of the R1 sensor operating range (22.21 GHz) are considered [7].			

[1] The deployment densities of clusters are extrapolated beyond the values computed in § 6.4 in order to assess the sensitivity of the interference predictions based on the deployment density assumptions. It is also remarked that deployment densities can vary by geographic regions, and it is useful to capture the results of a sensitivity analysis to reduce the need to re-run simulations and instead support extrapolation to different areas of the Earth. A single experimental simulation is performed for each density deployment and the repetition of the run may serve to establish bounds of uncertainty in a subsequent iteration of this study.

[2] The random walk algorithm applied in this scenario is assumed to adequately approximate the flight trajectories for the purposes of this study.

[3] A list of commercial air-routes is used to serve as the navigational reference basis for the movement of the clusters. This data set is freely available in public domain.

[4] See Table 3.

[5] 10 MHz for the links between the observation aircraft and the relay, and 20 MHz for the links between the relay and the observation aircraft. The links between the relay and the control centre is left out of consideration.

[6] The simulation performed in this Study B extrapolates the spectrum occupancy of the scenarios beyond what is described in § 6.5 of this Report. For instance, according to the Table 7 in § 6.5, in the scenario 6.2.1, the ADTs establish 55 MHz WBLOSDL with the GDT, but the GDT only establishes 500 kHz links with each of these ADTs. However, this simulation considers both directions with equal bandwidth 50 MHz (although not operating at the same time). In other terms, the simulation considered G2A WBLOSDL in scenario 6.2.1, whereas no such links have been considered relevant in the analysis of the scenario. This is also true for the three other scenarios 6.2.2, 6.2.3 and 6.2.4.

[7] The purpose of the study is to assess the impact on the R1 sensor of unwanted AM(OR)S emissions falling inside the passive band 22.21-22.5 GHz. Therefore, only the two closest channels from the passive band edge at 22.21 GHz are allocated to the AM(OR)S stations as the subsequent channels have significantly less impact. For instance, in scenario 6.2.1, the FDR of the first 50 MHz channel just under the band edge 22.21 GHz is −10.3 dB. The FDR of the second channel is −45.8 dB and the FDR of the third channel is −56 dB.

A9.2.3 Simulation parameters of Earth exploration-satellite service (passive)

The operational altitude of the EESS (passive) R1 sensor and antenna pattern are described in § A2.5 and are 833 km and Recommendation ITU-R RS.1813-1 respectively.

The analysis band for this study is 22.21-22.31 GHz centered at 22.26 GHz. An AM(OR)S emission center frequency of 22 160 MHz, 50 MHz from the band edge, with a 100 MHz bandwidth was chosen to be in line with the EESS (passive) protection criteria of −169 dB(W/100 MHz). Subsequent channels incorporate a 50 MHz offset further away from the band edge to accommodate channel assignment specific to AM(OR)S scenarios. Analysis was done along the band edge to determine the level of unwanted emissions into the EESS (passive) band. Table A9-6 elow gives the rest simulation parameters that were assumed for this simulation.

TABLE A9-6

General simulation parameters

Parameter	Units	Value
Simulation frequency	MHz	22 160
Duration	days	30
Time step	sec.	0.5 × π
Atmospheric losses	–	P.676-13
RF prop. models Air-space Ground-space		Rec. ITU-R P.1409-2 Rec. ITU-R P.619-5
Polarization losses	dB	3 (C-V)
FDR		10.3 (C1), 47.0 (C2)

The simulation was run for a 25-day duration with a 1 × π second time step to collect an appropriate amount of sample points to achieve statistical significance of results. Atmospheric losses (L_a) were calculated using Recommendation ITU-R P.676-12. According to guidance from WPs 3K and 3M liaison statement the preferred propagation model for ground-space interference computations is Recommendation ITU-R P.619-5 and the preferred propagation model for ground-air interference computations is Recommendation ITU-R P.1409-2. These were implemented to produce propagation losses noting that Recommendation ITU-R P.619-5 and Recommendation ITU-R P.1409-2 internally account for atmospheric losses attributed to use of Recommendation ITU-R P.676. The irrational time step of 1 × π was chosen to create a random non-uniform distribution of the EESS (passive) locations and azimuth pointing angles during satellite orbit within the simulation run time.

The RF and general parameters of the AM(OR)S system under simulation were derived from system 1 of Table A1-1 in § A1.1. In the absence of an explicit deployment, a generic one was considered and provisionally proposed to be representative. Two configurations were constructed which aim to approximate the description of "Wildfire Detection" found in § 6.2.1, "Search and Rescue" found in § 6.2.2, "Borer Surveillance Mission" found in § 6.2.3, and "Data Networks" found in § 6.2.4.

Note that for the following four configuration scenarios the operational parameters were adapted from § 6.3 "Technical setup of the scenarios". For instance, geometric spacing and relative location are adapted from Table 3. Additional technical parameters implemented (which may not be explicitly stated in § 6) in order to illustrate interaction with the EESS (passive) system are taken into account individually in the following descriptions.

For the first configuration (operational scenario 6.2.1, Wildfire observation), a density of randomly deployed ground central locations was placed in a ground centred 10 million km^2 EESS passive mission area of interest (MAI) centred at 52° W, 140° D, with associated ground stations taken in ratio 2 to 1 ground to air stations. See Figs A9-1 and A9-2, with associated ground stations taken in ratio 2 to 1 ground to air stations. Communication between air and ground station enforced a pointing arrangement consistent with § 6.2.1 were based on shortest distance to ground receiver. Channel assignment was allocated on a sequential basis in accordance with § 6.5 "Spectrum occupancy" Table 7. A single experimental simulation was performed for each transmitter density deployment and the repetition of the run may serve to establish bounds of uncertainty in a subsequent iteration of this study. The aim of this analysis was to determine what density of systems could operate a downlink main beam within the MAI without imposing harmful interference to the EESS (passive) service.

The second configuration (scenario 6.2.2, Search and Rescue), a density of randomly deployed clusters was placed in a ground centred 10 million km^2 EESS passive mission area of interest (MAI) centred at 68° W, 0° N. Each cluster was defined by seven coordinated aeronautical users operating bi-directional air-air links within the specially defined region. In this scenario, altitude is varied nominally, and average relative spacing between craft remains roughly constant with cluster centre and individual craft performing exploration similar to behaviour of a random walk (for purposes here adequately approximate expected flight trajectories).

The third configuration (scenario 6.2.3, Border Surveillance Mission), a density of randomly deployed clusters was placed in a ground centred 10 million km^2 EESS passive mission area of interest (MAI) centred at 68° W, 0° N. Each cluster was defined by two coordinated aeronautical observation users operating in relay (air-air bidirectional links) with an additional aircraft which communicates (return link) with a single ground station located within the specially defined region.

For the fourth configuration (operational scenario 6.2.4, Data Networks), a list of commercial air-routes was used to serve as the navigational reference basis for AM(OR)S device air platform station emissions. The density of flight paths is taken to be representative of the route traffic given by the dataset. Air-air transmissions consistent with the description in § 6.2.4 were established which enforced a pointing arrangement based on shortest distance to air-based receiver. Channel assignment was allocated on a sequential basis in accordance with § 6.5. Transmissions are assumed to be continual during nominal flight, and pointing assignment (pair-assignment) is on the basis of nearest neighbour. Operational altitude of a cluster is 10 km. A single experimental simulation was performed, and the repetition of the run may serve to establish bounds of uncertainty in a subsequent iteration of this study. The aim of this analysis was to determine the density of systems that could operate a return (air-air link) within the MAI without imposing harmful interference to the EESS passive service. Two 10 million km^2 EESS passive MAIs centred at (68° W, 0° N) and (91° W, 0° N) were considered as representatives of over ground and oversea areas, respectively. See Figs A9-1 and A9-2.

The example R1 MAI to be used for this simulation was selected over both Amazon River basin and oversea MAI.

When the EESS R1 sensor main beam is within the MAI, the active air-air and air-ground links with line-of-sight to the R1 were computed and aggregated receive power density computed using § A9.1.1. Interference events are considered only for that time that the EESS R1 sensor is making measurements from within the MAI. However, an extension of the MAI of 1 degree in each direction was used to determine those aeronautical systems that could additionally contribute interference.

Figure A9-15 shows the ground demark of the EESS R1 MAI utilized for all simulation runs of configurations 1 and 4 (over ground case).

Figure A9-16 shows the ground demark of the EESS R1 MAI utilized for all simulation runs of configurations 4 (oversea case).

Figure A9-17 shows the aeronautical flight paths utilized by subsequent simulation runs of configuration 4 (over ground case). The source of this data set given in public domain by link.

Figure A9-18 shows routes in and immediately around the MAI utilized by subsequent simulation runs of configuration 4 (over ground case).

Figures A9-19 and A9-20 show routes in and immediately around the MAI utilized by subsequent simulation runs of configuration 4 (oversea case), for low and high route density, respectively.

Figure A9-21 shows the ground station segment utilized by subsequent simulation runs of configuration 1. Also plotted is the EESS R1 MAI for reference.

Figure A9-22 shows the air station segment utilized by subsequent simulation runs of configuration 1. Also plotted is the EESS R1 MAI for reference.

Figure A9-22 shows the antenna pattern for sensor R1 utilized by subsequent simulation runs. Figure A9-23 shows the antenna pattern for AM(OR)S air-stations utilized by subsequent simulation runs.

Figure A9-24 shows the selectivity curves used by simulations including both the receiver and emission source for the case of the emission occupying the band subset immediately adjacent to the receiver allocated band. These curves are used to determine the FDR used by the simulations as described in § A9.1.2.

Figure A9-25 shows the antenna pattern for AM(OR)S systems 1 and 3 air-stations utilized by subsequent simulation runs.

FIGURE A9-15

Earth exploration-satellite service example of R1 over ground mission area of interest for Earth exploration-satellite service (passive) observations

FIGURE A9-16

Earth exploration-satellite service R1 mission area of interest (overseas) example of oversea mission area of interest for Earth exploration-satellite service (passive) observations

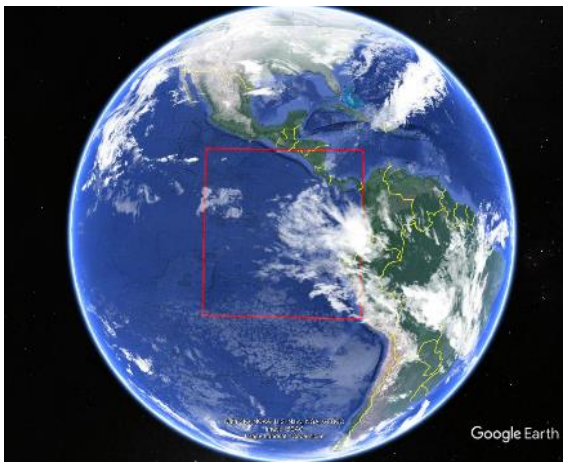

FIGURE A9-17

Aeronautical route deployment

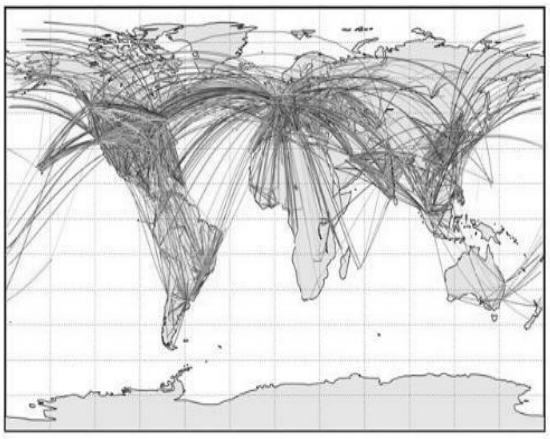

FIGURE A9-18

Aeronautical route deployment

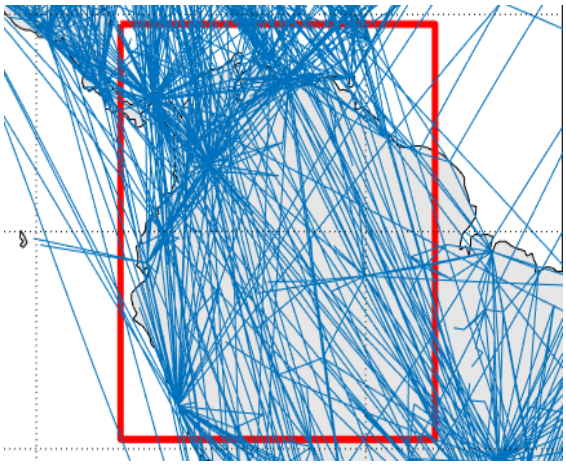

FIGURE A9-19

Aeronautical route deployment (low route number)

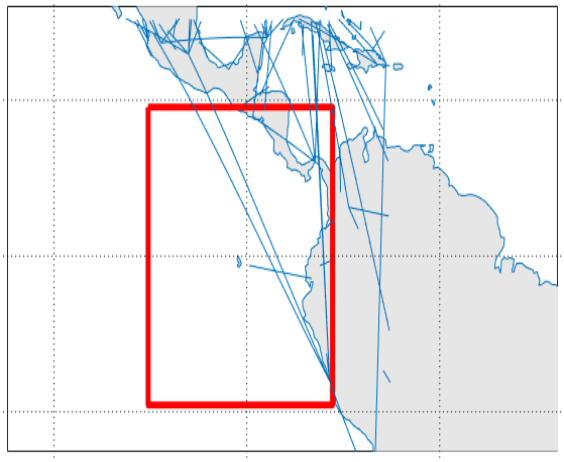

FIGURE A9-20

Aeronautical route deployment (high route number)

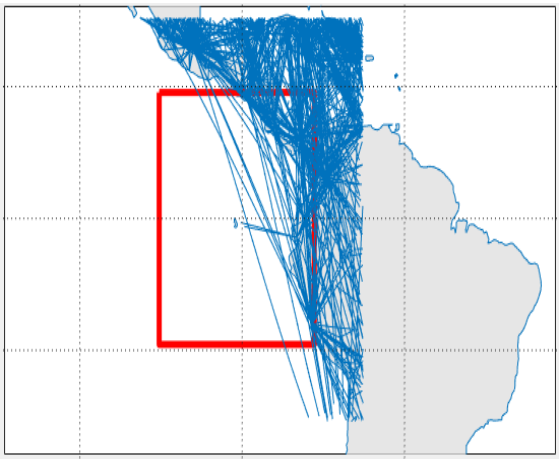

FIGURE A9-21

Ground station segment deployment (low density) (one blue dot represents a ground station in scenario 6.2)

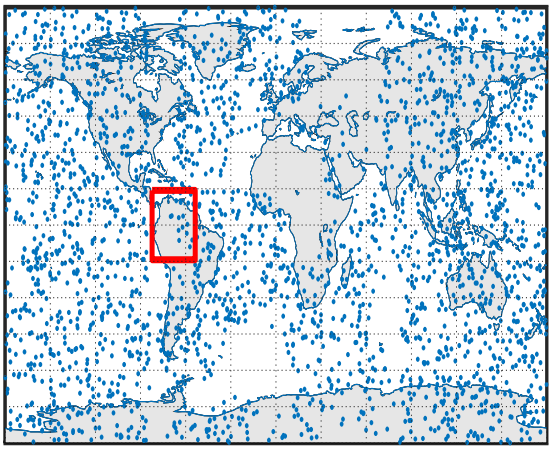

FIGURE A9-22

Ground station segment deployment (med. density) (one blue dot represents a ground station in scenario 6.2)

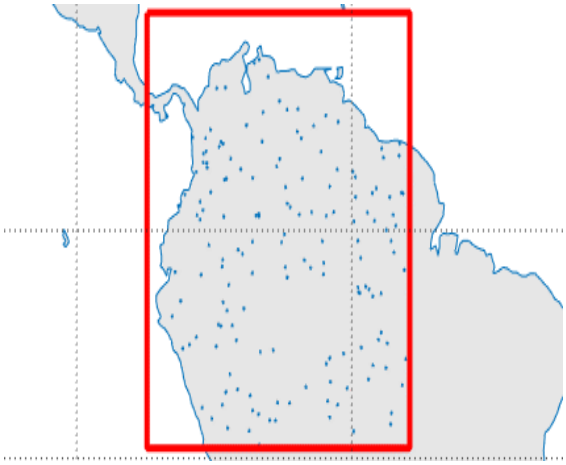

FIGURE A9-23

Earth exploration-satellite service (passive) sensor R1 gain

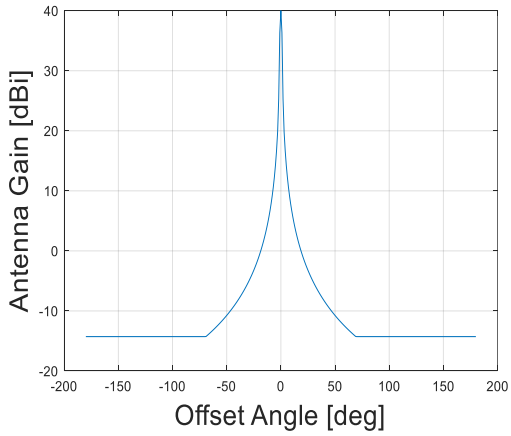

FIGURE A9-24

Emission and receiver selectivity curves

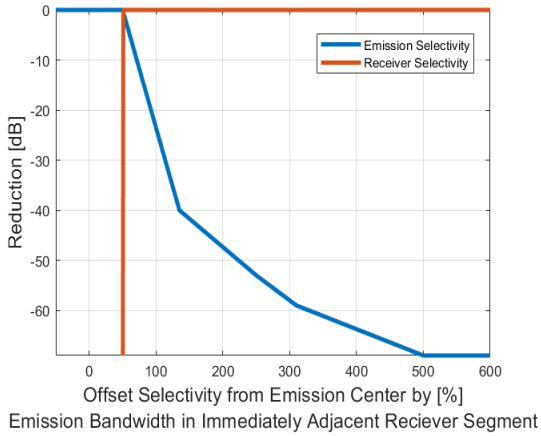

FIGURE A9-25

Aeronautical mobile (off-route) air-stations gain

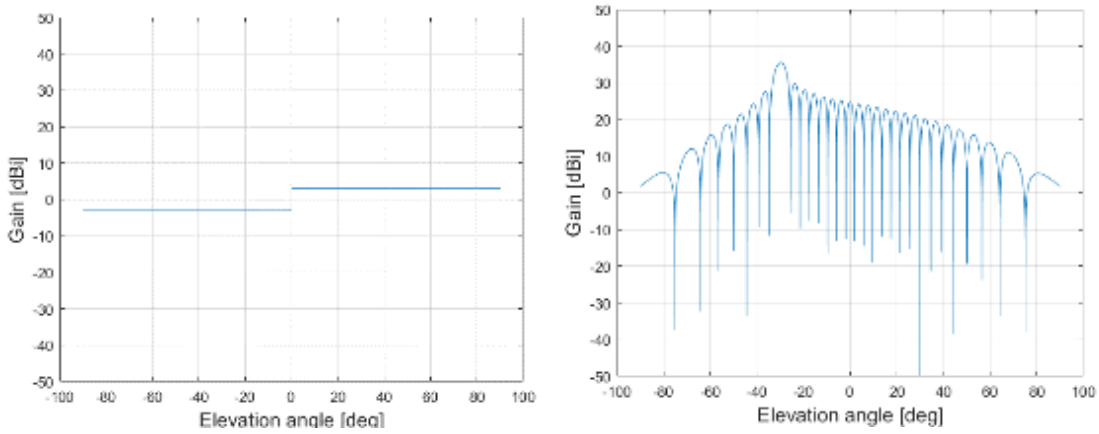

A9.2.4 Results

The following Figures illustrate the findings from the study of the RF interference impact of four scenarios on EESS R1 sensors.

Figures A9-26 to A9-33 show the simulation results in terms of ECDF of the variable $AggI_{n|\mathrm{dB}}$ (see equation (A9-14)). In each configuration, the different links established within an AM(OR)S cluster are considered separately (the other links are assumed to not operate):

– In the configuration n°1 (scenario 6.2.1), Fig. A9-26 shows the impact of A2G WBLOSDLs i.e. from the ADTs to the GDT whereas Fig. A9-27 shows the impact of G2A WBLOSDLs i.e. from the GDT to the ADTs.

– In the configuration n°2 (scenario 6.2.2), Fig. A9-28 shows the impact of upwards A2A WBLOSDLs i.e. from the observation aircraft to the central aircraft flying at a higher altitude whereas Fig. A9-29 shows the impact of downwards A2A WBLOSDL i.e. from the central aircraft to the observation aircraft.

– In the configuration n°3 (scenario 6.2.3), Fig. A9-30 shows the impact of A2A upwards WBLOSDLs i.e. from the observation aircraft to the relay whereas Fig. A9-31 shows the impact of downwards A2A WBLOSDLs i.e. from the relay to the observation aircraft.

– In the configuration n°4 (scenario 6.2.4), Fig. A9-32 shows the impact of horizontal A2A WBLOSDLs in the MAI n°1, and Fig. A9-33, the impact of the same links in the MAI n°2.

From Figs A9-30 to A9-32, the limits highlighted in Table A9-7 in terms of maximum density of WBLOSDLs (according to their type and pointing direction) can be summarized.

FIGURE A9-26

Empirical cumulative distribution function of $AggI_{n|dB}$ in the conf. n°1 (A2G omnidirectional links 50 MHz)

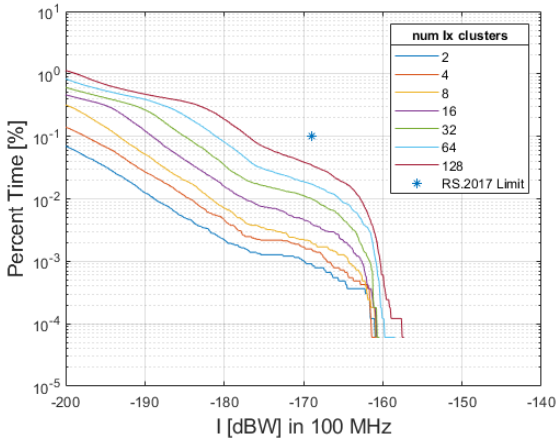

FIGURE A9-27

Empirical cumulative distribution function $AggI_{n|dB}$ in the conf. n°1 (G2A omnidirectional links 50 MHz limited to –17 dB(W/100 MHz) in 22.21-22.31 GHz)

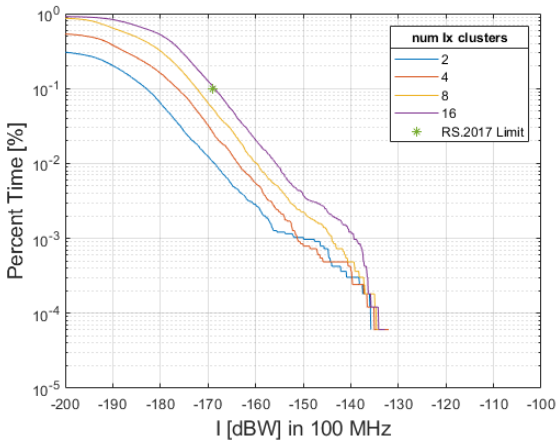

FIGURE A9-28

Empirical cumulative distribution function of $AggI_{n|dB}$ in the conf. n°2 (upwards A2A directional 30 MHz)

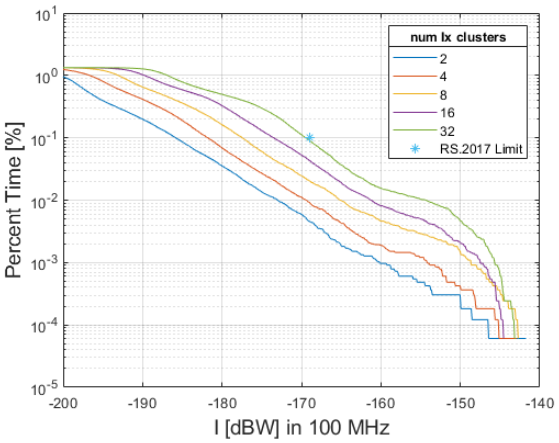

FIGURE A9-29

Empirical cumulative distribution function of $AggI_{n|dB}$ in the conf. n°2 (downwards A2A omnidirectional 30 MHz limited to −20 dB(W/100 MHz) in 22.21-22.31 GHz)

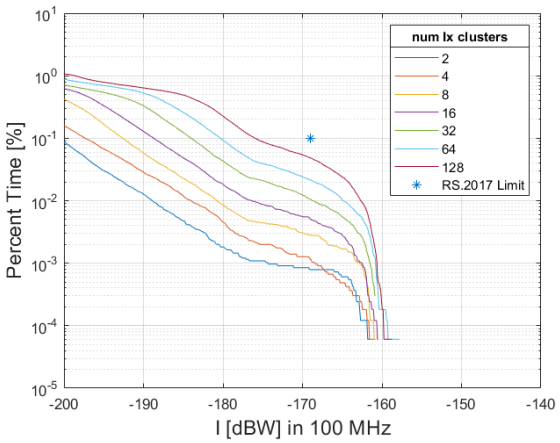

FIGURE A9-30

Empirical cumulative distribution function of $AggI_{n|dB}$ in the conf. n°3 (upwards A2A directional 10 MHz)

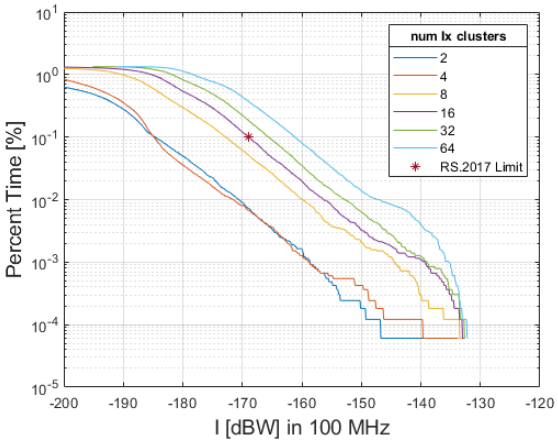

FIGURE A9-31

Empirical cumulative distribution function of $AggI_{n|dB}$ in the conf. n°3 (downwards A2A omnidirectional 20 MHz limited to −23 dB(W/100 MHz) in 22.21-22.31 GHz)

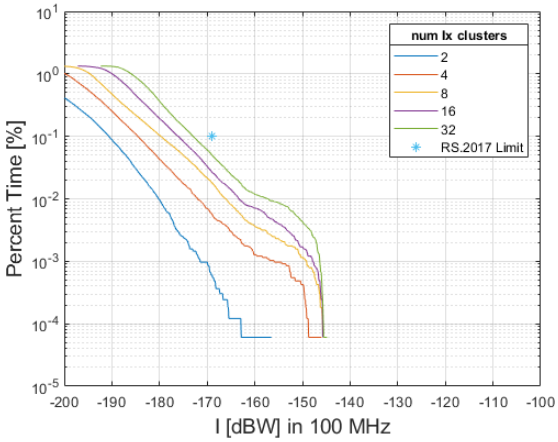

FIGURE A9-32

Empirical cumulative distribution function of $AggI_{n|dB}$ in the conf. n°4/mission area of interest N°1 (horizontal A2A directional 80 MHz limited to −22 dB(W/100 MHz) in 22.21-22.31 GHz)

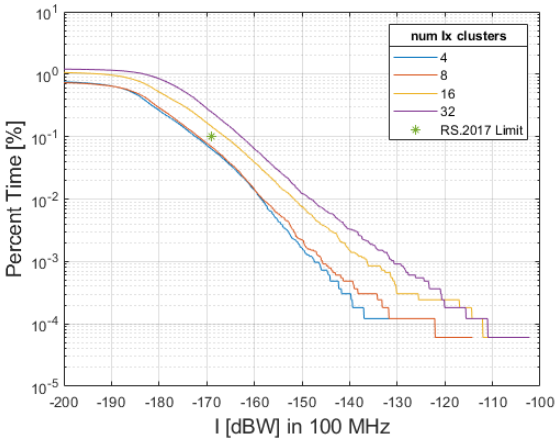

FIGURE A9-33

Empirical cumulative distribution function of $AggI_{n|dB}$ in the conf. n°4/mission area of interest N°2 (horizontal A2A directional 80 MHz limited to −22 dB(W/100 MHz) in 22.21-22.31 GHz)

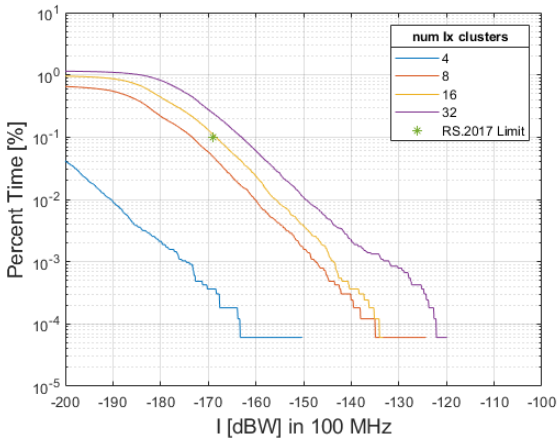

TABLE A9-7

Maximum allowable number of wideband line of sight datalinks in different configurations and associated unwanted emissions limits

	Conf. n°1		Conf. n°2		Conf. n°3		Conf. n°4
Type of WBLOS	(1)	omni (2)	Directional (+25 dBi peak gain)	omni	Directional (+25 dBi peak gain)	omni	Directional (+38 dBi peak gain)
Direction	G2A	A2G	A2A (upwards)	A2A (downwards)	A2A (upwards)	A2A (downwards)	A2A (horizontal)
Maximum number of links in a 10 000 000 km^2 MAI	8	64	128	32	32	16	20
Associated unwanted emissions limits in dB(W/100 MHz) in 22.21-22.31 GHz	−17	-	−4	−17	−11	−23	−22

(1) The whip antenna associated to the AM(OR)S system 4 that is used for G2A links in scenario 6.2.1 cannot be considered purely omnidirectional nor directional.

(2) In this Table, omni refers to the antenna used by the AM(OR)S system 2 that exhibits +3 dBi gain for negative elevation angles with respect to the local horizontal and –3 dBi for negative angles.

A9.2.5 Summary

The following results are based on studies conducted using densities below and above the typical deployment density numbers provided in § 6.4 of this Report. The purpose of this sensitivity analysis was to assess the sensitivity of the interference predictions based on the deployment density assumptions. It is also remarked that deployment densities can vary by geographic regions, and it is useful to capture the results of a sensitivity analysis to reduce the need to re-run simulations and instead support extrapolation to different areas of the Earth.

Note that this limit is based on the nominal average operational emission and adjusted to respect OOB emission levels in the EESS (passive).

Wildfire observation (operational scenario 6.2.1)

The results of § A9.1 indicate that the first configuration (operational scenario 6.2.1, wildfire observation) can support operations in the downlink transmission direction without imposing harmful interference into the EESS (passive), according to typical deployment densities, defined by ground station platforms and their associated aeronautical users operating within the specially defined region.

The air-ground link transmission direction (utilizing system 2 as described as an option in Table 3) appears to support the utilization of multiple clusters, which should be noted. Considering the return transmission direction, the interference potential is greater for the EESS passive, and a maximum number of clusters supporting operations in the ground-to-air transmission in the immediate adjacent two channels is approximately 8.

The study conducted found the majority of the contribution to this harmful interference from wildfire observation comes from non-safety-of-life AM(OR)S ground-to-air link systems operating immediately adjacent to the EESS (passive) band specifically within 50 MHz of the band edge of 22.21 GHz. The study shows it is necessary to limit the ground-to-air OOB emissions of the AM(OR)S to −17 dB(W/100 MHz) for operations within 50 MHz of the band edge in order to ensure the protection of the EESS passive service. Note that this limit is based on the nominal average operational emission and adjusted to respect OOB emission levels in the EESS (passive). It is advantageous (from a spectrum sharing perspective) to allocate ground-to-air link operations as far away from the 22.21 GHz band edge as possible.

Search and rescue (operational scenario 6.2.2)

The results of § A9.1 indicate that the second configuration (operational scenario 6.2.2, search and rescue) can support typical deployment densities, defined by seven coordinated aeronautical users operating bi-directional air-air links within the specially defined region, without imposing harmful interference into the EESS (passive). It is noted that this assumption is greater than the typical number of clusters defined in operational scenarios (see Table 8). The forward and return air-air transmission directions (utilizing systems 1 and 2 as described as options in Table 3) have a noted difference in impact to EESS. Considering the forward transmission direction, the interference potential is greater for the EESS passive, and a maximum number of clusters supporting operations in the forward transmission in the immediate adjacent two channels is approximately 4. This difference appeared to be exclusively due to the system configuration differences between 1 and 2.

The majority of the contribution to this harmful interference from search and rescue operations comes from non-safety-of-life AM(OR)S air-air systems operating immediately adjacent to the EESS (passive) band specifically within 30 MHz of the band edge in order to ensure the protection of the EESS passive service. This study found it is therefore necessary to limit the OOB emissions of specifically the return links to −17 dB(W/100 MHz) in order to ensure the protection of the EESS passive service.

Border surveillance (operational scenario 6.2.3)

The results of § A9.1 indicate that the third configuration (operational scenario 6.2.3, border surveillance) can, under certain system configurations, support two coordinated aeronautical observation users operating in relay (air-air bidirectional links) with an additional aircraft which communicates (return link) with a single ground station located within the specially defined region, without imposing harmful interference into the EESS (passive). This was taking into consideration typical deployment densities (see Table 7).

The observation/relay and exclusive relay transmission direction (utilizing systems 1 and 2 as described as options in Table 3) have a noted difference in impact to EESS. Considering the observation/relay transmission direction, the interference potential is greater for the EESS passive, and a maximum number of clusters supporting operations in the forward transmission in the immediate adjacent two channels is approximately 4. The use of system 1 for the observation/relay appeared to be primarily responsible for the greater interference levels compared to the relay exclusive transmission mode.

The majority of the contribution to this harmful interference from border surveillance operations comes from non-safety-of-life AM(OR)S air-air relay return systems operating immediately adjacent to the EESS (passive) band specifically within 20 MHz of the band edge in order to ensure the protection of the EESS passive service. This study found it is therefore necessary to limit the OOB emissions of specifically the observation/relay links to −23 dB(W/100 MHz) in order to ensure the protection of the EESS passive service.

Data networks (operational scenario 6.2.4)

The results of § A9.1 indicate that the fourth configuration (operational scenario 6.2.4, data networks above the clouds) cannot support without imposing harmful interference into the EESS (passive) more than approximately four aeronautical platforms operating over inland regions as well as not more than approximately four aeronautical platforms operating over oversea (near the shore) regions. The study found it is necessary to limit the OOB emissions of the AM(OR)S to −22 dB(W/100 MHz) immediately adjacent to the EESS (passive) band specifically within 80 MHz of the band edge of the frequency band 22.21 GHz in order to ensure the protection of the EESS passive service.

The majority of the contribution to this harmful interference from data networks above the clouds operations comes from non-safety-of-life AM(OR)S air-air relay forward systems operating immediately adjacent to the EESS (passive) band specifically within 80 MHz of the band edge in order to ensure the protection of the EESS passive service.

Summary of out-of-band limit

TABLE A9-8

Determination of out-of-band limit per system dB(W/100 MHz)

Scenario	Link	α (dBi)	β (dB)	γ	OOBL
6.2.1	DL	20	−177	T	T
6.2.1	UL	34	−177	8	−17
6.2.2	FWD	40	−177	32	−17
6.2.2	RET	33	−177	128	−4
6.2.3	OBS	42	−177	16	−23
6.2.3	RET	34	−177	32	−11
6.2.4	FWD A	40	−177	8	−23
6.2.4	FWD B	38	−177	16	−18

Table A9-8 shows the determination of the out-of-band limit per system to meet the protection criteria in the EESS (passive) band 100 MHz segment consisting of 22.21-22.31 GHz. The symbol T indicates incomplete information to compute.

General remarks

Study B is a Monte Carlo analysis that assessed the impact of AM(OR)S stations operating in the band 22-22.21 GHz onto the space-borne EESS (passive) R1 sensor introduced in § A2.5.1 and operating in the adjacent band 22.21-22.5 GHz. The effective trajectory of the spacecraft around the Earth was simulated according to the orbital parameters introduced in Table A2-10. The scanning behaviour of the sensor was also considered according to the information available in Table A2-10. The trajectory of AM(OR)S stations was also considered.

The study determines the maximum allowable density of AM(OR)S stations and the associated limits of unwanted emissions and concludes that:

– at most 32 omnidirectional WBLOSDLs limited to −23 dB(W/100 MHz) in the band 22.21-22.31 GHz; or

– at most 20 directional and horizontal WBLOSDLs limited to −22 dB(W/100 MHz) in the band 22.21-22.31 GHz; or

– at most 64 directional tilted WBLOSDLs;

– at most 4 ground to air WBLOSDLs in the scenario described in § 6.2.1 can operate simultaneously in the 10 000 000 km^2 MAI observed by the EESS (passive) sensor R1.

Annex 10

Compatibility study between future systems planned to operate in the non-safety aeronautical mobile (off-route) service in the frequency band 22-22.21 GHz and systems in the broadcasting-satellite service in the frequency band 21.4-22 GHz

TABLE OF CONTENTS

The frequency band 21.4-22 GHz is allocated to the BSS on a primary basis in Regions 1 and 3. This annex assesses potential compatibility issues between BSS operating this band and future non-safety AM(OR)S systems planned to operate in the band 22-22.21 GHz.

A10.1 Methodology

The compatibility study presented in this annex follows a Monte Carlo approach whose principle is explained in Annex 11 to this Report. Each of the five BSS carriers listed in § A2.9.1 are studied independently in the four AM(OR)S scenarios described in § 6.2.

A10.2 Results

Results are shown in Figs A10-1 to A10-4 below for the four scenarios. The long- and short-term protection criteria of BSS as highlighted in § A2.9.3 are also shown in the Figures. In the four scenarios, none of the 100 000 simulated snapshots resulted in an I/N exceeding −20 dB at the BSS receiver. This maximum I/N value is obtained in scenario 6.2.3 with BSS carrier 3 (Fig. A10-3B), which is smaller than any of the protection thresholds for BSS, which are 0 dB, −6 dB, and −10.5 dB according to § A2.9.3.

A10.3 Summary

The results presented in § A10.2 lead to the conclusion that coexistence between BSS operating in 21.4-22 GHz and non-safety AM(OR)S planned to operate in the frequency band 22-22.21 GHz can be achieved without any specific protection measures.

FIGURE A10-1A

Empirical cumulative distribution function in scenario 6.2.1 of aggregate *I*/*N* at the broadcast satellite receiver, caused by aeronautical mobile (off-Route) systems operating in the frequency band 22-22.21 GHz

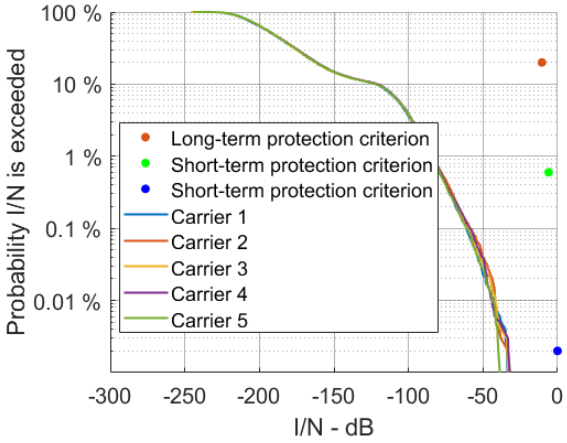

FIGURE A10-1B

Zoom of Fig. A10-1A around 10%

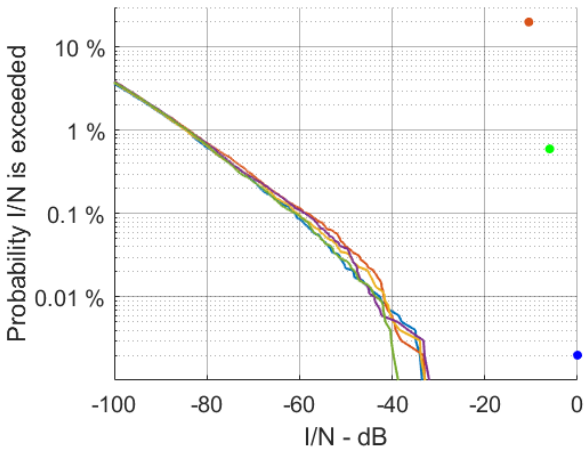

FIGURE A10-2A

As in Fig. A10-1A, in scenario 6.2.2

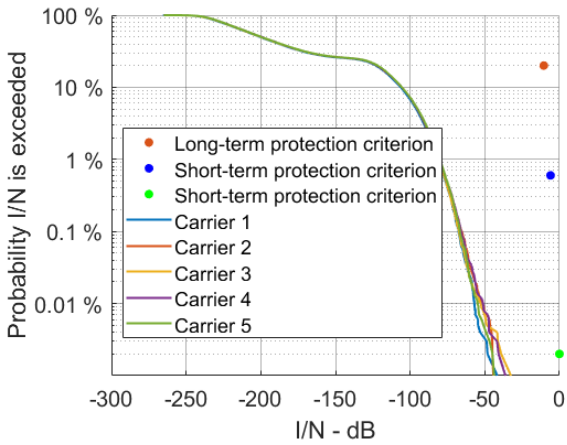

FIGURE A10-2B

Zoom of Fig. A10-2A around 10%

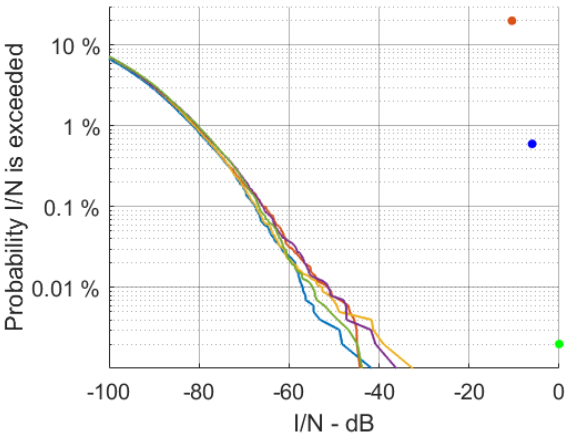

FIGURE A10-3A

As in Fig. A10-1A, in scenario 6.2.2

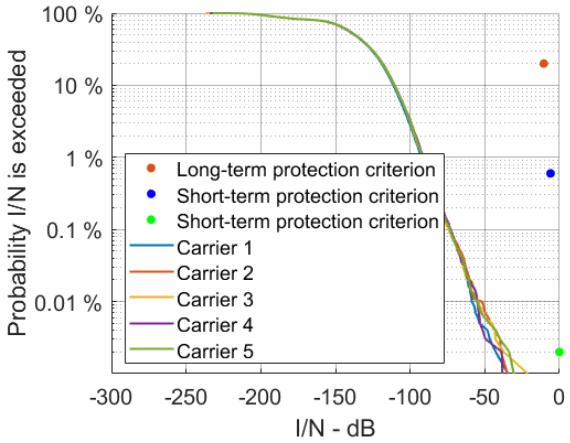

FIGURE A10-3B

Zoom of Fig. A10-3A around 10%

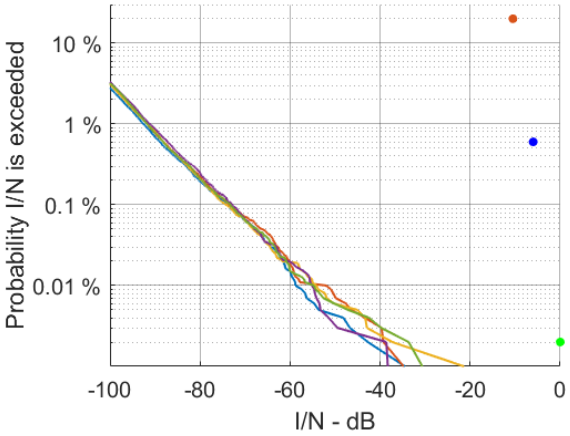

FIGURE A10-4A

As in Fig. A10-1A, in scenario 6.2.4

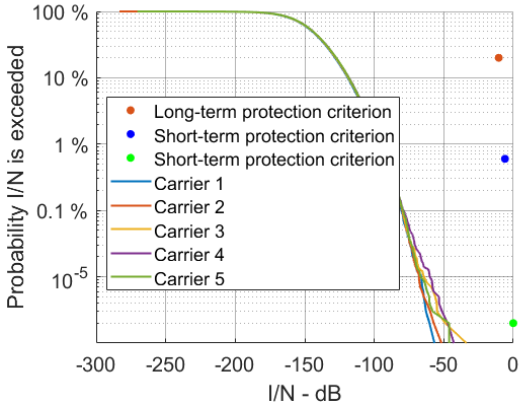

FIGURE A10-4B

Zoom of Fig. A10-4A around 10%

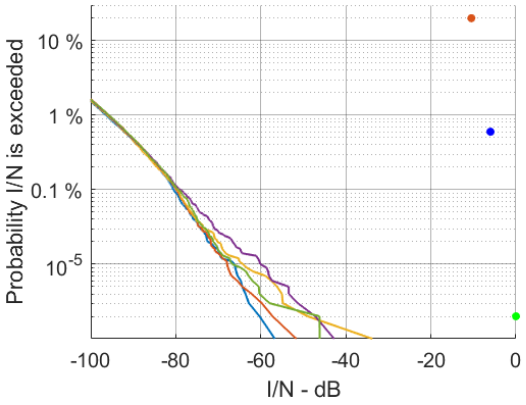

Annex 11

Proposed methodology for some Monte Carlo simulations

TABLE OF CONTENTS

This Annex describes a generic methodology used in this Report for Monte Carlo sharing and compatibility studies listed in Table A11-1. The steps described further in §§ A11.1 to A11.9 are applicable in a similar way to all sharing and compatibility studies referenced in this Table.

TABLE A11-1

List of studies using the methodology described in this annex

Interfered-with service	Frequency band (GHz)	Relevant section
RLS	15.4-17.3	Study B in Annex 3
ARNS ALS		Annex 4
ARNS DAA		Annex 5
FSS (Earth-to-space)	15.43-15.63	Annex 6
RAS	15.35-15.4	Study B in Annex 7
FS	21.2-23.6	Study B in Annex 8
RAS	22.21-22.5	Study B in Annex 7
BSS	21.4-22	Annex 10

A11.1 General principle

The Monte Carlo simulations performed in this Report have examined the impact of future non-safety AM(OR)S systems planned to operate in the frequency bands 15.4-15.7 GHz and 22-22.21 GHz onto incumbent services operating in the same, in an overlapping, or in an adjacent band. The analysis has been limited to the four operational scenarios described in § 6.2 of this Report. Due to the variety of these scenarios in terms of platform configuration and operational deployment, they are assumed to build an envelope of future applications of the AM(OR)S in the frequency bands 15.4-15.7 GHz and 22-22.21 GHz.

The Monte Carlo approach consists in placing a single IWS (representative of the victim) in the centre of a simulation area, and to deploy a number of AM(OR)S stations inside this area to assess potential interference effects. To that purpose, the contributions of the different AM(OR)S stations are aggregated at the IWS, which produces a single interference level at the IWS. To account for various configurations of the AM(OR)S stations in a given scenario, this process is repeated multiple times, and each run of the simulation (called a snapshot) produces an independent aggregate interference level. These interference levels can then be collected over all snapshots and visualized as an ECDF curve. This curve is then compared against the respective protection criterion of the IWS. The intermediary steps that lead to this ECDF curve are described in further detail in the subsequent sections.

A11.2 Deployment of the IWS

A single IWS (representative of the incumbent service under study) is deployed in the middle of the simulation area and remains at the same position and in the same configuration throughout the simulation of the snapshot. Note however that the configuration of the IWS is changed between successive snapshots.

The operational parameters of the IWS in a particular snapshot such as altitude, the direction of the antenna, and the position of the channel inside the tuning range are chosen with uniform probability from the description of the technical and operational parameters of the IWS, i.e. according to Table A11-2.

TABLE A11-2

Technical and operational characteristics of the services under study

Interfered-with service	Frequency band (GHz)	Technical and operational characteristics
RLS	15.4-17.3	Section A2.1
ARNS ALS		Section A2.2.2
ARNS DAA		Section A2.2.1
FSS (Earth-to-space)	15.43-15.63	Section A2.3
RAS	15.35-15.4	Section A2.4
FS	21.2-23.6	Section A2.5
RAS	22.21-22.5	Section A2.4
BSS	21.4-22	Section A2.9

For instance, in the case of the RLS operating in the frequency band 15.4-17.3 GHz, according to Table A2-1, the operational altitude can take any value with uniform probability within the range 300 to 13 700 m, and the radar channel can take any centre frequency within the range 15.4-17.3 GHz[26]. According to Table A2A-1 in Attachment A to Annex 2, the elevation of the antenna above the local horizontal can vary between +5° and −45°, and the azimuth between −45° and +45°. The IWS deployment in the simulation area is illustrated in Fig. A11-1.

FIGURE A11-1

Deployment of the IWS in the simulation area

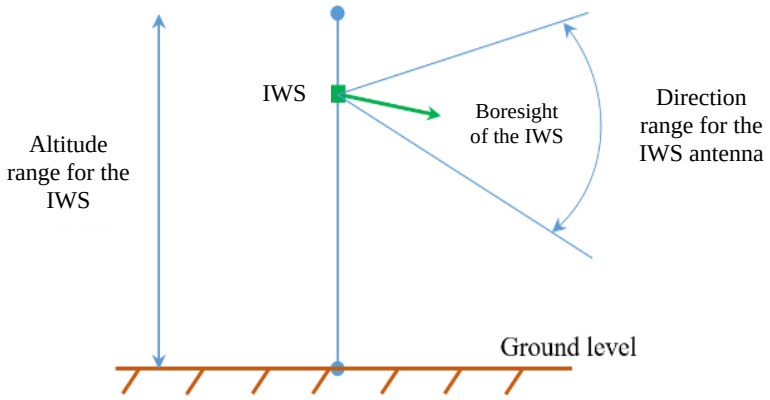

A11.3 Size of the simulation area

The second step consists in setting up a simulation area around the IWS in which AM(OR)S stations i.e. ADTs and GDTs, will be deployed. This area is represented as a spherical cap on the surface of the Earth whose radius[27] (from now onwards denoted by $R_{\text{simulation}}$) is chosen in such a way that the

[26] Note however that the channel edges may not cross the boundaries of the tuning range.

[27] The radius is understood here as the curved segment from the top to the edge of the spherical cap alongside the Earth surface.

IWS at its maximum altitude is always visible from any ADT inside the simulation area[28]. In that regard, the radius of the spherical cap is chosen as the sum of the RHD of the IWS at its maximum altitude and the RHD of the ADTs in the considered scenario, which is a fixed value provided in Table 3. This second step is illustrated in Fig. A11-2.

FIGURE A11-2

Size of the simulation area

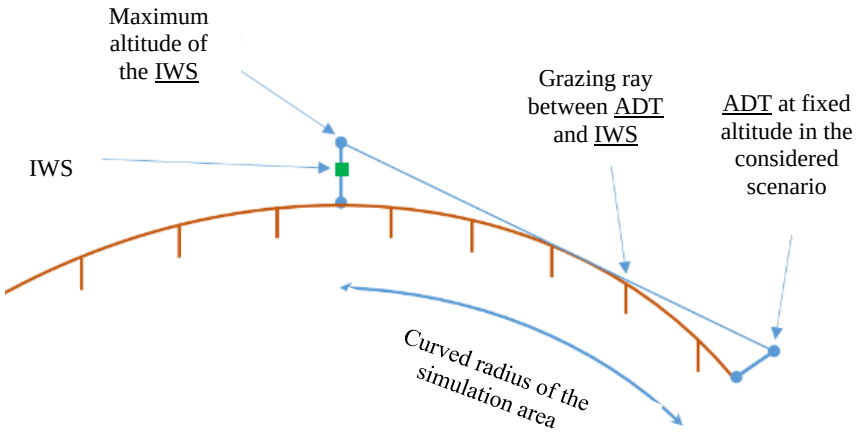

The RHD is calculated using Recommendation ITU-R P.528-5, i.e. the curvature of the rays inside the atmosphere due to the variation of the refractive index as a function of the altitude, has been taken into account. The RHD is plotted in Figs A11-3 and A11-4, together with the RHD considering free space propagation i.e. unbended rays.

FIGURE A11-3

RHD at 15.4 GHz as per Rec. ITU-R P.528-5 (blue) and considering unbended rays (red)

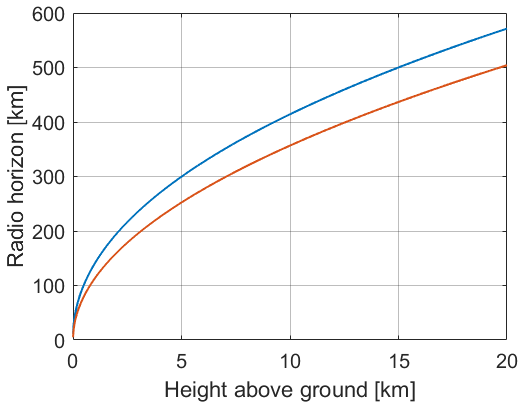

FIGURE A11-4

RHD at 22 GHz as per Rec. ITU-R P.528-5 (blue) and considering unbent rays (red)

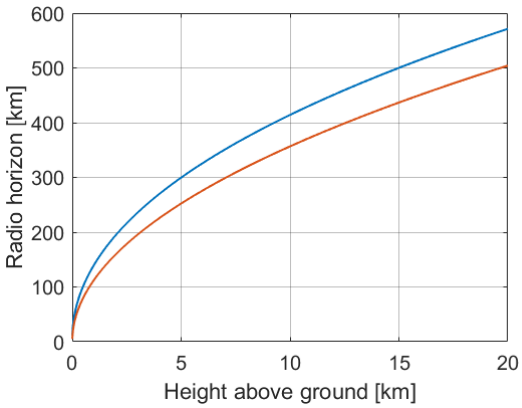

Note that Figs A11-3 and A11-4 are not linked to any time percentage because Recommendation ITU-R P.528-5 computes the RHD without any time variability.

[28] Note that the effect of BLOS interferers could have been considered as well. However, their impact was found to be negligible as compared to visible interferers. That is the rationale for limiting the simulation area to the “visibility area” of the IWS.

When the altitude of ADTs exceeds the upper bound of the applicability range of Recommendation ITU-R P.528-5, i.e. 20 km AGL, ray bending was neglected, and the simplified equation (A11-1) was used to compute the size of the simulation area.

$$RHD(h) = R_e \cdot \text{Acos}\left(\frac{R_e}{R_e+h}\right) \quad \text{(A11-1)}$$

where:

R_e: average Earth radius (km), i.e. 6 371 km

h: altitude AGL (km) of the IWS or ADT

$RHD(h)$: RHD (km) at the altitude h.

This approach leads to the values provided in Table A11-3 for the 15 GHz band, and Table A11-4 for the 22 GHz band. The simulation radius $R_{\text{simulation}}$ is called "preliminary" because it is adjusted in § A11.4 following the calculation of the number of AM(OR)S clusters to deploy in the simulation area.

TABLE A11-3

Preliminary simulation radius $R_{\text{simulation}}$ (km) in the 15 GHz frequency band

	Scenario			
	6.2.1	**6.2.2**	**6.2.3**	**6.2.4**
RLS	548	725	882	
ARNS DAA	640	817	974	
ARNS ALS	263	440	597	
FSS (Earth-to-space)	4 559	4 711	4 854	
RAS	80	257	414	

TABLE A11-4

Preliminary simulation radius $R_{\text{simulation}}$ (km) in the 22 GHz frequency band

	Scenario			
	6.2.1	**6.2.2**	**6.2.3**	**6.2.4**
FS	87	264	422	
RAS	80	257	414	
BSS				
EESS (passive)	3 156	3 308	3 451	

For instance, one can consider RLS as the IWS in scenario 6.2.1. In this example, the maximum altitude of RLS is 13.7 km AGL as per Table A2-1. The altitude of the ADTs is 300 m AGL as per Table 3. Using Fig. A11-1, these altitudes correspond to a RHD of 473.7 km and 73.9 km, respectively. The radius of the simulation area is therefore 473.7 + 73.9 = 547.6 ≈ 548 km.

In scenario 6.2.2, the maximum altitude of ADTs is 3.6 km as per Table 3, and the corresponding RHD is 214.2 km as per Fig. A11-1. The maximum height of FSS (Earth-to-space) satellites is 2 000 km as per Table A3-7 and the corresponding RHD_is 4 496.8 km as per equation (A11-1). Therefore, the radius of the simulation area is 214.2 + 4 496.8 = 4 711 km.

A11.4 Number and location of the clusters

The number of clusters N_{cluster} to deploy in the simulation area i.e. the number of groups of AM(OR)S stations in a particular scenario is calculated from $R_{\text{simulation}}$ computed in Tables A11-3 and A11-4, and from the reference cluster density associated to each scenario as evaluated in § 6.5 of this Report i.e. one cluster in a circle of radius 254 km in scenario 6.2.1, 484 km in scenario 6.2.2, 467 km in scenario 6.2.3, and 332 km in scenario 6.2.4). Equation (A11-2) is used:

$$N_{\text{cluster}} = \left(\frac{R_{\text{simulation}}}{R_{\text{density}}}\right)^2 \quad \text{(A11-2)}$$

where:

N: number of clusters to deploy in the simulation area

$R_{\text{simulation}}$: simulation radius as computed in Tables A11-3 and A11-4

R_{density}: radius in which one cluster is expected as computed in § 6.5.

The number of clusters obtained from equation (A11-2) being most of the time a non-integer value, it is rounded to the superior unit, which provides the values in Tables A11-5 and A11-6.

TABLE A11-5

Number of deployed clusters N_{cluster} in the 15 GHz frequency band

	Scenario			
	6.2.1	**6.2.2**	**6.2.3**	**6.2.4**
RLS	5	3	4	8
ARNS DAA	7		5	9
ARNS ALS	2	1	2	4
FSS (Earth-to-space)	322	95	107	212
RAS	1			2

TABLE A11-6

Number of deployed clusters N_{cluster} in the 22 GHz frequency band

	Scenario			
	6.2.1	**6.2.2**	**6.2.3**	**6.2.4**
FS	1			2
RAS				
BSS				
EESS (passive)	155	47	55	108

In order to maintain the cluster density constant, the simulation radius needs to be re-computed according to equation (A11-3):

$$R_{\text{simulation}} = \sqrt{N} \cdot R_{\text{density}} \quad \text{(A11-3)}$$

where:

$R_{\text{simulation}}$: adjusted simulation radius

N: number of clusters to deploy as shown in Tables A11-3 and A11-4

R_{density}: radius in which one cluster is expected as computed in § 6.5.

This calculation leads to the adjusted values of $R_{\text{simulation}}$ shown in Tables A11-7 and A11-8. Note that this approach can lead to considering some AM(OR)S stations that are slightly beyond the LOS distance (BLOS) of the IWS.

TABLE A11-7

Final simulation radius $R_{\text{simulation}}$ (km) in the 15 GHz frequency band

	Scenario			
	6.2.1	**6.2.2**	**6.2.3**	**6.2.4**
RLS	568	838	934	939
ARNS DAA	672		1 044	996
ARNS ALS	359	484	660	664
FSS (Earth-to-space)	4 559	4 711	4 831	4 834
RAS	254	484	467	469

TABLE A11-8

Final simulation radius $R_{\text{simulation}}$ (km) in the 22 GHz frequency band

	Scenario			
	6.2.1	**6.2.2**	**6.2.3**	**6.2.4**
FS	254	484	467	470
RAS				
BSS				
EESS (passive)	6 988	7 179	7 325	7 327

This step is illustrated in Fig. A11-5, taking as an example a snapshot where the IWS is an ARNS ALS receiver, and the scenario under study is the wildfire detection (scenario 6.2.1). According to Table A11-7, the radius of the simulation area is $R_{\text{simulation}}$ = 359 km , and N_{cluster} = 2 in accordance with Table A11-5. In this scenario, each cluster is composed of one GDT (the ground vehicle) that communicates with two ADTs (the helicopters equipped with optical and IR cameras).

FIGURE A11-5

Deployment of the aeronautical mobile (off-route) clusters in the simulation area

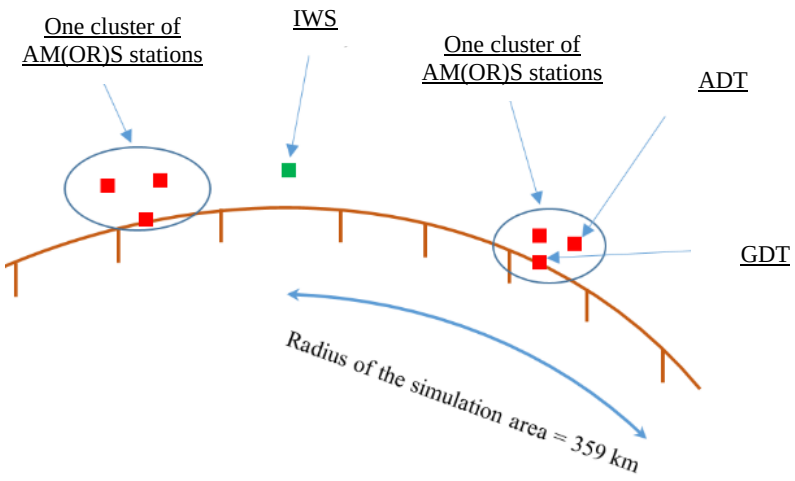

A11.5 Deployment of aeronautical mobile (off-route) stations inside a cluster

A11.5.1 Geometric deployment

FIGURE A11-6

Deployment of aeronautical mobile (off-route) stations inside a cluster

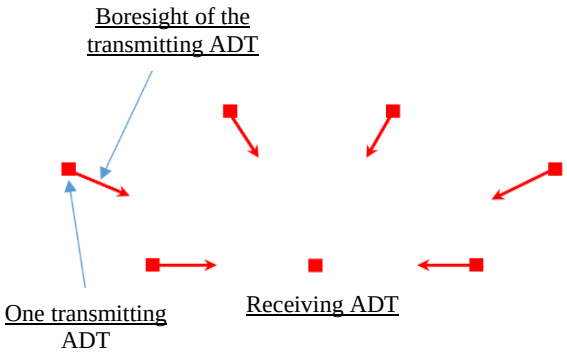

AM(OR)S stations i.e. ADTs and GDTs, are deployed within a cluster according to the technical setup shown in Table 3. When a range of values is provided rather that a single value (for example regarding the altitude of ADTs or the relative location of the AM(OR)S stations inside a cluster), a random value is chosen within this range with a uniform probability distribution.

Antennas are optimally configured to minimize the TPO of AM(OR)S stations i.e. the boresight of the transmitting station shows in the direction of the receiving station and vice-versa. This step is illustrated in Fig. A11-6, taking as an example scenario 6.2.2 (Search and Rescue). Note that in this scenario, the central aircraft is equipped with the omnidirectional AM(OR)S system and therefore there is no direction of maximum gain.

A11.5.2 Frequency and bandwidth allocation

The bandwidth BW of WBLOSDL depends on the supported throughput and the spectral efficiency. Numerical values have been provided for the various scenarios in Table 3. The centre frequency f_c is chosen with uniform probability inside the tuning range while respecting the following rules:

– The channel must be completely included inside the tuning range, in other words:

$$f_c - {BW}/{2} \geq F_{\min} \quad f_c + {BW}/{2} \leq F_{\max} \tag{A11-4}$$

where:

$F_{\min}$: lower bound of the frequency band 15.4-15.7 GHz or 22-22.21 GHz i.e. 15.4 or 22 GHz

$F_{\max}$: upper bound of the frequency band 15.4-15.7 GHz or 22-22.21 GHz i.e. 15.7 or 22.21 GHz.

– For the sake of simplicity, it is assumed that two different clusters can make use of the same frequency resources even though they are in LOS. In other words, self-interference effects between two clusters are not taken into account. This simplification however does not change the impact of interference onto the IWS under study.

– The assignment of AM(OR)S channels in a particular cluster is made on a sequential manner to maximize spectrum occupancy while respecting the condition that two links in the same cluster should be established on non-overlapping channels.

A11.6 Link budget of interfering paths

Each transmitting AM(OR)S station in the simulation area contributes a power I_i level to the aggregate interference measured at the IWS, which is evaluated using equation (A11-5). The different terms of this equation are addressed in subsequent sections.

$$I_i = (P_{Tx})_i + (G_{Tx})_i + (G_{Rx})_i - L_{i,IWS} - FDR_i \tag{A11-5}$$

where:

I_i: power level (dBm) received by the IWS from the *i*-th AM(OR)S transmitter inside the simulation area

$(P_{Tx})_i$: output power level (dBm) of the *i*-th AM(OR)S transmitter

$(G_{Tx})_i$: antenna gain (dBi) in the direction of the IWS of the *i*-th AM(OR)S transmitter

$(G_{Rx})_i$: gain (dBi) of the IWS in the direction of the *i*-th AM(OR)S transmitter

$L_{i,IWS}$: PL between the i-th AM(OR)S transmitter and the IWS

FDR_i: FDR (dB) between the channel used by the *i*-th AM(OR)S transmitter and the channel used by the IWS.

A11.6.1 transmit power output of aeronautical mobile (off-route) stations

The TPO of AM(OR)S stations inside a cluster is determined according to the simplified ATPC algorithm described in equation (A11-6). From this equation, it follows that the transmit power $(P_{Tx})_i$ of AM(OR)S stations depends upon the link distances between AM(OR)S stations that communicate using WBLOSDLs. Some examples are provided in Table 3 for different operational scenarios.

$$(P_{Tx})_i = \min\left(L_{i,\text{wanted}} - N_i + \left(\frac{C}{N}\right)_{i,targ} - (G_{Tx})_{i,\max} - (G_{Rx})_{i,\max}\,;\, P_{Tx,\max}\right) \tag{A11-6}$$

where:

$L_{i,\text{wanted}}$: PL (dB) between the *i*-th AM(OR)S transmitter and the corresponding AM(OR)S receiver, computed Recommendation ITU-R P.528-5 with a random time percentage value

N_i: thermal noise level (dBm) associated to the channel used by the i-th AM(OR)S transmitter, computed using equation (A11-7)

$\left(\frac{C}{N}\right)_{i,\text{targ}}$: target SNR (dB) at the receiver of the *i*-th AM(OR)S transmitter, as given in Table A1-1 in Annex 1

$(P_{Tx})_i$: TPO (dBm) of the *i*-th AM(OR)S transmitter[29]

$(G_{Tx})_{i,\max}$: peak gain (dBi) of the *i*-th AM(OR)S transmitter[4]

$(G_{Rx})_{i,\max}$: peak gain (dBi) of the AM(OR)S station receiving signal from the *i*-th AM(OR)S transmitter

$P_{Tx,\max}$: maximum TPO (dBm) of the *i*-th AM(OR)S transmitter, according to Table A1-1 in Annex 1.

The noise power N_i in equation (A11-6) depends on the BW used and on the receiver NF. It is computed using equation (A11-7):

$$N_i = -\frac{174\text{dBm}}{\text{Hz}} + 10\log_{10}(BW_i) + NF_i \quad \text{(A11-7)}$$

where:

N_i: thermal noise level (dBm) at the AM(OR)S station receiving signal from the *i*-the AM(OR)S transmitter

BW_i: BW of the channel used by the *i*-th AM(OR)S transmitter. Examples are provided Table 3 for different operational scenarios

NF_i: NF (dB) of the AM(OR)S station receiving signal from the *i*-th AM(OR)S transmitter, according to Table A1-1 in Annex 1.

Figures A11-7 to A11-10 show the ECDF of the TPO of AM(OR)S systems (denoted by $(P_{Tx})_i$) in the four scenarios described in § 6.2. The following remarks can be made:

– In the four scenarios, $(P_{Tx})_i$ is larger for data links than for control links. This is due to the difference in BW and hence in thermal noise between data and control links. Equation (A11-6) above explains in more details the relationship between thermal noise and TPO;

  For instance, in scenario 6.2.1 (Fig. A11-7), the difference is about 20 dB, where System 2 is used for data links, and System 4 for control links. This difference in power corresponds to the difference in BW between a control channel of 0.55 MHz and a data channel of 55 MHz, which are the respective BW of data and control links in this scenario according to Table 5;

  In scenario 6.2.2 (Fig. A11-8), the difference is about 17 dB, which corresponds in the same way to the ratio in dB between data and control channel in this scenario (see Table 5);

  In scenario 6.2.3, the difference cannot be seen from Fig. A11-9, because System 1 is used both for the link between the relay ADT and the GDT, and the links between the observation aircraft and the relay ADT. Therefore the ECDF of $(P_{Tx})_i$ for System 1 aggregates these two links;

  In scenario 6.2.4 (Fig. A11-10), no difference can be seen in terms of TPO between data and control links as they use the same system (System 3).

– In scenario 6.2.2 (Fig. A11-4), the blue plain curve corresponding to the System 1 in the frequency band 15.4-15.7 GHz (red in the frequency band 22-22.21 GHz) shows a step that separates observation ADTs that are close to the central ADT from those that are further

[29] Note that the antenna gain at the *i*-th AM(OR)S transmitter in the direction of the receiver (as well as in the other direction) equals the peak gain of the system because a perfect main beam to main beam alignment is assumed for the WBLOSDL (see § A11.5.1).

away. The step occurs at 33%, which can be explained by the fact that two observation ADTs out of six are further away than the others from the central ADT (aircraft 4), see Fig. 6-2 in scenario 6.2.2.

– In all four scenarios, the maximum power of AM(OR)S systems according to Table A1-1 is attained in at least one snapshot when they are used to implement data links:
  - 25 dBm for System 2 in both frequency bands in scenario 6.2.1, see Fig. A11-7;
  - 40 dBm for System 1 in both frequency bands in scenario 6.2.2, see Fig. A11-8;
  - 40 dBm for System 1 in both frequency bands in scenario 6.2.3, see Fig. A11-9;
  - 40 dBm for System 3 in the frequency band 15.4-15.7 GHz and 50 dBm in the frequency band 22-22.21 GHz in scenario 6.2.4, see Fig. A11-10.

– The curves related to System 5 in scenario 6.2.3 (Fig. A11-9) and System 3 in scenario 6.2.4 (Fig. A11-10) have the shape of a Gaussian cumulative distribution function (CDF) because the link distances vary within an interval with uniform probability:
  - between 50 and 250 km for System 5 in scenario 6.2.3, see Table 3;
  - between 150 and 800 km for System 3 in scenario 6.2.4, see Table 3.

FIGURE A11-7

Empirical cumulative distribution function of $(P_{Tx})_i$ in scenario 6.2.1 (Syst. 2 (data): plain line; system 4 (ctrl.): dotted line), blue in the frequency band 15.4-15.7 GHz and red in the frequency band 22-22.21 GHz

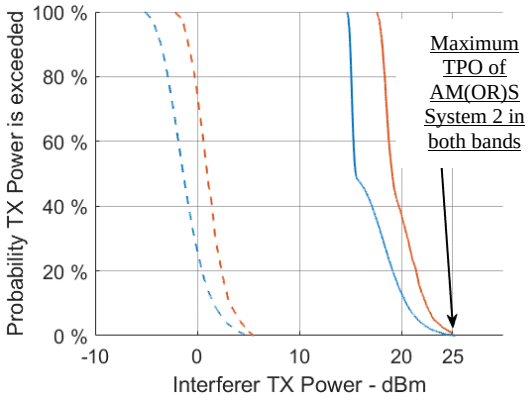

FIGURE A11-8

Empirical cumulative distribution function of $(P_{Tx})_i$ in scenario 6.2.2 (Syst. 1 (data): plain line; Syst. 2 (ctrl.): dotted line), blue in the frequency band 15.4-15.7 GHz and red in the frequency band 22-22.21 GHz

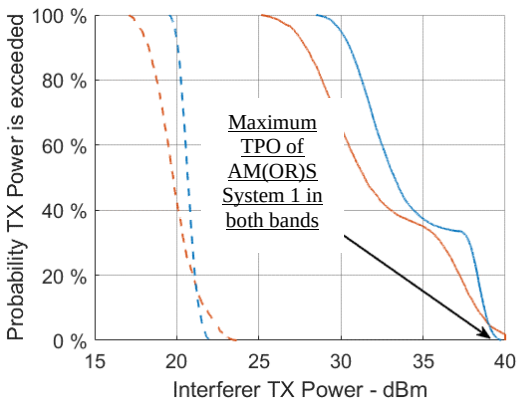

FIGURE A11-9

Empirical cumulative distribution function of $(P_{Tx})_i$ in scenario 6.2.3 (Syst. 1 (data): plain line; Syst. 2 (ctrl.): dash-dotted line; Syst. 5 (ctrl.): dotted line), blue in the frequency band 15.4-15.7 GHz and red in the frequency band 22-22.21 GHz

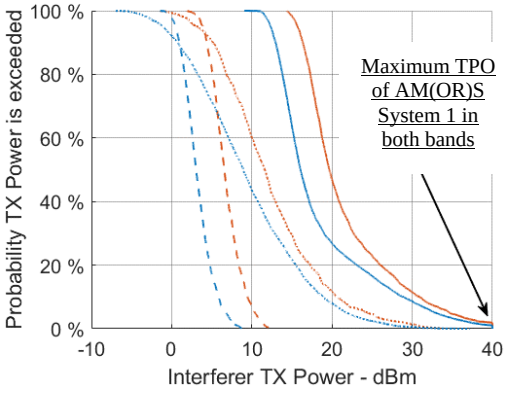

FIGURE A11-10

Empirical cumulative distribution function of $(P_{Tx})_i$ in scenario 6.2.4 (Syst. 3 (data + ctrl.): blue in the frequency band 15.4-15.7 GHz and red in the frequency band 22-22.21 GHz

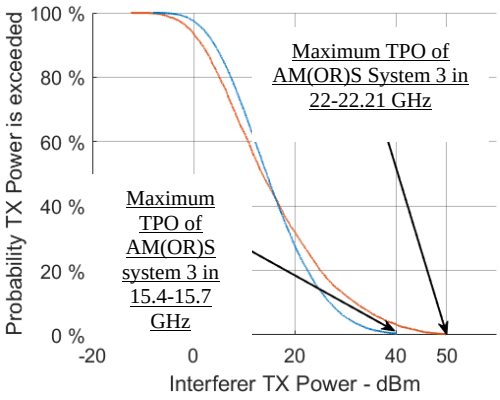

A11.6.2 Antenna gains

The antenna gain of the *i*-th AM(OR)S transmitter in the direction of the IWS antenna (denoted by $(G_{Tx})_i$ in equation (A11-5)), and conversely the gain of the IWS antenna in the direction of the *i*-th AM(OR)S transmitter (denoted by $(G_{Rx})_i$ in equation (A11-5)) are computed by first determining off-axis angles in azimuth and elevation at both ends, and then by using the appropriate antenna radiation pattern.

A11.6.3 Propagation losses for interfering paths

$L_{i,IWS}$ in equation (A11-5) is evaluated by using the appropriate model of the ITU-R P-Series, as detailed in § 8.2. The choice of the model depends on the position of the i-th AM(OR)S transmitter and the IWS. It is for instance possible that two different propagation models are used in a single snapshot, one for the interfering paths between GDTs and the IWS, and one for the interfering paths between ADTs and the same IWS.

Note that two of the three models actually used (Recommendations ITU-R P.528-5 and ITU-R P.1409-2) take as input a time percentage. In these two models, the PL between two points P_1 and P_2 fixed in space is not a constant, but a random variable denoted by $L_{P_1 \to P_2}$.

In order to generate a value of a random variable X, one must dispose of the inverse cumulative distribution function (ICDF)[30] (denoted by F_X) of this random variable i.e. a function from $[0; 1]$ into $[X_{\min}; X_{\max}]$, where $X_{\min}$ and $X_{\max}$ denote the minimum and maximum values that X can take[31]. Then, one must generate a number u with uniform probability between 0 and 1, and compute $F_X(u)$, which is a random draw of the variable X.

In the context of the propagation models, the function $L_{P_1 \to P_2}(u)$ is in general given in the appropriate Recommendation of the P-Series, and the variable u is a time percentage (denoted by p). Therefore, to generate a random sampling of $L_{i,IWS}$ between the *i*-th AM(OR)S transmitter and the IWS, one can

[30] The IDF is also called quantile function in some contexts. This is nothing else than the inverse of the CDF.
[31] This interval is also known as the support of X.

simply draw a number p with uniform probability between 0 and 100%[32] and compute a random sampling of $L_{i,IWS}(p)$.

A11.6.4 Frequency dependent rejection

The FDR between the *i*-th AM(OR)S transmitter and the IWS is computed using the methodology laid out in Annex 1 of Recommendation ITU-R SM.337-6. In particular, equation (A11-8) is adapted from equation (2) in Recommendation ITU-R SM.337-6.

$$FDR_i = 10\log_{10}\left(\frac{\int_0^{+\infty} M_{Tx}(\tau)d\tau}{\int_0^{+\infty} M_{Tx}(\tau)M_{Rx}(\Delta f_i+\tau)^2 d\tau}\right) \quad \text{(A11-8)}$$

where:

FDR_i: FDR between the i-th AM(OR)S transmitter and the IWS

τ: relative frequency offset defined as $\tau = \frac{f - f_{c,i}}{f_{c,i}}$, where $f_{c,i}$ denotes the centre frequency used by the i-th AM(OR)S transmitter

$M_{Tx}(\tau)$: relative SEM (in the linear domain) of the i-th AM(OR)S transmitter at the relative frequency τ defined above, as provided in Table A1-1. Note that the same SEM applies for AM(OR)S systems planned to operate in the frequency bands 15.4-15.7 GHz and 22-22.21 GHz

$M_{Rx}(\Delta f_i + \tau)$: relative SEM (in the linear domain) of the IWS at the relative frequency $\Delta f_i + \tau$, where $\Delta f_i = \frac{f_r - f_{c,i}}{f_{c,i}}$, where f_r denotes the centre frequency of the IWS. Note that in the case where this mask is not available for a particular IWS, a perfect selectivity mask is assumed i.e. a mask that equals 1 in the receiver band, and 0 everywhere else.

In the particular case where an AM(OR)S transmitter uses the same centre frequency as the IWS (for instance in some cases of sharing studies), equation (A11-8) can be approximated using equation (A11-9):

$$FDR_i \approx \begin{cases} 10\log_{10}\left(\frac{BW_r}{BW_i}\right) & \text{if} \quad BW_r \le BW_i \\ 0 & \text{otherwise} \end{cases} \quad \text{(A11-9)}$$

where:

BW_i: BW used by the i-th AM(OR)S transmitter

BW_r: BW used by the IWS.

A11.7 Aggregate interference

In a particular snapshot, the aggregate interference value $I_{\text{aggregate}}$ at the IWS is evaluated by summing the contributions of all active AM(OR)S transmitters in the linear domain i.e. using equation (A11-10):

$$I_{\text{aggregate}} = 10\log_{10}\left(\sum_{i=1}^{n} 10^{I_i/10}\right) \quad \text{(A11-10)}$$

where:

[32] It might be that some propagation models do not consider the full range of time percentage from 0 to 100%. In that case the number p is generated with uniform probability within the applicability range of the model.

I_i: contribution (dBm) of the *i*-th AM(OR)S transmitter to the aggregate interference value $I_{\text{aggregate}}$ at the receiver. For a particular AM(OR)S transmitter, I_i is computed using equation (A11-5)

n: number of active AM(OR)S transmitters in the simulation area in the current snapshot.

A11.8 Number of snapshots

The minimum number of snapshots chosen for the simulation i.e. the number of times that the simulation is iterated, is related to the minimum percentage of time associated to the protection criteria of the IWS. For instance, if this time percentage is 1%, 100 snapshots at least would be necessary. If the time percentage is 0.1%, 1 000 snapshots at least would be required.

The minimum number of snapshots is indicated in Table A11-9 for all IWS. Note that the actual number of simulation snapshots is in all cases greater than this minimum value in order to provide sufficient statistical diversity. Note also that the protection criteria associated to the RLS and to the ARNS in the 15 GHz frequency band is not associated to any time percentage, and therefore the number of snapshots is arbitrarily chosen equal to 100 000 to assess sufficiently low percentages.

TABLE A11-9

Number of simulated snapshots

IWS	Frequency band (GHz)	Maximum time percentage associated to the protection criterion	Relevant section	Minimum number of snapshots	Number of simulated snapshots
RLS	15.4-17.3	None	A3.2.2	–	100 000
ARNS ALS			A4.2		
ARNS DAA			A5.1.2		
FSS (Earth-to-space)	15.43-15.63	99.98	A6.2	5 000	10 000
RAS	15.35-15.4	98	A7.2.1	50	100 000
FS	21.2-23.6	99.9872	A8.2.2	7 813	100 000
RAS	22.21-22.5	98	A7.2.1	50	100 000
BSS	21.4-22	99.98	A10.2	5 000	100 000

A11.9 Empirical cumulative distribution function of the aggregate interference

Each of the simulated snapshot produces an aggregate interference value $I_{\text{aggregate}}$ that is computed according to equation (A11-10). Iterating the simulation multiple times allows one to plot the ECDF of the variable $I_{\text{aggregate}}$ and to compare it against the protection criteria of the IWS.